

DISSERTATION

MEMBRANE BEHAVIOR, DIFFUSION, AND COMPATIBILITY OF A
POLYMERIZED BENTONITE FOR CONTAINMENT BARRIER APPLICATIONS

Submitted by

Gretchen L. Bohnhoff

Department of Civil and Environmental Engineering

In partial fulfillment of the requirements

For the Degree of Doctor of Philosophy

Colorado State University

Fort Collins, Colorado

Fall 2012

Doctoral Committee:

Advisor: Charles D. Shackelford

Craig H. Benson

Thomas Borch

Thomas C. Sale

ABSTRACT

MEMBRANE BEHAVIOR, DIFFUSION, AND COMPATIBILITY OF A POLYMERIZED BENTONITE FOR CONTAINMENT BARRIER APPLICATIONS

Conventional (untreated or unmodified) bentonites are commonly used in hydraulic containment barriers to contain liquid flow and contaminant transport, because of the ability of bentonite to swell and achieve low hydraulic conductivity to water, substantial membrane behavior, and low solute diffusion coefficients. However, conventional bentonites also have been shown to be affected adversely by environmental conditions that promote multivalent-for-monovalent cation exchange. In this study, the membrane behavior and diffusive properties of a polyacrylic acid modified bentonite referred to as a bentonite polymer nanocomposite, or BPN, were determined through the simultaneous measurement of membrane efficiency coefficients, ω , and solute diffusion coefficients, D^* , during combined multi-stage membrane and diffusion tests using either potassium chloride (KCl) with concentrations ranging from 4.7 mM to 54 mM or calcium chloride (CaCl_2) with concentrations ranging from 5 mM to 20 mM. The BPN exhibited substantial membrane behavior when exposed to KCl with values of ω that were higher than those previously reported for conventional (unmodified) bentonite under similar testing conditions.

For example, the ω value measured in this study for a BPN specimen contained within a rigid-wall cell and based on circulation of 20 mM KCl was 0.43, whereas that previously reported for a GCL specimen containing a conventional bentonite under similar testing conditions except at a lower porosity (0.74 vs. 0.92) was only 0.30. Also, in contrast to previously reported results for conventional bentonite, the membrane behavior of the BPN was

sustained when exposed to 5 mM CaCl₂, and values of ω for the BPN were higher than those previously reported for conventional and other modified bentonites. For example, the value of ω for the BPN tested in a rigid-wall cell with 5 mM CaCl₂ was 0.95, whereas the ω values for an anionic polymer modified bentonite, known as Hyper clay, and a GCL were 0.13 and 0, respectively. However, exposure of specimens of the BPN to 10 mM CaCl₂ for a test conducted in a rigid-wall cell and 20 mM CaCl₂ for a test conducted in a flexible-wall cell did ultimately result in complete destruction of the membrane behavior. The destruction of the membrane behavior of the specimen in the rigid-wall test was attributed to short-circuiting along the side-walls of the rigid cell after shrinkage of the BPN specimen, whereas the destruction of the membrane behavior of the specimen in the flexible-wall test correlated with the time to reach steady-state diffusion of calcium (Ca²⁺).

Similar to a previous study involving a conventional bentonite, the diffusive properties of the BPN also were shown to correlate well with the membrane behavior of the BPN, such that that the diffusive solute mass flux decreased as the membrane efficiency of the BPN increased. However, in contrast to previous test results, the steady-state values of D^* for K⁺ and Ca²⁺ were not only not equal to but also lower than the D^* value for Cl⁻ at steady state, although the differences between the D^* for K⁺ or Ca²⁺ versus that for Cl⁻ diminished with increasing source concentration of KCl or CaCl₂, respectively. This inequality between salt cation and salt anion D^* values at steady state was attributed to the complicating existence of significant excess Na⁺ that was initially present within the specimen of BPN prior to testing and contributed to satisfying the requirement for electroneutrality, a contribution that diminished with time as the Na⁺ diffused out of the specimen.

Finally, the use of BPN in soil-bentonite (SB) backfills of vertical cutoff walls was investigated. The hydraulic conductivity, k , to tap water, the consolidation behavior, and the chemical compatibility (Δk) based on permeation with CaCl_2 solutions of SB backfills amended with BPN were evaluated and compared with those for a backfill comprised of a conventional bentonite. Although the backfills containing BPN were more sensitive to stress conditions than the backfill containing conventional bentonite, the overall hydraulic performance of a backfill containing 5 % dry BPN was better than that of the backfill containing 5 % dry conventional bentonite by approximately two orders of magnitude in terms of k .

Overall, the BPN exhibited improved membrane and diffusion properties relative to conventional and other modified bentonites previously tested under similar conditions. However, the improved membrane behavior of the BPN was ultimately destroyed upon exposure to 10 mM CaCl_2 in a rigid-wall cell and 20 mM CaCl_2 in a flexible-wall cell. Also, despite an overall lower k of the sand-BPN backfills relative to a backfill comprised of the same sand but a conventional bentonite upon permeation with a 50 mM CaCl_2 solution, the chemical resistance of the sand-BPN backfills in terms of changes in k was not any better than that for the sand-conventional bentonite backfill. Thus, the beneficial behavior of the BPN was not unlimited nor without issues, such that any perceived benefit of polymerized bentonites must first be properly characterized on a case-by-case basis prior to use.

ACKNOWLEDGEMENTS

I would like to extend my sincere gratitude to Dr. Charles Shackelford for serving as my advisor and for his helpful comments, guidance, and encouragement. I would like to thank Craig Benson, Thomas Borch, and Tom Sale for serving on my committee. Also, I would like to thank CETCO for providing the bentonites used in this study and the assistance of all the collaborators including Joe Scalia, Craig Benson, and Tuncer Edil at UW-Madison and Mike Donovan and Jerry Darlington of CETCO.

I would like to thank my fellow graduate students for their endless assistance and camaraderie including Kristin Sample, Catherine Soo Jung Hong, Jong Beom Kang, David Castelbaum, Zach Fox, and Gustavo Vianna. I also would like to acknowledge my undergraduate and graduate assistants who assisted in the building of the testing apparatuses and monitoring of the laboratory tests including Steve Middlekauff, Lance Heyer, Julie Heitland, and Stephanie Moore. Thanks to Joe Wilmetti for sharing his mechanical expertise and his continual assistance repairing components in the laboratory. I would like to thank my colleagues at the University of Wisconsin-Platteville for their encouragement as I completed my dissertation.

I would like to thank my parents, Charles and Jeanine Krupp, my mother- and father-in-law, Gene and Kathy Bohnhoff, and the rest of my family for their assistance, support, and encouragement. Thank you to my son August for being such a good baby that completion of this document was possible. Finally, thanks to my husband Andy for his patience and never-ending support and encouragement.

Financial support for this project was provided by the U.S. National Science Foundation (NSF), Arlington, VA under Grant No. CMMI-0757815. The opinions expressed in this document are solely those of the author and are not necessarily consistent with the policies or opinions of the NSF.

TABLE OF CONTENTS

ABSTRACT.....	ii
ACKNOWLEDGEMENTS.....	v
TABLE OF CONTENTS.....	vi
LIST OF TABLES.....	xii
LIST OF FIGURES.....	xiv
1 INTRODUCTION.....	1
1.1 BACKGROUND.....	1
1.2 GOALS AND OBJECTIVES OF RESEARCH.....	3
1.3 OVERVIEW OF DISSERTATION.....	5
REFERENCES.....	7
2 BACKGROUND.....	9
2.1 TRADITIONAL BENTONITE.....	9
2.1.1 Structure and Mineralogy of Bentonite.....	10
2.1.2 Index and Engineering Properties of Bentonite.....	11
2.1.2.1 Index Properties.....	12
2.1.2.2 Hydraulic Conductivity.....	14
2.1.2.3 Membrane Behavior.....	15
2.2 GEOENVIRONMENTAL ENGINEERING APPLICATIONS OF BENTONITE.....	17
2.2.1 Geosynthetic Clay Liners.....	18
2.2.2 Soil-Bentonite Cutoff Walls.....	25
2.2.3 Radioactive Waste Storage.....	28

2.3	MODIFIED BENTONITE.....	30
2.3.1	Pillared Layered Clay.....	31
2.3.2	Organoclays.....	33
2.3.3	Acid Modified Clay.....	35
2.3.4	Thermally Modified Clays.....	36
2.3.5	Polymer Modified Clay.....	37
2.4	GEOENVIRONMENTAL ENGINEERING APPLICATIONS OF MODIFIED BENTONITE.....	41
2.4.1	Geosynthetic Clay Liners.....	41
2.4.2	Soil-Bentonite Cutoff Walls.....	47
2.4.3	Sand-Bentonite Mixtures.....	48
	REFERENCES.....	51
3	ENHANCING MEMBRANE BEHAVIOR WITH A BENTONITE POLYMER NANOCOMPOSITE.....	58
3.1	INTRODUCTION.....	59
3.2	MATERIALS AND METHODS.....	62
3.2.1	Liquids.....	62
3.2.2	Soil.....	63
3.2.3	Membrane Testing.....	65
3.2.4	Measurement of Membrane Efficiency.....	71
3.2.5	Testing Program.....	73
3.3	RESULTS.....	74
3.3.1	Boundary Electrical Conductivity Values.....	74

3.3.2	Boundary Water Pressures.....	76
3.3.3	Chemico-Osmotic Pressures.....	78
3.3.4	Membrane Efficiency Coefficients.....	80
3.3.5	Volume Changes.....	81
3.3.6	Limits on Membrane Behavior.....	83
3.4	DISCUSSION.....	84
3.4.1	Comparison of Membrane Efficiency Coefficients.....	84
3.4.2	Comparison of the Limits to Membrane Behavior.....	85
3.4.3	Comparison of Volume Changes.....	86
3.4.4	Effect of Effective Stress and Boundary Salt Concentration.....	88
3.4.5	Practical Significance of Results.....	89
3.5	CONCLUSIONS.....	92
	REFERENCES.....	127
4	COUPLED SOLUTE DIFFUSION AND MEMBRANE BEHAVIOR OF A POLYMERIZED BENTONITE.....	133
4.1	INTRODUCTION.....	134
4.2	MATERIALS AND METHODS.....	137
4.2.1	Materials.....	137
4.2.2	Testing Apparatus and Procedures.....	138
4.2.3	Determination of Membrane Efficiency.....	139
4.2.4	Measurement of Transport Parameters.....	140
4.2.5	Testing Program.....	143
4.3	RESULTS.....	144

4.3.1	Membrane Efficiency Coefficients.....	144
4.3.2	Exit Concentrations and Charge Balances.....	144
4.3.3	Diffusion Results.....	146
4.3.4	Apparent Tortuosity Factors.....	149
4.4	DISCUSSION.....	150
4.4.1	Comparison of Effective Diffusion Coefficients.....	150
4.4.2	Comparison of Tortuosity Factors.....	152
4.4.3	Explanation of Diffusion Coefficients.....	153
4.5	CONCLUSIONS.....	156
	REFERENCES.....	183
5	POLYMERIZED BENTONITE FOR ENHANCED RESISTANCE TO MEMBRANE DEGRADATION.....	186
5.1	INTRODUCTION.....	187
5.2	MATERIALS AND METHODS.....	192
5.2.1	Liquids.....	192
5.2.2	Soil.....	193
5.2.3	Membrane Testing.....	194
5.2.4	Membrane Efficiency Coefficient.....	197
5.2.5	Determination of Diffusion Coefficients.....	198
5.2.6	Testing Program.....	200
5.3	RESULTS.....	200
5.3.1	Electrical Conductivity.....	200
5.3.2	Boundary Water Pressures.....	202

5.3.3	Chemico-Osmotic Pressures and Membrane Efficiency Coefficients.....	203
5.3.4	Volume Change.....	206
5.3.5	Exit Concentrations.....	208
5.3.6	Diffusion Results.....	209
5.4	DISCUSSION.....	211
5.4.1	Destruction of Membrane Behavior.....	211
5.4.2	Comparison of Membrane Efficiencies.....	212
5.4.3	Comparison of Diffusion Coefficients.....	213
5.5	CONCLUSIONS.....	214
	REFERENCES.....	244
6	POLYMERIZED BENTONITE AMENDED BACKFILLS FOR VERTICAL CUTOFF WALLS.....	249
6.1	INTRODUCTION.....	250
6.2	MATERIALS AND METHODS.....	253
6.2.1	Constituent Soils.....	253
6.2.2	Permeant Liquids.....	254
6.2.3	Slurries.....	255
6.2.4	Slump Tests.....	257
6.2.5	Preparation of Backfills for Testing.....	258
6.2.6	Consolidation.....	258
6.2.7	Flexible-Wall Hydraulic Conductivity Tests.....	259
6.3	RESULTS AND DISCUSSION.....	263
6.3.1	Stress-Strain Behavior.....	263

6.3.2	Coefficients of Volume Change, Compressibility, and Consolidation.....	265
6.3.3	Hydraulic Conductivity to Water.....	267
6.3.4	Hydraulic Conductivity to CaCl ₂ Solutions.....	269
6.3.5	Intrinsic Permeability to CaCl ₂ Solutions.....	271
6.4	SUMMARY AND CONCLUSIONS.....	273
	REFERENCES.....	301
7	SUMMARY AND CONCLUSIONS.....	305
7.1	SUMMARY.....	305
7.2	CONCLUSIONS.....	305
7.3	RECOMMENDATIONS FOR FUTURE RESEARCH.....	307
	APPENDIX A - CONSOLIDATION TEST DATA.....	308

LIST OF TABLES

Table 2.1	Properties of bentonite reported in literature.	50
Table 3.1	Chemical properties of liquids used in study.....	94
Table 3.2	Results of membrane testing on bentonite polymer nanocomposite using rigid-wall (RW) and flexible-wall (FW) cells.....	95
Table 3.3	Bulk porosities of test specimens during membrane testing in flexible-wall (FW) cells.....	97
Table 3.4	Results of regression analyses for the specimens of the bentonite polymer nanocomposite tested in this study (see Figs. 3.18 and 3.19).....	98
Table 3.5	Results of regression analyses shown based on data from the literature for geosynthetic clay liners (see Figs. 3.22 and 3.23).....	99
Table 4.1	Results of membrane testing and diffusion analysis for bentonite polymer nanocomposite using rigid-wall (RW) and flexible-wall (FW) cells.....	159
Table 5.1	Chemical properties of liquids used in study.....	217
Table 5.2	Results of swell index tests for lower quality bentonite (LQB), higher quality bentonite (HQB), and BPN.....	218
Table 5.3	Results of solution retention capacity tests for lower quality bentonite (LQB), higher quality bentonite (HQB), and BPN.....	219
Table 5.4	Membrane/diffusion test results for BPN.....	220
Table 5.5	Bulk porosities of test specimen during membrane testing in a flexible-wall cell.....	221
Table 5.6	Membrane/diffusion test results from literature for untreated and treated bentonites.....	222
Table 6.1	Index properties of two bentonites evaluated in this study.....	276
Table 6.2	Chemical properties of liquids used in study.....	277
Table 6.3	Compositions, designations, and characteristics at a slump, $-\Delta H$, of 125 mm for sand-bentonite backfills containing conventional bentonite (CB) or bentonite polymer nanocomposite (BPN).....	278

Table 6.4	Coefficients of volume change and compressibility for sand-bentonite backfills with 5 % conventional bentonite (CB) mixed with 5 % CB slurry (5CB5), 2 % bentonite polymer nanocomposite (BPN) mixed with 2 % BPN slurry (2BPN2), and 5% BPN mixed with 2 % BPN slurry (5BPN2).....	279
Table 6.5	Coefficients of consolidation for sand-bentonite backfills with 5 % conventional bentonite (CB) mixed with 5 % CB slurry (5CB5), 2 % bentonite polymer nanocomposite (BPN) mixed with 2 % BPN slurry (2BPN2), and 5% BPN mixed with 2 % BPN slurry (5BPN2).....	280
Table 6.6	Results of flexible-wall hydraulic conductivity tests on sand-bentonite backfills containing conventional bentonite (CB) or bentonite polymer nanocomposite (BPN).....	281

LIST OF FIGURES

Figure 3.1	Grain-size distributions (ASTM D 422) for replicate samples of the bentonite polymer nanocomposite (BPN).....	100
Figure 3.2	Photograph of traditional bentonite and bentonite polymer nanocomposite (BPN) plastic limit "worms.".....	101
Figure 3.3	Schematic of membrane testing apparatus.....	102
Figure 3.4	Schematic drawings of membrane testing cells: (a) rigid-wall cell (after Malusis et al. 2001); (b) flexible-wall cell (after Kang and Shackelford 2009).....	103
Figure 3.5	Pictorial views of membrane apparatuses: (a) apparatus with rigid-wall cell; (b) apparatus with flexible-wall cell.....	104
Figure 3.6	Calibration of electrical conductivity versus measured KCl concentration.....	105
Figure 3.7	Measured electrical conductivity across top and bottom boundaries during membrane testing of BPN specimens in rigid-wall cells: (a) RW1 @ $n = 0.92$; (b) RW2 @ $n = 0.80$ and flexible-wall cells (c) FW1 @ $\sigma' = 34.5$ kPa (5 psi); (d) FW2 @ $\sigma' = 103$ kPa (15 psi).	106
Figure 3.8	The change in electrical conductivity, ΔEC , of non-flushed BPN specimens during membrane testing in a rigid-wall cells (RW1 @ $n = 0.92$; RW2 @ $n = 0.80$) and a flexible-wall cells [FW1 @ $\sigma' = 34.5$ kPa (5 psi); FW2 @ $\sigma' = 103$ kPa (15 psi)] as a function of average salt (KCl) concentration across the specimen.....	107
Figure 3.9	Boundary water pressures for BPN specimens during membrane testing in a rigid-wall cells at two different porosities, n : (a) RW1 @ $n = 0.92$; (b) RW2 @ $n = 0.80$	108
Figure 3.10	Boundary water pressures for BPN specimens during membrane testing in a flexible-wall cells at different effective stresses, σ' : (a) FW1 @ $\sigma' = 34.5$ kPa (5 psi); (b) FW2 @ $\sigma' = 103$ kPa (15 psi).....	109
Figure 3.11	Boundary effective stresses in BPN [FW1 @ $\sigma' = 34.5$ kPa (5 psi)] during membrane testing in flexible-wall cells: (a) average boundary effective stress, σ'_{ave} ; (b) boundary effective stress at the top and bottom of the specimen, σ'_{Top} and σ'_{Bottom} , respectively.....	110
Figure 3.12	Boundary effective stresses in BPN [FW2 @ $\sigma' = 103$ kPa (15 psi)] during membrane testing in flexible-wall cells: (a) average boundary effective stress, σ'_{ave} ; (b) boundary effective stress at the top and bottom of the specimen, σ'_{Top} and σ'_{Bottom} , respectively.....	111

Figure 3.13	Measured chemico-osmotic pressure differences across BPN specimens at different porosities, n , during membrane testing in a rigid-wall cells: (a) RW1 @ $n = 0.92$; (b) RW2 @ $n = 0.80$	112
Figure 3.14	Measured chemico-osmotic pressure differences across BPN specimens at different initial effective stresses, σ' , during membrane testing in flexible-wall cells: (a) FW1 @ $\sigma' = 34.5$ kPa (5 psi); (b) FW2 @ $\sigma' = 103$ kPa (15 psi).....	113
Figure 3.15	Steady-state membrane efficiency coefficients of BPN specimens during membrane testing in a rigid-wall cell (RW1 @ $n = 0.92$, RW2 @ $n = 0.80$) and a flexible-wall cell [FW1 @ $\sigma' = 34.5$ kPa (5 psi), FW2 @ $\sigma' = 103$ kPa (15 psi)] as a function of average salt concentration across the specimen: (a) ω values based on initial (source) boundary concentrations, ω_o ; (b) ω values based on average boundary concentrations, ω_{ave}	114
Figure 3.16	Volume change versus time (a and b) and cumulative volume change versus time (c and d) during membrane testing of BPN specimens in a flexible-wall cell: (a and c) FW1 @ $\sigma' = 34.5$ kPa (5 psi); (b and d) FW2 @ $\sigma' = 103$ kPa (15 psi).....	115
Figure 3.17	Volumetric strain versus time (a and b) and cumulative volumetric strain versus time (c and d) during membrane testing of BPN specimens in a flexible-wall cell: (a and c) FW1 @ $\sigma' = 34.5$ kPa (5 psi); (b and d) FW2 @ $\sigma' = 103$ kPa (15 psi).....	116
Figure 3.18	Schematic illustration of membrane efficiency, ω , versus average boundary salt concentration (after Shackelford et al. 2003) [ω_{ref} = reference membrane efficiency coefficient at $\log C_{ave} = 0$; $C_{ave,\omega}$ = threshold concentration corresponding to $\omega = 0$; $C_{ave,pm}$ = perfect membrane concentration corresponding to $\omega = 1$; I_ω = the membrane index].....	117
Figure 3.19	Semi-log linear regressions of membrane efficiency coefficients for BPN specimens during membrane testing in a rigid-wall cell (RW1 @ $n = 0.92$, RW2 @ $n = 0.80$) and a flexible-wall cell [FW1 @ $\sigma' = 34.5$ kPa (5 psi), FW2 @ $\sigma' = 103$ kPa (15 psi)] as a function of average salt concentration difference across the specimen: (a) ω values based on initial (source) boundary concentrations, ω_o ; (b) ω values based on average boundary concentrations, ω_{ave}	118
Figure 3.20	Steady-state membrane efficiency coefficients of non-flushed BPN specimens versus a flushed GCL specimen (from Malusis et al. 2002a) tested in a rigid-wall cell as a function of average salt concentration across the specimen: (a) ω values based on initial (source) boundary concentrations, ω_o ; (b) ω values based on average boundary concentrations, ω_{ave} (n = total specimen porosity).....	119

Figure 3.21	Comparison of steady-state membrane efficiency coefficients, ω , of non-flushed BPN specimens versus flushed GCL specimens (from Kang and Shackelford 2010) tested in a flexible-wall cell as a function of average salt concentration across the specimen: (a) ω values based on initial (source) boundary concentrations, ω_o ; (b) ω values based on average boundary concentrations, ω_{ave} ($\sigma' =$ initial effective stress).....120
Figure 3.22	Comparison of steady-state membrane efficiency coefficients of a non-flushed BPN specimens versus those of flushed GCL specimens (from Malusis et al. 2002a) tested in a rigid-wall cell as a function of average salt concentration difference across the specimen: (a) ω values based on initial (source) boundary concentrations, ω_o ; (b) ω values based on average boundary concentrations, ω_{ave} ($n =$ total specimen porosity).....121
Figure 3.23	Comparison of steady-state membrane efficiency coefficients, ω , of non-flushed BPN specimens versus those of flushed GCL specimens (from Kang and Shackelford 2010) tested in a flexible-wall cell as a function of average salt concentration across the specimen: (a) ω values based on initial (source) boundary concentrations, ω_o ; (b) ω values based on average boundary concentrations, ω_{ave} ($\sigma' =$ initial effective stress).....122
Figure 3.24	Ratio of the membrane efficiency coefficient, ω , at σ' to ω at $\sigma' = 34.5$ kPa (5 psi), versus the average salt concentration across the specimen, C_{ave} : (a) ω based on initial (source) KCl concentrations, ω_o and (b) ω based on average KCl concentrations, ω_{ave} ($\sigma' =$ initial effective stress).....123
Figure 3.25	Ratio of the membrane efficiency coefficient in terms of average KCl concentrations, ω_{ave} , relative to that based on initial KCl concentrations, ω_o , or $R_{\omega,ss}$, versus the source KCl concentration, C_{ot} , for non-flushed BPN specimens [FW1 @ $\sigma' = 34.5$ kPa (5 psi), FW2 @ $\sigma' = 103$ kPa (15 psi)] and flushed GCL specimens (from Kang and Shackelford 2010).....124
Figure 3.26	Simplified analysis depicting the effect of chemico-osmotic counterflow through BPN ($L \leq 10$ mm) used as a containment barrier as a function of the KCl concentration in containment liquid [RW1 @ $n = 0.92$, RW2 @ $n = 0.80$, FW1 @ $\sigma' = 34.5$ kPa (5 psi), and FW2 @ $\sigma' = 103$ kPa (15 psi)].....125
Figure 3.27	Comparison of results of a simplified analysis of the potential effect of membrane behavior on the liquid flux through BPN or a GCL containment barrier: (a) based on results of rigid-wall tests (GCL data from Malusis et al. 2003); (b) based on results of flexible-wall tests (GCL data from Kang and Shackelford 2010) [$n =$ total porosity; $\sigma' =$ initial effective stress].....126

Figure 4.1	Measured exit concentrations of cations as a function of time at the top of the cell during membrane testing with KCl; (a & b) RW1 @ $n = 0.92$, (c & d) RW2 @ $n = 0.80$, (e & f) FW1 @ $\sigma' = 34.5$ kPa (5 psi), (g & h) FW2 @ $\sigma' = 103$ kPa (15 psi).....	161
Figure 4.2	Measured exit concentrations of cations as a function of time at the bottom of the cell during membrane testing; (a & b) RW1 @ $n = 0.92$, (c & d) RW2 @ $n = 0.80$, (e & f) FW1 @ $\sigma' = 34.5$ kPa (5 psi), (g & h) FW2 @ $\sigma' = 103$ kPa (15 psi)....	162
Figure 4.3	Measured exit concentrations of anions as a function of time at the bottom of the cell during membrane testing in a rigid-wall cell; (a & b) RW1 @ $n = 0.92$, (c & d) RW2 @ $n = 0.80$, (e & f) FW1 @ $\sigma' = 34.5$ kPa (5 psi), (g & h) FW2 @ $\sigma' = 103$ kPa (15 psi).....	163
Figure 4.4	Concentrations of anions and cations at the bottom of the testing cell during membrane testing of the bentonites polymer nanocomposite as a function of time: (a) Test RW 1 ($n = 0.92$); (b) Test RW2 ($n = 0.80$); (c) Test FW1 ($\sigma' = 34.5$ kPa (5 psi)); (d) Test FW2 ($\sigma' = 103$ kPa (15 psi)).....	164
Figure 4.5	Charge balance at the bottom of the testing cell during membrane testing of the bentonites polymer nanocomposite as a function of time: (a) Test RW 1 ($n = 0.92$); (b) Test RW2 ($n = 0.80$); (c) Test FW1 ($\sigma' = 34.5$ kPa (5 psi)); (d) Test FW2 ($\sigma' = 103$ kPa (15 psi)).....	165
Figure 4.6	BPN diffusion test results with chloride and potassium in terms of cumulative mass per unit area, Q_t , versus elapsed time, t for (a) RW1 @ $n = 0.92$, (b) RW2 @ $n = 0.80$, (c) FW1 @ $\sigma' = 34.5$ kPa (5 psi), (d) FW2 @ $\sigma' = 103$ kPa (15 psi).....	166
Figure 4.7	Diffusion test results from Test RW1 ($n = 0.92$) for chloride. Linear regression of steady-state data and non-linear regression of all data.....	167
Figure 4.8	Diffusion test results from Test RW2 ($n = 0.80$) for chloride. Linear regression of steady-state data and non-linear regression of all data.....	168
Figure 4.9	Diffusion test results from Test FW1 for chloride. Linear regression of steady-state data and non-linear regression of all data.....	169
Figure 4.10	Diffusion test results from Test FW2 for chloride. Linear regression of steady-state data and non-linear regression of all data.....	170
Figure 4.11	Diffusion test results from Test RW1 for potassium. Linear regression of steady-state data and non-linear regression of all data.....	171
Figure 4.12	Diffusion test results from Test RW2 for potassium. Linear regression of steady-state data and non-linear regression of all data.....	172

Figure 4.13	Diffusion test results from Test FW1 for potassium. Linear regression of steady-state data and non-linear regression of all data.....	173
Figure 4.14	Diffusion test results from Test FW2 for potassium. Linear regression of steady-state data and non-linear regression of all data.....	174
Figure 4.15	Effective diffusion coefficient (D^*) versus potassium chloride source concentration (C_{ot}) for bentonite polymer nanocomposite (BPN) for tests (a) RW1 @ $n = 0.92$, (b) RW2 @ $n = 0.80$, (c) FW1 @ $\sigma' = 34.5$ kPa (5 psi), (d) FW2 @ $\sigma' = 103$ kPa (15 psi). The D^* for the BPN was estimated using a steady state (SS) linear regression and using a non-linear regression.....	175
Figure 4.16	Ratio of chloride-to-potassium effective diffusion coefficient ratio at steady state versus source KCl concentration (C_{ot}) for bentonite polymer nanocomposite (BPN) for both rigid-wall (RW) and flexible-wall (FW) tests [Note: n = specimen porosity; σ' = initial effective stress in specimen].....	176
Figure 4.17	Effective diffusion coefficient (D^*) based on both linear regression of steady-state data and non-linear regression of all data as a function of the membrane efficiency coefficient for a bentonite polymer nanocomposite: (a) Test RW1 @ $n = 0.92$; (b) Test RW2 @ $n = 0.80$; (c) Test FW1 @ $\sigma' = 34.5$ kPa (5 psi); (d) Test FW2 @ $\sigma' = 103$ kPa (15 psi).....	177
Figure 4.18	Tortuosity factors of a bentonite polymer nanocomposite based on rigid-wall (RW) and flexible-wall (FW) test results for chloride (Cl^-) as a function of membrane efficiency: (a) apparent tortuosity factor; (b) restrictive tortuosity factor, τ_r . [Note: τ_m = matrix tortuosity factor].....	178
Figure 4.19	Effective diffusion coefficient (D^*) for chloride or potassium versus potassium chloride source concentration (C_{ot}) for bentonite polymer nanocomposite (BPN) and GCL (from Malusis and Shackelford 2002b). The D^* for the BPN was estimated using a steady state (SS) linear regression. BPN RW1, $n = 0.92$; BPN RW2, $n = 0.80$; BPN FW1, $n_i = 0.95$; BPN FW2, $n_i = 0.84$; GCL $n = 0.78 - 0.80$	179
Figure 4.20	Comparison of results for a bentonite polymer nanocomposite (BPN) versus those for a geosynthetic clay liner (GCL) from Malusis and Shackelford (2002b) as a function of membrane efficiency: (a) effective diffusion coefficients for chloride; (b) apparent tortuosity factors. [Note: RW = rigid-wall cell; FW = flexible-wall cell].....	180
Figure 4.21	Matrix tortuosity factor versus specimen porosity for the bentonites polymer nanocomposite (BPN) evaluated in this study versus that for a geosynthetic clay liner (GCL) as reported by Malusis and Shackelford (2002b).....	181

Figure 4.22	Schematic illustration of diffusion of dominant ionic species in test specimens of bentonite polymer nanocomposite (BPN): (a) directions of diffusion at top and bottom boundaries; (b) time-dependent concentration profiles.....	182
Figure 5.1	Index test results for lower quality bentonite (LQB), higher quality bentonite (HQB) from Lee and Shackelford (2005c) and BPN versus CaCl_2 concentration of solution: (a) swell index; (b) solution retention capacity.....	223
Figure 5.2	Change in (a) swell index, SI , and (b) solution retention capacity, SRC , for higher quality bentonites (HQB) and lower quality bentonites (LQB) (from Lee and Shackelford 2003b) relative to the SRC of the BPN (PN) versus CaCl_2 concentration of solution.....	224
Figure 5.3	Measured electrical conductivity across top and bottom boundaries during membrane testing of BPN specimens in rigid-wall cell (a) RW @ $n = 0.87$ and a flexible-wall cell (b) FW @ $\sigma' = 103$ kPa (15 psi).....	225
Figure 5.4	Boundary water pressures for BPN specimens during membrane testing in a rigid-wall cell (a) RW @ $n = 0.87$ and a flexible-wall cell (b) FW @ $\sigma' = 103$ kPa (15 psi).....	226
Figure 5.5	Boundary effective stresses in BPN during membrane testing in flexible-wall cell (a) boundary effective stress at the top and bottom of the specimen, σ'_{Top} and σ'_{Bottom} , respectively; (b) average boundary effective stress, σ'_{ave}	227
Figure 5.6	Measured chemico-osmotic pressure differences across BPN specimens during membrane testing in a rigid-wall cell (a) RW @ $n = 0.87$ and a flexible-wall cell (b) FW @ $\sigma' = 103$ kPa (15 psi).....	228
Figure 5.7	Photographs of potential short-circuiting of 10 mM CaCl_2 during membrane testing of BPN in rigid-wall cell, RW @ $n = 0.87$. Rhodamine dye (pink color) was added to top reservoir to indicate migration pathways.....	229
Figure 5.8	Photographs of BPN specimen after circulation of 10 mM CaCl_2 with rhodamine dye during membrane testing of BPN in rigid-wall cell, RW @ $n = 0.87$. (a) Showing stained outer surface of the BPN specimen and (b) showing the cross-section through the specimen where only the upper surface is stained.....	230
Figure 5.9	Volume change versus time (a) and cumulative volume change versus time (b) during membrane testing on BPN in a flexible-wall cell @ $\sigma' = 103$ kPa (15 psi).....	231
Figure 5.10	Volumetric strain versus time (a) and cumulative volumetric strain versus time (b) during membrane testing on BPN in a flexible-wall cell @ $\sigma' = 103$ kPa (15 psi).....	232

Figure 5.11	Photographs depicting BPN specimen volume change during membrane testing in a flexible-wall cell: (a) before circulation of DIW; (b) after circulation of DIW but before circulation of 5 mM CaCl ₂ ; (c) during circulation of 10 mM CaCl ₂ ; (d) after circulation of 20 mM CaCl ₂ ; (e) after termination of test.....	233
Figure 5.12	Measured exit concentrations of cations as a function of time at the bottom of the cell during membrane testing with CaCl ₂ ; (a & b) RW @ $n = 0.87$ and (c & d) FW @ $\sigma' = 103$ kPa (15 psi).....	234
Figure 5.13	Measured exit concentrations of anions as a function of time at the bottom of the cell during membrane testing with CaCl ₂ ; (a & b) RW @ $n = 0.87$ and (c & d) FW @ $\sigma' = 103$ kPa (15 psi).....	235
Figure 5.14	BPN diffusion test results with chloride and calcium in terms of cumulative mass per unit area, Q_t , versus elapsed time, t for (a) RW @ $n = 0.87$ and (b) FW @ $\sigma' = 103$ kPa (15 psi).....	236
Figure 5.15	Diffusion results for chloride (a, c) or calcium (b, d) for test conducted in the rigid-wall cell.....	237
Figure 5.16	Diffusion results for chloride (a, c, e) or calcium (b, d, f) for test conducted in the flexible-wall cell.....	238
Figure 5.17	Effective diffusion coefficient (a) and ratio of chloride-to-calcium effective diffusion coefficient s(b) versus calcium chloride source concentration (C_{ot}) for bentonite polymer nanocomposite (BPN) for tests RW @ $n = 0.87$ and FW @ $\sigma' = 103$ kPa (15 psi).....	239
Figure 5.18	Effective diffusion coefficient (D^*) as a function of the membrane efficiency coefficient for a bentonite polymer nanocomposite: RW @ $n = 0.87$; FW @ $\sigma' = 103$ kPa (15 psi).....	240
Figure 5.19	Measured chemico-osmotic pressure differences versus time for membrane testing of bentonite polymer nanocomposite: (a) flexible-wall test at 20 mM CaCl ₂ with $t'_{ss,Cl^-} = 80$ d and $t'_{ss,Ca^{2+}} = 86$ d; (b) rigid-wall tests with $t'_{ss,Cl^-} = 84$ d and $t'_{ss,Ca^{2+}} = 96$ d.....	241
Figure 5.20	Results of steady-state membrane efficiency coefficients for specimens of bentonite polymer nanocomposite tested in rigid-wall and flexible-wall cells (BPN-RW, BPN-FW), a GCL from Shackelford and Lee (2003), and untreated bentonite, multi-swellable bentonite (MSB), and Hyper clay from Di Emidio (2010) as a function of average salt concentration across the specimen.....	242

Figure 5.21	Effective diffusion coefficient for (a) chloride and (b) calcium versus source concentration of calcium chloride for bentonite polymer nanocomposite tested in rigid-wall and flexible-wall cells (BPN-RW, BPN-FW), a GCL from Shackelford and Lee (2003), and untreated bentonite, multi-swellable bentonite (MSB), and Hyper clay from Di Emidio (2010) as a function of average salt concentration across the specimen.....	243
Figure 6.1	Particle-size distributions, ASTM D 422 (ASTM 2007), for silica sand (SS) and replicated samples of conventional bentonite (CB), bentonite polymer nanocomposite (BPN), and. [Notes: number in () is the sample number; SP = poorly graded sand and CH = high plasticity clay according to ASTM D 2487 (ASTM 2010a)]......	282
Figure 6.2	Properties of slurries of conventional bentonite (CB) and bentonite polymer nanocomposite (BPN) as a function of bentonite content: (a) Marsh viscosity; (b) density; (c) filtrate loss; (d) <i>pH</i>	283
Figure 6.3	Backfill slump versus backfill gravimetric water content for sand-bentonite backfills with 5 % conventional bentonite (CB) mixed with 5 % CB slurry (5CB5), 2 % bentonite polymer nanocomposite (BPN) mixed with 2 % BPN slurry (2BPN2), and 5% BPN mixed with 2 % BPN slurry (5BPN2).....	284
Figure 6.4	Schematic diagram illustrating falling headwater-constant tailwater permeation system for measuring hydraulic conductivity.....	285
Figure 6.5	Effective consolidation stress versus (a) void ratio and (b) strain for sand-bentonite backfills with 5 % conventional bentonite (CB) mixed with 5 % CB slurry (5CB5), 2 % bentonite polymer nanocomposite (BPN) mixed with 2 % BPN slurry (2BPN2), and 5% BPN mixed with 2 % BPN slurry (5BPN2).....	286
Figure 6.6	Coefficient of volume change (a) and coefficient of compressibility (b) as a function of average effective stress during loading for sand-bentonite backfills with 5 % conventional bentonite (CB) mixed with 5 % CB slurry (5CB5), 2 % bentonite polymer nanocomposite (BPN) mixed with 2 % BPN slurry (2BPN2), and 5% BPN mixed with 2 % BPN slurry (5BPN2).....	287
Figure 6.7	Coefficient of consolidation based on (a) Casagrande's method (b) Taylor's method and (c) a ratio of Taylor's method to Casagrande's method as a function of average effective stress during loading for sand-bentonite backfills with 5 % conventional bentonite (CB) mixed with 5 % CB slurry (5CB5), 2 % bentonite polymer nanocomposite (BPN) mixed with 2 % BPN slurry (2BPN2), and 5% BPN mixed with 2 % BPN slurry (5BPN2).....	288

Figure 6.8	Comparisons of coefficient of consolidation based on (a) Casagrande's method (b) Taylor's method as a function of average effective stress during loading for sand-bentonite backfills with 5 % conventional bentonite (CB) mixed with 5 % CB slurry (5CB5), 2 % bentonite polymer nanocomposite (BPN) mixed with 2 % BPN slurry (2BPN2), and 5% BPN mixed with 2 % BPN slurry (5BPN2) and backfill mixtures with 2 to 5 % bentonite by dry weight from Yeo et al. (2005).....	289
Figure 6.9	Effective consolidation stress versus measured hydraulic conductivity for sand-bentonite backfills with 5 % conventional bentonite (CB) mixed with 5 % CB slurry (5CB5), 2 % bentonite polymer nanocomposite (BPN) mixed with 2 % BPN slurry (2BPN2), and 5% BPN mixed with 2 % BPN slurry (5BPN2).....	290
Figure 6.10	Measured hydraulic conductivity versus void ratio for sand-bentonite backfills with 5 % conventional bentonite (CB) mixed with 5 % CB slurry (5CB5), 2 % bentonite polymer nanocomposite (BPN) mixed with 2 % BPN slurry (2BPN2), and 5% BPN mixed with 2 % BPN slurry (5BPN2).....	291
Figure 6.11	Comparison between measured and estimated hydraulic conductivity for (a) sand-bentonite backfills with 5 % conventional bentonite (CB) mixed with 5 % CB slurry (5CB5), (b) 2 % bentonite polymer nanocomposite (BPN) mixed with 2 % BPN slurry (2BPN2), (c) and 5% BPN mixed with 2 % BPN slurry (5BPN2).....	292
Figure 6.12	Hydraulic conductivity measured in flexible-wall cells based on permeation with water versus (a) time and (b) pore volumes of flow for replicated specimens of sand-bentonite backfills 5 % conventional bentonite (CB) mixed with 5 % CB slurry (5CB5), and individual specimens of sand-bentonite backfills with 2 % bentonite polymer nanocomposite (BPN) mixed with 2 % BPN slurry (2BPN2) and 5% BPN mixed with 2 % BPN slurry (5BPN2).....	293
Figure 6.13	Correlation between geometric mean hydraulic conductivity measured in a flexible-wall cell at an average effective stress, σ' , of 20 kPa (2.9 psi) versus the hydraulic conductivity measured in a consolidometer cell at 23 kPa (3.3 psi) $\leq \sigma' \leq 1485$ kPa (215 psi) for sand-bentonite backfills with 5 % conventional bentonite (CB) mixed with 5 % CB slurry (5CB5), 2 % bentonite polymer nanocomposite (BPN) mixed with 2 % BPN slurry (2BPN2), and 5% BPN mixed with 2 % BPN slurry (5BPN2).....	294
Figure 6.14	Hydraulic conductivity to tap water as a function of bentonite content for different backfills (modified after Malusis and McKeehan 2012).....	295
Figure 6.15	Swell index of different backfills as a function of CaCl_2 concentration (modified after Malusis and McKeehan 2012).....	296

Figure 6.16	Hydraulic conductivity measured in flexible-wall cells versus (a) elapsed time and (b) pore volumes of flow for sand-bentonite backfills with 5 % conventional bentonite (CB) mixed with 5 % CB slurry (5CB5).....	297
Figure 6.17	Hydraulic conductivity measured in flexible-wall cells versus (a) elapsed time and (b) pore volumes of flow for sand-backfills with 2 % bentonite polymer nanocomposite (BPN) mixed with 2 % BPN slurry (2BPN2) and 5 % BPN mixed with 2 % BPN slurry (5BPN2).....	298
Figure 6.18	Hydraulic conductivity measured in flexible-wall cells versus (a) elapsed time and (b) pore volumes of flow measured in flexible-wall cells for sand-bentonite backfills with 5 % conventional bentonite (CB) mixed with 5 % CB slurry (5CB5), 2 % bentonite polymer nanocomposite (BPN) mixed with 2 % BPN slurry (2BPN2), and 5% BPN mixed with 2 % BPN slurry (5BPN2).....	299
Figure. 6.19	Hydraulic conductivity ratios (k_c/k_w) and intrinsic permeability ratios (K_c/K_w) for soil-bentonite backfills containing NaturalGel (NG) bentonite, SW101 bentonite, and multi-swellable bentonite (MSB), a compacted sand-attapulgite-bentonite (S-A-B) mixture containing 10 % attapulgite clay and 10 % bentonite, granular bentonite GCLs, and sand-bentonite backfills with 5 % conventional bentonite (CB) mixed with 5 % CB slurry (5CB5), 2 % bentonite polymer nanocomposite (BPN) mixed with 2 % BPN slurry (2BPN2), and 5% BPN mixed with 2 % BPN slurry (5BPN2) (modified after Malusis and McKeehan 2012).....	300

Chapter 1

Introduction

1.1 BACKGROUND

Bentonite is commonly used for a variety of geoenvironmental applications because bentonite exhibits a low hydraulic conductivity, k , to water and dilute aqueous solutions (i.e., $k \leq 10^{-10}$ m/s) and semipermeable membrane behavior (Malusis et al. 2001; Malusis and Shackelford 2002a; Kang and Shackelford 2009). Membrane behavior and low k are beneficial in geoenvironmental engineering applications because membrane behavior results from solute (e.g., contaminant) restriction which promotes hyperfiltration, chemico-osmotic flow, and reduced diffusion, and the lower the k of the barrier material, the lower the advective (hydraulically driven) component of contaminant transport. Example applications where bentonite is commonly used include as a backfill component in groundwater cutoff walls, as a barrier or barrier component in waste containment (e.g., landfills, wastewater ponds, manure lagoons, nuclear storage, etc.) and secondary containment (e.g., tank farms) applications, and as a seal in monitoring and water supply wells (Estornell and Daniel 1992; Evans 1994; Kajita 1997; Christman et al. 2002; Smith et al. 2003). Sodium bentonite (Na-bentonite), where Na^+ is the primary or predominant exchangeable cation, is preferred in these applications because Na-bentonite exhibits greater osmotic swell relative to calcium or magnesium bentonites, resulting in lower k and the presence of semipermeable membrane behavior.

However, the beneficial properties of Na-bentonite (i.e., low k and membrane behavior) can be adversely affected by environments where multivalent cations are present or predominant, as is common in most naturally occurring pore waters in earthen materials (Sposito 1989). Na-

bentonite is thermodynamically unstable in these environments, leading to cation exchange or replacement of Na^+ with multivalent cations (e.g., Ca^{2+} or Mg^{2+}). Such cation exchange can limit the osmotic swell and cause collapse of the hydrated interlayer of the bentonite, thereby increasing the k and decreasing the magnitude and/or existence of membrane behavior and, therefore, potentially increasing the magnitude of contaminant flux through the bentonite (Malusis and Shackelford 2002b; Manassero and Dominijanni 2003). Recent case histories and laboratory studies have illustrated the detrimental effects of long-term cation exchange on k and membrane behavior (Lin and Benson 2000; Jo et al. 2001; Shackelford and Lee 2003; Kolstad et al. 2004; Jo et al. 2005; Lee and Shackelford 2005a; Lee and Shackelford 2005b). For example, partial or complete destruction of membrane behavior in bentonite has been correlated with diffusion of invading salt cations into the bentonite (Malusis and Shackelford 2002a; Shackelford and Lee 2003; Kang and Shackelford 2009; Kang and Shackelford 2011).

Based on the aforementioned background, the purpose of this study was to evaluate the ability of a polymer modified bentonite to provide superior engineering performance relative to conventional (unmodified) bentonites commonly used as barriers or components of barriers in waste containment and hydraulic control applications. The bentonite evaluated in this study was a conventional (unmodified) bentonite that was modified by insertion of polyacrylic acid (PAA) within the interlayer regions of the montmorillonite mineral comprising the bentonite, and then polymerized *in situ* to form an interconnected structure within the bentonite nanoscale in an attempt to ensure that the swollen structure of the bentonite is retained upon exposure to aggressive chemical solutions. Because this polymer modification method was similar to those used for production of polymer nanocomposites, the PAA polymerized bentonite in this study is frequently referred to as a bentonite-polymer nanocomposite, or BPN. The BPN was produced

and supplied by Colloid Environmental Technologies Co. (CETCO, Hoffman Estates, IL). The overall evaluation represented a collaborative effort among CETCO, the University of Wisconsin-Madison (UW), and Colorado State University (CSU). The results presented in this dissertation are those based on the component of the evaluation conducted at CSU.

1.2 GOALS AND OBJECTIVES OF RESEARCH

Bentonite-polymer nanocomposites (BPNs) may be a viable alternative to conventional bentonite used in geoenvironmental engineering applications. Preliminary test results indicated that BPNs may have superior engineering properties relative to conventional bentonite. However, long-term testing was still needed to confirm the sustainability of the low k (UW) and the existence of membrane behavior (CSU). Therefore, the primary goal of this research was to evaluate the existence and persistence of significant membrane behavior for the BPN. A secondary goal of the proposed research was to evaluate the feasibility of using BPN as the bentonite component in the slurry and backfills for SB vertical cutoff walls. These goals were accomplished by evaluating the following hypothesis:

Bentonite-polymer nanocomposites (BPNs) will exhibit better engineering properties and more sustainable and chemically resistant membrane behavior relative to those of conventional bentonites commonly used in geoenvironmental containment applications.

This hypothesis was evaluated by completing the following objectives:

- (1) characterize the BPN through evaluation of the physical and chemical properties, and compare and contrast these properties with those previously reported for conventional bentonites;

- (2) determine the existence and sustainability of membrane behavior for a BPN exposed to solutions of potassium chloride (KCl) and compare this behavior with that previously reported for conventional bentonites;
- (3) determine the effective diffusion coefficients, D^* , for the BPN exposed to solutions of KCl and compare the these D^* values with those previously reported for conventional bentonites;
- (4) complete objectives (2) and (3) for a BPN exposed to solutions of calcium chloride (CaCl_2); and
- (5) evaluate the potential to use BPN in soil-bentonite (SB) vertical cutoff walls for hydraulic containment applications.

The primary goal of this research was achieved by characterizing the physical and chemical properties of the BPN, measuring the existence, magnitude, and sustainability of any membrane behavior (i.e., the membrane efficiency coefficient) for the BPN exposed to KCl or CaCl_2 and determining the effective diffusion coefficient, D^* , for the BPN exposed to KCl or CaCl_2 . All of these measured properties were compared and contrasted with those of conventional Na-bentonites and other modified bentonites, where applicable.

The secondary goal of this research was achieved by evaluating the potential to use BPN in soil-bentonite (SB) vertical cutoff walls for hydraulic containment applications through viscosity, API filtrate loss, and slump tests. After the use of BPN in soil-bentonite backfill was determined to be feasible, the compressibility, hydraulic conductivity, and chemical compatibility of BPN in soil-bentonite backfills were investigated.

1.3 OVERVIEW OF DISSERTATION

This dissertation includes seven chapters. Chapters 1 and 7 represent the introduction and conclusions, respectively, for the overall dissertation, and Chapter 2 contains background information for the study. The substantive results of the research are included in Chapters 3 through 6, which are written in the form of draft manuscripts for subsequent submission to archival journals.

Chapter 3 on “Enhancing Membrane Behavior with a Bentonite Polymer Nanocomposite,” presents the results of four membrane tests conducted on specimens of BPN with potassium chloride (KCl), which has been established in the literature as the predominant salt upon which the membrane behavior of conventional bentonites has been measured. The membrane behavior of the BPN was measured in the laboratory by establishing differences in KCl concentrations ranging from 4.7 mM to 54 mM across specimens of the BPN contained in both rigid-wall and flexible-wall cells under closed-system boundary conditions. The membrane efficiency coefficients, ω , were determined and compared with those of a conventional Na-bentonite. The practical significance of the results is illustrated in an analysis showing a reduction in liquid flux across a barrier composed of BPN.

Chapter 4 on “Coupled Solute Diffusion and Membrane Behavior of a Polymerized Bentonite,” presents the diffusive properties of BPN using KCl. The diffusive properties of BPN were determined through the simultaneous measurement of values of ω and the effective diffusion coefficients, D^* , of chloride (Cl^-) and potassium (K^+) during combined multi-stage membrane and diffusion tests. The steady-state D^* values of both Cl^- and K^+ are correlated with the ω values of the BPN, and compared with similar correlations previously reported for a conventional bentonite contained in the form of a geosynthetic clay liner (GCL).

Chapter 5 on “Polymerized Bentonite for Enhanced Resistance to Membrane Degradation,” presents the results of two membrane tests on specimens of BPN using solutions of calcium chloride (CaCl_2) to evaluate the chemical resistance of the BPN subjected to a more chemically aggressive electrolyte solution containing divalent calcium (Ca^{2+}). The diffusive properties of BPN are determined through the simultaneous measurement of ω and D^* during combined multi-stage membrane and diffusion tests in both rigid-wall and flexible-wall cells under closed-system boundary conditions. The values of ω and D^* for both Cl^- and Ca^{2+} were determined and compared with those previously reported in the literature based on tests conducted using specimens of conventional (unmodified) and other modified bentonites.

Chapter 6 on “Polymerized Bentonite Amended Backfills for Vertical Cutoff Walls,” presents the investigation into using BPN as an alternative to conventional bentonite in soil-bentonite (SB) backfills for vertical cutoff walls. The consolidation behavior, k , to tap water, and chemical compatibility (Δk) based on permeation with CaCl_2 solutions of SB backfills amended with BPN were evaluated and compared with those for a backfill comprised of conventional bentonite.

References

- Christman, M., Benson, C., and Edil, T. (2002). "Geophysical evaluation of annular well seals." *Ground Water Monitoring and Remediation*, 22(3), 104-112.
- Estornell, P., and Daniel, D. E. (1992). "Hydraulic conductivity of 3 geosynthetic clay liners." *Journal of Geotechnical Engineering-Asce*, 118(10), 1592-1606.
- Evans, J. C. (1994). "Hydraulic Conductivity of Vertical Cutoff Walls." *Hydraulic Conductivity and Waste Contaminant Transport in Soil*, STP 1142, D. E. Daniel and S. Trautwein, eds., ASTM, West Conshohocken, PA, 79-94.
- Jo, H. Y., Benson, C. H., Shackelford, C. D., Lee, J. M., and Edil, T. B. (2005). "Long-term hydraulic conductivity of a geosynthetic clay liner permeated with inorganic salt solutions." *Journal of Geotechnical and Geoenvironmental Engineering*, 131(4), 405-417.
- Jo, H. Y., Katsumi, T., Benson, C. H., and Edil, T. B. (2001). "Hydraulic conductivity and swelling of nonprehydrated GCLs permeated with single-species salt solutions." *Journal of Geotechnical and Geoenvironmental Engineering*, 127(7), 557-567.
- Kajita, L. S. (1997). "An improved contaminant resistant clay for environmental clay liner applications." *Clays and Clay Minerals*, 45(5), 609-617.
- Kang, J.-B., and Shackelford, C. D. (2009). "Clay membrane testing using a flexible-wall cell under closed-system boundary conditions." *Applied Clay Science*, 44(1-2), 43-58.
- Kang, J.-B., and Shackelford, C. D. (2011). "Consolidation enhanced membrane behavior of a geosynthetic clay liner." *Geotextiles and Geomembranes*, 29(6), 544-556.
- Kolstad, D. C., Benson, C. H., and Edil, T. B. (2004). "Hydraulic conductivity and swell of nonprehydrated geosynthetic clay liners permeated with multispecies inorganic solutions." *Journal of Geotechnical and Geoenvironmental Engineering*, 130(12), 1236-1249.
- Lee, J.-M., and Shackelford, C. D. (2005a). "Concentration dependency of the prehydration effect for a geosynthetic clay liner." *Soils and Foundations*, 45(5), 27-41.
- Lee, J. M., and Shackelford, C. D. (2005b). "Impact of bentonite quality on hydraulic conductivity of geosynthetic clay liners." *Journal of Geotechnical and Geoenvironmental Engineering*, 131(1), 64-77.
- Lin, L. C., and Benson, C. H. (2000). "Effect of wet-dry cycling on swelling and hydraulic conductivity of GCLs." *Journal of Geotechnical and Geoenvironmental Engineering*, 126(1), 40-49.

- Malusis, M. A., and Shackelford, C. D. (2002a). "Chemico-osmotic efficiency of a geosynthetic clay liner." *Journal of Geotechnical and Geoenvironmental Engineering*, 128(2), 97-106.
- Malusis, M. A., and Shackelford, C. D. (2002b). "Theory for reactive solute transport through clay membrane barriers." *Journal of Contaminant Hydrology*, 59(3-4), 291-316.
- Malusis, M. A., Shackelford, C. D., and Olsen, H. W. (2001). "A laboratory apparatus to measure chemico-osmotic efficiency coefficients for clay soils." *Geotechnical Testing Journal*, 24(3), 229-242.
- Manassero, M., and Dominijanni, A. (2003). "Modelling the osmosis effect on solute migration through porous media." *Geotechnique*, 53(5), 481-492.
- Scalia, J. (2012). "Bentonite-polymer composites for containment applications," PhD Dissertation, University of Wisconsin - Madison, Madison, WI.
- Scalia, J., Benson, C. H., Edil, T. B., Bohnhoff, G. L., and Shackelford, C. D. (2011). "Geosynthetic clay liners containing bentonite polymer nanocomposite." *Geo-Frontiers 2011: Advances in Geotechnical Engineering*, J. Han and D. Alzamora, eds., ASCE, Reston, VA, 2001-2009.
- Shackelford, C. D., and Lee, J. M. (2003). "The destructive role of diffusion on clay membrane behavior." *Clays and Clay Minerals*, 51(2), 186-196.
- Smith, J. A., Bartelt-Hunt, S. L., and Burns, S. E. (2003). "Sorption and permeability of gasoline hydrocarbons in organobentonite porous media." *Journal of Hazardous Materials*, 96(1), 91-97.
- Sposito, G. (1989). *The Chemistry of Soils*, Oxford University Press, New York.

Chapter 2

Background

2.1 TRADITIONAL BENTONITE

Bentonite is a natural clay composed mostly of the mineral montmorillonite. Bentonite has unique characteristics that are useful in a variety of industries. These characteristics include a large surface area, a net negative charge on the order of 80 to 150 meq/100 g (80 to 150 cmol/kg), and exchangeable surface cations (Grim 1968). Bentonite has a strong affinity for water resulting in swelling, sealing, and adhesive characteristics (Bergaya et al. 2006b; Eisenhour and Brown 2009).

Bentonite has been used extensively since the 20th century in a variety of industries. Bentonite is used (1) in metal casting in a process called green sand molding, (2) as pet adsorbents, (3) in drilling fluid for oil and gas exploration and small wells for water, mineral exploration, and environmental monitoring, (4) in iron-ore pelletizing, (5) as desiccants, (6) as environmental sealants, (7) in the manufacture of bricks and ceramics, and (8) in Civil Engineering applications such as slurry trenches. Acid modified bentonite is used in bleaching and clarifying, and polymer modified bentonite is used in paper making (Deer et al. 1992; Eisenhour and Brown 2009). Additional discussion of modified bentonite materials and their uses is provided in the following sections.

Bentonite is generally extracted via surface mines, and deposits of bentonite can be found on every continent except Antarctica. The most significant bentonite deposits were formed from the devitrification of volcanic ash that fell into shallow brackish water. These deposits tend to be layered as a result of multiple volcanic eruptions (Eisenhour and Brown 2009). As a result, the

quality of the bentonite can vary significantly throughout a deposit. Associated minerals, or non-phyllosilicate minerals that are part of the clay fraction of a deposit, reduce the commercial value of deposits (Bergaya et al. 2006b). After mining, the processing that the bentonite undergoes depends on the quality of the bentonite and the expected end use. Common processing steps include extrusion, drying, milling, screening, air classification, centrifugation, agglomeration, acid leaching, and cation exchange (Eisenhour and Brown 2009).

2.1.1 Structure and Mineralogy of Bentonite

The principle mineralogical constituents of bentonite clay are montmorillonite and beidellite, both of which are dioctahedral smectites. Smectites are a group of 2:1 layered alumino-silicates with hydrated interlayer cations and can be either dioctahedral as in montmorillonite, beidellite, and nontronite, or trioctahedral as in saponite, hectorite, and saunonite (Deer et al. 1992; Brigatti et al. 2006).

The smectites display several properties including a layered structure, several types of surfaces (i.e., external basal and edge surfaces and internal surfaces), a high specific surface area (50 to 120 m²/g), a large cation exchange capacity (80 to 150 meq/100g or 80 to 150 cmol_c/kg), a relatively minor pH-dependent anion exchange capacity, and a variable interlayer separation or basal spacing (d_{001}) that depends on the degree of hydration and the interlayer cation (Grim 1968; Mitchell 1993; Bergaya et al. 2006b; Brigatti et al. 2006). The d_{001} varies from 9.6 Å when fully collapsed to more than 19 Å when hydrated (Deer et al. 1992). Substitution of divalent for trivalent cations in the octahedral sheet, substitution of Al³⁺ for Si⁴⁺ in the tetrahedral sheets, and/or vacancies within a sheet result in a net negative charge. This negative charge is balanced by interlayer exchangeable cations, most often Na⁺ or Ca²⁺. The interlayer cations can

form inner-sphere or outer-sphere complexes with the clay mineral. Inner-sphere complexes occur when the cation is directly bound to the clay surface on one side and water molecules on the other side, whereas outer-sphere complexes occur when the interlayer cation is surrounded by water molecules that interact with the clay mineral via hydrogen bonding. The charge of the edge surfaces, where broken bonds form Si-OH and Al-OH groups, is dependent on the *pH* and point of zero charge (*PZC*) of the system. In general, the cation exchange in the interlayer is reversible, diffusion controlled, and stoichiometric, and includes selectivity of one cation over another (Brigatti et al. 2006).

2.1.2 Index and Engineering Properties of Bentonite

Hydraulic conductivity, volume change, and deformation and strength are important engineering properties of bentonite (Mitchell and Soga 2005). Additional engineering properties of bentonite that are important in geoenvironmental engineering applications include compatibility and membrane behavior. Compatibility refers to the effect of a non-standard liquid (e.g., permeant liquid) on the magnitude of an engineering property (e.g., *k*) of a material (e.g., bentonite) relative to the magnitude of the same engineering property when exposed to water (Kashir and Yanful 1997; Shackelford et al. 2000). Incompatibility results when non-standard liquids cause changes in the engineering property that are deemed to be significant. Membrane behavior refers to the ability of the clay to restrict the migration of aqueous miscible solutes.

Engineering properties of bentonite are affected by compositional factors and environmental factors. The compositional factors include the type of mineral and amount of each mineral, the absorbed cations, the particle-size distribution, and the pore-water composition. The environmental factors include the water content, density, confining pressure, fabric, and

availability of water.

Several index tests commonly conducted on fine-grained soils can provide an indication of the expected engineering properties of the soil via empirical correlations. These index tests include the Atterberg limits, particle-size distribution, and swell index. In addition, there are several other tests that are commonly conducted to directly determine the engineering properties of soil. These other tests and index tests are discussed subsequently.

2.1.2.1 Index Properties

Atterberg limits are used in the classification of fine grained soils, and also are used as correlations with engineering properties of soil, such as k , compressibility, shrink-swell potential, and chemical compatibility. The Atterberg limits describe the relationship between moisture (water) content and soil consistency. The plastic limit, or PL , is the gravimetric water content of the soil at which the soil changes from a semi-solid consistency to a plastic consistency. The liquid limit, or LL , is the gravimetric water content of the soil at which the soil changes from a plastic consistency to the consistency of a liquid. The plasticity index, PI , is the range of water contents at which the soil is in a plastic state and, therefore, is represented as the difference between the liquid limit and the plastic limit (i.e., $PI = LL - PL$).

As shown in Table 2.1, the liquid limits and plasticity indices of bentonites reported in literature vary widely, with values of LL ranging from as low as 399.3 to as high as 767.8, and values of PI ranging from as low as 376.1 to as high as 737.7, respectively (Kenney et al. 1992; Komine and Ogata 1996; Kolstad et al. 2004b; Lee and Shackelford 2005b; Ito 2006; Katsumi et al. 2007; Meer and Benson 2007; Benson and Meer 2009). This variability in Atterberg limits of bentonites found worldwide reflects, in part, the variability in the mineralogy of the bentonites

and the overall quality of bentonites. In general, the greater the *LL* and *PI*, the higher the quality of the bentonite (Lee and Shackelford 2005b).

For example, Lee and Shackelford (2005b) evaluated the *k* of two different quality bentonites taken from GCLs, a higher quality bentonite (HQB) with a *LL* of 589 and a *PI* of 548, and a lower quality bentonite (LQB) with a *LL* of 430 and a *PI* of 393. They found that the *k* of the HQB permeated with DIW was 7.0×10^{-10} cm/s, whereas the *k* of the LQB permeated with DIW was 2.4×10^{-9} cm/s. The *LL* of the HQB decreased to 102 when 500 mM CaCl₂ was used as the permeant liquid, whereas the *k* of the HQB to 500 mM CaCl₂ increased to 6.0×10^{-5} cm/s. Thus, the *k* of the HQB as defined by Lee and Shackelford (2005b) when permeated with DIW was lower than that of the LQB, but the HQB was much more reactive than the LQB when the salt solution was used as the permeant liquid, resulting in a significant increase in *k* of the HQB.

The aggregate-size distribution of bentonite clay depends on the expected end use. Bentonite can be found in granular form, powdered form, or even in chips (commonly used to seal boreholes or the annulus in monitoring wells). The aggregate-size distribution is determined with a dry sieve analysis. The aggregate-size distribution of dry bentonite taken from four GCLs classified the dry bentonite aggregates as sand (SP and SW-SC, ASTM D 2487) (Shackelford et al. 2000). The aggregate-size distribution does not tend to affect the *k* of the bentonite to DIW. However, when the bentonite is exposed to liquids that limit the swell of bentonite, the *k* of the material is similar to material with a similar grain-size distribution (i.e., 10^{-4} cm/s, or the *k* of sand and silty sand).

Swell tests give an indication of the swell potential. These tests also can be conducted with non-standard liquids (i.e., liquids other than water) where limited swell compared to that with DIW can indicate incompatibility. However, there are potential issues with the testing

procedures (e.g., user inconsistencies, insufficient test duration) that make correlations with k inconsistent; such that swell tests should be used only as an indicator rather than as a replacement of long-term k tests (Shackelford et al. 2000). For example, the swell index of bentonite with DIW typically varies from 25 mL/2g to 36 mL/2g, whereas the swell index of bentonite with salt solutions can be less than 10 mL/2g (Kenney et al. 1992; Jo et al. 2001; Lee and Shackelford 2005c; Meer and Benson 2007).

2.1.2.2 Hydraulic Conductivity

Hydraulic conductivity tests can be conducted using several different types of permeameters, but flexible-wall permeameters have been recommended because flexible-wall permeameters provide better contact between the membrane and test specimen and limit the potential for side-wall leakage (Shackelford et al. 2000). Several termination criteria also have been recommended, including: (1) achieving inflow equal to outflow ± 25 %, (2) reaching a steady state k (four or more measurements within ± 25 % to 50 % of the mean k), (3) permeating two or more pore volumes of flow (PVF), and (4) achieving similar influent and effluent chemical composition. The fourth criterion is important because tests have shown that k may increase after more than five PVF (Shackelford et al. 2000). Electrical conductivity (EC) and pH measurements can be used in place of chemical composition to indicate when the influent and effluent chemical compositions are similar. Since the method of prehydration may affect the measured k , and an increase in confining stress decreases k , the hydration and degree of confinement during k testing should simulate the conditions expected in the field. The k of bentonite in GCLs permeated with DIW typically ranges from approximately 1×10^{-9} to 3×10^{-9} cm/s (Daniel et al. 1997), whereas the k of GCLs permeated with salt solutions (e.g., 500 mM

CaCl₂) and non-standard liquids (e.g., benzene, gasoline, TCE) can be greater than 10⁻⁵ cm/s (Shackelford et al. 2000; Jo et al. 2001; Lee and Shackelford 2005b).

2.1.2.3 Membrane Behavior

Membrane behavior has been exhibited by clay soils used for waste containment barriers. As a result, there is increased interest in the membrane behavior of clay soils. Semipermeable clay membranes restrict the flow of solute and produce solvent flow in the opposite direction of the concentration gradient (Kang and Shackelford 2009). Clay membranes may exhibit salt exclusionary properties, chemico-osmosis, and hyperfiltration. A membrane is a semipermeable barrier that permits transport of only some components of a solution. Solutes are rejected because of size or electrical restrictions. The pores of clay typically are large enough to accommodate flow of common ions in groundwater; therefore, the salt exclusionary properties are a result of electrical restrictions resulting from an overlap of the Guoy double layer (Fritz 1986). The degree of salt exclusion of clay membranes is a function of several clay properties (e.g., cation exchange capacity, density, porosity) and the concentration of the solute. In ideal membranes, only chemico-osmosis (water flowing from higher water activity to lower water activity) occurs. However, in non-ideal membranes such as clay membranes, salt also diffuses in the opposite direction of water flow. The chemico-osmotic pressure difference ($\Delta\pi$) is a function of the difference in water activity across the membrane. However, this chemico-osmotic pressure difference can be estimated based on the differences of the solute concentration across the membrane via the van't Hoff expression (Fritz 1986). The chemico-osmotic efficiency coefficient, ω , also referred to as the membrane efficiency or, in the science literature, the reflection coefficient (σ), describes the ideality of chemico-osmotic systems. Fine grained soils

can act as semipermeable membranes, with ω ranging from zero for no membrane behavior to unity for an ideal (perfect) membrane (i.e., $0 \leq \omega \leq 1$) (Malusis et al. 2001).

Several methods have been used to test the membrane behavior of clay soils (e.g., Kemper and Rollins 1966; Olsen 1969; Malusis et al. 2001; Heister et al. 2005). Boundary conditions can consist of open or closed systems and test cells may be either rigid (rigid-wall cells) or flexible (flexible-wall cells). Open-system tests consist of hyperfiltration tests (applying a hydraulic gradient and quantifying the amount of filtered salt) or tests where the amount of chemico-osmotic liquid flow is measured. Under closed conditions, no liquid flow is allowed and the chemico-osmotic pressure difference is measured and used to determine ω (Kang and Shackelford 2009). The apparatus proposed by Malusis et al. (2001) and subsequently used by Yeo et al. (2005), Evans et al. (2008), and Kang and Shackelford (2009, 2010, 2011), has several advantages for measuring ω relative to other methods. With the apparatus proposed in Malusis et al. (2001), the maximum chemico-osmotic pressure difference ($\Delta\pi$) established to induce chemico-osmotic flow can be controlled and maintained approximately constant throughout the test, and the transport parameters (effective diffusion, D^* and retardation factor, R_d) can be determined simultaneously with ω .

This test set-up consists of a test cell connected to a flow-pump system. The rigid-wall cell is equipped with a top piston that allows control of the vertical total stress and prevents expansion of the specimen, and ports exiting the top piston and base pedestal that allow electrolyte circulation and measurements of differential pressures (ΔP) across the specimen established in response to the tendency for membrane behavior (i.e., a closed system). The flexible-wall cell is similar to the rigid-wall cell except that, with rigid-wall cells, the volume of the specimen is controlled; whereas the state of stress in the specimen is controlled with flexible-

wall cells (Kang and Shackelford 2009). A dual-syringe flow pump circulates the liquids via syringes housed in actuators (syringes) through the top piston and base pedestal at a constant rate in an attempt to maintain a constant $\Delta\pi$ across the specimen and mimic "perfectly flushing" boundary conditions. The outflow from the cell is collected for measurement of the electrolyte concentrations used to calculate D^* and R_d , whereas ΔP and $\Delta\pi$ are used to calculate ω (Malusis et al. 2001).

2.2 GEOENVIRONMENTAL ENGINEERING APPLICATIONS OF BENTONITE

Bentonite is used in several geoenvironmental engineering applications, including groundwater cutoff walls, seals in monitoring and water supply wells, and as components of waste containment systems for municipal, hazardous, and radioactive waste. The low k of bentonite limits the flow of fluids, making bentonite very useful in engineered containment systems constructed to isolate waste. The k of bentonite is affected by several factors, including the mineralogical composition, swell potential, exposed surface area, mineral layer charge deficiency, exchangeable cations, pore structure and connectivity, and the permeant solution. Sodium-bentonite (Na-bentonite) is most useful for geoenvironmental engineering applications because Na-bentonite has an extremely low k to water (typically $k < 10^{-8}$ cm/s). However, exchange of multivalent cations for the sodium cations (Na^+) on the exchange complex of Na-bentonites can result in reduced swell and an increase in k (Vasko et al. 2001; Kolstad et al. 2004a; Lee et al. 2005; Lee and Shackelford 2005b; Gates et al. 2009). Because of their high swell potential and low k to water permeation, bentonites commonly are used as barriers or components of barriers in hydraulic containment applications. Such bentonite based barriers included manufactured geosynthetic clay liners (GCLs), highly compacted bentonites for

radioactive waste storage, compacted soil-bentonite mixtures, especially sand-bentonite mixtures, comprised of low percentages of bentonite (typically < 10 % by dry weight) and used as compacted clay liners (CCLs), and soil-bentonite (SB) backfills used in vertical cutoff walls for *in situ* containment of contaminated groundwater.

2.2.1 Geosynthetic Clay Liners

Geosynthetic clay liners (GCLs) are comprised of a thin layer (typically ≤ 10 mm) of sodium bentonite sandwiched between two geotextiles (GTs) typically held together via needle punching or stitching. Because GCLs are manufactured and shipped to the site, the engineering properties generally are more controlled and better known relative to other types of hydraulic barriers constructed in the field, such as CCLs and SB vertical cutoff walls. The primary advantages of GCLs relative to other hydraulic containment barriers, such as non-bentonite based CCLs, are a typically lower cost resulting from the relative ease of installation, and greater containment space due to the relative thinness of GCLs. However, there are several disadvantages including the potential for incompatibility with permeant liquids other than water and desiccation problems that lead to increases in k , and the potential for greater flux through the GCL because of a reduction in bentonite thickness (Bouazza 2002; Jo et al. 2005; Gates et al. 2009). The bentonite clay in GCLs consists of approximately 65 % to 90 % montmorillonite. The small particle size, interlayer swelling, and thick layer of bound water results in low k and membrane behavior. However, these same characteristics make the clay susceptible to incompatibility (Jo et al. 2001). Recent laboratory and field investigations have illustrated the potential for these incompatibility effects (James et al. 1997; Shackelford et al. 2000; Jo et al. 2001; Shackelford and Lee 2003; Guyonnet et al. 2005; Jo et al. 2005; Benson et al. 2007;

Benson and Meer 2009). The results of several of these investigations are described subsequently.

One of the earliest investigations of GCL incompatibility was a case study of five Victorian water reservoirs renovated with geosynthetic clay liners (GCLs) as roof sealants described by James et al. (1997). The study was initiated when leaking roofs that caused potential threats to the potable water supply were discovered. The GCL was placed above the clay between the brick arches of the reservoirs and overlain by non-calcareous gravel containing a drainage system and calcareous topsoil with grass. Following the detection of leaks, laboratory tests were conducted on the GCLs exhumed from the reservoirs, unused GCLs, and unused GCLs that had been exposed to the elements. The Ca^{2+} on the exchange sites of the bentonite contained in the GCLs from the site was greater than the Ca^{2+} in the unused GCLs (i.e., greater than 76.9 meq/100 g versus less than 42.5 meq/100 g, respectively). The calcite content in the GCL was approximately 2 % and the gravel was non-calcareous. Conversely, the calcium carbonate of the cover soil was 52 mg/kg.

This investigation by James et al. (1997) led to several conclusions. The predominantly sodium-bentonite in the original GCL was altered to predominantly calcium-bentonite via cation exchange. The Ca^{2+} cations could have been from several sources, including calcite within the GCL, test water, or overlying soil. However, the calcium carbonate content of the cover soil was sufficient to provide Ca^{2+} to exchange the Na^+ in the GCL. Lastly, the wetter GCL had increased cation exchange. As a result, James et al. (1997) concluded that considerations of the overlying and underlying soils must be taken into account when using GCLs.

The study by Jo et al. (2001) investigated the effect of single species salt solutions on the swelling and k of nonprehydrated GCLs. Several salt solutions were used as permeant liquids in

the study, including NaCl, KCl, LiCl, CaCl₂, MgCl₂, ZnCl₂, CuCl₂, and LaCl₃. The effects of cation size, valence, solution concentration, and *pH* on free swell and *k* were investigated. The valence, ion size, solution concentration, and *pH* of the salt solutions were found to affect the free swell of the bentonite. The solutions with monovalent cations resulted in the most swell, whereas the trivalent cation resulted in the least swell. For the monovalent cations, the ion size also affected the amount of swell, such that cations with the largest hydrated radius resulted in the most swell. The size of the divalent and trivalent cations did not affect the swell. The swell decreased with increasing solution concentration regardless of the cations in solution. The greatest effect was displayed for monovalent solutions at high concentrations. The *pH* affected the free swell significantly for monovalent solutions. For *pH* in the range $3 > pH > 12$, the free swell decreased substantially. When Ca²⁺ was in the solution, the swelling increased with increasing *pH*, perhaps due to precipitation of Ca(OH)₂ at high *pH* (Jo et al. 2001).

Similar results were observed for the *k* of the bentonite subjected to the different salt solutions. The *k* increased with increasing valence, although the differences were more pronounced at the intermediate concentrations. The *k* increased with increasing concentration for all salt solutions. At intermediate concentrations ranging from 0.025 to 0.1 M, the valence of the cation affected the *k*, whereas at lower concentrations and at a concentration of 1 M, the effect of valence on *k* was insignificant. For example, for the 0.1 M solutions, a change in valence from +1 to +3 caused a 100,000-fold increase in *k*. However, the same change in valence for 0.01M solutions only caused a two-fold increase in *k*. The changes in *k* were less apparent for cation species and size. The *k* was mildly sensitive to cation size (varied less than a factor of ten). Although the *k* was sensitive to *pH* for monovalent species, the effect of *pH* was masked when divalent cations were in the system (Jo et al. 2001).

As previously described, GCLs used in waste containment systems can undergo cation exchange. This cation exchange can alter the microstructure and k of the GCL. A study by Guyonnet et al. (2005) investigated the correlations between the changes in k at the macroscopic scale with changes in the chemistry and structure at the microscopic scale. Two GCLs, a sodium bentonite GCL (GCL_a) and a sodium-activated calcium bentonite GCL (GCL_b), were placed in oedometer cells and subjected to combinations of three different liquids. The liquids consisted of a prehydration fluid (PF) with an ionic strength, I , of 10^{-3} M NaCl, a synthetic leachate (SL) with I of 0.3 M CaCl₂, and a real leachate (RL) with I of 0.25 M collected from a leachate disposal pond at a municipal solid waste landfill (Guyonnet et al. 2005). Testing included a prehydration period and a percolation period consisting of different sequences of the liquids. The k of each GCL was monitored over time. The microstructure and chemistry of the bentonite was investigated using small-angle x-ray scattering (SAXS), transmission electron microscopy (TEM), and exchangeable cation analysis.

Guyonnet et al. (2005) found that the k of GCL_a was lower than that of GCL_b for all tests. The k of both GCLs increased when permeated with SL and RL relative to k of the GCL permeated with PF. According to the SAXS analysis, GCL_a exhibited a gel phase when subjected to PF or RL and no gel phase when subjected to the SL. These results also were verified visually with the TEM images. The proportion of the gel phase in GCL_b was smaller than GCL_a. The TEM images for GCL_b depicted closely spaced particles. Both GCL_a and GCL_b consisted of primarily sodium before hydration. However, after hydration of GCL_b with PF, the amount of Ca²⁺ and Mg²⁺ cations on the exchange complex increased, although there was no source of these cations in the hydration fluid. After exposure to SL, both GCLs consisted primarily of Ca²⁺ cations on the exchange complex. However, after exposure to the RL, NH₄⁺

and K^+ were more prevalent than Ca^{2+} , which was the reason given as to why the GCLs still exhibited gel phase after being subjected to the RL (Guyonnet et al. 2005).

Geosynthetic clay liners used in covers for waste containment systems may be subjected to countless wet/dry cycles throughout the lifetime of the cover. Cation exchange in addition to wet/dry cycling has been shown to result in large increases in k rendering the GCL useless as a hydraulic barrier. For example, Benson and Meer (2009) reported the results of a study investigating the effect of wet and dry cycles and solutions with different relative abundances of monovalent and multivalent cations on the swell index and k of a GCL. GCLs were subjected to 11 different solutions with varying ionic strength, I , and ratio of monovalent-to-divalent cations, RMD . The RMD is equal to the ratio of total molarity of the monovalent cations to the square root of the total molarity of multivalent cations. Sodium (Na^+) and calcium (Ca^{2+}) were the monovalent and divalent cations used in the solutions. Batch tests, falling head k tests, and free swell tests, all with wet/dry cycling, were conducted on the GCLs.

The RMD was found to control the behavior of the swell index, the cations on the exchange complex, and the k of the GCLs. The I affected the number of wet/dry cycles required to produce a change in the swell index or k of the GCL. When the RMD was less than $0.07 M^{1/2}$, the k increased at least three orders of magnitude and the swell potential decreased from more than 23 mL/2g to less than 15 mL/2g. In contrast, when the RMD was greater than $0.14 M^{1/2}$, only modest to small changes in k and swell were observed ($\Delta k \leq \pm 10$ and swell index > 25 mL/2g). Desiccation cracks were observed in the bentonite after wet/dry cycling. The self-healing capacity of the bentonite (ability of the cracks to close) was affected by the RMD of the solutions. The self-healing capacity decreased with decreasing RMD , that is, when Na^+ was exchanged with Ca^{2+} (Benson and Meer 2009).

Geosynthetic clay liners (GCLs) also have been shown to exhibit membrane behavior. Malusis et al. (2001) investigated the membrane behavior of 10-mm-thick specimens of Bentomat[®] GCL using a closed (no-flow) system. Tests with initial KCl concentration differences of 8.7 mM and 47 mM reached steady state in 6 d and 16 d, respectively, resulting in values for ω of 0.49 and 0.14, respectively. These results correlated with the expected behavior of clay soils in that, as the concentration of the electrolyte solution increases, the time required to reach steady-state conditions increases and the membrane efficiency of the clay decreases (Malusis et al. 2001).

The membrane efficiency of clay has been shown to decrease when the clay is subjected to an electrolyte solution with increasing valence (charge) and/or concentration. This behavior has been attributed to the collapse of the diffuse double layer (DDL) resulting from the diffusion of ions into the clay. Test results have indicated that diffusion and collapse of the DDL is the probable cause of the decreased membrane behavior; however, no previous studies had been conducted to demonstrate this correlation between membrane behavior and diffusion. The objective of the work by Shackelford and Lee (2003) was to demonstrate the correlation between diffusion and the destruction of membrane behavior.

The test set-up and analysis used by Shackelford and Lee (2003) were similar to those described by Malusis et al. (2001) and Malusis and Shackelford (2002b). The apparatus consisted of a rigid-wall cell with a flow pump and actuators, and the membrane behavior was measured in a closed (no-flow) system with constant boundary concentrations. In this type of system, diffusion and chemico-osmotic flow are the only processes that can occur. Tests were conducted on a Bentofix[®] NS GCL. A 5 mM CaCl₂ solution was circulated through the porous stone at the top of the specimen and deionized (DI) water was circulated through the porous

stone at the base of the specimen resulting in a concentration gradient, ΔC , across the specimen. The concentration gradient induced a pressure difference, ΔP , across the specimen and also induced diffusion of the solute through the specimen. The ΔP and concentrations of Ca^{2+} and Cl^- exiting the top and base of the specimen were monitored with time. The chemico-osmotic efficiency coefficient, ω , was calculated as the ratio of ΔP to the theoretical chemico-osmotic pressure difference, $\Delta\pi$. The time at which steady-state diffusion commenced, t_{ss} , was determined by plotting the change in cumulative mass per unit area of solute, ΔQ_t , versus the change in time, Δt , and determining the time at which the slope, $\Delta Q_t/\Delta t$, became constant (Shackelford and Lee 2003).

If diffusion is the cause of reduced membrane efficiency, ω should decrease to a steady state after time t_{ss} . The ω of the GCL reached a peak of 0.52 after 9 d, decreased to 0.016 after 35 d, and then decreased to zero after approximately 48 d. Based on a regression analysis, t_{ss} for the Ca^{2+} was 35 ± 2 d. Thus, the times to reach $\omega \sim 0$ and t_{ss} for Ca^{2+} correlated very well. These results provided direct evidence that diffusion of solutions can completely destroy membrane behavior. Also, compression of the DDL was a result of increased Ca^{2+} concentration in the clay (Shackelford and Lee 2003).

Kang and Shackelford (2009) describe the use of a flexible-wall cell to test membrane behavior under closed boundary conditions. The pros and cons of the rigid-wall versus flexible-wall cells for membrane testing are similar to those described in Daniel et al. (1985) for hydraulic conductivity testing. The flexible-wall membrane test apparatus is similar to that described by Malusis et al. (2001), except that a flexible-wall cell is used, in-line pressure transducers were added to the system, and volume change of the specimen was monitored. Geosynthetic clay liners (GCLs) were tested in the flexible-wall membrane apparatus and were

subjected to the same solutions as the rigid-wall tests conducted by Malusis et al. (2001). Therefore, the test results obtained using the flexible-wall membrane apparatus were compared with those using a rigid-wall membrane apparatus as reported by Malusis et al. (2001). The ω for the flexible-wall cell was slightly less than the ω for the rigid-wall cell. The ω values obtained with both types of cell decreased with increasing KCl concentration, although the trend for the flexible-wall cell was non-linear on a semi-logarithmic scale, whereas the trend for the rigid-wall cell was approximately semi-log linear (Kang and Shackelford 2009).

2.2.2 Soil-Bentonite Cutoff Walls

Bentonite is used in bentonite-water slurry and as an additive to the backfill for use in soil-bentonite vertical cutoff walls. Cutoff walls have been used since the early 1940s to control seepage into excavations, in dams, as a barrier to salt-water intrusion, and more recently to control contaminant migration in groundwater (D'Appolonia 1980; Ressi and Cavalli 1985). Cutoff walls typically are constructed by first excavating a trench 0.6 to 1.5 m wide through permeable material to an underlying impermeable stratum. The trench is held open by placing a bentonite slurry consisting of a mixture of water and about 5 % bentonite by dry weight in the open excavation, usually to a level that is somewhat higher than the surrounding groundwater, resulting in an outward gradient for flow of the slurry into the surrounding soil(s). The penetration of the slurry into the surrounding soil(s) results in the formation of thin (e.g., several mm) filter cake with a low k (i.e., $< 10^{-9}$ cm/s). Trenches up to 30-m deep and 300-m long have stayed open as long as the slurry extends to the top of the trench and the groundwater level is several feet lower than the slurry level. The trench then is backfilled with the trench spoils that typically have been combined with bentonite slurry and occasionally, if the trench spoils consist

of coarse-grained materials, additional dry bentonite (D'Appolonia 1980).

Detailed methods of slurry trench construction depend on site conditions. Backhoes, clamshells, and draglines may be used to excavate the trench depending on the required depth. The bentonite slurry is mixed on site using ponds or large vortex or propeller type mixers. The target viscosity of the slurry is approximately 40 s Marsh viscosity. The soil-bentonite backfill, consisting of trench spoils, bentonite slurry, and additional bentonite for coarse grained formations, is mixed adjacent to the trench. The ideal consistency of the backfill material is at a water content that produces a slump ranging from 100 mm to 150 mm. The unit weight of the backfill material should be approximately 2.35 kN/m^3 (15 lb/ft^3) greater than the unit weight of the slurry to ensure displacement of the slurry by the backfill (D'Appolonia 1980; Evans 1993, 1994).

The k , compressibility, and strength of the backfill material is of great importance and has been thoroughly investigated (D'Appolonia 1980). The k of the backfill depends on the soil gradation and the amount of bentonite added to the backfill. In general, greater than 1 % bentonite and greater than 20 % fines are recommended for the backfill in order to reach the desired k for the completed wall, typically less than $1 \times 10^{-7} \text{ cm/s}$. Although increasing the amount of fines decreases k , increasing the amount of fines also increases the compressibility of the backfill (D'Appolonia 1980).

A potential for incompatibility between the soil-bentonite cutoff wall and the surrounding contaminated groundwater typically exists when such cutoff walls are used for environmental containment applications. Such incompatibility results in an increase in k due to physico-chemico interactions between the permeant liquid and the soil-bentonite backfill. Incompatibility also can lead to piping failure in scenarios involving granular backfill soils and small amounts of

bentonite (D'Appolonia 1980).

In addition to low k , soil-bentonite cutoff walls may exhibit membrane behavior because of the presence of sodium montmorillonite in the soil-bentonite (SB) mixture and the slurry. Studies by Yeo et al. (2005) and Henning et al. (2006) document the membrane behavior exhibited by SB cutoff wall backfills.

Yeo et al. (2005) investigated the membrane behavior of two model SB backfills. The model SB backfills consisted of either a natural clay or a sand-bentonite mixture with 5 % bentonite by weight mixed with the amount of bentonite-water slurry necessary to achieve 100-mm of slump (standard practice for SB cutoff walls). The apparatus used to measure membrane efficiency was the same as that used by Malusis et al. (2001) and Malusis and Shackelford (2002a) and consisted of a rigid-wall cell and a closed system. The membrane efficiency, ω , was measured for the model backfills subjected to a concentration gradient of 3.88 mM KCl. The membrane efficiency was measured at 3 different void ratios for each sample. The ω of the natural clay ranged from 0.018 to 0.024 (1.8 to 2.4 %), whereas the ω of the sand-bentonite mixture ranged from 0.118 to 0.166 (11.8 to 16.6 %) (Yeo et al. 2005; Evans et al. 2008). The ω increased with increasing consolidation stress, decreasing void ratio, and decreasing k for both samples.

To verify that membrane behavior is exhibited by slurry walls in the field, Henning et al. (2006) collected SB backfill samples from actual cutoff walls constructed in New Jersey and Delaware. At both sites, the local soil was mixed with 3 to 4 % bentonite by dry weight. The backfills were classified as clayey sands (SC and SP-SC). The membrane behavior was measured in the laboratory using the same apparatus as used by Yeo et al. (2005). The results indicated that both soils exhibited membrane behavior, with ω for the New Jersey backfill ranging from

0.0119 to 0.0140 (1.19 to 1.4 %) and ω for the Delaware backfill ranging from 0.0019 to 0.0172 (0.19 to 1.72 %). However, these membrane efficiencies were significantly lower than those previously reported by Yeo et al. (2005) for model SB backfills. Henning et al. (2006) attributed the lower membrane efficiencies for the field constructed backfills relative to the laboratory produced model backfills to a lower percentage of clay in the field constructed backfills, differences in preparation of the specimens (i.e., field constructed backfills were mixed on site with a backhoe and laboratory produced backfills were prepared under controlled conditions in a laboratory), and the higher solute concentration used to test the field constructed backfills versus the model backfills (11.0 and 14.0 mM KCl versus 3.8 mM KCl solution, respectively). Nonetheless, even with these lower membrane efficiencies, the calculated reduction in the total liquid flux due to membrane behavior for the field sites may be as much as 10 % (Evans et al. 2008).

2.2.3 Radioactive Waste Storage

Bentonite also is used as a component in radioactive waste storage. Spent radioactive fuel is placed in stainless steel or other corrosion resistant canisters. The canisters then are placed in boreholes or tunnels and embedded in bentonite. The bentonite acts as a buffer and is intended to limit the entry of water into the waste, retain radionuclides, provide heat dissipation, and provide a cushion to the canisters. The bentonite may be subjected to thermal, hydraulic, mechanical, and chemical stresses. Potential issues include heat-induced desiccation resulting in an increase in k and compression resulting in a decrease in k but also a decrease in thickness (Gates et al. 2009). One such storage facility is being planned in Japan. The depth of the proposed facility is 300 to 1000 m (Komine 2008).

Compacted bentonite and sand-bentonite mixtures can be used as a buffer material surrounding the containers or canisters of radioactive waste, and as a backfill. The bentonite or sand-bentonite mixtures may be compacted around the canisters under controlled conditions in a factory and then placed in a borehole or tunnel. A small space is left between the bentonite and the borehole or tunnel to accommodate bentonite swelling upon exposure to groundwater (Komine and Ogata 2004). This buffer material also must have a sufficiently low k to prevent exposing the radioactive waste to the surrounding environment. The compacted bentonite or sand-bentonite mixtures also may be used as a backfill material to backfill the access tunnel and create a low- k zone. For example, in Japan, the k of the buffer material must be less than 4.5×10^{-11} cm/s, and the k of the backfill must be between 1×10^{-9} to 1×10^{-10} cm/s.

In order to specify the materials to be used in these disposal facilities, the required dry density and sand-bentonite mass ratio, the swelling characteristics and swell pressures, and the k of the material must be known. Equations for estimating the swelling behavior and the k of compacted bentonite and sand-bentonite mixtures have been promulgated (Komine and Ogata 1996; Komine and Ogata 2004; Komine 2008). The predictions are based on equations that describe attractive and repulsive forces between clay minerals, a parameter called the swelling volumetric strain of montmorillonite, the specific surface of the bentonite and the influence of the pore water, and a flow model that describes flow between two parallel montmorillonite layers. The equations were verified through comparison with laboratory test results and results reported by Kenney et al. (1992) and Sivapullaiah et al. (2000). The predicted and measured k results were similar for sand-bentonite mixtures when the bentonite content was greater than 20 %. For radioactive disposal facilities, bentonite contents are typically greater than 20 % (Komine 2008).

Ahn and Jo (2009) investigated the effect of exchangeable cation on the k of compacted bentonite which may be used for radioactive waste disposal because laboratory results showed that the k of Ca-bentonite could be very low. For instance, Komine (2008) reported that the k of the Ca-bentonite varied from 3×10^{-11} cm/s to 1×10^{-11} cm/s at dry densities of 1.34 and 1.46 Mg/m³, respectively. Ahn and Jo (2009) investigated the effect of exchangeable cations on the compaction characteristics and k of compacted bentonites with different initial dry densities and under varying effective stresses. They found that the maximum dry density and the k decreased with increasing equivalent fraction of Na⁺ ions (i.e., Na-bentonite). In addition, the k decreased with increased final dry density. However, the k of Ca-bentonite was also very low ($< 1 \times 10^{-9}$ cm/s) at high final dry densities (> 1.25 Mg/m³) which could be maintained at high effective stresses (> 290 kPa).

2.3 MODIFIED BENTONITE

The use of modified clays for pollution prevention and remediation has been growing for several decades. Several classes of modified clay materials are used for various applications including immobilization of contaminants, slow release formulas of agrochemicals, enhanced degradation of organic toxic chemicals, waste water purification, and groundwater pollution prevention. Prost and Yaron (2001) describe the new clay materials and the general mechanisms controlling the interactions with contaminants.

A diverse group of contaminants can be treated with various forms of modified clays. Prost and Yaron (2001) divided modified clays that are used for controlling soil environmental quality into five categories *viz.*, pillared layered clays, organoclays, nanocomposites, acid and salt modified clays, and thermally and mechanically modified clays. Pillared layered clays are

formed when 1:2 clays are propped open with metal oxides or small organic cations. Organoclays are formed when organic cations are exchanged with the inorganic cations creating an organophilic surface. Nanocomposites are formed when changes at the nanometer scale result in property enhancement; the authors' definition of nanocomposites consists of a polymer reinforced by clay. For a true nanocomposite to exist the clay must be dispersed uniformly in the polymer matrix. Acid induced modifications usually improve the catalytic properties of the clay minerals. Acid treatment modifies the active sites and removes impurities. Thermally induced modification of clay removes free, absorbed, and structural water and results in modifications of the surface properties and index properties of the clay. Mechanically induced modifications of clay result from grinding and reaggregation of the clay resulting in new minerals with changes in the surface properties (e.g., specific surface area, cation exchange capacity, and water retention) (Prost and Yaron 2001).

In addition to the categories used by Prost and Yaron (2001), several additional types of modified bentonites that have been investigated for geoenvironmental engineering applications are discussed in the following sections. These include dense-prehydrated bentonite used in GCLs, multi-swellable bentonite, and polymer modified bentonite.

2.3.1 Pillared Layered Clay

Pillared layered clays (PLC), also referred to as pillared interlayered clays (PILC), pillared layered structures (PLS), cross-linked smectites (CLS), and layered double hydroxides (LDH), have been used in cracking (a method where complex organic molecules are broken down into simpler molecules), as molecular sieves, selective adsorbents, and thermal insulators, in electrochemical and optical devices, as pigments, and as membranes (Bergaya et al. 2006a;

Kloprogge 1998). Pillared layered clays have an increased interlayer distance (d_{001}), increased porosity, and higher accessible specific surface area (SSA) compared to the host clay. Pillared layered clays often are formed using a natural swelling clay mineral such as the smectites (e.g., montmorillonite, hectorite, beidelitte, saponite) as a host and an organic, organometalic, or inorganic pillaring material. The most common pillared layered clays are Al-pillared clays. However, other cations also have been used as pillars (Zr, Cr, Fe, Ti, etc.), as well as mixed Al and other cation pillars, metal complexes, and inorgano-organo pillaring agents (Kloprogge 1998; Prost and Yaron 2001; Bergaya et al. 2006a).

The classic method of creating pillared layered clays consists of two steps. The first step is the intercalation of the pillaring agent, where a dilute pillaring solution is added to dilute clay mineral dispersion. The second step involves heating the mixture. Industrial scale methods are also being developed. Two potential industrial scale methods include adding clay mineral powder to pillaring solution to create slurry or placing a concentrated clay suspension in a dialysis bag and then placing the dialysis bag in a dilute pillaring solution (Bergaya et al. 2006a). However, industry is still working on an efficient method for large-scale production of pillared layered clays.

Several criteria must be met for a clay to be considered pillared, including replacement of the inorganic cations and intercalation of the cationic pillars, a free height, and unaltered basal spacing and free height when heated, under anhydrous or hydrothermal conditions, or when the pH is varied. Pillared layered clays are thermally stable, although the linkage between the clay and pillars is not well understood and there is no generally accepted mechanism for this stable linkage (Bergaya et al. 2006a).

2.3.2 Organoclays

The study and use of organoclays has increased greatly during the last two decades because of the use of organoclays in the development of polymer-clay nanocomposites (PCNs). The exchange of organic cations for inorganic exchangeable cations changes the surface properties of the clay such that the clay becomes organophilic (i.e., hydrophobic). The organophilic clay is dispersed in a polymer matrix to form PCNs that have improved properties over conventional composites (Prost and Yaron 2001). Other uses of organoclays include adsorbents of organic pollutants in the environment, rheological control agents, paints, cosmetics, refractory varnish, and thixotropic fluids (de Paiva et al. 2008). Organoclays have been used in geoenvironmental engineering applications, including multi-swelling bentonite, which is a bentonite treated with propylene carbonate (Katsumi et al. 2008), organoclays formed with quaternary ammonium compounds (Lorenzetti et al. 2005), and dense-prehydrated geosynthetic clay liners which contain bentonite treated with carboxymethyl cellulose and methanol (Kolstad et al. 2004b; Katsumi et al. 2008). Often the composition of the modified clay is proprietary and the exact chemistry of the clay is unknown (Ashmawy et al. 2002; Benson et al. 2010; Shackelford et al. 2010).

To create organoclays, organic molecules must be intercalated, meaning that organic cations must penetrate into the interlayer space of the clay crystalline structure. Interactions between organics and 2:1 clay minerals include displacement of water in the interlayer with polar organic molecules, complexation between interlayer cations and neutral organic ligands, and replacement of interlayer cations by organic cations (Lagaly et al. 2006). The most common form of organoclay is created through ion exchange of alkylammonium ions with the interlayer cations. However, other commonly used materials include cationic dyes, cationic complexes, and

polymers (Lagaly et al. 2006; de Paiva et al. 2008).

Organic and organometallic cations are exchanged with the interlayer cations through solution or solid-state reactions. Solutions of excess organo-ammonium salts are mixed with aqueous clay dispersion for the solution reactions. The salts are in concentrations in excess of the *CEC* of the clay. With solid-state reactions, the clay mineral and solid organo-ammonium salt are ground together (Lagaly et al. 2006). The structure of the organoclay depends on the layer charge of the clay mineral and the length of the alkyl chain of the organic cation. Short alkyl chains form monolayers with interlayer spacing, d_{001} , ~ 1.4 nm and longer chains form bilayers of chains oriented parallel to the silicate layers with $d_{001} \sim 1.8$ nm. Highly charged clays or long, surfactant cations tend to have a pseudotrimolecular arrangement ($d_{001} \sim 2.2$ nm), whereas paraffin-type arrangements are formed when the quaternary alkylammonium ions consist of two or more long alkyl chains. As the number of carbon atoms in a chain increases, the structure of the chains become more ordered (Lagaly et al. 2006; de Paiva et al. 2008).

Smectites swell in water but have limited swell in electrolyte solutions. Montmorillonite-organic complexes are influenced by the interlayer cations in the montmorillonite (MMT), which influence the stability and orientation of the organic molecules. Addition of propylene carbonate (PC) to MMT activates osmotic swelling of the MMT, even in the presence of electrolyte solutions.

For example, Onikata et. al. (1999) conducted a study where sodium-rich MMT saturated with various cations (Li^+ , Na^+ , K^+ , Ca^{2+} , Mg^{2+} , Ba^{2+} , or Ni^{2+}) was mixed with different amounts of PC to form PC-MMT complexes (also referred to as multi-swelling bentonite). The mechanisms of osmotic swelling of the PC-MMT complexes in aqueous electrolyte solutions were investigated. Specimens were prepared and then investigated using X-ray diffraction

(XRD), Fourier transform infrared (FTIR) absorption spectroscopy, thermogravimetric analysis (TGA), and swelling power. Sodium-rich MMT was saturated with the aforementioned cations. The cation exchanged MMT then was mixed with different amounts of PC (15 to 45 % by weight of MMT).

Results of the investigation by Onikata et al. (1999) were presented in terms of saturation cation and amount of PC. The XRD indicated the interlayer spacing (d_{001}) of the PC-MMT complexes. The more polarizing cations had larger interlayers. The more polarizing monovalent cations (Na^+ and Li^+) indicated mono-layer and bi-layer PC molecules between the layers, where the bi-layers were present with higher concentrations ($> 20\%$) of PC. The divalent cation-MMT mixed with large amounts ($>20\%$) of PC indicated bi-layers of PC molecules in the interlayer. In general, the interlayer spacing increased with increasing amounts of PC. The weight loss of the specimen increased with increasing polarizing power (the ratio of the charge to the ionic radius of the cation) indicating that the PC molecules were bound more strongly to the cations with greater polarizing power (e.g., $\text{Li}^+ \gg \text{K}^+$). FTIR results showed a red-shift in the C=O stretching band of the PC indicating absorption of the PC in the interlayer of the MMT. The swelling power of the PC-MMT mixed with 0.5 M NaCl solution increased with increasing PC, and swelling of the PC-MMT was evident at concentrations of NaCl as high as 0.75 M versus 0.3 M for MMT without PC.

2.3.3 Acid Modified Clay

Acid modifications improve the catalytic properties of bentonite. Acid treatment leads to a modification of the original active sites within the clay (Prost and Yaron 2001). During acid treatment, cations may be leached from the tetrahedral and octahedral sheets, impurities such as

calcite may be dissolved, and exchangeable cations are replaced with H^+ . Acid treatment may lead to an increase in the specific surface area (*SSA*) and pore volume of the clay (Vukovic et al. 2006). According to Komadel (2003), a common chemical treatment of smectites is the dissolution of smectites in inorganic acids. Acid activation, or partial dissolution, is conducted to produce sorbents and catalysts. The final product from the acid activation depends on the temperature, acid concentration, acid to clay ratio and the stirring mechanism that is used to create the acid modified clays (Komadel 2003).

Acid activated bentonites, also called bleaching earths, are used in food technology for clarification of beer, wine, animal feed, and food additives and bleaching of edible oil. The bentonite is treated with inorganic acids to remove impurities and obtain maximum adsorptive capacity. During the bleaching process, interactions between the oil and the bleaching earth include physical and chemical adsorption, ion exchange, and chemical decomposition of pigments and other impurities in the oil. The bleaching earth behaves as a solid acid in that the surface contains proton donors and electron pair acceptors. The bleaching power (BP) of the bleaching earth is affected by properties of the bentonite (e.g., specific surface area, *SSA*; surface acidity, n_m ; and porosity, n), the mineralogical and chemical composition of the bentonite, the type and concentration of inorganic acid, and the temperature at the time synthesis (Noyan et al. 2007).

2.3.4 Thermally Modified Clays

The structure and composition of bentonite is changed by heating. The observed changes depend on many factors including the type of mineral, the particle size, and the heating regime. Thermal treatment can be broken into four temperature ranges including the following (Heller-

Kalai 2006): (1) low temperatures which provide partial freezing of the water associated with the clay, (2) temperatures above dehydration but below dehydroxylation where the clay loses absorbed and hydration water resulting in a collapse of the interlayer and a change in the acidity of the surface and interlayer, (3) temperatures above dehydroxylation but below total destruction of the clay structure, and (4) temperatures above which new crystalline phases are formed.

Dehydration of smectites leads to changes in the macro- and microporosity of the clay, interlayer collapse, changes in clay index properties such as plasticity, grain-size distribution, and specific gravity, a decrease in *CEC*, and an increase hydrophilicity and surface acidity (Prost and Yaron 2001; Heller-Kalai 2006). Studies have indicated that the absorption-desorption of Na-bentonite is hysteretic. As a result, calcination (i.e., thermal treatment) of bentonite may be advantageous in applications such as slow-release agrochemicals (Bojemueller et al. 2001).

2.3.5 Polymer Modified Clay

Clay minerals modified with polymers have many potential uses including catalysts, adsorbents, soil conditioners, flocculants, and composite materials (Lagaly et al. 2006; Liu 2007). Modification of clay minerals with polymers can change the surface properties of the clay. Two methods, physical adsorption and chemical grafting, are generally used to produce polymer modified clays.

Physical adsorption may produce weak bonds between the clay mineral and the polymer, but does not change the structure of the clay mineral (Liu 2007). Adsorption of uncharged and positively charged polymers (polycations) is driven by entropy and electrostatic interactions, respectively. Uncharged and positively charged polymers can expand the interlayer space of 2:1 layer silicates. High concentrations of polycations may lead to surface charge reversal (negative

to positive) of the clay mineral. Polyanions do not intercalate unless under acidic or high ionic strength conditions (Theng 1982). However, polyanions attach to the edges of clay minerals and, thus, are used as flocculants (Lagaly et al. 2006).

Chemical grafting can be conducted in one step or two steps. The two-step method provides a better density of polymer. The first step of the two-step method involves covalently bonding a polymerizable or initiator molecule. In the second step, activation occurs and the polymer chain grows (Liu 2007). If hydrophobic molecules are to be intercalated, the clay must first be made hydrophobic by reaction with alkylammonium ions. Complex macromolecules cannot penetrate the interlayer space unless the mineral is first propped open or a disaggregation-reaggregation mechanism is used (Lagaly et al. 2006).

Sodium montmorillonite (Na-montmorillonite) is used in polymer-clay nanocomposites (PCN) to improve the thermal and mechanical properties of the nanocomposite. The Na-montmorillonite must be chemically modified before the nanocomposite can be formed. Typically, surfactants such as alkyl ammonium compounds are used to create hydrophobic clay that can interact with the organic polymers to form a nanocomposite.

An alternative method of modifying the Na-montmorillonite with poly(acrylic acid) was investigated by Tran et al. (2005). The chemical-structural modifications were investigated with x-ray photoemission spectroscopy (XPS) and x-ray diffraction (XRD). The Na-montmorillonite and poly(acrylic acid) (PAA) was mixed at different temperatures (room temperature, 30 °C, and 60 °C). The mixtures were allowed to sit for 24 hours, after which the solids were separated via a centrifuge, washed with DIW, and air dried. The resulting solid mixture was investigated with low angle XRD and XPS (Tran et al. 2005).

The results from the XRD and XPS provided an indication of the modifications that occurred when the Na-montmorillonite was mixed with PAA. The XRD results showed an increasing interlayer distance (d_{001}) with increasing reaction temperatures. The d_{001} for the pure Na-montmorillonite was approximately 13 Å, whereas, d_{001} was 16 Å and 20 Å for the PAA modified Na-montmorillonite formed at room temperature (approximately 20 °C) and 60 °C, respectively. The XRD results indicated absorption of PAA into the interlayer of the Na-montmorillonite. The XPS results indicated that sodium ions were removed from the surface of Na-montmorillonite and replaced with PAA molecules. Physisorption and chemisorption of the PAA molecules onto the silicate surface of the Na-montmorillonite occurred. However, the proportions of physisorption versus chemisorption could not be distinguished (Tran et al. 2005).

The bentonite polymer nanocomposites (BPNs) investigated as part of the research described in this document were formed by modifying clay with PAA. However, BPNs, also referred to as clay-polymer nanocomposites (CPNs), are formed when a small amount of polymer is dispersed within the clay matrix. In contrast, PCNs are formed when a small percentage of clay (typically < 10 % by weight) is dispersed within a polymer matrix.

Trauger and Darlington (2000) describe the deficiencies of traditional GCLs that led to the formulation of a polymer modified bentonite for use in GCLs. Polymer treatment of bentonite has been common in the drilling industry where dry anionic polymers are mixed with bentonite. Slurry is created for drilling applications and the polymer reacts with the bentonite in the slurry. However, mixing dry polymer and bentonite for use in lining applications is not sufficient because the materials are not dispersed in water, such that little interaction between the polymer and bentonite occurs.

The first attempt to create an improved GCL included replacement of traditional bentonite with contaminant-resistant clay (CRC). The CRC was formed by mixing polymer with semi-wetted bentonite and then blending the mixture to maximize the interaction between the polymer and the bentonite. The performance of the CRC was improved compared to a traditional bentonite (i.e., lower k when exposed to leachate). However, the improved performance was limited and production of the CRC was costly (Trauger and Darlington 2000).

Subsequent to the consideration of CRC came the creation of a bentonite polymer nanocomposite (BPN), also referred to as a bentonite polymer alloy (BPA). The BPN was formed through polymerization of an organic monomer in a bentonite slurry, and is referred to as a nanocomposite because nanometer sized particles of bentonite are dispersed in a polymer matrix. The polymerization occurred in the interlayer region of the bentonite, such that the interlayer spacing (d_{001}) of the BPN increased to between 10 and 15 Å relative to the 3.5 Å of the dry bentonite, indicating that the polymer was intercalated (Trauger and Darlington 2000). Preliminary investigations of the k of BPN slurry deposited in a needle-punched non-woven geotextile (GT) indicated that the k of the BPN-GT to seawater was 5×10^{-10} cm/s compared to the k of 2×10^{-6} cm/s measured for a traditional GCL exposed to seawater.

Trauger and Darlington (2000) provided four potential explanations for the improved performance of the BPN compared to traditional bentonite, viz.: (1) the polymer interacts with the sodium and prevents exchange of the sodium; (2) the polymer provides a physical restriction to the entry of exchangeable ions (e.g., Ca^{2+}); (3) the polymer absorbs water keeping the clay hydrated under a wide range of environmental conditions; and/or (4) the polymer serves as a structural reinforcement (i.e., a pillar) maintaining the interlayer spacing even after cation exchange occurs.

2.4 GEOENVIRONMENTAL ENGINEERING APPLICATIONS OF MODIFIED BENTONITE

2.4.1 Geosynthetic Clay Liners

A study conducted by Kolstad et al. (2004b) investigated the hydraulic conductivity and free swell of a dense pre-hydrated GCL (DPH-GCL). The results of the DPH-GCL were compared with those for a conventional GCL. The DPH-GCL was prehydrated to a gravimetric water content of 43 % with dilute solutions of sodium carboxymethyl cellulose and methanol. Then the DPH-GCL was calendared to a uniform thickness of 5 mm with a void ratio of 1.2. The dry mass of bentonite per unit area for the DPH-GCL was 6.0 kg/m^2 , whereas the conventional GCL had a dry mass per unit area of 4.3 kg/m^2 . The free swell of the DPH-GCL and the conventional GCL to DIW were similar at 35.0 mL/2g and 35.5 mL/2g , respectively.

The free swell and k of the DPH-GCL were investigated for a variety of permeant liquids that have been shown to adversely affect conventional GCLs, including a 1 M CaCl_2 solution, a 1 M NaCl solution, an acidic HCL solution ($pH = 1.2$), and a basic NaOH solution ($pH = 13.1$). The free swell for the DPH-GCL was similar to the free swell of the conventional GCL for all solutions except the basic solution, where the free swell was 41.0 mL/2g for the DPH-GCL and 22.0 mL/2g for the conventional GCL. The k of the DPH-GCL was several orders of magnitude lower than the k of the conventional GCL for most permeant liquids. For example, the k for the DPH-GCL was approximately $1 \times 10^{-10} \text{ cm/s}$ for all permeant liquids except the strong acid where the k was $1.6 \times 10^{-8} \text{ cm/s}$. In contrast, the k for the conventional GCL was approximately $1 \times 10^{-5} \text{ cm/s}$ for all permeant solutions except the strong base and DIW where the k was $2.2 \times 10^{-9} \text{ cm/s}$ and $1.2 \times 10^{-9} \text{ cm/s}$, respectively (Kolstad et al. 2004b). Kolstad et al. (2004b) concluded that, unlike conventional GCLs, the k and the free swell of the DPH-GCL did not

correlate well. Therefore, the free swell should not be used as a screening tool for compatibility of DPH-GCLs. In addition, the k tests suggest the DPH-GCL may be less sensitive to incompatibility when compared with a conventional GCL.

Katsumi et al. (2008) investigated the hydraulic conductivity of two modified bentonite materials, multiswellable bentonite (MSB) and dense-prehydrated geosynthetic clay liner (DPH-GCL), permeated with NaCl and CaCl₂ solutions. The goals of the study were to determine the long-term stability of the MSB and DPH-GCL, specifically, (1) to compare the long-term stability and chemical compatibility of MSB and DPH-GCL with that of natural bentonite (NB) and (2) to determine if the k values of the MSB and the DPH-GCL were sufficiently low for hydraulic barriers.

Index tests and long-term k tests (up to 7 yr) were conducted on specimens of four different materials (NB, GCL, MSB, and DPH-GCL). The MSB used in this study was a NB combined with 25 % by weight propylene carbonate (PC). The DPH-GCL was a factory manufactured product that was prehydrated with a dilute aqueous solution of sodium carboxymethyl cellulose and methanol, sandwiched between two geotextiles, and consolidated. Four permeant liquids were used in the testing: DIW, and three solutions containing either NaCl, CaCl₂, or NaCl and CaCl₂. Properties determined from the testing included liquid limit, swell index, chemical composition, and k .

The hydraulic performances of the NB and the MSB were similar when permeated with DIW. However, when the permeant liquid was NaCl, the MSB maintained a k of 1×10^{-9} cm/s up to a concentration of 1 M. At a concentration of 2 M, the k values of the MSB and the NB were approximately equal ($\sim 2-3 \times 10^{-5}$ cm/s). The DPH-GCL had superior hydraulic performance when compared to the GCL permeated with CaCl₂. The DPH-GCL maintained a k of

approximately 1×10^{-10} cm/s for all concentrations of CaCl_2 . The k of the DPH-GCL was up to 5 orders of magnitude lower than that of the GCL. However, the duration of the k tests for the DPH-GCL was insufficient to satisfy all of the termination criteria, such that the testing was still ongoing. Katsumi et al (2008) also noted that the free swell of the bentonite can be correlated with k . Specifically, they concluded that excellent barrier performance ($k < 1 \times 10^{-8}$ cm/s) can be expected when the free swell is greater than 20 mg/2 g solid.

The k and effective diffusion coefficient (D_e) for organobentonite (OB) modified geosynthetic clay liners (GCLs) was investigated Lorenzetti et al. (2005). Two OB amendments were used in this study, benzytriethylammonium-bentonite (BTEA-bentonite) and hexacyltrimethylammonium-bentonite (HDTMA-bentonite). The percentage of OB added to the GCL was varied and the results were compared with that of an unmodified GCL. In addition, one-dimensional transport simulations were conducted to assess the effect of OB content on the transport of benzene through the GCLs.

Although GCLs are used as hydraulic barriers in many geoenvironmental engineering applications, GCLs are thin and, therefore, provide little resistance to diffusion. One remedy is to add a highly sorptive material to the bentonite such as organophilic bentonite. Sorptive capacities of OBs have been shown to increase four to five orders of magnitude when compared to that of natural clay. To synthesize OBs, organic cations are exchanged with sodium and calcium ions on the internal and external surfaces of the clay crystalline structure. In this study, two quaternary ammonium compounds (QACs), HDTMA-bromide and BTEA-chloride, were used to synthesize the OB. The bentonite in the GCL was replaced by OB in 10 % increments (10 % to 90 % for the BTEA-bentonite and 10 % to 80 % for the HDTMA-bentonite) (Lorenzetti et al. 2005).

The k of the modified GCL increased with increasing OB content. The increase in k was as much as three orders of magnitude for OB contents above 20 % due to the hydrophobic behavior of the OB and resulting reduced swelling potential. The swelling ratio decreased to unity with increasing OB contents. The D_e was similar for both modified and unmodified GCLs (3.6×10^{-10} to 5×10^{-10} m²/s), with the lower D_e correlating with the higher OB content. Solute transport simulations indicated that BTEA-bentonite GCLs would decrease the transport while HDTMA-bentonite GCLs would increase transport. Also, higher percentages of OB would result in advective and diffusive transport because of the higher k with respect to the unmodified GCLs (Lorenzetti et al. 2005).

Recent advances in GCL technology have led to the creation of treated GCLs composed of contaminant-resistant clays (CRC) or polymer treated bentonites (PTB). In the study by Ashmawy et al. (2002), four polymer-treated GCLs and three untreated GCLs were permeated with leachate from three incinerator ash disposal facilities, two ash disposal/MSW landfills and one ash monolith. All leachates had high levels of Ca²⁺ and Mg²⁺. Falling head permeability tests were conducted on the GCLs. The majority of the tests were conducted using saturation with leachate which simulates the worst-case scenario. Several tests also were conducted with prehydration with water to investigate the influence of prehydration on the k and swell of the GCL.

The k of all of the GCLs increased with time. The GCLs permeated with LH-3, the leachate with the highest concentrations, resulted in the highest k (up to 1.3×10^{-5} cm/s). The k reached steady state quickly, which was attributed to the high concentration of divalent cations in the leachate. The k of the specimens permeated with leachates LH-1 and LH-2 were within the acceptable range of k for most waste containment applications (i.e., $< 1 \times 10^{-8}$ cm/s). However,

for LH-3, the k were high ($> 1.2 \times 10^{-6}$ cm/s) even for the treated GCLs. Polymer treated clay had slightly lower swell indices and only minor improvements in k compared to the untreated GCLs. Thus, Ashmawy et al. (2002) recommended that compatibility tests be conducted on treated clay expected to be subjected to aggressive environments before approving the use of the treated clay.

Benson et al. (2010) investigated the hydraulic conductivity of two treated GCLs, GCL A and GCL B, permeated with hyperalkaline solutions. Each GCL contained powdered bentonite that was treated with different quantities of a proprietary additive meant to reduce the effects of incompatibility with the surrounding environment. The GCLs were permeated with three different liquids, viz., DIW, a 1.3 mM CsCl solution, and a solution containing 1M NaOH and 1.3 mM CsCl. The NaOH-CsCl solution with a pH of 12.4 was meant to simulate the hyperalkalinity of leachate from an Al refining operation. Triplicate k tests were conducted with each GCL and liquid except for DIW. The tests were broken down at different times varying from 72 to 213 d in order to evaluate the changes in the bentonite with time. The final tests were terminated after eight months because of time constraints, such that chemical equilibrium between the effluent and influent solutions may not have been achieved. Nonetheless, the k had stabilized or was decreasing upon termination and the exchangeable cations in the effluent were constant or decreasing, indicating that the k would be an accurate or conservative (high) estimate of the long-term k of the GCLs.

Test results indicated that the different quantities of the additive had no measurable effect on the k of the GCL. For example, the k values of the treated GCLs permeated with the NaOH-CsCl solution ranged from 2.3×10^{-9} cm/s to 4.8×10^{-9} cm/s. However, GCL B with the higher dosage of the additive showed buffering to changes in pH and a reduction in the degree of cation

exchange, indicating that the additional additive altered the chemical reactions within the GCL. Permeation with CsCl had no impact on the k of either GCLs with the k decreasing slightly (by a factor of 1.5 to 1.8). Permeation with NaOH-CsCl solutions caused an increase in k from 9×10^{-10} cm/s for permeation with DIW to as much as 4.1×10^{-8} cm/s for permeation with NaOH-CsCl solutions. This increase in k was attributed to the possibility of decreased osmotic swelling and dissolution of the montmorillonite. The NaOH-CsCl solution also caused an accumulation of sodium in the bentonite, or sodicity, and the resulting free swell of the GCLs increased, because of the abundance of Na^+ in the solution (Benson et al. 2010).

The k of a typical GCL and a contaminant resistant GCL subjected to three solutions expected during tailings impoundment at a proposed zinc and copper mine was investigated by Shackelford et al. (2010). The study investigated the effect of prehydration, type of GCL, permeant liquid, and duration of backpressure saturation. The permeant liquids used in this study included a low ionic strength groundwater (GW) taken from the site ($pH \sim 7.24$ and $I \sim 3.2$ mM), a process water (PW) that would be similar to the leachate expected at the site ($pH = 6.9$ to 9.8 and $I = 32$ to 51 mM), and a synthetic leachate (SL) that simulated worst case scenario conditions where oxidation of the tailings leads to an acidic leachate ($pH = 2.5$ and $I = 350$ mM). The two GCLs included a typical GCL (referred to as GCL) that is commercially available and a chemical resistant GCL (CR GCL) that has been treated to be resistant to chemicals. The exact treatment of the CR GCL is proprietary and, therefore, unavailable. A total of 22 flexible-wall hydraulic conductivity tests were conducted on the GCLs varying the factors mentioned above.

The k of both GCLs with GW was 1.7×10^{-9} cm/s, which is typical for a GCL subjected to low I liquids. However, the k of the GCLs permeated with SL and PW (k_{SL} and k_{PW}) were significantly greater than the k for GW (k_{GW}) (k_{SL}/k_{GW} and $k_{PW}/k_{GW} = 45$ to $15,000$). Compared

to the effect of the permeant liquid, the other factors had a minimal effect on the k of the GCLs. Prehydration with GW resulted in a lower k ; however, the k of the GCL permeated with SL and PW was still higher than the k of the GCL permeated with GW. For the majority of the tests, the CR GCL performed worse than the typical GCL ($k_{CRGCL}/k_{GCL} = 9.1$ to 21). The increase in k from permeation with the SL was expected because of the low pH and high I of the SL. However, the increase in k from the PW was less expected. In addition, the poorer performance of the CR GCL when compared to the typical GCL was considered surprising and reemphasized the importance of testing the k of the GCLs with site specific liquids (Shackelford et al. 2010).

2.4.2 Soil-Bentonite Cutoff Walls

Soil-bentonite cutoff walls (SB cutoff walls or SB vertical barriers) can be used as low- k barriers to prevent the spread of contaminated groundwater. However, the k of the wall may increase due to chemical incompatibility between the bentonite component of the soil comprising the wall and the liquid permeating through the wall. Malusis et al. (2010) investigated the use of multi-swellable bentonite (MSB) for use in SB cutoff walls. The MSB has been shown to exhibit swelling and maintain low k upon permeation with strong salt solutions (e.g., 0.6 M NaCl) and, therefore, may be a viable alternative to traditional bentonite in cutoff walls where chemical incompatibility may occur.

Three bentonites were investigated as part of the study, an MSB, a natural sodium bentonite (NB), and a commercially available “salt-resistant” bentonite (SW101). Properties of the slurry and a model backfill were investigated. Slurries were prepared with bentonite contents ranging from 2 to 5 % by weight. The Marsh viscosity, mud density, filtrate loss, and pH of all of the slurries were within acceptable ranges except for the SW101 with 5 % bentonite, where

the Marsh viscosity was 200 s (Malusis 2010).

Model backfills were prepared with mortar sand, slurry (5 % bentonite), and 3 to 4 % bentonite. The slurry was added to the backfill until a slump of 125 ± 12.5 mm was achieved. The final bentonite content of the backfills was 4.5 to 5.7 %. The model backfills were permeated with tap water, and three of the backfills with a similar k to tap water also were permeated with 50 mM CaCl_2 . The values of k for the MSB and the NB with 4.6 % bentonite were 7.6×10^{-7} cm/s and 8.2×10^{-8} cm/s, respectively, which were close to or greater than the target k of 10^{-7} cm/s. The values of k for the SW101 with 4.6 % bentonite, the MSB with 5.6 % bentonite, and the NB with 5.7 % bentonite were between 2.2×10^{-8} and 2.7×10^{-8} cm/s. These three specimens then were permeated with 50 mM CaCl_2 . The k of all three specimens increased when permeated with 50 mM CaCl_2 . The least increase in k based on permeation with the salt solution, k_c , relative to k based on permeation with tap water, k_w , or k_c/k_w , occurred with the MSB (i.e., $k_c/k_w=1.9$), whereas the greatest increase in k_c/k_w (3.8) occurred with the SW101. This preliminary assessment indicates that MSB may be used in as an alternative to NB in SB cutoff walls. However, additional study is necessary (Malusis 2010).

2.4.3 Sand-Bentonite Mixtures

Haug and Boldt-Leppin (1994) investigated the effect of adding polymer to a marginal quality (MQ) bentonite used in compacted sand-bentonite. The rheology and hydraulic conductivity of the MQ bentonite mixed with 0 to 0.5 % polymer were compared with the properties of a high quality (HQ) bentonite.

The materials used in this testing program included a HQ bentonite ($SSA = 668 \text{ m}^2/\text{g}$, $CEC = 90 \text{ meq}/100 \text{ g}$) or a MQ bentonite ($SSA = 490 \text{ m}^2/\text{g}$, $CEC = 69 \text{ meq}/100 \text{ g}$) mixed with

Ottawa sand. The MQ bentonite also was mixed with 0 to 0.5 % polymer. The commercially available polymer, Alcomer 228 (Allied Colloids Ltd), is an anionic polyacrylamide that was specially formulated to improve the hydraulic properties of bentonite. First, the polymer was mixed with the bentonite followed by the addition of sand. The final bentonite content of the mixtures was eight percent. Then, the specimens were moisture conditioned to near optimum water content and compacted to 100 % of the standard compactive effort. The specimens were permeated with distilled water (Haug and Boldt-Leppin 1994).

Ten hydraulic conductivity tests were conducted on compacted MQ bentonite and sand mixtures with 0 to 0.5 % by weight of bentonite polymer. Several of the k tests failed. Failure occurred when the bentonite "blew out" filling the outflow with a brown bentonite slurry. This "blow out" occurred in the specimens with little to no polymer. The k of the specimens with 0.05 % to 0.5 % polymer varied from 1.80×10^{-9} to 1.05×10^{-9} cm/s and was similar to the k of the HQ bentonite sand mixtures, which was approximately 1.45×10^{-9} cm/s. The k of the MQ bentonite sand mixtures decreased from 10^{-5} cm/s to 10^{-9} cm/s with the addition of 0.05 % polymer. However, the addition of more than 0.05 % polymer resulted in diminishing returns, i.e., the k did not decrease substantially with > 0.05 % polymer (Haug and Boldt-Leppin 1994).

Table 2.1. Properties of bentonite reported in literature.

Reference	Specific Gravity of Solids, G_s	Cation Exchange Capacity, CEC (meq/100g)	Liquid Limit, LL (%)	Plastic Limit, PL (%)	Plasticity Index, PI (%)	Activity, A	% Clay (< 2 μ m)	Swell Index, SI (mL/2g)	% Montmorillonite	Specific Surface Area, SSA (m ² /g)
Kenney et al. (1992)	2.74	100	500	40	-----	-----	-----	25	-----	-----
Komine and Ogata (1996)	-----	-----	473.9	26.6	447.3	6.9	64.5	-----	-----	46 - 51
Jo et al. (2005)	2.74 \pm 0.04	53 - 75	479 \pm 90	-----	441 \pm 86	-----	90	-----	-----	-----
Kolstad et al. (2004)	2.65	-----	-----	-----	-----	-----	90	35.5	-----	-----
Lee and Shackelford (2005a)	2.74 - 2.78	63.9 - 93.4	430 - 548	-----	393 - 548	-----	-----	27.5 - 30	-----	-----
Ito (2006) ^a	2.66 - 2.72	62.7 - 79.7	399.3 - 767.8	23.3 - 30.1	376.1 - 737.7	-----	-----	-----	45 - 70	-----
Ito (2006) ^b	2.68 - 2.78	62.1 - 82.8	511.3 - 690.3	33 - 38.8	473.3 - 651.6	-----	-----	-----	60 - 71	-----
Katsumi et al. (2007)	-----	-----	619.5	51	-----	-----	-----	33	-----	-----
Meer and Benson (2007), Benson and Meer (2010)	-----	-----	504	-----	465	-----	87	34 - 36	-----	-----
Guyonnet (2008) ^c	-----	66.2 - 76.2	-----	-----	-----	-----	-----	-----	68.8 - 76.5	-----
Guyonnet (2008) ^d	-----	33.7 - 72.5	-----	-----	-----	-----	-----	-----	29.6 - 76.8	-----

^a Japanese bentonites

^b Wyoming bentonites

^c Na-bentonite and Na-activated Ca-bentonite

^d Ca-bentonite

Notes:

"-" = not reported

References

- Ahn, H. S., and Jo, H. Y. (2009). "Influence of exchangeable cations on hydraulic conductivity of compacted bentonite." *Applied Clay Science*, 44(1-2), 144-150.
- Ashmawy, A. K., Darwish, E. H., Sotelo, N., and Muhammad, N. (2002). "Hydraulic performance of untreated and polymer-treated bentonite in inorganic landfill leachates." *Clays and Clay Minerals*, 50(5), 546-552.
- Benson, C. H., and Meer, S. R. (2009). "Relative Abundance of Monovalent and Divalent Cations and the Impact of Desiccation on Geosynthetic Clay Liners." *Journal of Geotechnical and Geoenvironmental Engineering*, 135(3), 349-358.
- Benson, C. H., Ören, A. H., and Gates, W. P. (2010). "Hydraulic conductivity of two geosynthetic clay liners permeated with a hyperalkaline solution." *Geotextiles and Geomembranes*, 28(2), 206-218.
- Benson, C. H., Thorstad, P. A., Jo, H. Y., and Rock, S. A. (2007). "Hydraulic performance of geosynthetic clay liners in a landfill final cover." *Journal of Geotechnical and Geoenvironmental Engineering*, 133(7), 814-827.
- Bergaya, F., Aouad, A., Mandalia, T., Faïza Bergaya, B. K. G. T., and Gerhard, L. (2006a). "Chapter 7.5 Pillared Clays and Clay Minerals." *Developments in Clay Science*, Elsevier, 393-421.
- Bergaya, F., Lagaly, G., Faïza Bergaya, B. K. G. T., and Gerhard, L. (2006b). "Chapter 1 General Introduction: Clays, Clay Minerals, and Clay Science." *Developments in Clay Science*, Elsevier, 1-18.
- Bojemueller, E., Nennemann, A., and Lagaly, G. (2001). "Enhanced pesticide adsorption by thermally modified bentonites." *Applied Clay Science*, 18(5-6), 277-284.
- Bouazza, A. (2002). "Geosynthetic clay liners." *Geotextiles and Geomembranes*, 20(1), 3-17.
- Brigatti, M. F., Galan, E., Theng, B. K. G., Faïza Bergaya, B. K. G. T., and Gerhard, L. (2006). "Chapter 2 Structures and Mineralogy of Clay Minerals." *Developments in Clay Science*, Elsevier, 19-86.
- D'Appolonia, D. J. (1980). "Soil-bentonite slurry trench cutoffs." *Journal of the Geotechnical Engineering Division-Asce*, 106(4), 399-417.
- Daniel, D. E., Anderson, D. C., and Boynton, S. S. (1985). "Fixed-wall versus flexible-wall permeameters." *Hydraulic Barriers in Soil and Rock*. ASTM STP 874, A. I. Johnson, R. K. Frobel, N. J. Cavalli, and C. B. Pettersson, eds., ASTM, West Conshohocken, PA, 107-126.

- Daniel, D. E., Bowders, J. J., and Gilbert, R. B. (1997). "Laboratory hydraulic conductivity testing of GCLs in flexible-wall permeameters." *SAE Special Publications*(1308), 208-226.
- de Paiva, L. B., Morales, A. R., and Valenzuela Díaz, F. R. (2008). "Organoclays: Properties, preparation and applications." *Applied Clay Science*, 42(1-2), 8-24.
- Deer, W. A., Howie, R. A., and Zussman, J. (1992). *An introduction to the rock-forming minerals - 2nd ed.*, Addison Wesley Longman Limited, Essex.
- Eisenhour, D. D., and Brown, R. K. (2009). "Bentonite and Its Impact on Modern Life." *ELEMENTS*, 5(2), 83-88.
- Estornell, P., and Daniel, D. E. (1992). "Hydraulic conductivity of 3 geosynthetic clay liners." *Journal of Geotechnical Engineering-Asce*, 118(10), 1592-1606.
- Evans, J. C. (1993). "Vertical cutoff walls." *Geotechnical Practices for Waste Disposal*, D. E. Daniel, ed., Chapman & Hall, London, 430 - 454.
- Evans, J. C. (1994). "Hydraulic conductivity of vertical cutoff walls." *Hydraulic Conductivity and Waste Contaminant Transport in Soil*, STP 1142, D. E. Daniel and S. Trautwein, eds., ASTM, West Conshohocken, PA, 79-94.
- Evans, J. C., Shackelford, C. D., Yeo, S. S., and Henning, J. (2008). "Membrane behavior of soil-bentonite slurry-trench cutoff walls." *Soil & Sediment Contamination*, 17(4), 316-322.
- Fritz, S. J. (1986). "Ideality of clay membranes in osmotic processes – a review." *Clays and Clay Minerals*, 34(2), 214-223.
- Gates, W. P., Bouazza, A., and Churchman, G. J. (2009). "Bentonite clay keeps pollutants at bay." *ELEMENTS*, 5(2), 105-110.
- Grim, R. E.-. (1968). *Clay mineralogy*, McGraw-Hill, New York.
- Guyonnet, D., Gaucher, E., Gaboriau, H., Pons, C. H., Clinard, C., Norotte, W., and Didier, G. (2005). "Geosynthetic clay liner interaction with leachate: Correlation between permeability, microstructure, and surface chemistry." *Journal of Geotechnical and Geoenvironmental Engineering*, 131(6), 740-749.
- Haug, M. D., and Boldt-Leppin, B. (1994). "Influence of polymers on the hydraulic conductivity of marginal quality bentonite-sand mixtures." *Hydraulic Conductivity and Waste Contaminant Transport in Soil*, ASTM STP 1142, D. E. Daniel and S. J. Trautwein, eds., American Society for Testing and Materials, Philadelphia.

- Heister, K., Kleingeld, P. J., Keijzer, T. J. S., and Loch, J. P. G. (2005). "A new laboratory set-up for measurements of electrical, hydraulic, and osmotic fluxes in clays." *Engineering Geology*, 77(3-4), 295-303.
- Heller-Kalai, L. (2006). "Thermally modified clay minerals." Handbook of Clay Science, F. Bergaya, B. K. G. Theng, and G. Lagaly, eds., Elsevier, Amsterdam, The Netherlands, 289-308.
- Henning, J. T., Evans, J. C., and Shackelford, C. D. (2006). "Membrane behavior of two backfills from field-constructed soil-bentonite cutoff walls." *Journal of Geotechnical and Geoenvironmental Engineering*, 132(10), 1243-1249.
- Ito, H. (2006). "Compaction properties of granular bentonites." *Applied Clay Science*, 31(1-2), 47-55.
- James, A. N., Fullerton, D., and Drake, R. (1997). "Field performance of GCL under ion exchange conditions." *Journal of Geotechnical and Geoenvironmental Engineering*, 123(10), 897-901.
- Jo, H. Y., Benson, C. H., Shackelford, C. D., Lee, J. M., and Edil, T. B. (2005). "Long-term hydraulic conductivity of a geosynthetic clay liner permeated with inorganic salt solutions." *Journal of Geotechnical and Geoenvironmental Engineering*, 131(4), 405-417.
- Jo, H. Y., Katsumi, T., Benson, C. H., and Edil, T. B. (2001). "Hydraulic conductivity and swelling of nonprehydrated GCLs permeated with single-species salt solutions." *Journal of Geotechnical and Geoenvironmental Engineering*, 127(7), 557-567.
- Kajita, L. (1997). "An improved contaminant resistant clay for environmental clay liner applications." *Clays and Clay Minerals*, 45(5), 609-617.
- Kang, J.-B., and Shackelford, C. D. (2009). "Clay membrane testing using a flexible-wall cell under closed-system boundary conditions." *Applied Clay Science*, 44(1-2), 43-58.
- Kang, J.-B., and Shackelford, C. D. (2011). "Consolidation enhanced membrane behavior of a geosynthetic clay liner." *Geotextiles and Geomembranes*, 29(6), 544-556.
- Kang, J. B., and Shackelford, C. D. (2010). "Membrane Behavior of Compacted Clay Liners." *Journal of Geotechnical and Geoenvironmental Engineering*, 136(10), 1368-1382.
- Kashir, M., and Yanful, E. K. (1997). "A flow pump system for assessing clay barrier-permeant compatibility." *Geotechnical Testing Journal*, 20(2), 179-190.
- Katsumi, T., Ishimori, H., Ogawa, A., Yoshikawa, K., Hanamoto, K., and Fukagawa, R. (2007). "Hydraulic conductivity of nonprehydrated geosynthetic clay liners permeated with inorganic solutions and waste leachates." *Soils and Foundations*, 47(1), 79-96.

- Katsumi, T., Ishimori, H., Onikata, M., and Fukagawa, R. (2008). "Long-term barrier performance of modified bentonite materials against sodium and calcium permeant solutions." *Geotextiles and Geomembranes*, 26(1), 14-30.
- Kemper, W. D., and Rollins, J. B. (1966). "Osmotic efficiency coefficients across compacted clays." *Soil Science Society of America Proceedings*, 30(5), 529-534.
- Kenney, T. C., Vanveen, W. A., Swallow, M. A., and Sungaila, M. A. (1992). "Hydraulic conductivity of compacted bentonite sand mixtures." *Canadian Geotechnical Journal*, 29(3), 364-374.
- Klopprogge, J. T. (1998). "Synthesis of smectites and porous pillared clay catalysts: A review." *Journal of Porous Materials*, 5(1), 5-41.
- Kolstad, D. C., Benson, C. H., and Edil, T. B. (2004a). "Hydraulic conductivity and swell of nonprehydrated geosynthetic clay liners permeated with multispecies inorganic solutions." *Journal of Geotechnical and Geoenvironmental Engineering*, 130(12), 1236-1249.
- Kolstad, D. C., Benson, C. H., Edil, T. B., and Jo, H. Y. (2004b). "Hydraulic conductivity of a dense prehydrated GCL permeated with aggressive inorganic solutions." *Geosynthetics International*, 11(3), 233-241.
- Komadel, P. (2003). "Chemically modified smectites." *Clay Minerals*, 38(1), 127-138.
- Komine, H. (2008). "Theoretical equations on hydraulic conductivities of bentonite-based buffer and backfill for underground disposal of radioactive wastes." *Journal of Geotechnical and Geoenvironmental Engineering*, 134(4), 497-508.
- Komine, H., and Ogata, N. (1996). "Prediction for swelling characteristics of compacted bentonite." *Canadian Geotechnical Journal*, 33(1), 11-22.
- Komine, H., and Ogata, N. (2004). "Predicting swelling characteristics of bentonites." *Journal of Geotechnical and Geoenvironmental Engineering*, 130(8), 818-829.
- Lagaly, G., Ogawa, M., Dékány, I., Faïza Bergaya, B. K. G. T., and Gerhard, L. (2006). "Chapter 7.3 Clay Mineral Organic Interactions." *Developments in Clay Science*, Elsevier, 309-377.
- Lee, J. M., and Shackelford, C. D. (2005a). "Concentration dependency of the prehydration effect for a geosynthetic clay liner." *Soils and Foundations*, 45(4), 27-41.
- Lee, J. M., and Shackelford, C. D. (2005b). "Impact of bentonite quality on hydraulic conductivity of geosynthetic clay liners." *Journal of Geotechnical and Geoenvironmental Engineering*, 131(1), 64-77.

- Lee, J. M., and Shackelford, C. D. (2005c). "Solution retention capacity as the swell index test for sodium an alternative to bentonite." *Geotechnical Testing Journal*, 28(1), 61-70.
- Lee, J. M., Shackelford, C. D., Benson, C. H., Jo, H. Y., and Edil, T. B. (2005). "Correlating index properties and hydraulic conductivity of geosynthetic clay liners." *Journal of Geotechnical and Geoenvironmental Engineering*, 131(11), 1319-1329.
- Liu, P. (2007). "Polymer modified clay minerals: A review." *Applied Clay Science*, 38(1-2), 64-76.
- Lorenzetti, R. J., Bartelt-Hunt, S. L., Burns, S. E., and Smith, J. A. (2005). "Hydraulic conductivities and effective diffusion coefficients of geosynthetic clay liners with organobentonite amendments." *Geotextiles and Geomembranes*, 23(5), 385-400.
- Malusis, M. A. (2010). "Multiswellable bentonite for soil-bentonite vertical barriers." Sixth International Congress on Environmental Geotechnics, New Dehli, India.
- Malusis, M. A., and Shackelford, C. D. (2002a). "Chemico-osmotic efficiency of a geosynthetic clay liner." *Journal of Geotechnical and Geoenvironmental Engineering*, 128(2), 97-106.
- Malusis, M. A., and Shackelford, C. D. (2002b). "Coupling effects during steady-state solute diffusion through a semipermeable clay membrane." *Environmental Science & Technology*, 36(6), 1312-1319.
- Malusis, M. A., Shackelford, C. D., and Olsen, H. W. (2001). "A laboratory apparatus to measure chemico-osmotic efficiency coefficients for clay soils." *Geotechnical Testing Journal*, 24(3), 229-242.
- Meer, S. R., and Benson, C. H. (2007). "Hydraulic conductivity of geosynthetic clay liners exhumed from landfill final covers." *Journal of Geotechnical and Geoenvironmental Engineering*, 133(5), 550-563.
- Mitchell, J. K.-. (1993). *Fundamentals of soil behavior*, Wiley, New York.
- Mitchell, J. K.-., and Soga, K. i. (2005). *Fundamentals of soil behavior*, John Wiley & Sons, Hoboken, N.J.
- Noyan, H., Muserref, O., and Sarikaya, Y. (2007). "The effect of sulphuric acid activation on the crystallinity, surface area, porosity, surface acidity, and bleaching power of a bentonite." *Food Chemistry*, 105(1), 156-163.
- Olsen, H. W. (1969). "Simultaneous fluxes of liquid and charge in saturated kaolinite." *Soil Science Society of America Proceedings*, 33(3), 338-344.

- Onikata, M., Kondo, M., Hayashi, N., and Yamanaka, S. (1999). "Complex formation of cation-exchanged montmorillonites with propylene carbonate: Osmotic swelling in aqueous electrolyte solutions." *Clays and Clay Minerals*, 47(5), 672-677.
- Prost, R., and Yaron, B. (2001). "Use of modified clays for controlling soil environmental quality." *Soil Science*, 166(12), 880-895.
- Ressi, A., and Cavalli, N. (1985). "Bentonite slurry trenches." *Engineering Geology*, 21(3-4), 333-339.
- Shackelford, C. D., Benson, C. H., Katsumi, T., Edil, T. B., and Lin, L. (2000). "Evaluating the hydraulic conductivity of GCLs permeated with non-standard liquids." *Geotextiles and Geomembranes*, 18(2-4), 133-161.
- Shackelford, C. D., and Lee, J. M. (2003). "The destructive role of diffusion on clay membrane behavior." *Clays and Clay Minerals*, 51(2), 186-196.
- Shackelford, C. D., Sevick, G. W., and Eykholt, G. R. (2010). "Hydraulic conductivity of geosynthetic clay liners to tailings impoundment solutions." *Geotextiles and Geomembranes*, 28(2), 149-162.
- Sivapullaiah, P. V., Sridharan, A., and Stalin, V. K. (2000). "Hydraulic conductivity of bentonite-sand mixtures." *Canadian Geotechnical Journal*, 37(2), 406-413.
- Theng, B. K. G. (1982). "Clay-polymer interactions – Summary and perspectives." *Clays and Clay Minerals*, 30(1), 1-10.
- Tran, N. H., Dennis, G. R., Milev, A. S., Kannangara, G. S. K., Wilson, M. A., and Lamb, R. N. (2005). "Interactions of sodium montmorillonite with poly(acrylic acid)." *Journal of Colloid and Interface Science*, 290(2), 392-396.
- Trauger, R., and Darlington, J. "Next generation geosynthetic clay liners for improved durability and performance." *14th GRI Conference, Geosynthetic Institute, Folsom, PA, USA*, 255-267.
- Vasko, S., Jo, H. Y., Benson, C. H., Edil, T. B., and Katsumi, T. (2001). "Hydraulic conductivity of partially prehydrated geosynthetic clay liners permeated with aqueous calcium chloride solutions." *Geosynthetics 2001*, Industrial Fabrics Assoc. International, St. Paul, MN, 685-699.
- Vukovic, Z., Milutonic, A., Rozic, L., Rosic, A., Nedic, Z., and Jovanovic, D. (2006). "The influence of acid treatment on the composition of bentonite." *Clays and Clay Minerals*, 54(6), 697-702.

Yeo, S. S., Shackelford, C. D., and Evans, J. C. (2005). "Membrane behavior of model soil-bentonite backfills." *Journal of Geotechnical and Geoenvironmental Engineering*, 131(4), 418-429.

Chapter 3

Enhancing Membrane Behavior with a Bentonite Polymer Nanocomposite

SUMMARY: Traditional bentonite used in geosynthetic clay liners (GCLs) has been shown to exhibit substantial semipermeable membrane behavior, or the ability to restrict the migration of solutes. Although such membrane behavior represents a beneficial aspect to the containment function of GCLs, partial or complete degradation of the membrane behavior due to diffusion of invading salt cations into the bentonites also has been observed. In this study, a polyacrylate modified bentonite, referred to as a bentonite polymer nanocomposite or BPN, was investigated as a potential substitute for traditional (non-treated or unmodified) bentonite for the purpose of providing increased resistance to salt degradation of the membrane behavior. The membrane behavior of the BPN was measured in the laboratory by establishing differences in salt (KCl) concentrations ranging from 4.7 mM to 54 mM across specimens of the BPN contained in both rigid-wall and flexible-wall cells under closed-system boundary conditions. The membrane efficiency coefficients at steady state, ω , for the BPN were higher than those previously reported for GCLs containing traditional bentonites under similar, albeit more favorable, testing conditions for the GCLs, including reduced salt concentrations in the pore waters of the GCL specimens due to flushing of the specimens prior to membrane testing (i.e., the BPN specimens were not preflushed). For example, the ω value measured in this study for a BPN specimen contained within a rigid-wall cell and based on circulation of 20 mM KCl was 0.43, whereas that previously reported for a GCL specimen under similar testing conditions except a lower porosity (0.74 vs. 0.92) was only 0.30. Similarly, the ω value measured in this study for a BPN specimen during circulation of 9.3 mM KCl in a flexible-wall cell at an effective stress of 34.5 kPa (5 psi)

was 0.32, whereas that previously reported for a GCL specimen under similar test conditions during the circulation of a slightly lower (more favorable) concentration, 8.7 mM KCl, was only 0.20. Thus, the BPN exhibited enhanced membrane behavior under conditions that were somewhat less favorable than those previously reported for a GCL with a traditional bentonite. The practical significance of the results is illustrated in an analysis showing a reduction in liquid flux across a barrier composed of BPN.

KEY WORDS: Chemico-osmosis; Clay membranes; Membrane efficiency; Geosynthetic clay liner; Polymer modified bentonites; Semipermeable membrane

3.1 INTRODUCTION

Bentonite is a clay comprised primarily of the mineral montmorillonite, a member of the smectite group of clay minerals (Mitchell and Soga 2005). Bentonite commonly is used in a variety of hydraulic containment applications to control liquid flow and contaminant transport. Example applications include use as a compositional component in soil-bentonite (SB) groundwater cutoff walls, as a barrier or barrier component for waste containment (e.g., landfills, wastewater ponds, manure lagoons, nuclear storage, etc.) and secondary containment (e.g., oil tank farms), and as a seal in monitoring and water supply wells (Estornell and Daniel 1992; Evans 1993; Kajita 1997; Christman et al. 2002; Smith et al. 2003). In general, sodium bentonite (Na-bentonite), meaning that the sodium cation, Na^+ , dominates the exchange sites of the individual montmorillonite-based clay particles, is preferred in these applications. This preference for Na-bentonite is based primarily on the superior engineering properties of Na-bentonite, such as a typically low hydraulic conductivity, k , to water ($k < 10^{-10}$ m/s), relative to

the same properties of other bentonites, such as Ca- and Mg-bentonites (Shackelford et al. 2000; Jo et al. 2001; Kolstad et al. 2004; Jo et al. 2005). In addition, Na-bentonite has been shown to exhibit semipermeable membrane behavior, which can significantly improve the containment function of barriers comprised of Na-bentonite via processes known as hyperfiltration, chemico-osmosis, and reduced diffusion of aqueous-phase solutes (Shackelford et al. 2003; Shackelford 2011; Shackelford 2012).

Unfortunately, Na-bentonite is thermodynamically unstable in environments where multivalent cations are present or predominant, including most naturally occurring pore waters in earthen materials (Sposito 1989). Under such conditions, multivalent cations (e.g., Ca^{2+} and Mg^{2+}) gradually replace monovalent cations (e.g., Na^+ and K^+), originally dominating the exchange sites, thereby reducing or eliminating osmotic swelling of the bentonite and the ability of the bentonite to function effectively (Vasko et al. 2001; Kolstad et al. 2004; Lee et al. 2005; Lee and Shackelford 2005b). For example, several field studies have shown that Ca^{2+} -for- Na^+ exchange in the bentonite portion of geosynthetic clay liners (GCLs) can result in reduced swelling capability of the bentonite upon hydration, and ultimately to poor hydraulic performance (ATU 1992; James et al. 1997; Shackelford et al. 2000; Egloffstein 2001; Jo et al. 2001; Benson et al. 2004; Jo et al. 2004; Benson et al. 2007; Meer and Benson 2007; Scalia and Benson 2011; Bradshaw et al. 2012). The Ca^{2+} typically is derived from surrounding soils, and migrates into the GCL usually in response to hydraulic (e.g., suction) and/or diffusive (chemical) gradients.

Recent laboratory studies have illustrated the deleterious effects of long-term cation exchange on both k and membrane behavior (Lin and Benson 2000; Egloffstein 2001; Jo et al. 2001; Shackelford and Lee 2003; Kolstad et al. 2004; Jo et al. 2005; Lee and Shackelford 2005b;

Lee and Shackelford 2005a). For example, partial or complete destruction of membrane behavior in bentonite has been correlated with diffusion of invading salt cations into the bentonite (Malusis and Shackelford 2002a; Shackelford and Lee 2003). These field and laboratory data paint an unsettling picture regarding the long-term effectiveness of traditional (non-treated or unmodified) bentonite used for hydraulic containment applications.

However, methods exist to chemically modify bentonite so that the bentonite properties are compatible with the surrounding environment. For example, anionic polymers are added to bentonite to attain rheological properties needed for drilling fluids (Heller and Keren 2003). Organobentonites, or bentonites where cationic organic molecules such as the quaternary ammonium cations (QACs) are exchanged for inorganic cations comprising the exchange complex of the bentonite, also have been created for applications where increased sorption of hydrophobic organic compounds is desired (Lo et al. 1996; Gullick and Weber 2001; Smith et al. 2003).

The objective of this study was to evaluate the potential use of a polyacrylic acid (PAA) polymerized bentonite as a potential substitute for traditional Na-bentonite commonly used in GCLs, compacted soil-bentonite liners, and soil-bentonite (SB) backfills in vertical cutoff walls (Yeo et al. 2005; Henning et al. 2006; Evans et al. 2008) for the purpose of enhancing semipermeable membrane behavior. Since the polymerized modification of the traditional bentonite occurs at the nanoscale, the PAA polymerized bentonite is commonly referred to as a bentonite-polymer nanocomposite, or BPN (Scalia et al. 2011; Scalia 2012).

The BPN evaluated in this study is different from other treated or modified bentonites, such as the aforementioned organobentonites and anionic polymer modified bentonites. For example, the polymerized bentonite evaluated in this study is formed when polyacrylic acid

molecules are polymerized after insertion into the interlayers of the montmorillonite mineral structure. In contrast, organobentonites typically are synthesized either by solution, whereby clay is suspended and mixed within aqueous solutions of excess QACs, or by solid-state reactions, whereby the clay mineral and solid organo-ammonium salt are ground together (Lagaly et al. 2006). Also, typical anionic polymer modified bentonites employ long-chain anionic polymers (e.g., anionic polyacrylimides) that are electrostatically associated with the positively charged edges of the bentonite platelets (e.g., Boels and van der Wal 1999; Heller and Keren 2003), rather than bonded in the interlayer space of the montmorillonite mineral structure as occurs in the BPN evaluated in this study.

Evaluation of the semipermeable membrane behavior of the BPN consisted of four laboratory membrane tests, two performed using a rigid-wall cell and two performed using a flexible-wall cell. The tests performed in the rigid-wall cells were conducted at different porosities. The tests performed in the flexible-wall cells were conducted at different initial effective stresses. The results are compared with previously published results based on evaluation of a GCL containing traditional bentonite under similar initial and boundary conditions.

3.2 MATERIALS AND METHODS

3.2.1 Liquids

The liquids used in this study included de-ionized water (DIW) and solutions of DIW with potassium chloride (KCl) (certified A.C.S.; Fisher Scientific, Fair Lawn, NJ). The KCl solutions were used as circulating liquids in membrane tests to allow for direct comparison of results from previous membrane tests conducted on GCLs using similar KCl solutions (Malusis

and Shackelford 2002a; Kang and Shackelford 2009; Kang and Shackelford 2011). Solutions were prepared and stored in 20-L carboys (Nalgene[®]; Thermo Fisher Scientific, Rochester, NY). The *pH* and electrical conductivity, *EC*, of the solutions were measured using a *pH* meter (Accumet[®] AB15 meter, Fisher Scientific Co., Pittsburgh, PA) and an *EC* meter (150 A+ Conductivity Meter, Thermo Orion, Beverly, MA), respectively. Ion chromatography (Dionex[®] 4000i IC Module, Dionex Co., Sunnyvale, CA) was used to measure chloride (Cl^-) concentrations, and inductively coupled plasma-atomic emission spectrometry (IRIS[®] Advantage/1000 ICAP Spectrometer, Thermo Jarrel Ash Co., Franklin, MA) was used to measure potassium (K^+) concentrations. The measured *EC* and *pH* of the KCl solutions are given in Table 3.1.

3.2.2 Soil

The BPN evaluated in this study was supplied by Colloid Environmental Technologies Co. (CETCO, Hoffman Estates, IL). The BPN was produced with PAA using methods similar to those used for the production of polymer nanocomposites (e.g., Muzney et al. 1996). First, a monomer solution was prepared by dissolving acrylic acid in water followed by neutralization with sodium hydroxide and addition of the initiator sodium persulfate. Then, a traditional sodium bentonite was added to the monomer solution in concentrations ranging from 30 to 50 % by weight to form a bentonite-monomer slurry. Polymerization was initiated by raising the temperature of the bentonite-monomer slurry above the decomposition temperature of the initiator molecule (180°C), causing the initiator molecule to decompose into free radicals ($\text{R}\bullet$). The $\text{R}\bullet$ react with the acrylic acid monomer to form more free radicals ($\text{RM}\bullet$), which in turn react with additional monomer to proliferate the polymer chain ($\text{RMM}\bullet$). Following

polymerization, the PAA polymerized bentonite was oven dried, milled, and screened (Scalia et al. 2011).

Based on the grain-size distributions from the hydrometer analysis shown in Fig. 3.1, 100 % of the BPN was fine grained, with the BPN comprised of 97 % clay-sized ($< 5 \mu\text{m}$) material. The BPN classified as a high-plasticity clay or CH according to the Unified Soil Classification System (ASTM D 2487, ASTM 2010). Mineralogical analyses conducted by Mineralogy, Inc. (Tulsa, OK) using x-ray diffraction indicated the composition of the BPN as 76 % montmorillonite, 15 % quartz, 7 % plagioclase feldspar, and 2 % illite/mica.

The Atterberg limits of the BPN also were measured according to ASTM D 4318 (ASTM 2005). The measured liquid limit, *LL*, was 255, which is significantly lower than that of traditional bentonites with values of *LL* that typically vary from 400 to 700 (e.g., Kenney et al. 1992; Lee and Shackelford 2005b; Ito 2006). However, the value of *LL* for other modified bentonites materials also have been reported as being lower relative to those of traditional bentonites. For example, Di Emidio (2010) reported a *LL* of 375 for dense pre-hydrated, or DPH, GCL which is a GCL that is prehydrated with sodium-carboxymethylcellulose (CMC) and methanol and densified via calendaring.

In contrast to the *LL*, the plastic limit, *PL*, of the BPN could not be determined. As shown in Fig. 3.2, the consistency of the BPN during the test for *PL* was similar to "silly putty" at low gravimetric water contents ($< 150 \%$), and the soil "worm" did not exhibit the same cracking pattern that a traditional bentonite would exhibit as the water content approaches the *PL*. As a result, the plasticity index or *PI* of the BPN could not be determined.

Tests to measure both the swell index, *SI*, and the solution retention capacity, *SRC*, using DIW also were conducted. The *SI* tests were conducted in general accordance with ASTM D

5890 (ASTM 2006). Briefly, two grams of oven dried BPN were dusted over the test solution in 0.1-g increments. The *SI* (mL/2g) was monitored initially after 16 h and subsequently every 4 h thereafter up to a total elapsed time of 48 h, at which swelling had ceased. The *SRC* tests were conducted following the procedures described in Lee and Shackelford (2005c), except that the centrifuge speed was set at 3000 rpm versus the 5000 rpm used by Lee and Shackelford (2005c) to allow for an increased sensitivity of the resulting measurements.

The resulting values of *SI* and *SRC* for the BPN were 73 mL/2g and 11 mL/1g, respectively. These values are noticeably higher than those reported for traditional bentonites (e.g., Lee and Shackelford 2005c). For example, values of *SI* and *SRC* for traditional bentonites typically range from 25 to 36 mL/2g and 5.7 to 7.2 mL/g, respectively (Kenney et al. 1992; Kolstad et al. 2004; Lee and Shackelford 2005b; Katsumi et al. 2007; Benson and Meer 2009). The greater swelling behavior of the BPN is most likely attributable to the contribution of the swelling resulting from the superabsorbent polymer (PAA) portion of the BPN (Scalia et al. 2011).

3.2.3 Membrane Testing

As shown schematically in Figs. 3.3 and 3.4 and pictorially in Fig. 3.5, two membrane testing apparatuses were assembled as a part of this study, i.e., one with a rigid-wall cell similar to that described by Malusis et al. (2001), and the other with a flexible-wall cell similar to that described by Kang and Shackelford (2009). The rigid-wall cell is used to test specimens under constant-volume conditions throughout the test. As explained by Kang and Shackelford (2009), the flexible-wall cell also maintains constant specimen volume during the stages of the test devoted to measuring membrane behavior, as required by the constant-volume assumption

inherent in the equation used to calculate the membrane efficiency (described subsequently). However, some volume change generally does occur during the brief (< 5 min) liquid refilling and sampling periods that are required periodically between the longer (typically either 24 or 48 h) membrane testing stages. Also, the flexible-wall cell allows for back-pressure saturation of the specimen prior to membrane testing and for control of the stress conditions imposed on the specimen (Kang and Shackelford 2009).

Both rigid-wall and flexible-wall cells were connected via stainless steel tubing to a hydraulic control system consisting of a flow-pump with syringes (actuators) used to circulate chemical solutions or across both the top and bottom boundaries of the specimen contained in the cell at the same, constant displacement rate (Malusis et al. 2001; Kang and Shackelford 2009). Stainless steel tubing was used to minimize volume change within the testing apparatus and to provide chemical resistance to electrolyte solutions. Two in-line pressure transducers (model Nos. PX181-100G5V or PX209-015G10V, Omega Engineering Inc., Stamford, CT) were used to measure the pressures existing in the boundary liquids, and a differential pressure transducer (model DP15-64, Validyne Engineering Corp., Northridge, CA) was used to measure the generation of pressure difference across the specimen due to specimen membrane behavior. These pressures were recorded via a data acquisition (DAQ) system consisting of a circuit board (SCB-68, National Instruments, Austin, TX), a DAQ device (National Instruments, Austin, TX), and the LabVIEW software (National Instruments, Austin, TX). Refilling and sampling reservoirs were used to replenish the syringes with fresh chemical solutions or DIW and to collect circulation outflow for measurement of chemical parameters (e.g., solute concentrations, electrical conductivity) during the aforementioned replenishment and sampling periods at the end of each circulation cycle.

The rigid-wall cell (Fig. 3.4a) consists of an acrylic cylinder with a 71.0-mm (2.8-in) inner diameter, a top piston, and a base pedestal. The acrylic cylinder slides over the base pedestal and the top piston slides into the acrylic cylinder. O-rings on both the base pedestal and top piston and vacuum grease provide a tight seal between the acrylic cylinder and the base pedestal and top piston. The top piston is used to control the thickness (i.e. volume) of the specimen and can be locked in place during testing. The base pedestal and top piston have three ports. The inflow and outflow ports allow circulation of liquids (e.g., electrolyte solutions) through the porous plastic disks (GenPore porous sheet TO-6, General Polymer Corp., Reading, PA) located along the top and bottom boundaries of the specimen, whereas third ports located in the center of the top piston and the base pedestal provide connections to the individual in-line pressure transducers for measurement of the boundary water pressures at the top and bottom of the specimen, or u_{Top} and u_{Bottom} , respectively, and the differential pressure transducer used to measure the pressure difference, $\Delta P (= u_{Bottom} - u_{Top})$, across the specimen.

The flexible-wall cell is a triaxial cell with special top and bottom caps as described in Kang and Shackelford (2009). The cell shown schematically in Fig. 3.4b, consists of an acrylic outer cylinder, top and bottom plates, and top and bottom caps. Each top and bottom cap has three ports, i.e., one port to allow for a circulation inflow, one port to allow for circulation outflow, and a third port to allow for measurement of the boundary water pressures (i.e., u_{Top} and u_{Bottom}) and the pressure difference across the specimen (i.e., ΔP). The bottom cap is attached to a bottom plate.

For the flexible-wall tests, a test specimen with a diameter of 102 mm (4.0 in) was placed above a heat-bonded, 140 g/m², non-woven geotextile on the bottom cap followed by a top cap and a flexible (polymer) membrane that is sealed with o-rings. The flexible membrane separated

the specimen from the cell water. The outer cylinder was filled with de-aired water, which may be pressurized to apply a confining pressure (i.e., total stress) to the specimen. An cell-water accumulator was connected to the cell water to monitor volume change. Backpressure was applied to the specimen through the inflow and outflow ports in the top and bottom caps.

The flow-pump system is essentially the same as that described by Malusis et al. (2001) and consists of a dual carriage syringe pump (Model 940 or 944, Harvard Apparatus, Holliston, MA), two stainless steel actuators (syringes), and stainless steel tubing. Stainless steel components are used to minimize corrosion and apparatus volume change. The syringes displace liquids at the same, constant rate into the top and bottom caps of the cell via the inflow port, the liquids circulate through the porous plastic disks, and then exit via the outflow ports. In addition, infusion and withdrawal of the liquids occur at constant rates, such that the incremental volume of liquid that enters the cell, ΔV_{in} , is equal to the incremental volume of liquid that exits the cell, ΔV_{out} . As a result, the volume change in the circulation system during circulation is zero, such that there can be no flow of liquid through the specimen during circulation. Thus, the circulation system represents a closed system, i.e., at least during the periods of the test devoted to measurement of the membrane behavior of the specimen.

Operation of the flow-pump system consists of a circulation (i.e., testing) phase and a sampling and refilling phase. During the testing phase, the syringes are open to the cell, but closed to the reservoirs by opening valves 1 and 3 and closing valves 6 and 7 (see Fig. 3.3). The syringes circulate liquids (DIW or electrolyte solutions) through the top and bottom of the specimens, such that a constant concentration difference (ΔC) is maintained across the specimen. If the specimen behaves as a semipermeable membrane, then a pressure difference, ΔP , is generated in response to the ΔC to counteract the tendency for chemico-osmotic flow, which is

prevented from occurring due to maintaining a constant volume during circulation. This pressure difference is measured directly by differential transducer and indirectly as the difference in pressures measured by the two in-line pressure transducers.

The circulation rate of the liquid is adjustable by changing the displacement rate for the syringes of the flow pump. The measured displacement rates for the pumps and syringes that were used in this study varied from 9.2×10^{-12} to 4.7×10^{-7} m³/s. The circulation rate was adjusted to mimic "perfectly flushing" boundary conditions such that a steady-state ΔP was achieved during the circulation period, i.e., the time between the sampling and refilling periods (e.g., see Malusis et al. 2001). The circulation rate used in this study was 2.3×10^{-10} m³/s, which amounted to a circulation of approximately 40 mL every two days, after which the syringes were sampled and refilled before the start of a new circulation cycle.

During the brief (< 5 min) sampling and refilling periods, the syringes were closed to the cell and opened to the reservoirs by closing valves 1 and 3 and opening valves 6 and 7 (see Fig. 3.3), and the directions of the syringe displacement were reversed. The front (inflow) chambers of the syringes were refilled with fresh circulation liquid from the refilling reservoirs, whereas the circulation outflow liquids from the back chambers of the syringes were emptied into the sampling reservoirs. The outflow liquids were collected and stored for subsequent analysis (e.g., *EC* and solute concentration, *C*).

The membrane tests consisted of two stages, a permeation stage and a chemico-osmotic testing stage. During the permeation stage, specimens were permeated for periods from weeks to months in order to saturate the specimens. Despite those durations of permeation, little effluent was collected due to the affinity of the BPN for water, the low k (< 3×10^{-8} m/s) of the BPN, and the presence of excess low molecular weight polymer clogging the system (Scalia 2012).

Therefore, the BPN specimens tested in this study essentially represented specimens that were not flushed of soluble salts prior to membrane testing. This precondition of the BPN specimens was unlike that for the majority of previous studies evaluating the membrane behavior of GCL specimens, whereby the specimens purposely were permeated with DIW to reduce the soluble salt content in the pores of the bentonite and, therefore, enhance the overall potential for significant membrane behavior (Malusis et al. 2001; Malusis and Shackelford 2002a; Shackelford and Lee 2003; Kang and Shackelford 2009; Kang and Shackelford 2010; Kang and Shackelford 2011). Thus, the precondition of the BPN specimens tested in this study was less favorable towards the existence and magnitude of semipermeable membrane behavior than that for previously tested GCLs.

Rigid-wall specimens were prepared and permeated directly in the rigid-wall membranes cells, whereas flexible-wall specimens were permeated in separate flexible-wall permeameters prior to being transferred to the flexible-wall membrane cell for the second stage of the test. The required mass of dry granular BPN was measured on a precision balance (Sartorius GP 5202, Goettingen, Germany). The dry BPN then was poured into the mold (rigid-wall cell) or membrane (flexible-wall cell) and leveled off using a plastic top cap to create a flat surface. The dry mass per unit area of the bentonite specimens was controlled to be 4.8 kg/m^2 , a typical value for a GCL (Scalia 2012). The flexible-wall specimens were permeated under 172 kPa (25 psi) backpressure at an average effective stress of 34.5 kPa (5 psi) using the falling headwater-rising tailwater method (ASTM D 5084). Specimens were permeated from the bottom to the top to minimize the entrapment of any air by simultaneously increasing the headwater pressure by 17.2 kPa (2.5 psi) to 189.2 kPa (27.5 psi) and decreasing the tailwater pressure by 17.2 kPa (2.5 psi) to 154.8 (22.5 psi). The thickness of the specimens varied from 7 to 11 mm resulting in

hydraulic gradients ranging from approximately 500 to 300, respectively. As described by Shackelford et al. (2000), these relatively high magnitudes of hydraulic gradients are typical for permeation of GCLs due to the low k values typically associated with GCLs permeated with water or dilute chemical solution (i.e., $\leq 3 \times 10^{-11}$ m/s), and should not have a significant influence on the resulting measured k values.

After the permeation stage was complete, the specimens were transferred to the membrane testing apparatus for measurement of membrane behavior. First, the baseline pressure difference, ΔP , was established by simultaneously circulating DIW across both the top and bottom boundaries of the specimen (i.e., $C_{ot} = C_{ob} = 0$). Then, the circulating liquid on the top boundary was switched to KCl solutions (i.e., $C_{ot} > 0$), and the generated pressure difference was recorded continuously.

3.2.4 Measurement of Membrane Efficiency

Under closed-system boundary conditions such as those imposed in this study, the membrane efficiency coefficient, ω , is defined as follows (Groenevelt and Elrick 1976; Malusis et al. 2001):

$$\omega = \frac{\Delta P}{\Delta \pi} \quad (3.1)$$

where ΔP (< 0 , since the positive x-direction is assumed downward from the top of the specimen) is the measured chemico-osmotic pressure difference induced across the specimen as a result of prohibiting chemico-osmotic flux of liquid, and $\Delta \pi$ (< 0) is the theoretical chemico-osmotic pressure difference across an "ideal" semipermeable membrane (i.e., $\omega = 1$) subjected to

an applied difference in solute (electrolyte) concentration (e.g., Olsen et al. 1990). The value of $\Delta\pi$ can be calculated in accordance with the van't Hoff expression in terms of either the source concentrations of KCl in the circulation inflows across the top and bottom of the specimen, or the average of the boundary salt concentrations (Malusis et al. 2001). The membrane efficiency coefficient in terms of the source KCl concentrations, designated as ω_o , is given as follows (e.g., Kang and Shackelford 2011):

$$\omega_o = \frac{\Delta P}{\Delta\pi}_o = \frac{\Delta P}{\Delta\pi_o} = \frac{\Delta P}{vRT\Delta C_o} = \frac{\Delta P}{vRT(C_{ob} - C_{ot})} = \frac{\Delta P}{-vRTC_{ot}} \quad (3.2)$$

where v is the number of ions per molecule of the salt (= 2 for KCl), R is the universal gas constant [8.314 J mol⁻¹K⁻¹], T is the absolute temperature (293 K in this study corresponding to 20 °C), and C_{ot} (> 0) and C_{ob} (= 0) are the initial concentrations of KCl (M) in the source solutions introduced across the top and bottom specimen boundaries, respectively. In terms of average KCl concentrations, the membrane efficiency coefficient, ω_{ave} , is given as follows (e.g., Kang and Shackelford 2011):

$$\omega_{ave} = \frac{\Delta P}{\Delta\pi}_{ave} = \frac{\Delta P}{\Delta\pi_{ave}} = \frac{\Delta P}{vRT\Delta C_{ave}} = \frac{\Delta P}{vRT(C_{b,ave} - C_{t,ave})} \quad (3.3)$$

where $C_{t,ave}$ and $C_{b,ave}$ are the average KCl concentrations across the top and bottom of the specimen boundaries defined as follows:

$$C_{t,ave} = \frac{C_{ot} + C_t}{2} \quad ; \quad C_{b,ave} = \frac{C_{ob} + C_b}{2} \quad (3.4)$$

and C_b and C_t are the measured KCl concentrations (i.e., via calibration with *EC*) in the circulation outflows from the bottom and top of the specimen boundaries, respectively (see Fig. 3.6). Since $C_{t,ave} < C_{ot}$ and $C_{b,ave} \geq C_{ob}$, the magnitude of $\Delta\pi_o$ will be greater than that of $\Delta\pi_{ave}$ such that, for the same measured value of ΔP , $\omega_o < \omega_{ave}$. Thus, membrane efficiency coefficients based on source salt concentrations typically are more conservative (lower) than those based on average salt concentrations. However, in the limit as $\omega \rightarrow 1$, solutes can neither enter nor exit the specimen, such that $C_{t,ave} \rightarrow C_{ot}$, $C_{b,ave} \rightarrow C_{ob}$, and $\omega_{ave} \rightarrow \omega_o$ (Kang and Shackelford 2009).

3.2.5 Testing Program

Multiple-stage membrane tests were conducted in this study by sequentially circulating four KCl solutions (4.7, 9.3, 20, and 54 mM KCl) across the top boundary of the specimen for each test, while simultaneously circulating DIW across the bottom boundary of the specimen. After steady-state conditions were achieved for each stage of the test (i.e., after ΔP and *EC* were constant), the source circulating solution was replaced with the subsequent solution containing a higher concentration of KCl, and this process was repeated until all four stages were completed. This procedure resulted in test durations ranging from 96 to 154 d. The two rigid-wall membrane tests designated as RW1 and RW2 corresponded to specimen thicknesses, L , of 16.7 mm and 8.6 mm and total specimen porosities, n , of 0.92 and 0.80, respectively. The two flexible-wall membrane tests designated as FW1 and FW2 corresponded to initial effective stresses, σ' , of 34.5 kPa (5 psi) and 103 kPa (15 psi), respectively, and initial values of n immediately after consolidation, but prior to membrane testing, of 0.95 and 0.84, respectively.

3.3 RESULTS

3.3.1 Boundary Electrical Conductivity Values

The measured EC of the circulation outflow liquids versus time for the rigid-wall and flexible-wall membrane tests are presented in Fig. 3.7. The EC of the outflow liquid from both the top and the bottom of the specimen increased as the solute concentration of the circulation liquid increased. The increase in EC at the bottom of the specimen can be attributed initially to diffusion of any remnant ions contained within the pores of the BPN specimens and eventually to diffusion of Cl^- and K^+ completely through the specimen from the top boundary.

The differences in electrical conductivity, ΔEC , between the steady-state electrical conductivities, measured in the circulation outflows across the top and the bottom of the specimens, or EC_t or EC_b , relative to the limiting values of EC in the circulation inflows, i.e., $\Delta EC_t = EC_t - EC_{ot}$ and $\Delta EC_b = EC_b - EC_{ob}$, are plotted versus the average salt concentration across the specimen, C_{ave} , in Fig. 3.8. The values of ΔEC for the top of the specimen are negative, because $EC_t < EC_{ot}$ due to diffusion K^+ and Cl^- ions into the specimen at the top, whereas the values of ΔEC for the base of the specimen are positive, because $EC_b > EC_{ob}$ due to diffusion of any remnant ions in the pore water of the specimen, including K^+ and Cl^- ions, out of the bottom of the specimen. As shown in Fig. 3.8, the magnitude of ΔEC (positive or negative) increases with an increase in C_{ave} for all four tests due to the increase in concentration difference, ΔC , across the specimens during the sequential circulation of higher concentration KCl solutions in the multistage tests. This trend in ΔEC with C_{ave} is consistent with increased diffusion through the specimen with increasing C_{ave} .

For example, consider the following form of Fick's first law for steady-state diffusive solute mass flux, J_d , in soil (Shackelford and Daniel 1991):

$$J_d = -nD^* \frac{\Delta C}{L} \quad (3.5)$$

where n is the porosity of the soil, D^* is the effective diffusion coefficient of the diffusing chemical species, and ΔC is the difference in the concentration of chemical species across a specimen of length L . As defined by Shackelford and Daniel (1991), D^* in Eq. 3.5 is the product of the aqueous-phase or free solution diffusion coefficient for a specific chemical species, D_o , and the apparent tortuosity factor, τ_a , or $D^* = \tau_a D_o$, where $0 < \tau_a \leq 1$. As further defined by Malusis and Shackelford (2002b), τ_a equals the product of the matrix tortuosity factor, τ_m ($0 < \tau_m < 1$), representing the portion of the apparent tortuosity factor attributed to the geometry of the interconnected pore structure, and a restrictive tortuosity factor, τ_r ($0 \leq \tau_r < 1$), resulting from other factors that can affect solute diffusion through soil, such as anion exclusion and increased viscosity of the liquid adjacent to clay particles. In the case where semipermeable membrane behavior is evident, Manassero and Dominijanni (2003) propose that τ_r be taken as an inverse linear function of the membrane efficiency coefficient, ω , or $\tau_r = 1 - \omega$, which was supported by the experimental results reported by Malusis and Shackelford (2002a). Thus, as ω approaches unity corresponding to a perfect membrane, τ_r and, therefore, D^* and J_d approach zero as required by definition for ideal or perfect membrane behavior.

Of the factors affecting J_d , n and L should be relatively constant for a given test specimen. In terms of D^* , results of numerous tests have clearly shown that ω decreases

approximately semi-log linearly with increasing C_{ave} (e.g., Shackelford et al. 2003). Thus, J_d also would be expected to increase with increasing C_{ave} , since D^* is expected to increase with decreasing ω . Finally, when C_{ave} is defined with respect to the initial source concentrations, such that $C_{ave} = (C_{ot} + C_{ob})/2$ and C_{ob} is zero (i.e., DIW), $\Delta C (= C_{ob} - C_{ot})$ in Eq. 3.5 is directly related to C_{ave} , or $\Delta C = -C_{ot} = 2C_{ave}$. Thus, as C_{ave} increases, ΔC increases and, therefore, J_d increases.

As a result, as ΔC across the specimen increases from 4.7 to 54 mM during a given test, J_d across the top and bottom boundaries increases, resulting in a parallel effect on the magnitude of the ΔEC . In addition, the ΔEC is lower for the tests with lower porosity (i.e., RW2 vs. RW1) and for the test with a higher initial effective stress (i.e., FW2 vs. FW1). Finally, the ΔEC values for the flexible-wall membrane tests, FW1 and FW2, are greater than those for the rigid-wall membrane tests, RW1 and RW2, which is consistent with the lower membrane efficiencies measured for the specimens in the flexible-wall cells.

3.3.2 Boundary Water Pressures

The boundary water pressures measured at the top, u_{top} , and bottom, u_{bottom} , of the cell by the in-line pressure transducers are presented in Figs. 3.9 and 3.10 for the rigid-wall and flexible-wall cells, respectively. As shown in Figs. 3.9a and 3.10a, the magnitudes of u_{top} and u_{bottom} were essentially the same (i.e., $u_{top} \approx u_{bottom}$) for tests RW1 and FW1 during the first stage of the test when DIW was circulated across both the top and bottom specimen boundaries. However, for tests RW2 and FW2 (Fig. 3.9.b and 3.10.b), the magnitudes of u_{top} and u_{bottom} were slightly different resulting in a baseline pressure difference, $-\Delta P_o$. However, upon commencement of the circulation with the 4.7 mM KCl solution across the top of the specimens in all tests, the magnitude of u_{top} increased relative to that measured during the circulation of DIW, and u_{top} was

greater than u_{bottom} ($u_{top} > u_{bottom}$). Also, in the case of the rigid-wall tests, u_{bottom} was less than the backpressure ($u_{bottom} < u_{bp} \approx 2.0$ kPa) throughout the duration of these tests. However, u_{bottom} for the flexible-wall tests initially was less than the backpressure ($u_{bottom} < u_{bp}$) during circulation with 4.7 mM KCl, but eventually increased during the circulation of higher concentration KCl solutions (9.3 and 20 mM KCl for FW1 and FW2, respectively) and remained greater than the backpressure ($u_{bottom} > u_{bp}$) for the remainder of the test. Although, both trends (i.e., $u_{bp} < u_{bottom} < u_{top}$ and $u_{bottom} < u_{bp} < u_{top}$) have been reported by others (e.g., Kang and Shackelford 2010), the exact causes for these trends remain unknown at this time.

For the flexible-wall test, the confining stress, σ_c , was held constant at 207 kPa (30 psi) and 172 kPa (25 psi) for FW1 and FW2, respectively. However, since the boundary water pressures (u_{bottom} and u_{top}) changed with time, the boundary effective stresses at the top, σ'_{top} ($= \sigma_c - u_{top}$), and the bottom, σ'_{bottom} ($= \sigma_c - u_{bottom}$), of the specimen also changed with time (see Fig. 3.11a and Fig. 3.12.a), such that the average effective stress, σ'_{ave} , based on these boundary effective stress $((\sigma'_{top} + \sigma'_{bottom})/2)$ also was not constant (see Fig. 3.11.b and Fig. 3.12.b). In general, the σ'_{ave} for FW1 decreased from greater than 48 kPa (7 psi) during circulation of DIW to less than 10 kPa (1.5 psi) during circulation of 54 mM KCl, whereas σ'_{ave} for FW2 decreased from greater than 128 kPa (18.6 psi) during circulation of DIW and 4.7 mM KCl to less than 55 kPa (8 psi) during circulation of 54 mM KCl. Because the values of σ_c for each test were constant throughout the durations of the tests, the trends in σ'_{ave} are a direct result of the aforementioned trends in u_{bottom} and u_{top} .

3.3.3 Chemico-Osmotic Pressures

The measured chemico-osmotic pressure differences ($-\Delta P > 0$) are presented in Figs. 3.13 and 3.14 for the rigid-wall tests and the flexible-wall tests, respectively. The baseline differential pressure, $-\Delta P_o$, induced during the circulation of DIW along both boundaries (i.e., $C_{ot} = C_{ob} = 0$) varied from 6.7 kPa for RW2 to -5.0 kPa for FW2. As described in Malusis et al. (2001), possible reasons for a nonzero baseline differential pressure include slight differences in the hydraulic resistance of the porous plastic disks along the top and bottom of the specimen, which would result in different head losses within the disks between the points where the circulation liquids enter the disks and the middle of the disk where the pressure difference is measured, and slightly different flow rates across the top and bottom of the specimen due to slight differences in the machining of the syringes. Therefore, corrected or effective values of the differential pressure, $-\Delta P_e [= -\Delta P_{ss} - (-\Delta P_o)]$, as summarized in Table 3.2, were used to calculate ω_o and ω_{ave} .

The values of $-\Delta P_e$ for test RW1 with $n = 0.92$ increased from 18.4 kPa during the circulation of 4.7 mM KCl across the top to the specimen to 59.0 kPa during the circulation of 54 mM KCl (see Fig. 3.13a). The $-\Delta P_e$ for RW2 with $n = 0.80$ was higher than that for the RW1, in that the $-\Delta P_e$ for RW2 increased from 21.3 kPa during the circulation of 4.7 mM KCl across the top of the specimen to 59.0 kPa during the circulation of 54 mM KCl for RW2 (see Fig. 3.13b). The steady-state $-\Delta P_e$ for RW1 and RW2 during the circulation of 54 mM KCl was lower than the aforementioned peak value of $-\Delta P_e$ as a result of post-peak degradation resulting from diffusion of solutes into and subsequently through the specimen (e.g., maximum $-\Delta P_e = 59.0$ kPa versus steady-state $-\Delta P_e = 44.3$ kPa for RW1). This time-dependent, post-peak degradation of $-\Delta P_e$, especially at higher KCl concentrations, is consistent with the same trend previously

reported by others (e.g., Malusis and Shackelford 2002a), and has been attributed to progressive compression of the diffuse double layer surrounding individual clay particles due to increasing salt concentration within the pores resulting from diffusion of KCl from the upper boundary (Fritz 1986; Malusis and Shackelford 2002a; Shackelford and Lee 2003; Shackelford et al. 2003).

The values of $-\Delta P_e$ for the flexible-wall membrane tests were lower than those for the rigid-wall tests, with $-\Delta P_e$ for FW1 increasing from 12.4 kPa during circulation of 4.7 mM KCl to 14.6 kPa during circulation of 20 mM KCl (see Fig. 3.14a), and $-\Delta P_e$ for FW2 increasing from 10.3 kPa during circulation of 4.7 mM KCl to 35.7 kPa during circulation of 20 mM KCl (see Fig. 3.14b). This trend of a slightly lower $-\Delta P_e$ for the flexible-wall versus rigid-wall membrane tests also was observed by Kang and Shackelford (2009) for their tests performed using a specimen of a GCL, and was attributed to the different stress conditions and volume control conditions in the two types of cells.

One possible explanation for the difference in performance between the rigid-wall tests and the flexible-wall tests may be the circumstances under which the BPN was initially exposed to water. In the rigid-wall cell, the BPN was permeated with water in a confined (fixed volume) cell that restricted swelling of the superabsorbent polymer portion of the BPN and limited flushing of the excess low molecular weight polymer from the system, resulting in smaller hydraulically active pores (i.e., pores are smaller and more pores are clogged with excess low molecular weight polymer that exists in the BPN), as described by Scalia (2012). In contrast, the BPN in the flexible-wall cell was permeated with water under an essentially constant σ' , average value for σ' of 34.5 kPa (5 psi) or 103 kPa (15 psi), but the specimen was able to swell due to the propensity for montmorillonite and the superabsorbent polymer portion of the BPN to sorb

water. This swelling resulted in larger hydraulically active pores and additional flushing of the excess low molecular weight polymer from the system and, therefore, less clogging of pores prior to the membrane testing stage of the test.

3.3.4 Membrane Efficiency Coefficients

The values of ω_o and ω_{ave} for the membrane tests based on Eqs. 3.2 and 3.3, respectively, are shown as a function of C_{ave} ($= \Delta C_o/2$) in Fig. 3.15. With the exception of the values of ω_o and ω_{ave} for test FW2 with the 4.7 mM KCl solution, the results are consistent with previous results reported by Malusis and Shackelford (2002a), Kang and Shackelford (2009) in that (1) the values of ω_{ave} are generally greater than the values of ω_o for a given average salt concentrations across the specimen, (2) the values of both ω_o and ω_{ave} decrease approximately semi-log linearly with increasing difference in KCl concentration across the specimens, (3) the values of ω_o or ω_{ave} from the rigid-wall tests are greater than those from the flexible-wall tests, and (4) the values of ω_o or ω_{ave} are greater for specimens at higher initial effective stresses and specimens with lower initial porosities.

The values of ω_o and ω_{ave} for test FW2 with the 4.7 mM KCl solution are anomalous due to a loss of system pressure resulting in loss of the applied cell pressure during this particular stage of this particular test. The applied system pressure unexpectedly failed approximately 14 d into the circulation of 4.7 mM KCl for FW2. Upon restoration of the system pressure, both the in-line and differential pressures returned to the same values prior to loss of system pressure. However, the calculated ω_o and ω_{ave} were lower than the expected values, in that the values of ω_o and ω_{ave} for test FW2 were expected to be greater than the same respective values for test FW1, because test FW2 was conducted at a higher effective stress than test FW1 [103 kPa (15 psi) vs. 34.5 kPa (5 psi), respectively].

3.3.5 Volume Changes

As described in Kang and Shackelford (2009), although drainage was not allowed to occur during the circulation stages of the membrane tests, drainage from the specimen did occur during the brief (< 5 min) refilling and sampling stages of the test when the valves to the reservoirs and the cell (valves 1, 3, 6 and 7 in Fig. 3.3) were simultaneously and temporarily opened to re-establish the backpressure. Kang and Shackelford (2009) attributed the drainage to an increment in effective stress resulting from physico-chemico interactions between the pore water in the bentonite and the individual particles of bentonite. Theoretically, an increase in salt concentration in the pore water results in decrease in the repulsive electrical forces relative to the adsorptive forces between individual soil particles (i.e., so-called R – A effect), such that the effective stress in the soil also increases resulting in compression of the soil (i.e., provided drainage is allowed). Such an increase in salt (KCl) concentration in the pore water is consistent with diffusion of the KCl into the specimens as previously described. This phenomenon has been referred to as osmotic consolidation (e.g., Mitchell 1976; Barbour and Fredlund 1989; Di Maio 1996).

This increase in effective stress in response to the increased salt concentrations is in contrast to the previously noted decrease values of σ'_{ave} measured at the boundaries of the specimen (see Section 3.2.2.). A decrease in σ'_{ave} should lead to an increase in volume (i.e., swelling of the specimens). However, the specimens compressed instead of swelled with an increase in the salt concentrations and corresponding decrease in σ'_{ave} , indicating that the R – A effect likely was the dominant mechanism in terms of volume change of the specimens. In addition, when the back pressure was re-established momentarily during the sampling/refilling intervals, the initial σ' of 34.5 kPa (5 psi) or 103 kPa (15 psi) also was re-established

momentarily, resulting in a brief increase in σ' relative to the value established during the membrane testing stage. This brief increase in σ' also could have caused specimen compression during the refilling and sampling stages.

Accordingly, volume changes were recorded for the membrane tests conducted in the flexible-wall cell using the cell-water accumulator attached to the flexible-wall cell (see Fig. 3.4b). The resulting measured values of incremental volume change, $-\Delta V$, and cumulative volume change, $\sum(-\Delta V)$, are presented in Fig. 3.16 and the resulting changes in bulk specimen porosities are summarized in Table 3.3. The ΔV values generally were negative, indicating that the volume of the specimen decreased during the test (i.e., a final volume less than the initial volume). The magnitude of $-\Delta V$ increased with increasing concentration of KCl. For FW1 with $\sigma' = 34.5$ kPa (5 psi), $-\Delta V$ was less than ± 0.5 mL during the circulation of DIW and 4.7 mM KCl, whereas $-\Delta V$ was as much as 3.2 mL during the circulation of 54 mM KCl. The $\sum(-\Delta V)$ was 46.3 mL which corresponds with a cumulative volumetric strain, $\sum(-\Delta V)/V_o$, of 25 % (see Fig. 3.17.c). The incremental volumetric strains, $(-\Delta V)/V_o$, for FW1 were less than -0.5 % during the circulation of DIW, 4.7 mM KCl, and 9.3 mM KCl, but increased to as much as 1.7 % during the circulation of 54 mM KCl, which is consistent with an increasing R – A effect with increasing salt concentration.

In contrast, for FW2 with $\sigma' = 103$ kPa (15 psi), $-\Delta V$ was as much as -2 mL during circulation of DIW and 4.7 mM KCl, but $-\Delta V$ was less than 1.5 mL during circulation of 54 mM KCl. During the circulation of both DIW and the 4.7 mM KCl solution after the loss of cell pressure, the specimen swelled likely as a result of the affinity for water of the superabsorbent polymer portion of the BPN. However, during the remainder of the test, the specimen compressed, i.e., volume of the specimen decreased, which is similar to the results for FP1 and

consistent with the R-A effect with increasing salt concentrations. The $\sum(-\Delta V)$ was 20.7 mL, which corresponds with a value for $\sum(-\Delta V)/V_o$ of 27 % (refer to Fig. 3.17.d). The incremental volumetric strains, $(-\Delta V)/V_o$, were as much as -2.5 % during the circulation of DIW and 4.7 mM KCl after the loss of cell pressure, were generally less than 1.0 % during the circulation of 9.3 mM KCl and 20 mM KCl, and then increased to as much as 2.0 % during the circulation of 54 mM KCl.

3.3.6 Limits on Membrane Behavior

As previously described, an approximately semi-log linearly relationship between ω and C_{ave} has been shown to exist on the basis of numerous experimental results (e.g., see Shackelford et al. 2003). This relationship is shown schematically in Fig. 3.18, where the slope of relationship is defined as the membrane index, I_ω , and the limiting values of C_{ave} are defined as the threshold concentration, $C_{ave,\omega}$, corresponding to the concentration below which membrane behavior occurs (i.e., $\omega > 0$ for $C_{ave} < C_{ave,\omega}$), and the perfect membrane concentration, $C_{ave,pm}$, corresponding to the concentration below which the material behaves as a perfect membrane (i.e., $\omega = 1$ for $C_{ave} < C_{ave,pm}$). As depicted in Fig. 3.18, the trend between ω versus C_{ave} in reality likely becomes non semi-log linear as the concentrations approach $C_{ave,pm}$ and $C_{ave,\omega}$. However, the exact functional forms of this non semi-log linear behavior are unknown, such that semi-log linear regressions can be used as a first approximation (Shackelford et al. 2003).

Accordingly, semi-log linear regressions to the data presented in Fig. 3.15 are shown in Fig. 3.19, and the resulting regression coefficients along with the corresponding coefficients of determination (r^2) are summarized in Table 3.4. The r^2 values indicate that the regressions are reasonable ($r^2 \geq 0.98$) over the range of measured data with somewhat better regressions based

on the results of the rigid-wall tests (i.e., $r^2 > 0.99$) versus those for the flexible-wall tests (i.e., $r^2 > 0.94$). The threshold concentrations range from 25 mM for FW1 based on ω_o to 68 mM for RW2 based on ω_{ave} . The values for the membrane index, I_ω , ranged from 0.60 to 0.67 for tests RW1 based on ω_{ave} and RW2 based on ω_o , respectively, whereas the I_ω values ranged from 0.38 to 0.55 for tests FW2 based on ω_o and FW1 based on ω_{ave} , respectively. In general, the threshold concentrations based on the two flexible-wall tests were lower than those based on the two rigid-wall tests. The higher threshold concentrations for the rigid-wall tests indicate that the BPN under these test conditions will exhibit membrane behavior at higher C_{ave} which is advantageous in practical applications. This increased performance of BPN in the rigid wall relative to BPN in the flexible wall cannot be attributed to the porosity alone because the porosities of the RW and FW tests are similar (RW1 similar to FW1 and RW2 similar to FW2, refer to Table 3.4.).

3.4 DISCUSSION

3.4.1 Comparison of Membrane Efficiency Coefficients

The measured values of ω from this study are compared with those previously reported for tests conducted using GCLs (Malusis and Shackelford 2002a; Kang and Shackelford 2009) in Fig. 3.20 and Fig. 3.21. For the rigid-wall membrane tests performed using the BPN, values of both ω_o and ω_{ave} are higher than those reported by Malusis and Shackelford (2002a) for a GCL that was 8-mm thick (i.e., $L = 8$ mm) with a lower porosity of 0.74 (see Fig. 3.20). Also, values of both ω_o and ω_{ave} for the flexible-wall membrane tests conducted in this study are higher than those reported by Kang and Shackelford (2009) for a GCL under similar effective confining stresses of 34.5 kPa (5 psi) and 103 kPa (15 psi) (see Fig. 3.21). In addition, unlike the GCL specimens that were flushed (leached) of soluble salts prior to membrane testing to enhance their

potential for reflecting a measureable membrane efficiency, the higher values of ω_o and ω_{ave} for the tests performed in this study using the BPN were achieved without flushing (leaching) of soluble salts from the BPN specimens prior to membrane testing. Thus, the BPN specimens not only reflected greater membrane efficiencies than previously reported for specimens of a GCL containing a traditional bentonite, but also did so under more disadvantageous initial conditions.

There are at least two possible mechanistic explanations for the improved performance of the BPN compared to the bentonite in a GCL (e.g. see Scalia 2012). One explanation is that the superabsorbent polymer portion of the BPN swells in low *EC* solutions, resulting in osmotic swelling and smaller hydraulically active pores than those in the bentonite typically found in GCLs. Another explanation relates to an excess of low molecular weight polymer in the BPN during the manufacturing process resulting from incomplete polymerization (chain termination), leading to a need to remove excess polymer from the outflow during permeability testing of the BPN to prevent the permeameters from clogging (Scalia 2012). This excess low molecular weight polymer is hypothesized to clog the hydraulically active pores resulting in low *k* of the BPN. These mechanisms that have been postulated to result in lower *k* of the BPN compared to traditional bentonites in GCLs also may contribute to the improved performance of the BPN in terms of membrane behavior.

3.4.2 Comparison of the Limits to Membrane Behavior

Semi-log linear regressions to the results reported by Malusis and Shackelford (2002a) and Kang and Shackelford (2009) for traditional GCLs are included in Figs. 3.22 and 3.23, respectively. The resulting limits on membrane behavior for the GCLs also are summarized in Table 3.5. The threshold concentrations, $C_{ave,\omega}$, for the BPN are greater than those for the GCLs

tested both the rigid-wall cells and the flexible-wall cells. The highest $C_{ave,\omega}$ determined for the BPN in the rigid-wall cell was 67.7 mM compared to 48.0 mM for the GCL. Whereas the highest $C_{ave,\omega}$ of 62.2 mM for the flexible-wall cell membrane test on the BPN with $\sigma' = 103$ kPa (15 psi) is significantly greater than $C_{ave,\omega} = 26.1$ mM reported for the GCL under similar stress conditions.

As previously mentioned (Section 3.3.6), the higher $C_{ave,\omega}$ for the BPN compared to the GCL would be beneficial in practical applications in that the BPN would presumably exhibit membrane behavior at higher concentrations. The superior performance of the BPN compared to a GCL is likely due, in part, to the superabsorbent polymer portion of the BPN resulting in higher swell and smaller hydraulically active pores resulting in enhanced membrane behavior. In addition, clogging of any hydraulically active pores by excess low molecular weight polymer also may have contributed to the enhanced membrane behavior of the BPN relative to that of a GCL containing a traditional bentonite.

3.4.3 Comparison of Volume Changes

The extent of the volume changes that occurred with the BPN specimens in this study was far greater than that previously reported for membrane tests in flexible-wall cells using GCLs containing traditional bentonites (Kang and Shackelford 2009; Kang and Shackelford 2011). For example, the cumulative volume change, $\sum(-\Delta V)$, for a traditional GCL tested at $\sigma' = 34.5$ kPa (5 psi) as reported by Kang and Shackelford (2011) was 5.98 mL, whereas, the $\sum(-\Delta V)$ for BPN tested at the same effective stress in this study was 46.3 mL, or almost eight times greater. However, similar to the traditional GCL, the $\sum(-\Delta V)$ for the BPN decreased with increased σ' [$\sum(-\Delta V) = 20.7$ mL versus 46.3 mL for $\sigma' = 103$ kPa (15 psi) for FW2 and $\sigma' = 34.5$

kPa (5 psi) for FW1, respectively].

The volume changes observed for the traditional GCL were attributed to compression of the diffuse double layers as the concentration of the salts in the pore water increased (Kang and Shackelford 2009). In addition to this explanation, the increased volume change of the BPN may be attributed, in part, to the unique properties of the BPN. The initial volume, V_o , of the BPN specimen was greater than that of the GCL (e.g., 191 mL versus 75.5 mL, respectively) for tests conducted at $\sigma' = 34.5$ kPa (5 psi), because of the greater swelling of the BPN versus a traditional GCL ($SI = 73$ mL/2g vs 25 to 35 mL/2g). This increased swelling for the BPN is a result of the superabsorbent polymer in the BPN (Scalia et al. 2011), which likely caused greater volume changes throughout the membrane test compared to that of a GCL.

The swelling capacity of the superabsorbent polymer in the BPN is affected by the applied load (i.e., σ') and the salt concentration in the pores (Buchholz and Graham 1998). In addition, for superabsorbent polymers, the effect of the salt concentration in the pores on the swelling capacity decreases with increasing load (Buchholz and Graham 1998). These properties of superabsorbent polymer correlate with the observed volume changes of the BPN. For example, for the membrane test on the BPN at the higher σ' [i.e., $\sigma' = 103$ kPa (15 psi) for FW2], the specimen swelled less resulting in a lower V_o ($V_o = 75$ mL versus 191 mL for FW2 and FW1, respectively), and consequently less volume change throughout the membrane test (i.e., $\sum(-\Delta V) = 20.7$ mL versus 46.3 mL for FW2 versus FW1, respectively). In addition, the volume change of the BPN decreased with increasing σ' . For example, the value of $-\Delta V$ was less than 1.5 mL during circulation of 54 mM KCl for FW2 [$\sigma' = 103$ kPa (15 psi)], whereas that for FW1 [$\sigma' = 34.5$ kPa (5 psi)] was as much as 3.2 mL during the circulation of 54 mM KCl.

3.4.4 Effect of Effective Stress and Boundary Salt Concentration

The effect of the σ' and the boundary salt concentrations on the measured membrane efficiencies is illustrated in Figs. 3.24 and 3.25. The ratio of the membrane efficiency coefficient at any σ' , relative to that at σ' of 34.5 kPa (5 psi), or $R_{\omega, \sigma'} [= \omega @ \sigma' / \omega @ \sigma' = 34.5 \text{ kPa (5 psi)}]$, is plotted as a function of C_{ave} for the BPN and a GCL (Kang and Shackelford 2011) in Fig. 3.24. In general, the values of $R_{\omega, \sigma'}$ are greater than unity as would be expected on the basis of studies that have shown that an increase in σ' results in a higher membrane efficiency (Kang and Shackelford 2010). In addition, the effect of increasing effective stress is greater with higher average source concentrations across the specimen. However, this increase $R_{\omega, \sigma'}$ is lower for the BPN relative to that of the GCL at similar σ' , especially for higher concentrations (e.g., $C_{ave} = 27$ mM KCl or $C_{ot} = 54$ mM KCl). As described in Kang and Shackelford (2011), the pore sizes decrease with increasing σ' , which tends to offset the effect of an increase in C_{ot} on the membrane efficiency. The lower increase in values of $R_{\omega, \sigma'}$ for the BPN specimens relative to that of the GCL suggests that the BPN is less sensitive to σ' than the GCL, likely due, in part, to the differences in the compressibility of the BPN relative to that for the GCL. As previously discussed (Section 3.4.3), the compressibility of the BPN likely is greater than that of the GCL as a result of the superabsorbent polymer portion of the BPN.

The ratio of steady-state membrane efficiencies, $R_{\omega, ss} (= \omega_{ave} / \omega_o)$, are plotted versus the source KCl concentration in Figure 3.25. The values of $R_{\omega, ss}$ are shown to increase approximately semi-log linearly with increasing C_{ot} . The increase in $R_{\omega, ss}$ versus C_{ot} indicates that the system deviates further from the assumed "perfectly flushing" boundary conditions as the source KCl concentration increases. At higher source KCl concentrations, the increase in the diffusive mass flux through the specimens as previously described results in a greater decrease in

the KCl concentration during circulation of the solution across the top of the specimen and increasingly higher solute concentrations at the bottom of the specimen. Thus, the difference between ω_{ave} , which is calculated using C_{ave} (Eq. 3.3), and ω_o , which is calculated using C_o (Eq. 3.2), increases with increasing C_{ot} , such that the values of $R_{\omega,ss}$ increase with increasing C_{ot} . In addition, the slope of this semi-log linear regression, B , is significantly greater for the tests using BPN versus those using GCLs ($B = 0.710$ and 0.392 for the BPN versus 0.203 and 0.199 for the GCLs), indicating that boundary conditions for the tests using the BPN were further from "perfectly flushing" than those for the tests on the GCL. This result was expected, because the circulation rate for the tests using the BPN was $2.3 \times 10^{-10} \text{ m}^3/\text{s}$ which is almost two times slower than the circulation rate for the tests using the GCL of $4.2 \times 10^{-10} \text{ m}^3/\text{s}$. In general, the slower the circulation rate, the further the boundary conditions are from the limiting case of "perfectly flushing" conditions (e.g., see Malusis et al. 2001).

3.4.5 Practical Significance of Results

As shown previously by others (Malusis et al. 2003; Kang and Shackelford 2010; Kang and Shackelford 2011), the practical significance of the results of this study can be illustrated using a simplified analysis showing the influence of chemico-osmosis due to membrane behavior on the total liquid flux through a containment barrier. This simplified analysis has been conducted using the membrane tests results for the BPN evaluated in this study, and the results of this analysis are compared with the results of previous analyses based on the membrane behavior of a traditional GCL to illustrate the comparatively improved performance of the BPN.

The total liquid flux, q , through a soil that behaves as a semi-permeable membrane is the sum of the hydraulic flux, q_h , the flow in response to a hydraulic gradient in accordance with

Darcy's Law, and the chemico-osmotic liquid flux, q_π , the flow in response to a solute concentration gradient, or $q = q_h + q_\pi$ (Barbour and Fredlund 1989; Malusis et al. 2003; Kang and Shackelford 2010). The contribution of the q_π to the q can be illustrated by normalizing q with respect to q_h as follows (e.g., Yeo et al. 2005; Henning et al. 2006; Kang and Shackelford 2010, 2011):

$$\frac{q}{q_h} = \frac{q_h + q_\pi}{q_h} = 1 + \frac{q_\pi}{q_h} = 1 - \frac{\Delta P}{\gamma_w \Delta h} \quad (3.6)$$

where γ_w = unit weight of water (i.e., 9.81 kN/m³ assuming dilute solutions), Δh = total hydraulic head loss across the barrier, and ΔP is the chemico-osmotic pressure difference. As indicated in Fig. 3.26, the value of Δh in Eq. 3.6 will be negative, since the final hydraulic head, h_f , at the base of the barrier will be less than the initial hydraulic head at the top of the barrier, h_i , or $\Delta h = h_f - h_i < 0$. Typically, the pressure head at the base of the barrier is assumed to be zero such that $\Delta h = -(L + h_l)$ where L is the thickness of the barrier and h_l is the height of liquid contained above the barrier. This scenario is similar to the membrane testing scenario where the concentration of the liquid on the top or the containment side of the barrier is greater than the concentration on the bottom or the outer side of the barrier. The resulting ΔP is also negative, such that the q_π is directed inward reducing the total liquid flux, q , through the barrier.

The results of this simplified analysis are presented in Fig. 3.26 in terms of q/q_h versus the source salt concentration in the containment liquid, C_o . To calculate the magnitude of Δh , the typical thickness of a GCL barrier ($L \leq 10$ mm) was considered to be negligible compared to the h_l ($h_l \gg L$) which was assumed to be 0.3 m (1 ft), the typical regulatory maximum height of liquid allowed on top of a barrier used in solid waste disposal. Therefore, Δh was assumed to be

equal to h_l . Also, the values of ΔP_e presented in Table 3.2 were used for the ΔP in Eq. 3.6.

Several observations are apparent from the results presented in Fig. 3.26. First, all of the values of q/q_h are negative implying inward liquid flux through a BPN barrier for the range concentrations considered in this study. Second, the results for the analyses based on all of the tests except FW1, the magnitudes of q/q_h increase with increasing C . This trend is a result of an increase in $-\Delta P_e$ with increasing C . Similar trends were reported in Malusis et al. (2003) for a GCL, whereas the opposite trend was reported in Kang and Shackelford (2010) for a compacted clay liner (CCL) amended with 5 % (by dry wt.) of sodium bentonite. This difference in trends was attributed by Kang and Shackelford (2010) to an increase in the resistance to the potential degradation of membrane behavior with increase in the content of bentonite in the barrier. In addition, the magnitude of q/q_h increases with decreasing n (e.g., RW2 vs. RW1) and, in general, increases with increasing σ' (e.g., FW2 vs. FW1) as a result of higher values of $-\Delta P_e$ and the corresponding ω for barriers with lower n or higher σ' .

The results of this analysis also are compared with analyses from previous studies based on the results of membrane tests on GCLs in Fig. 3.27 (Malusis et al. 2003; Kang and Shackelford 2010). For a given C , the ratio of q/q_h is higher for the BPN than for the GCL regardless of n or σ' (refer to Figs. 3.27a and 3.27b, respectively). The liquid flux is always upward for the BPN, whereas the liquid flux is downward for the GCL at a lower σ' of 34.5 kPa (5 psi) and higher C of 47 mM (see Fig. 3.27 b). This upward liquid flux results in negative advection, or advection in the direction opposite to that of diffusion, potentially decreasing the contaminant migration through the barrier. Thus, the improved performance of a barrier composed of BPN compared to a GCL is expected based on the values of ω for BPN compared to values of ω for GCLs (see Fig. 3.23).

3.5 CONCLUSION

The results of a laboratory experimental program to determine the existence of semipermeable membrane behavior for a polyacrylic acid (PAA) polymerized bentonite material known as a bentonite polymer nanocomposite, or BPN, were presented. The results indicate that the BPN exhibited membrane behavior when exposed to KCl initial concentration differences ranging from 4.7 to 54 mM. A comparison of the measured membrane behavior for the BPN with that previously reported for an non-polymerized bentonite contained in a GCL based on similar testing conditions shows that the BPN exhibited greater membrane behavior.

For example, the membrane efficiency coefficient, ω , for a specimen of the BPN with a porosity of 0.92 contained within a rigid-wall cell was 0.43 based on an initial concentration difference of 20 mM KCl, whereas ω for a GCL specimen with a lower (more favorable) porosity of 0.74 also contained within a rigid-wall cell and subjected to the same initial concentration difference was only 0.30. Similarly, the ω for a specimen of the BPN contained within a flexible-wall cell at an initial effective stress of 34.5 kPa (5 psi) and subjected to an initial concentration difference of 9.3 mM KCl was 0.32, whereas ω for a GCL specimen also contained within a flexible-wall cell at the same initial effective stress but subjected to a slightly lower (more favorable) concentration difference of 8.7 mM KCl was only 0.20. Also, unlike the GCL specimens, the BPN specimens were not permeated with deionized water (DIW) prior to membrane testing to remove soluble salts and enhance the potential for membrane behavior as were the specimens. Thus, relative to values of ω previously reported for GCL specimens containing a traditional sodium bentonite, the BPN evaluated in this study exhibited enhanced membrane behavior under conditions that more adverse to those for the GCL specimens.

The measured values of ω for the BPN depended on the type of cell used for the test (i.e.,

rigid-wall cell versus flexible-wall cell), the concentration of the KCl solution that was circulated across the boundaries of the test specimen, and either the porosity, n , for the specimens contained in rigid-wall cells or the initial effective stress, σ' , for specimens contained in the flexible-wall cells. In general, the values of ω were greater the lower the initial value of n or the higher the initial value of σ' , the lower the difference in concentration of KCl established across the test specimen, and for specimens tested in rigid-wall cells. These results are consistent with previously reported results based on similar tests conducted using traditional sodium bentonites.

The limits on membrane behavior for the BPN and for natural bentonites used in GCLs also were compared. The threshold concentrations, $C_{ave,\omega}$, for the BPN were greater than those based on the results previously reported for a GCL under similar test conditions. Higher values of $C_{ave,\omega}$ correlate with the existence of membrane behavior, (i.e., $\omega > 0$) over higher ranges in salt concentrations and, therefore, are advantageous in geoenvironmental containment applications.

The results of a simplified analysis based on the use of the BPN as a containment barrier indicate that the existence of membrane behavior can have a significant beneficial impact on the performance of a barrier. For example, the results of the analyses indicated that the magnitude of the chemico-osmotic counter flow was greater than that of the hydraulic flow resulting in a net inward liquid flux, such that no outward solute flux would be expected over the range of salt concentrations considered in this study. This result is more significant than that previously reported for a GCL used as the containment barrier in the same situation, such that the use of the BPN would be expected to provide an improved containment performance.

Table 3.1. Chemical properties of liquids used in study.

Liquid	Concentration		<i>pH</i>	Electrical Conductivity, <i>EC</i> (mS/m), @ 25°C
	(mM)	(mg/L)		
De-ionized Water	0	0	7.35	0.06
KCl Solutions	4.7	350	5.31	70.7
	9.3	690	5.20	139.2
	20	1500	5.28	276
	54	4000	5.24	661

Table 3.2. Results of membrane testing on bentonite polymer nanocomposite using rigid-wall (RW) and flexible-wall (FW) cells.

Test No.	Porosity, n	Initial Effective Stress, σ' [kPa (psi)]	Source KCl Concentration. C_{ot} (mM)	Maximum Chemico-Osmotic Pressure Difference (kPa)		Effective (Measured) Chemico-Osmotic Pressure Difference, $-\Delta P_e$ (kPa)	Membrane Efficiency Coefficient @ Steady-State	
				$-\Delta\pi_o^{(a)}$	$-\Delta\pi_{ave}^{(b)}$		$\omega_o^{(a)}$	$\omega_{ave}^{(b)}$
RW1	0.92	NA	4.7	22.9	21.9	18.4	0.80	0.84
			9.3	45.3	43.6	30.1	0.65	0.69
			20	97.4	83.2	41.6	0.43	0.50
			54	263	206	44.3	0.17	0.21
RW2	0.80	NA	4.7	22.9	22.8	21.3	0.88	0.88
			9.3	45.3	44.5	34.9	0.73	0.76
			20	97.4	88.0	47.5	0.46	0.51
			54	263	213	54.3	0.20	0.25

Table 3.2 Results of membrane testing on bentonite polymer nanocomposite using rigid-wall (RW) and flexible-wall (FW) cells. (continued).

Test No.	Porosity, n	Initial Effective Stress, σ' [kPa (psi)]	Source KCl Concentration. C_{ot} (mM)	Maximum Chemico-Osmotic Pressure Difference (kPa)		Effective (Measured) Chemico-Osmotic Pressure Difference, $-\Delta P_e$ (kPa)	Membrane Efficiency Coefficient @ Steady-State	
				$-\Delta\pi_o^{(a)}$	$-\Delta\pi_{ave}^{(b)}$		$\omega_o^{(a)}$	$\omega_{ave}^{(b)}$
FW1	0.94 – 0.95	34.5 (5)	4.7	22.9	19.3	12.4	0.55	0.63
			9.3	45.3	32.2	14.6	0.32	0.45
			20	97.4	60.7	13.4	0.14	0.22
			54	263	150	9.9	0.04	0.07
FW2	0.78 – 0.84	103 (15)	4.7	22.9	22.5	10.3	0.46	0.45
			9.3	45.3	37.6	17.3	0.38	0.46
			20	97.4	70.0	24.2	0.25	0.35
			54	263	165	26.0	0.10	0.15

(a) Based on difference in initial (source) KCl concentrations; (b) based on difference in average, boundary KCl concentrations

Table 3.3. Bulk porosities of test specimens during membrane testing in flexible-wall (FW) cells.

Stage of Test	Test Designation	
	FW1 [$\sigma' = 34.5 \text{ kPa (5 psi)}$]	FW2 [$\sigma' = 103 \text{ kPa (5 psi)}$]
After Consolidation	0.95	0.84
After DIW Circulation	0.95	0.87
After 4.7 mM KCl Circulation	0.95	0.84
After 9.3 mM KCl Circulation	0.95	0.84
After 20 mM KCl Circulation	0.95	0.82
After 54 mM KCl Circulation	0.94	0.78

Table 3.4. Results of regression analyses for the specimens of the bentonite polymer nanocomposite tested in this study (see Figs. 3.18 and 3.19).

Test No.	Porosity, (n)	Initial Effective Stress, σ' [kPa (psi)]	Definition of Membrane Efficiency Coefficient ^(a)	Regression Results: $\omega = \omega_{ref} - I_{\omega} \cdot \log C_{ave}$ ^(b)			Limiting Average Concentrations, C_{ave} (mM)	
				ω_{ref}	I_{ω}	r^2	@ $\omega = 0, C_{ave,\omega}$	@ $\omega = 1, C_{ave,pm}$
RW1	0.92	NA	ω_o	1.0	0.62	1.0	50	1.2
			ω_{ave}	1.1	0.60	1.0	61	1.4
RW2	0.80	NA	ω_o	1.1	0.67	0.99	52	1.6
			ω_{ave}	1.1	0.62	0.99	68	1.7
FW1	0.94 - 0.95	34.5 (5)	ω_o	0.68	0.49	0.94	25	0.22
			ω_{ave}	0.81	0.55	0.98	30	0.46
FW2	0.78 - 0.84	103 (15)	ω_o	0.62	0.38	1.0	47	0.10
			ω_{ave}	0.75	0.42	0.99	62	0.25

^(a) ω_o = membrane efficiency coefficient based on initial (source) salt concentrations

ω_{ave} = membrane efficiency coefficient based on average boundary salt concentrations

^(b) ω_{ref} = reference membrane efficiency coefficient corresponding to $\log C_{ave} = 0$; I_{ω} = the membrane index as defined by Shackelford et al. (2003) and illustrated schematically in Fig. 3.18

Table 3.5. Results of regression analyses shown based on data from the literature for geosynthetic clay liners (see Figs. 3.22 and 3.23).

Type of Cell	Porosity, n	Initial Effective Stress, σ' [kPa (psi)]	Definition of Membrane Efficiency Coefficient (a)	Regression Results for: $\omega = \omega_{ref} - I_{\omega} \cdot \log C_{ave}$ (b)			Limiting Average Concentrations, C_{ave} (mM)	
				ω_{ref}	I_{ω}	r^2	@ $\omega = 0$, $C_{ave,\omega}$	@ $\omega = 1$, $C_{ave,pm}$
Rigid-Wall ^(c)	0.74	NA	ω_o	0.81	0.50	1.0	44	0.42
			ω_{ave}	0.83	0.49	1.0	48	0.45
Flexible-Wall ^(d)	0.79-	34.5 (5)	ω_o	0.49	0.39	0.92	18	0.049
	0.81		ω_{ave}	0.65	0.51	0.94	19	0.21
Flexible-Wall ^(d)	0.79-	103 (15)	ω_o	0.57	0.41	0.94	24	0.092
	0.80		ω_{ave}	0.68	0.48	0.95	26	0.22

(a) ω_o = membrane efficiency coefficient based on initial (source) salt concentrations

ω_{ave} = membrane efficiency coefficient based on average boundary salt concentrations

(b) ω_{ref} = reference membrane efficiency coefficient corresponding to $\log C_{ave} = 0$; I_{ω} = the membrane index as defined by Shackelford et al. (2003) and illustrated schematically in Fig. 3.18

(c) From Malusis and Shackelford (2002a).

(d) From Kang and Shackelford (2011).

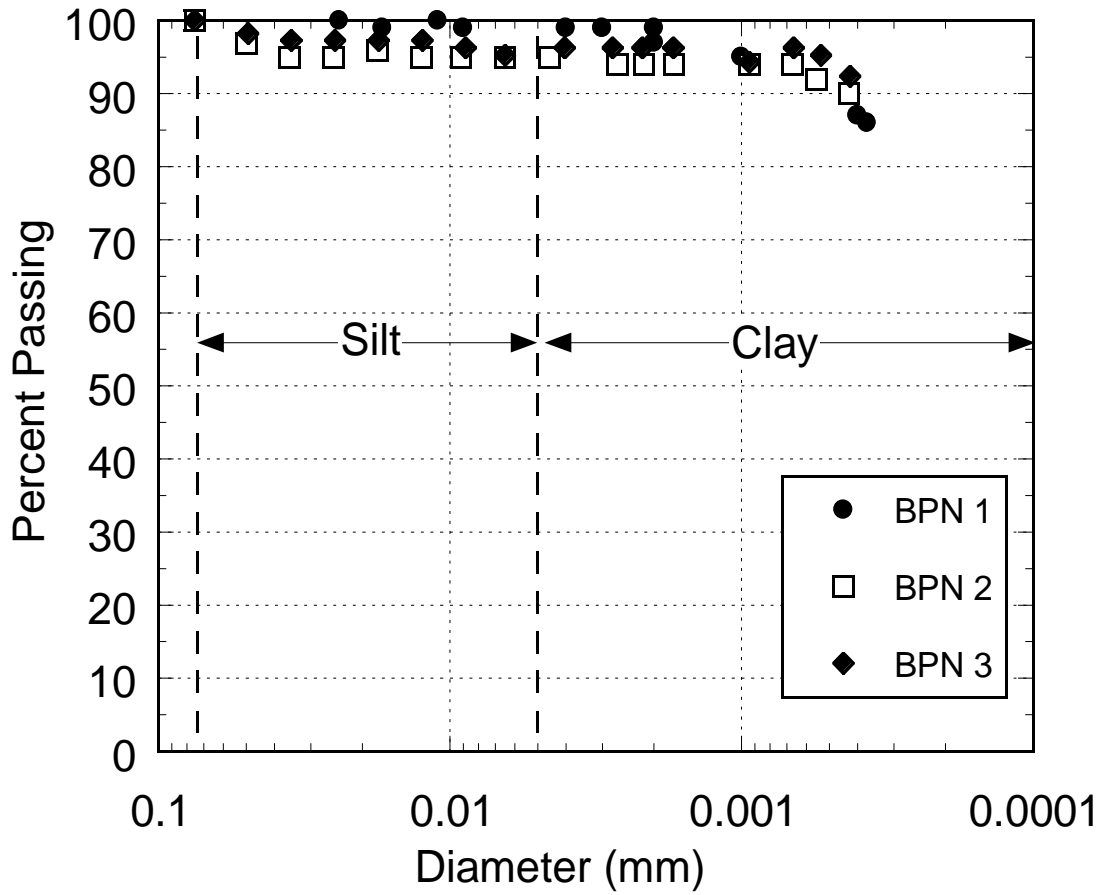


Figure 3.1. Grain-size distributions (ASTM D 422) for replicate samples of the bentonite polymer nanocomposite (BPN).



Figure 3.2. Photograph of traditional bentonite and bentonite polymer nanocomposite (BPN) plastic limit "worms."

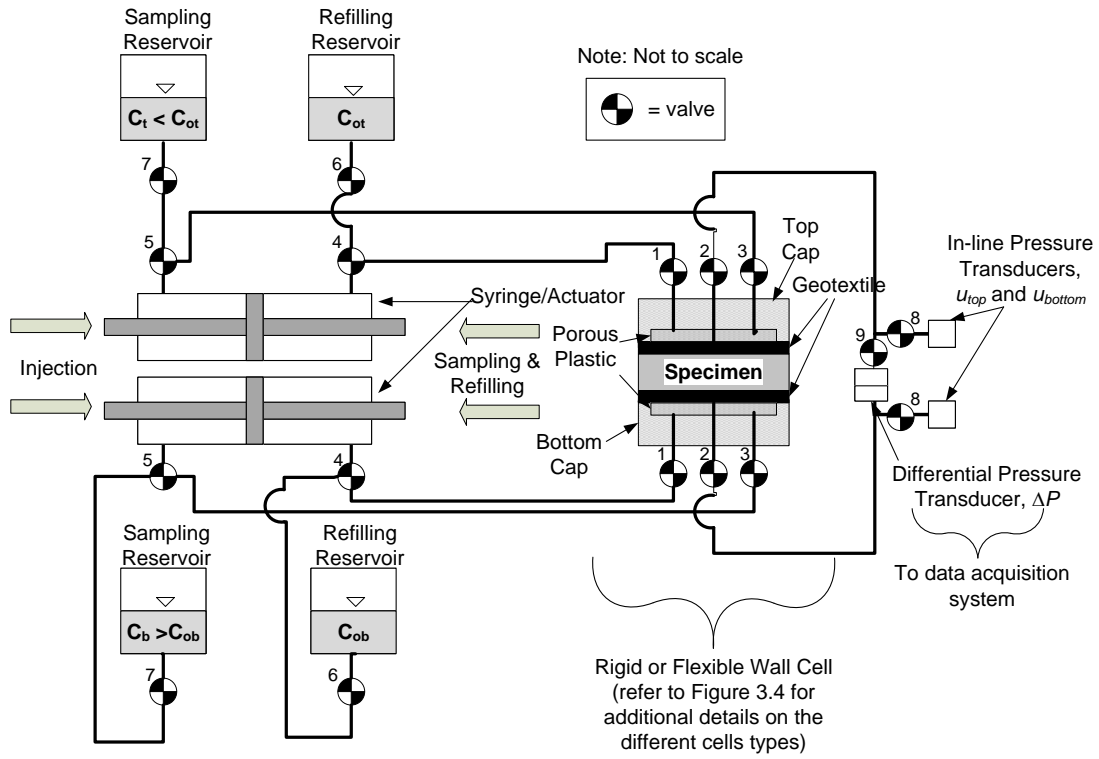


Figure 3.3. Schematic of membrane testing apparatus.

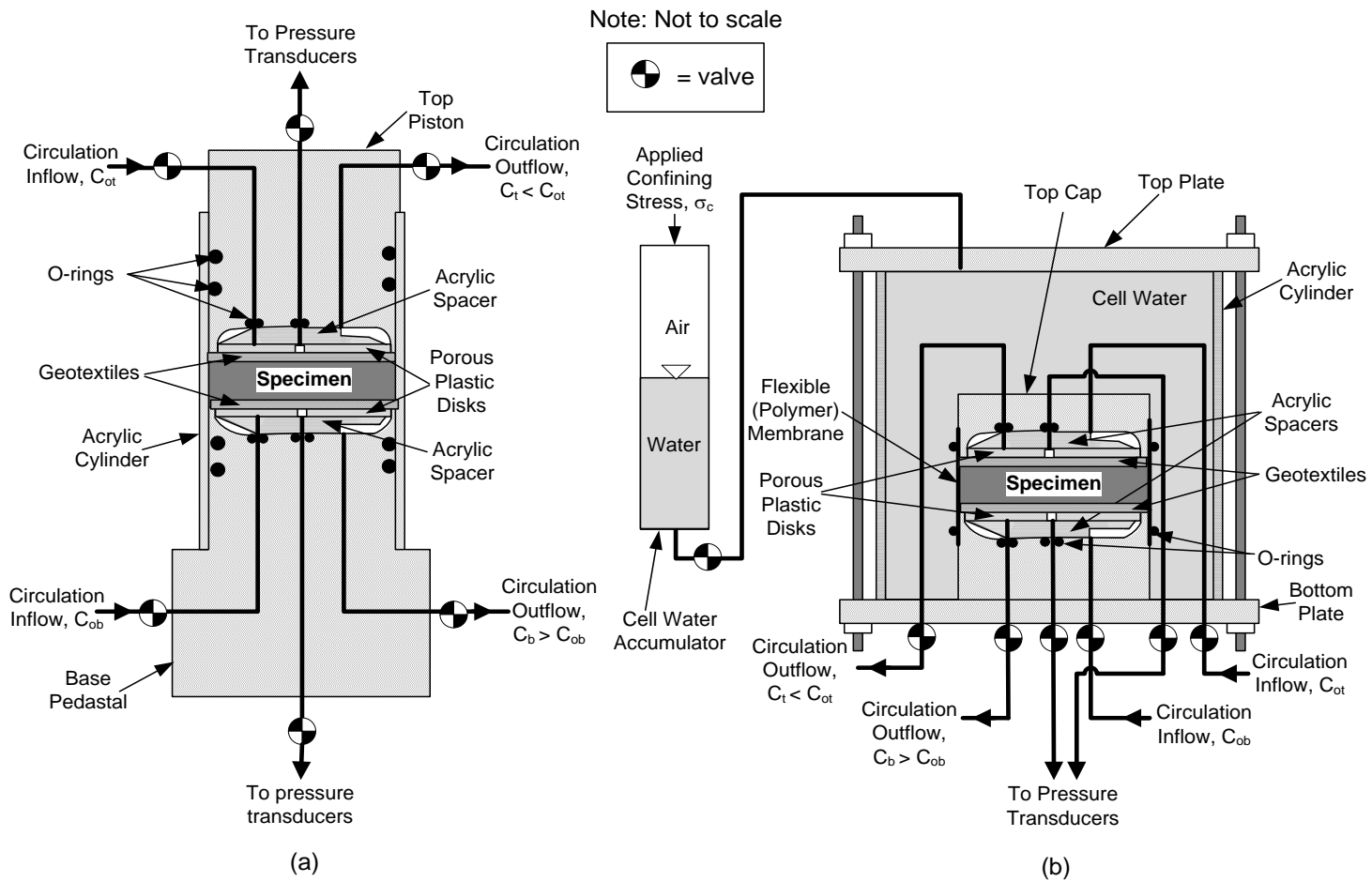
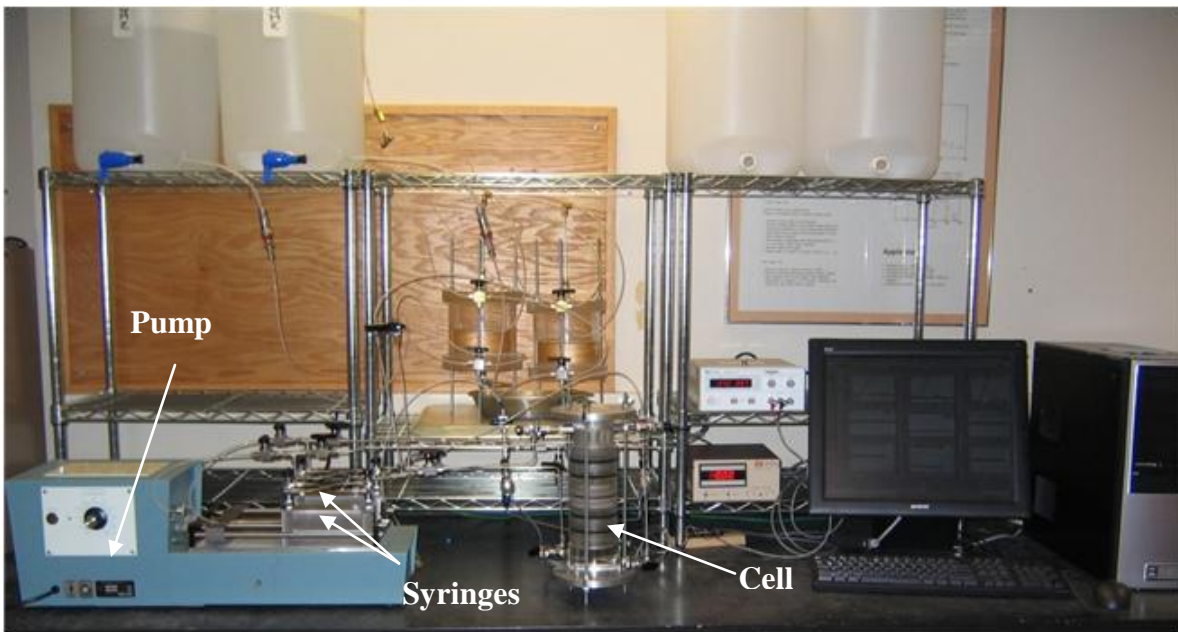
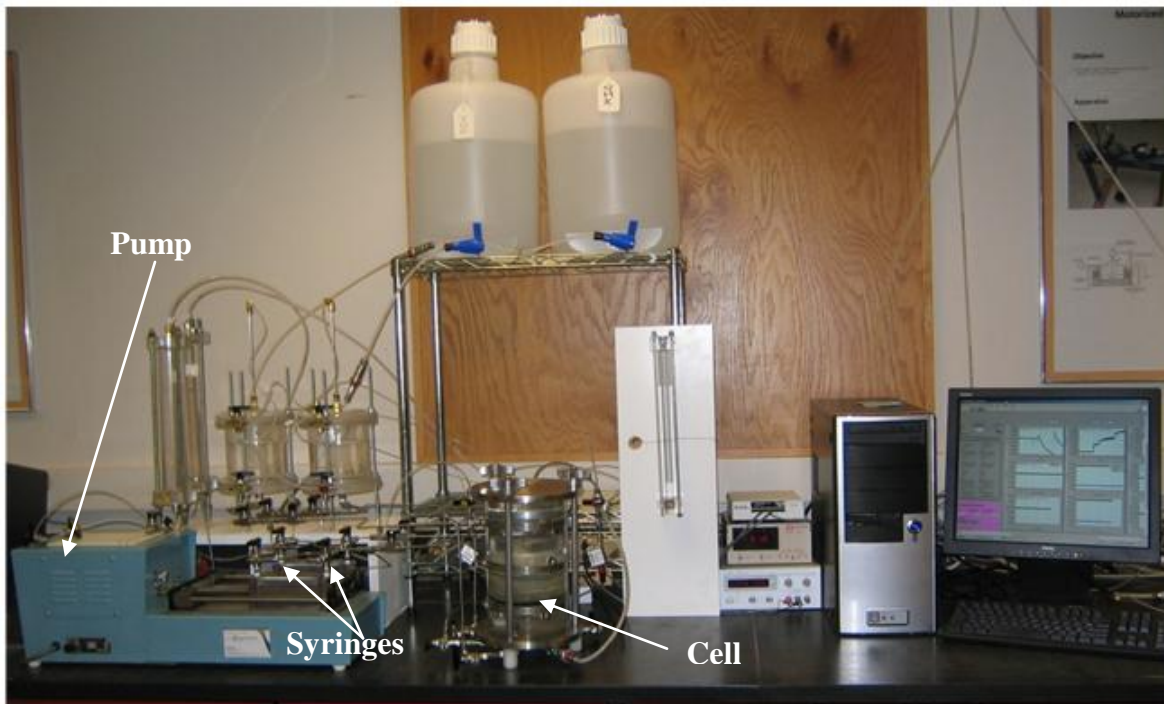


Figure 3.4. Schematic drawings of membrane testing cells: (a) rigid-wall cell (after Malusis et al. 2001); (b) flexible-wall cell (after Kang and Shackelford 2009).



(a)



(b)

Figure 3.5. Pictorial views of membrane apparatuses: (a) apparatus with rigid-wall cell; (b) apparatus with flexible-wall cell.

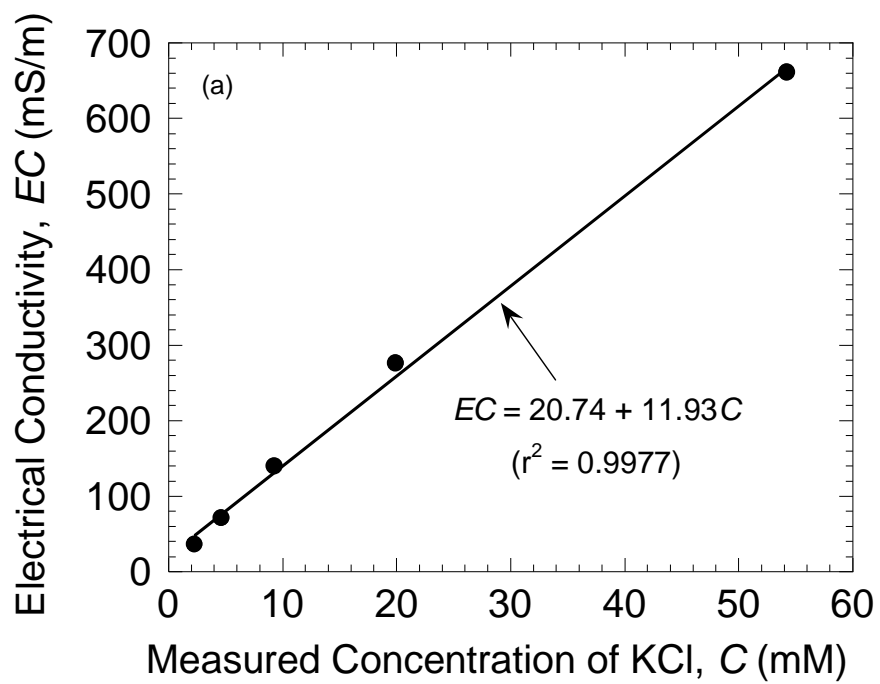


Figure 3.6. Calibration of electrical conductivity versus measured KCl concentration.

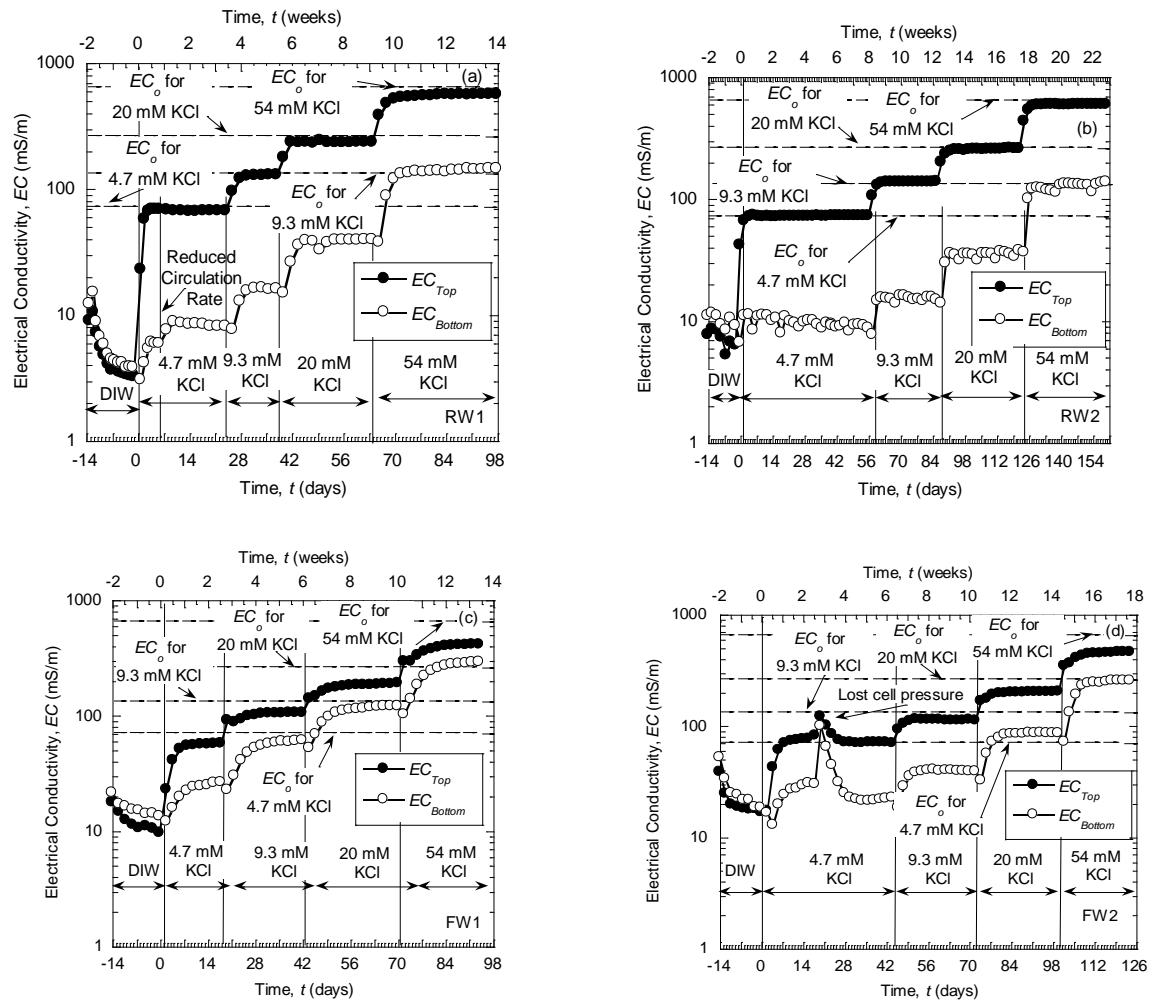


Figure 3.7. Measured electrical conductivity across top and bottom boundaries during membrane testing of BPN specimens in rigid-wall cells: (a) RW1 @ $n = 0.92$; (b) RW2 @ $n = 0.80$ and flexible-wall cells (c) FW1 @ $\sigma' = 34.5$ kPa (5 psi); (d) FW2 @ $\sigma' = 103$ kPa (15 psi).

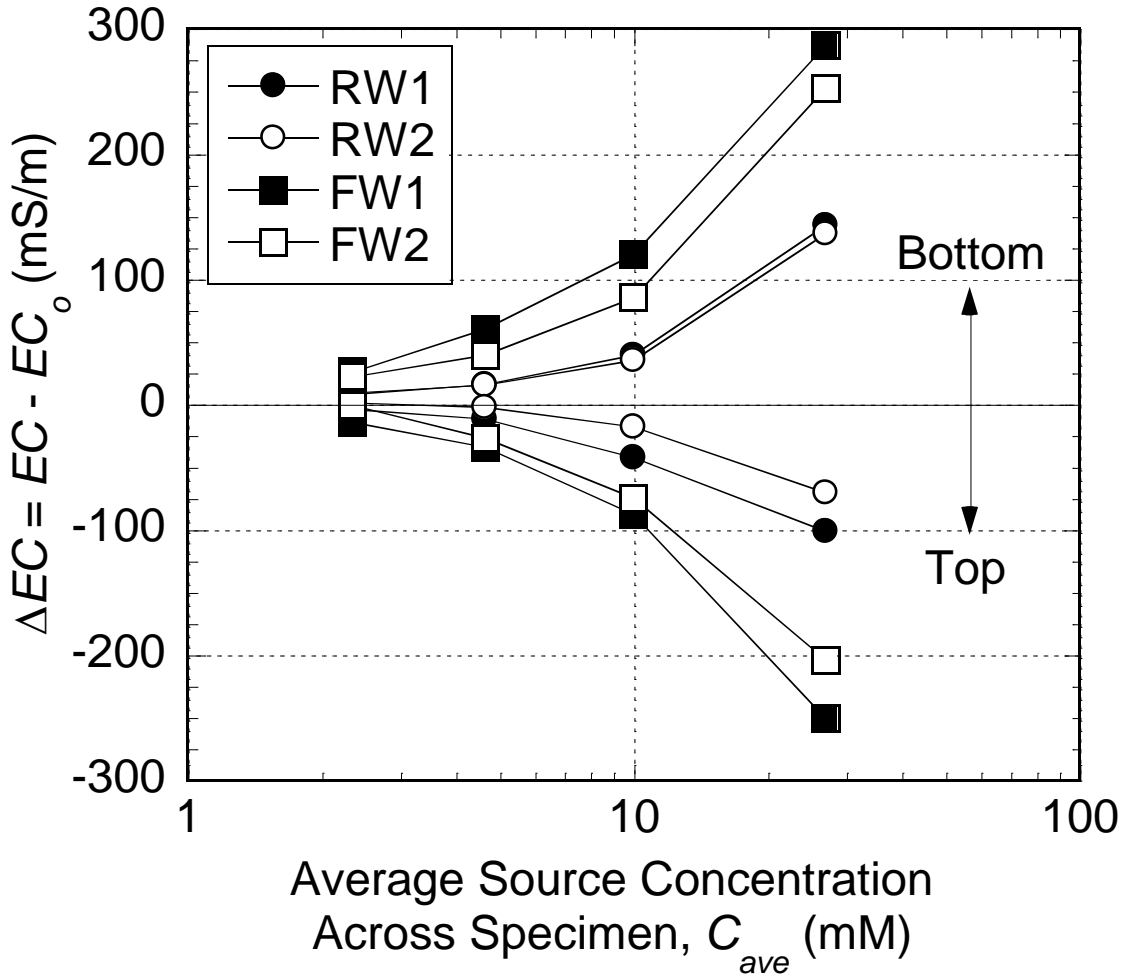


Figure 3.8. The change in electrical conductivity, ΔEC , of non-flushed BPN specimens during membrane testing in a rigid-wall cells (RW1 @ $n = 0.92$; RW2 @ $n = 0.80$) and a flexible-wall cells [FW1 @ $\sigma' = 34.5$ kPa (5 psi); FW2 @ $\sigma' = 103$ kPa (15 psi)] as a function of average salt (KCl) concentration across the specimen.

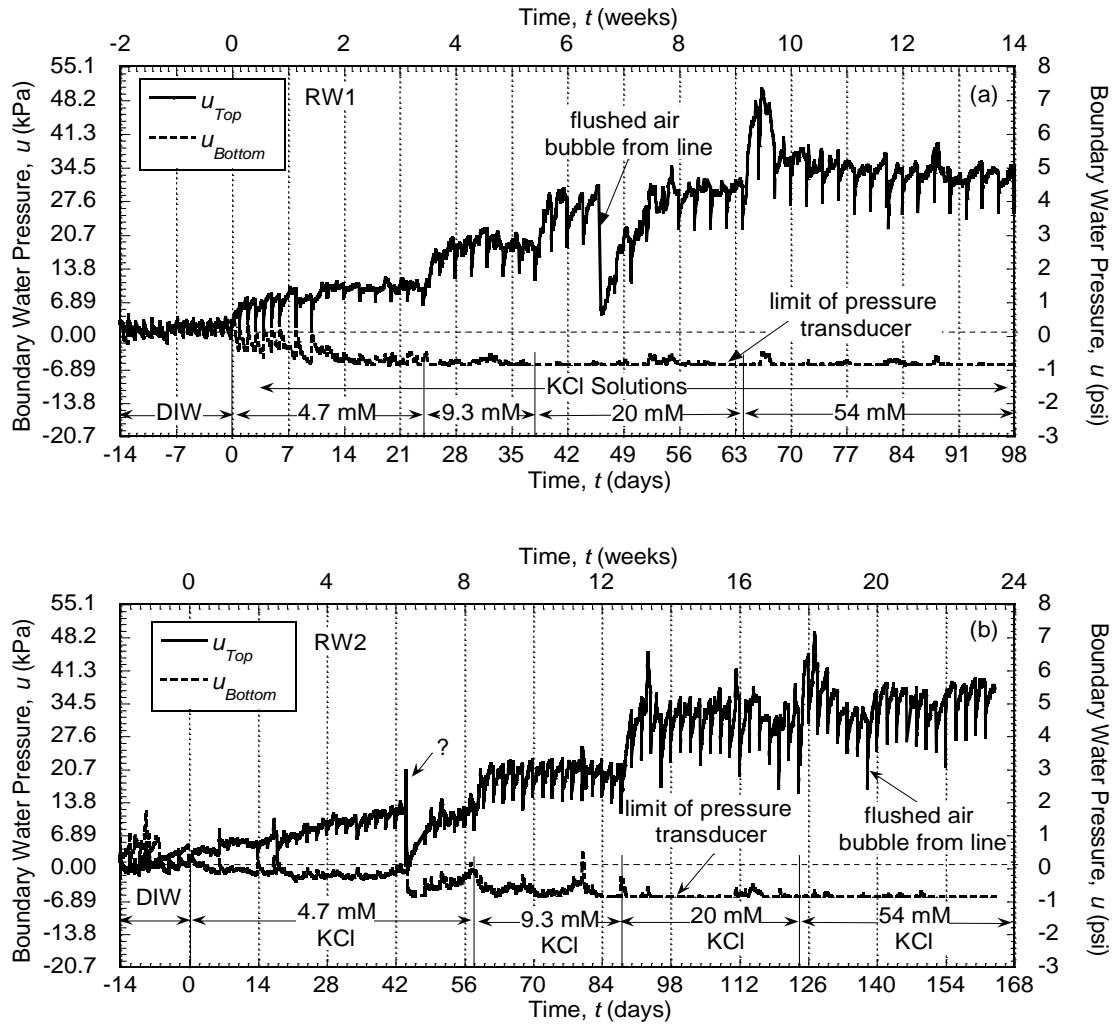


Figure 3.9. Boundary water pressures for BPN specimens during membrane testing in a rigid-wall cells at two different porosities, n : (a) RW1 @ $n = 0.92$; (b) RW2 @ $n = 0.80$.

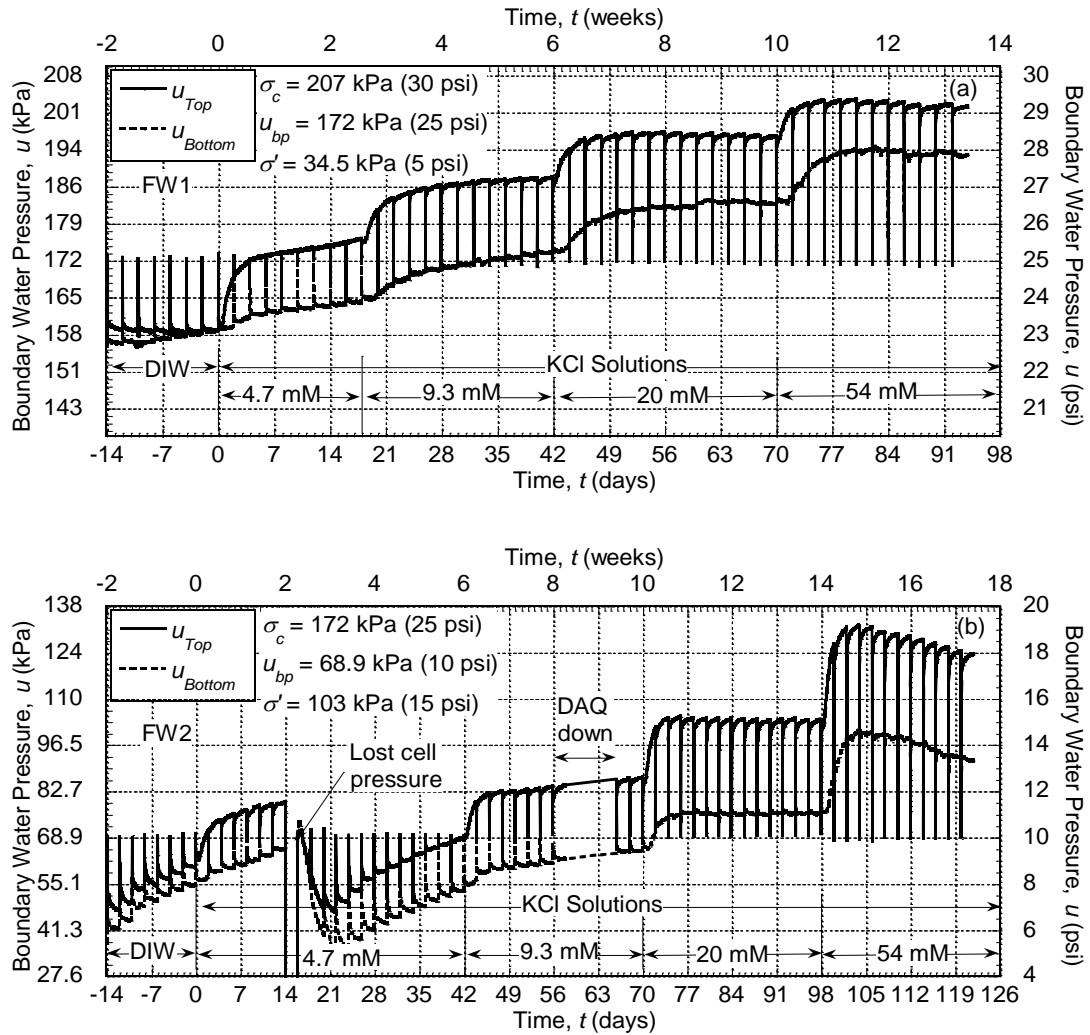


Figure 3.10. Boundary water pressures for BPN specimens during membrane testing in a flexible-wall cells at different effective stresses, σ' : (a) FW1 @ $\sigma' = 34.5$ kPa (5 psi); (b) FW2 @ $\sigma' = 103$ kPa (15 psi).

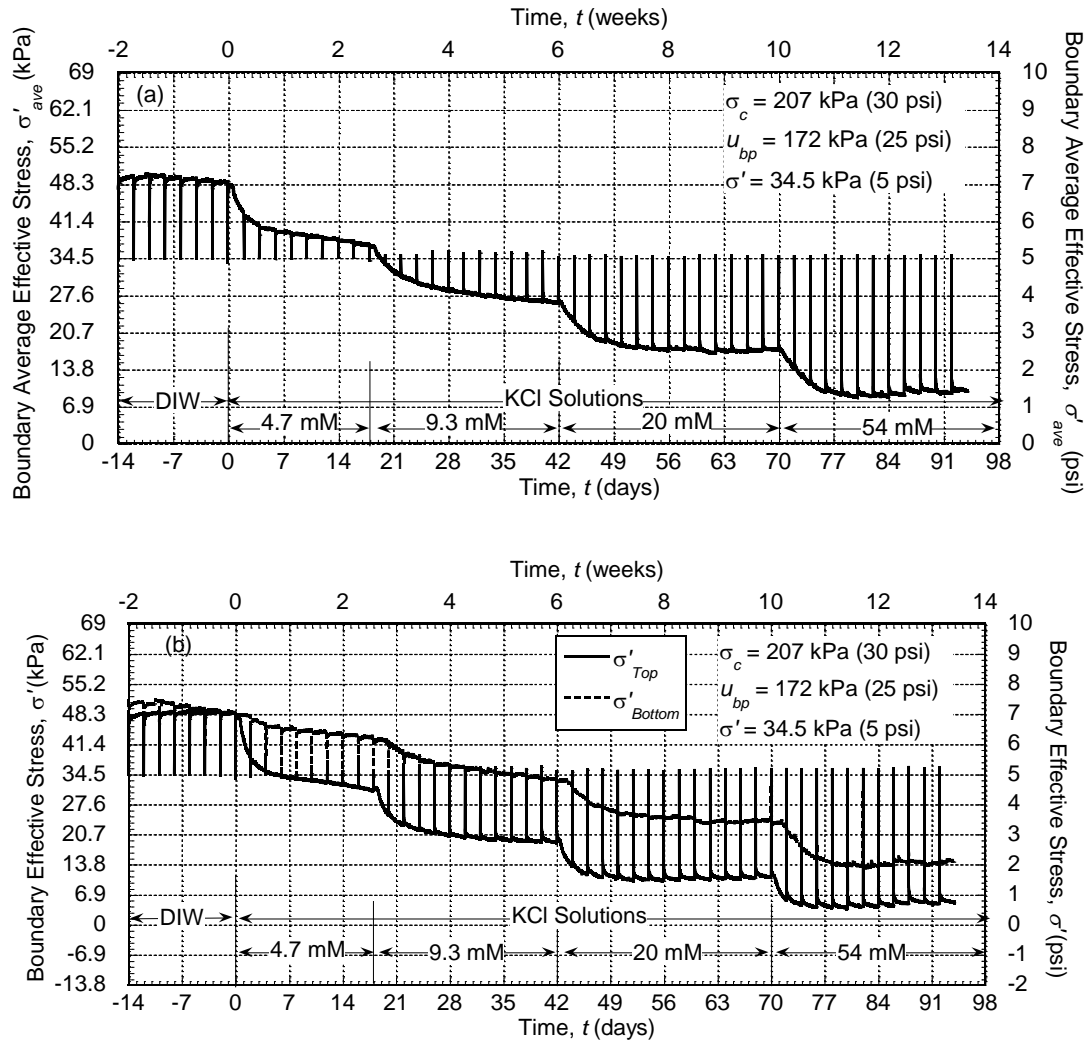


Figure 3.11. Boundary effective stresses in BPN [FW1 @ $\sigma' = 34.5 \text{ kPa (5 psi)}$] during membrane testing in flexible-wall cells: (a) average boundary effective stress, σ'_{ave} ; (b) boundary effective stress at the top and bottom of the specimen, σ'_{Top} and σ'_{Bottom} , respectively.

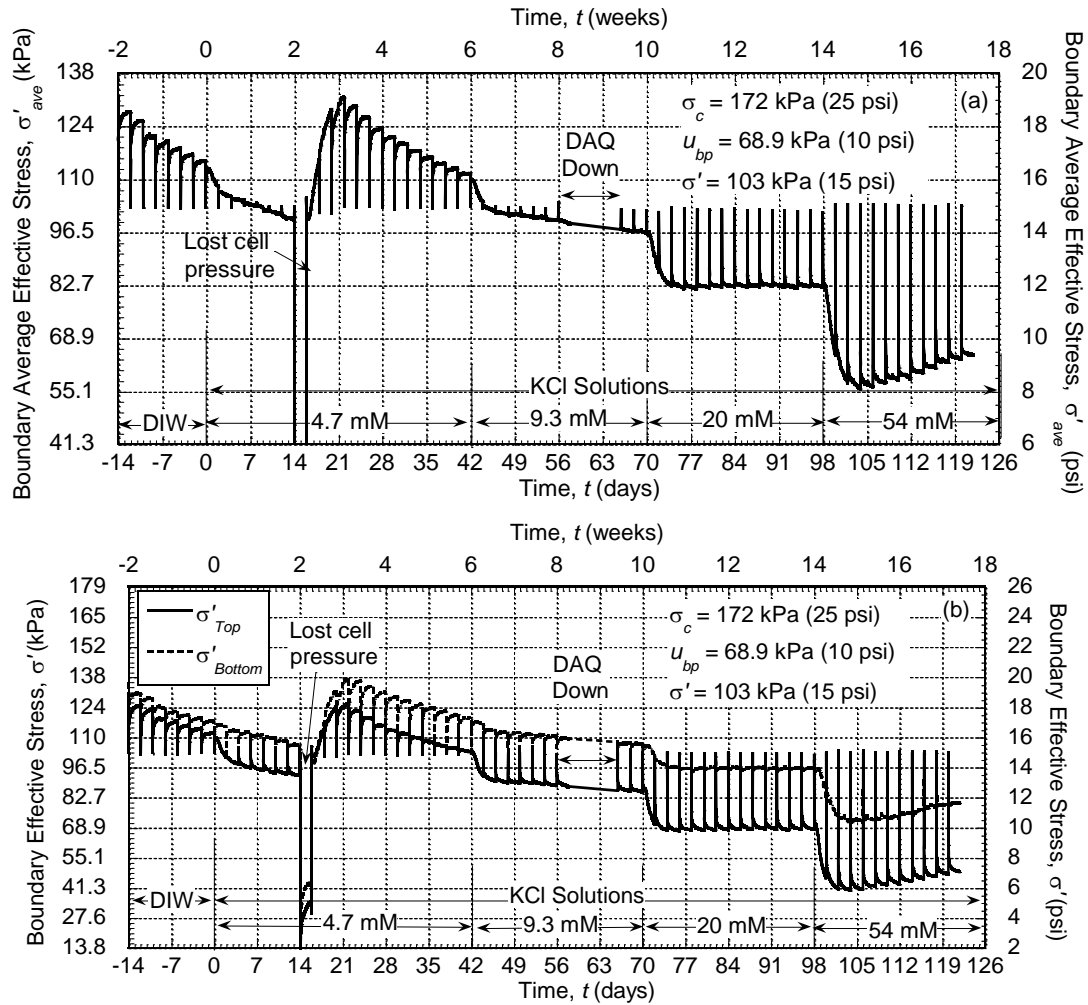


Figure 3.12. Boundary effective stresses in BPN [FW2 @ $\sigma' = 103$ kPa (15 psi)] during membrane testing in flexible-wall cells: (a) average boundary effective stress, σ'_{ave} ; (b) boundary effective stress at the top and bottom of the specimen, σ'_{Top} and σ'_{Bottom} , respectively.

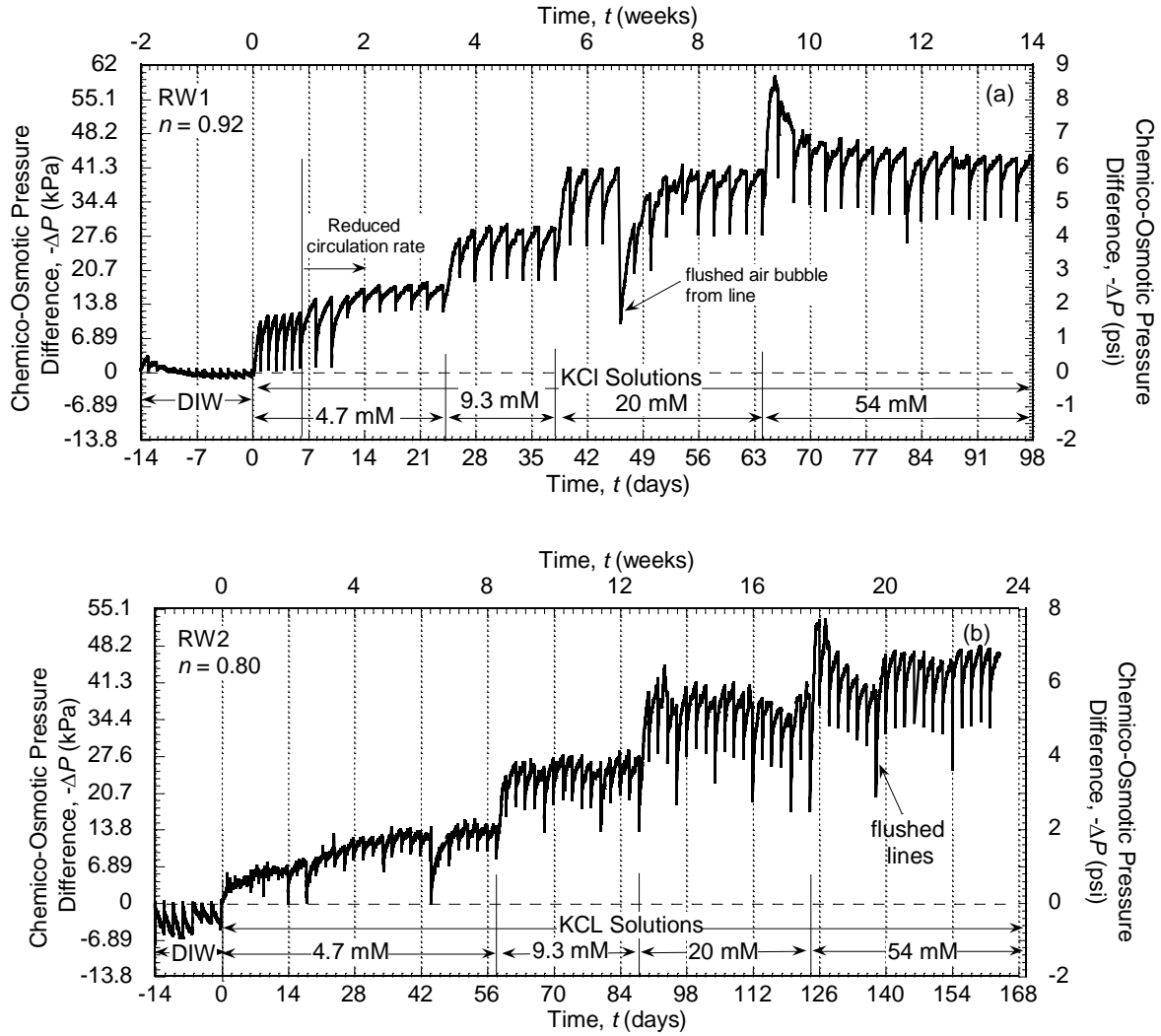


Figure 3.13. Measured chemico-osmotic pressure differences across BPN specimens at different porosities, n , during membrane testing in a rigid-wall cells: (a) RW1 @ $n = 0.92$; (b) RW2 @ $n = 0.80$.

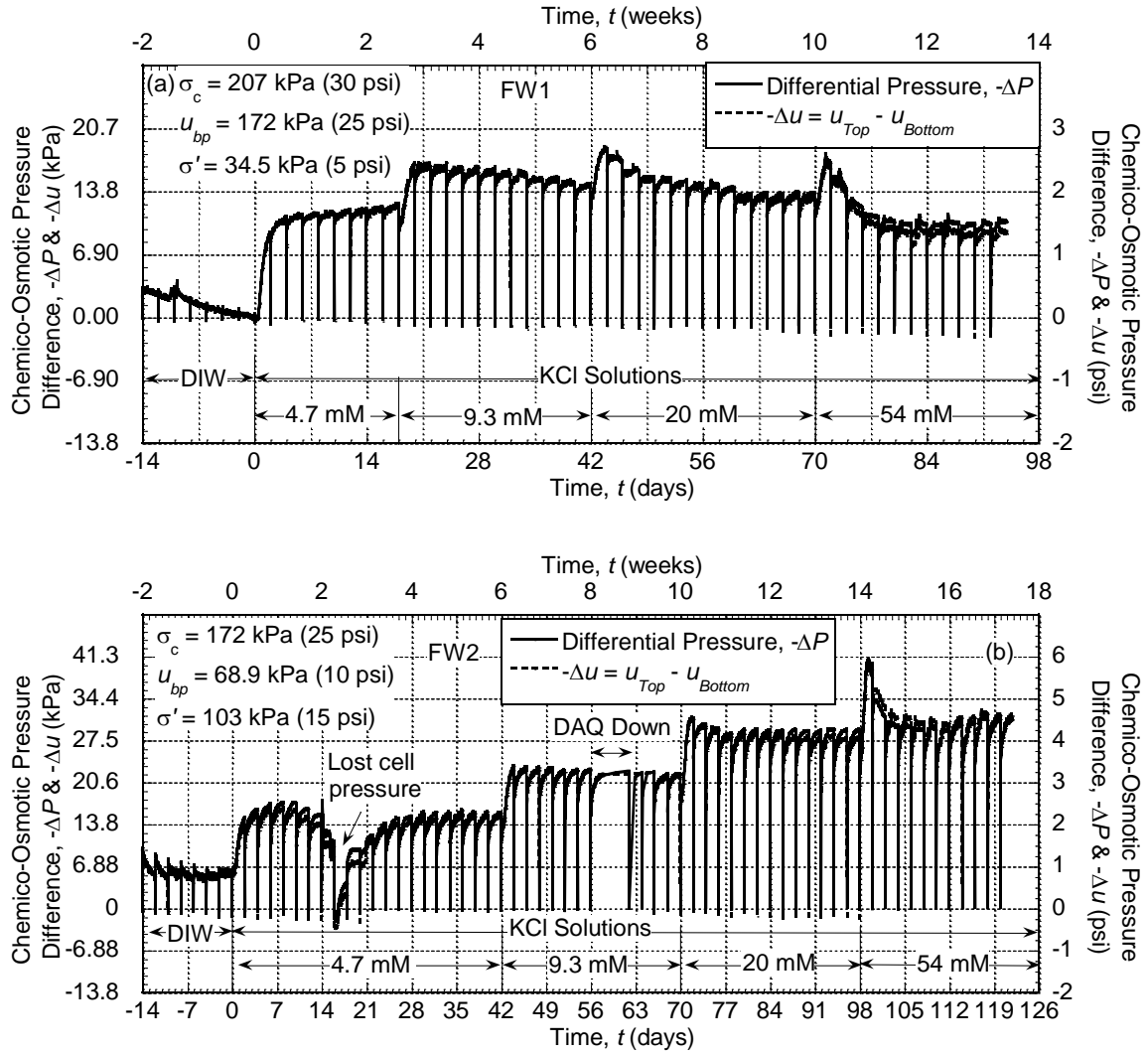


Figure 3.14. Measured chemico-osmotic pressure differences across BPN specimens at different initial effective stresses, σ' , during membrane testing in flexible-wall cells: (a) FW1 @ $\sigma' = 34.5$ kPa (5 psi); (b) FW2 @ $\sigma' = 103$ kPa (15 psi).

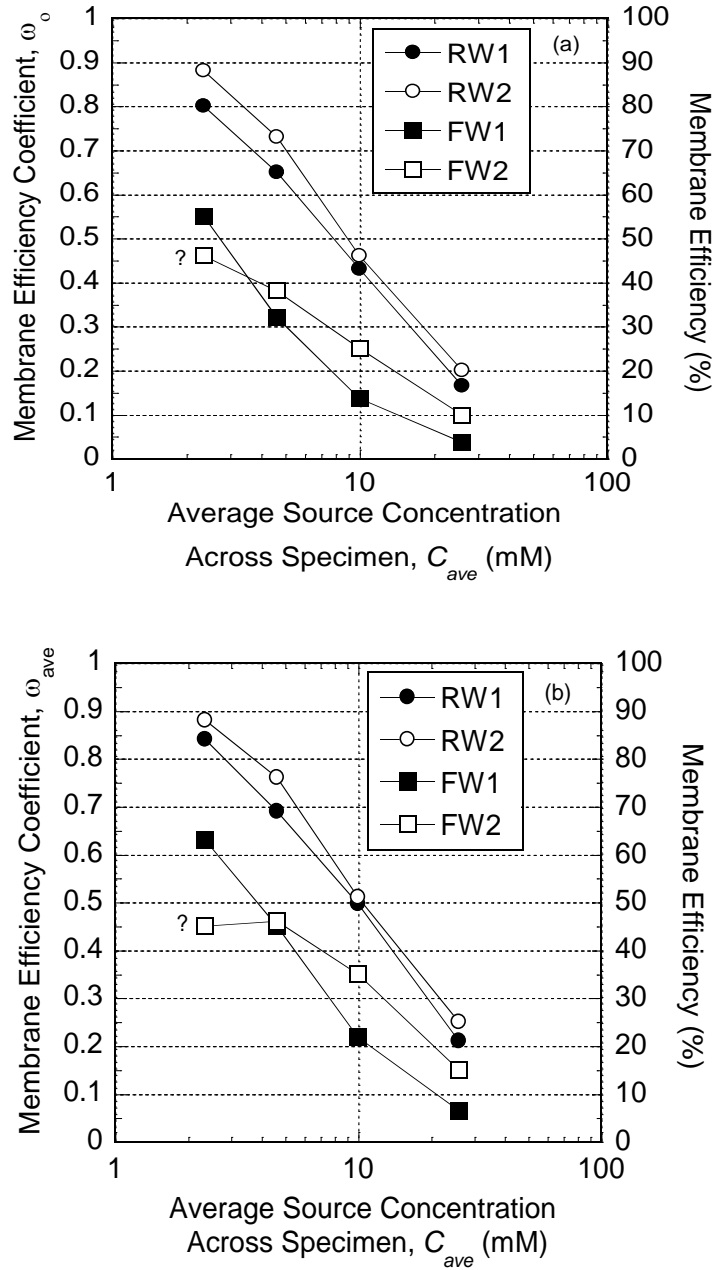


Figure 3.15. Steady-state membrane efficiency coefficients of BPN specimens during membrane testing in a rigid-wall cell (RW1 @ $n = 0.92$, RW2 @ $n = 0.80$) and a flexible-wall cell [FW1 @ $\sigma' = 34.5$ kPa (5 psi), FW2 @ $\sigma' = 103$ kPa (15 psi)] as a function of average salt concentration across the specimen: (a) ω values based on initial (source) boundary concentrations, ω_0 ; (b) ω values based on average boundary concentrations, ω_{ave} .

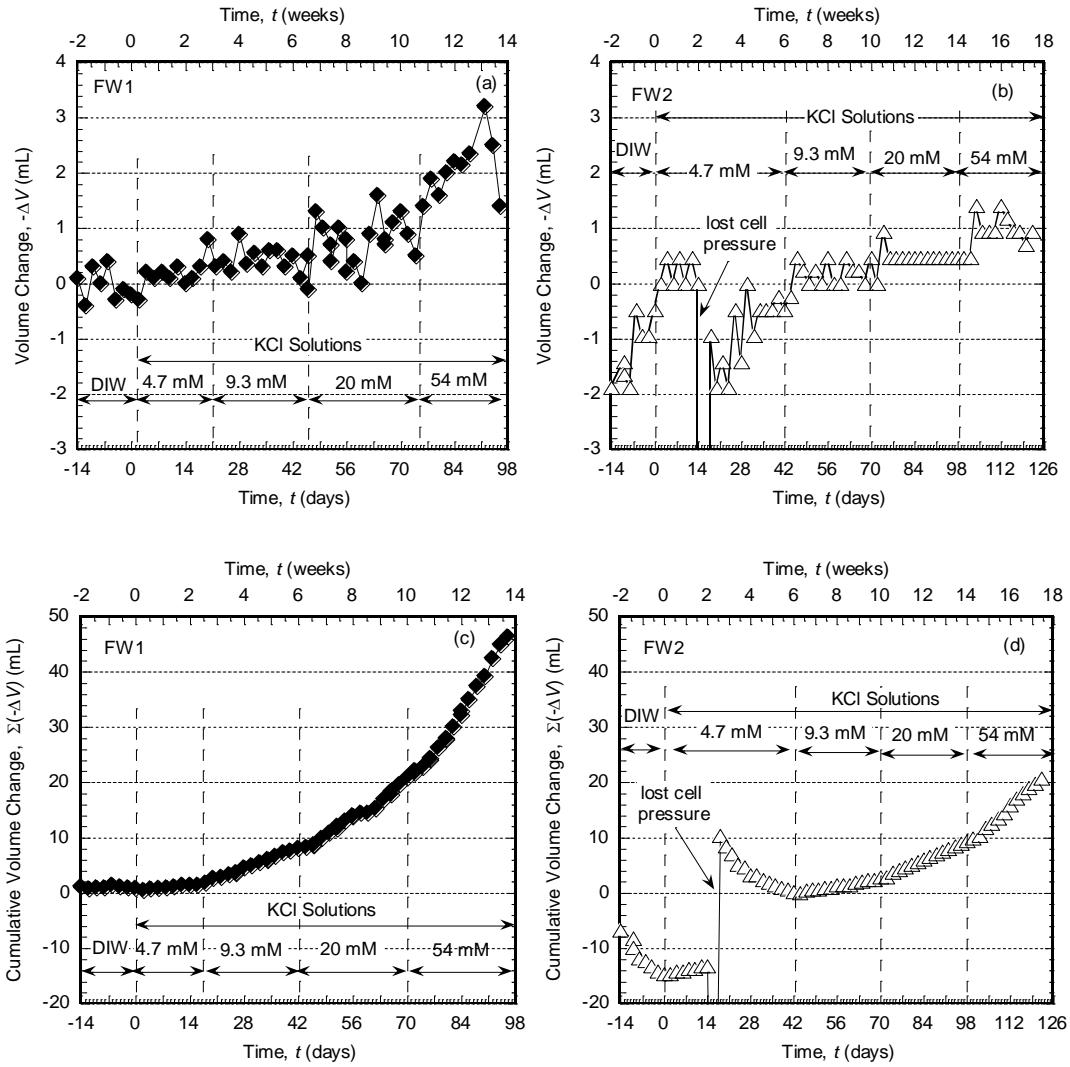


Figure 3.16. Volume change versus time (a and b) and cumulative volume change versus time (c and d) during membrane testing of BPN specimens in a flexible-wall cell: (a and c) FW1 @ $\sigma' = 34.5$ kPa (5 psi); (b and d) FW2 @ $\sigma' = 103$ kPa (15 psi).

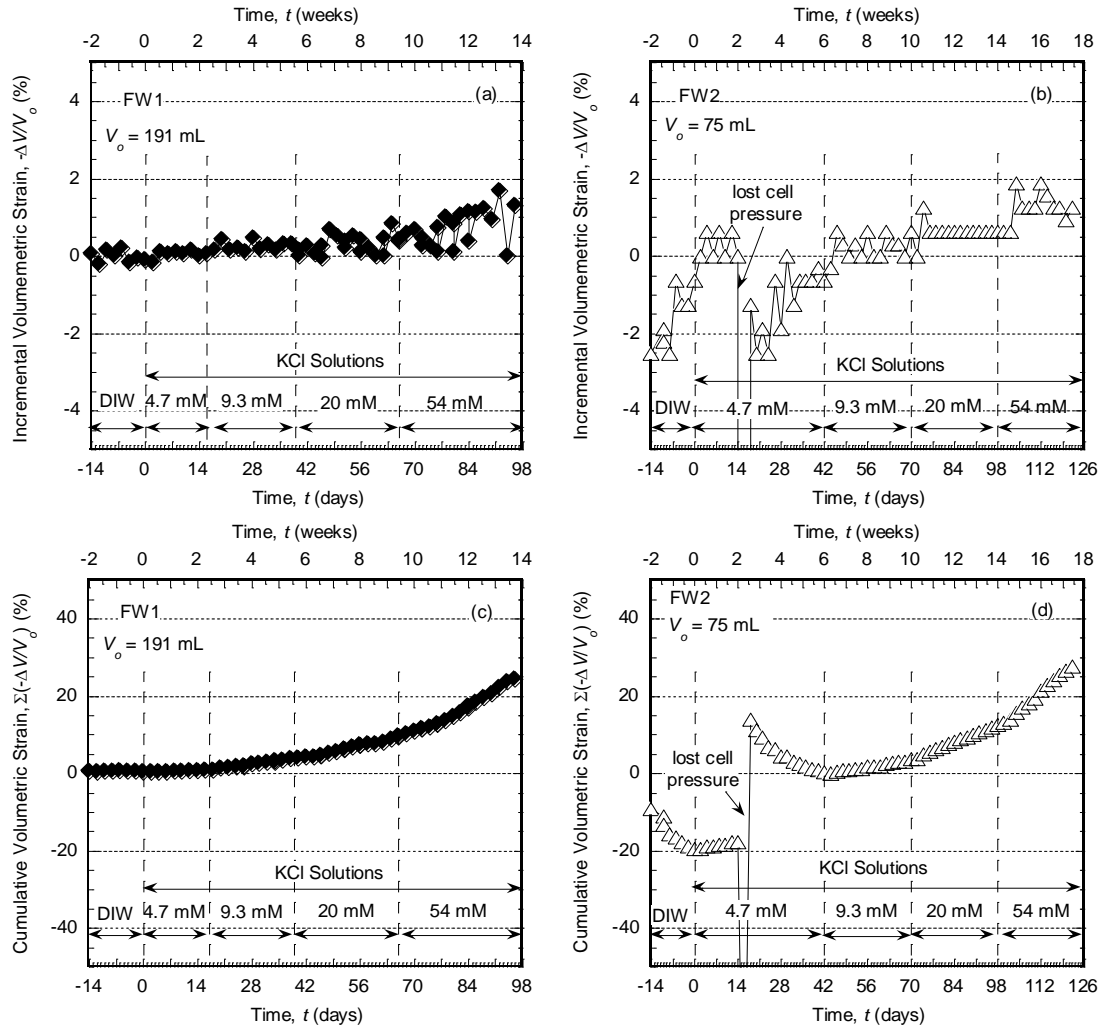


Figure 3.17. Volumetric strain versus time (a and b) and cumulative volumetric strain versus time (c and d) during membrane testing of BPN specimens in a flexible-wall cell: (a and c) FW1 @ $\sigma' = 34.5$ kPa (5 psi); (b and d) FW2 @ $\sigma' = 103$ kPa (15 psi).

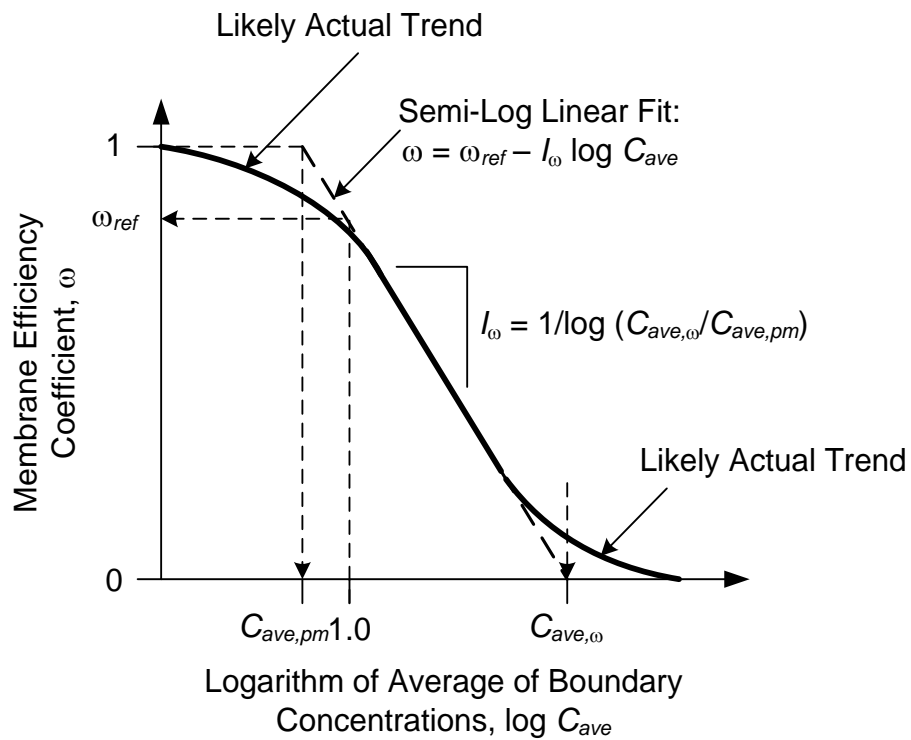


Figure 3.18. Schematic illustration of membrane efficiency, ω , versus average boundary salt concentration (after Shackelford et al. 2003) [ω_{ref} = reference membrane efficiency coefficient at $\log C_{ave} = 0$; $C_{ave,\omega}$ = threshold concentration corresponding to $\omega = 0$; $C_{ave,pm}$ = perfect membrane concentration corresponding to $\omega = 1$; I_{ω} = the membrane index].

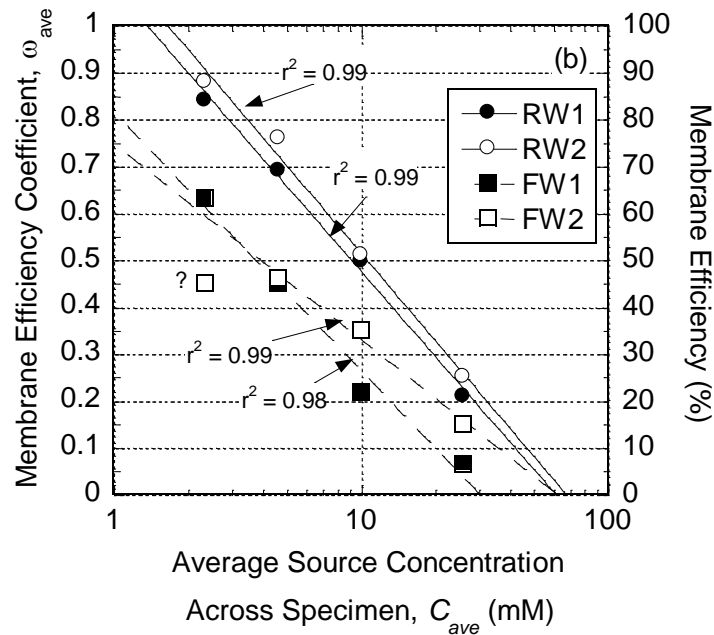
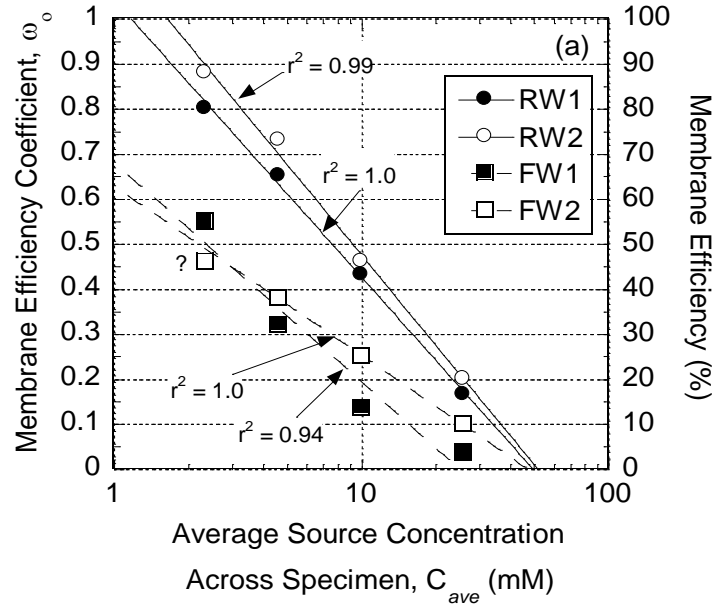


Figure 3.19. Semi-log linear regressions of membrane efficiency coefficients for BPN specimens during membrane testing in a rigid-wall cell (RW1 @ $n = 0.92$, RW2 @ $n = 0.80$) and a flexible-wall cell [FW1 @ $\sigma' = 34.5$ kPa (5 psi), FW2 @ $\sigma' = 103$ kPa (15 psi)] as a function of average salt concentration difference across the specimen: (a) ω values based on initial (source) boundary concentrations, ω_0 ; (b) ω values based on average boundary concentrations, ω_{ave} .

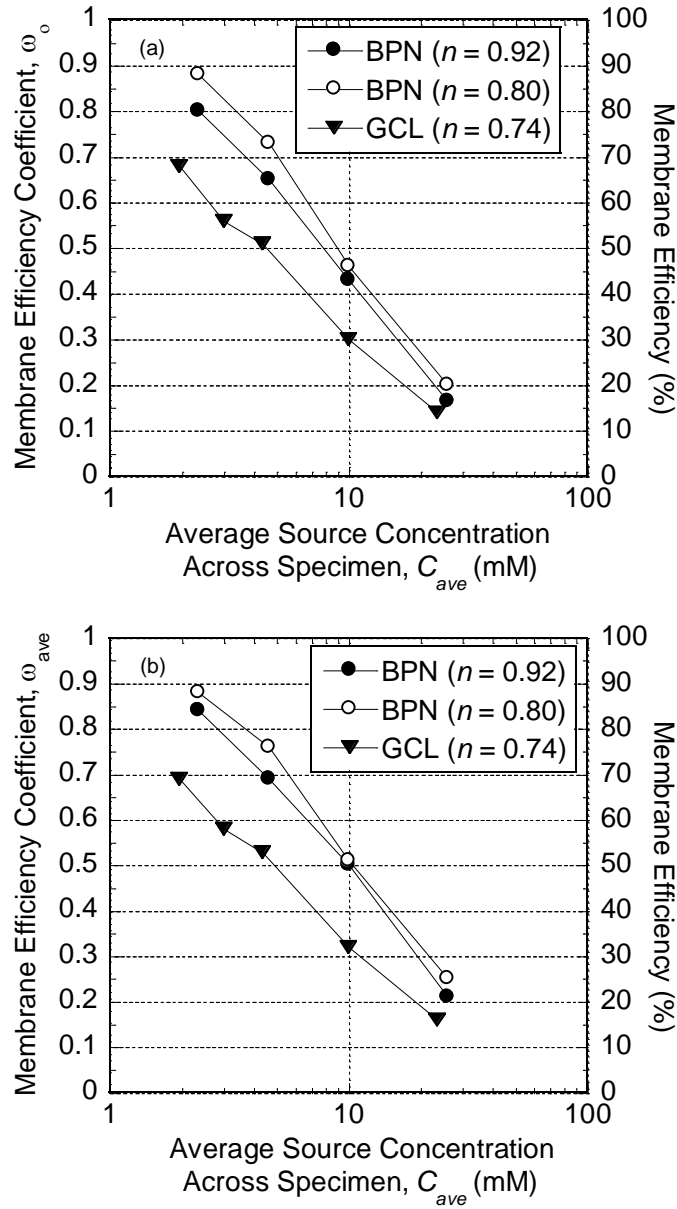


Figure 3.20. Steady-state membrane efficiency coefficients of non-flushed BPN specimens versus a flushed GCL specimen (from Malusis et al. 2002a) tested in a rigid-wall cell as a function of average salt concentration across the specimen: (a) ω values based on initial (source) boundary concentrations, ω_0 ; (b) ω values based on average boundary concentrations, ω_{ave} (n = total specimen porosity).

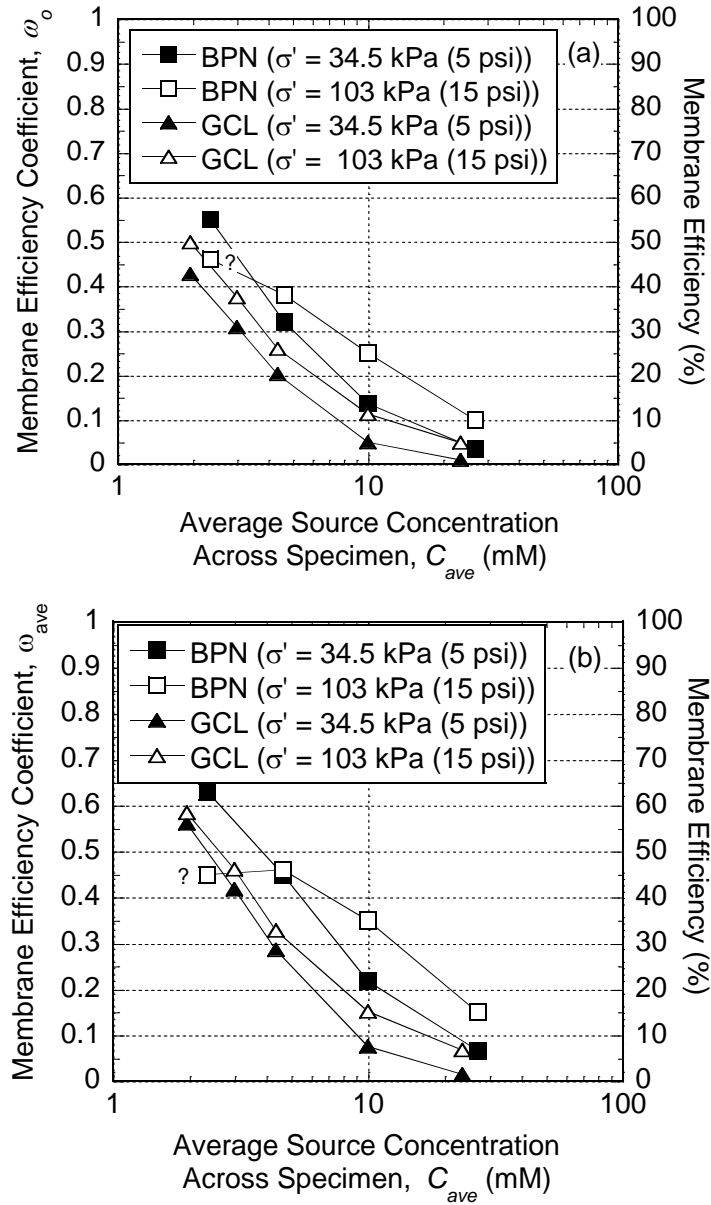


Figure 3.21. Comparison of steady-state membrane efficiency coefficients, ω , of non-flushed BPN specimens versus flushed GCL specimens (from Kang and Shackelford 2010) tested in a flexible-wall cell as a function of average salt concentration across the specimen: (a) ω values based on initial (source) boundary concentrations, ω_0 ; (b) ω values based on average boundary concentrations, ω_{ave} ($\sigma' =$ initial effective stress).

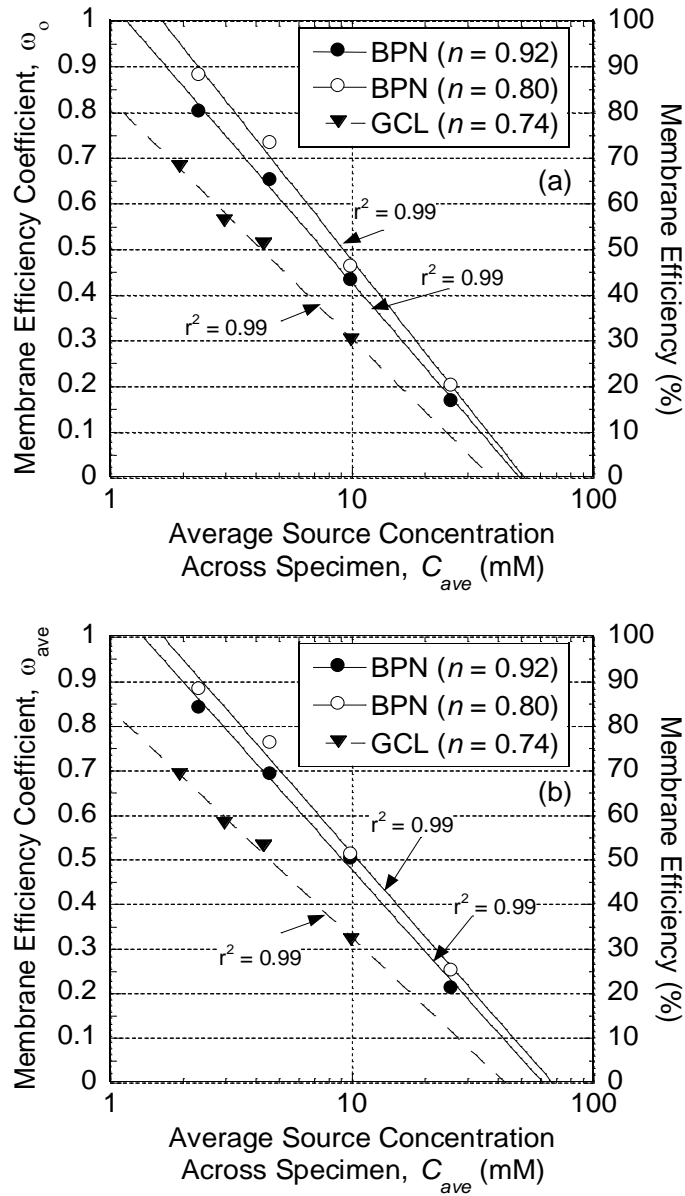


Figure 3.22. Comparison of steady-state membrane efficiency coefficients of a non-flushed BPN specimens versus those of flushed GCL specimens (from Malusis et al. 2002a) tested in a rigid-wall cell as a function of average salt concentration difference across the specimen: (a) ω values based on initial (source) boundary concentrations, ω_0 ; (b) ω values based on average boundary concentrations, ω_{ave} (n = total specimen porosity).

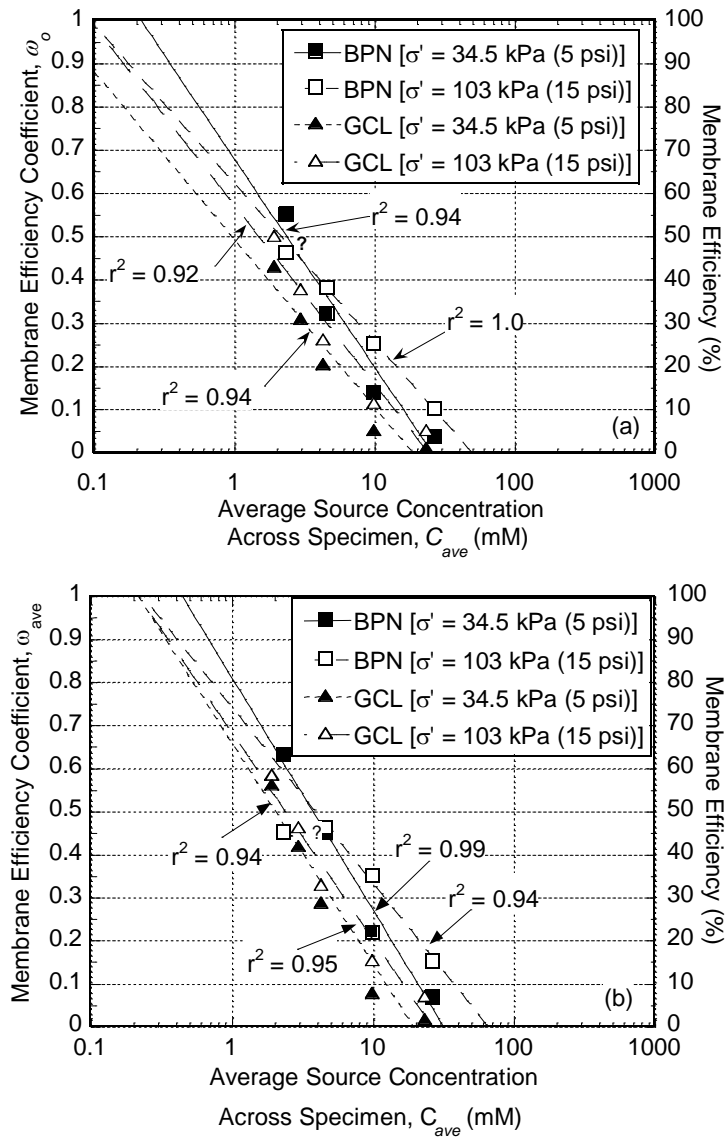


Figure 3.23. Comparison of steady-state membrane efficiency coefficients, ω , of non-flushed BPN specimens versus those of flushed GCL specimens (from Kang and Shackelford 2010) tested in a flexible-wall cell as a function of average salt concentration across the specimen: (a) ω values based on initial (source) boundary concentrations, ω_0 ; (b) ω values based on average boundary concentrations, ω_{ave} ($\sigma' =$ initial effective stress).

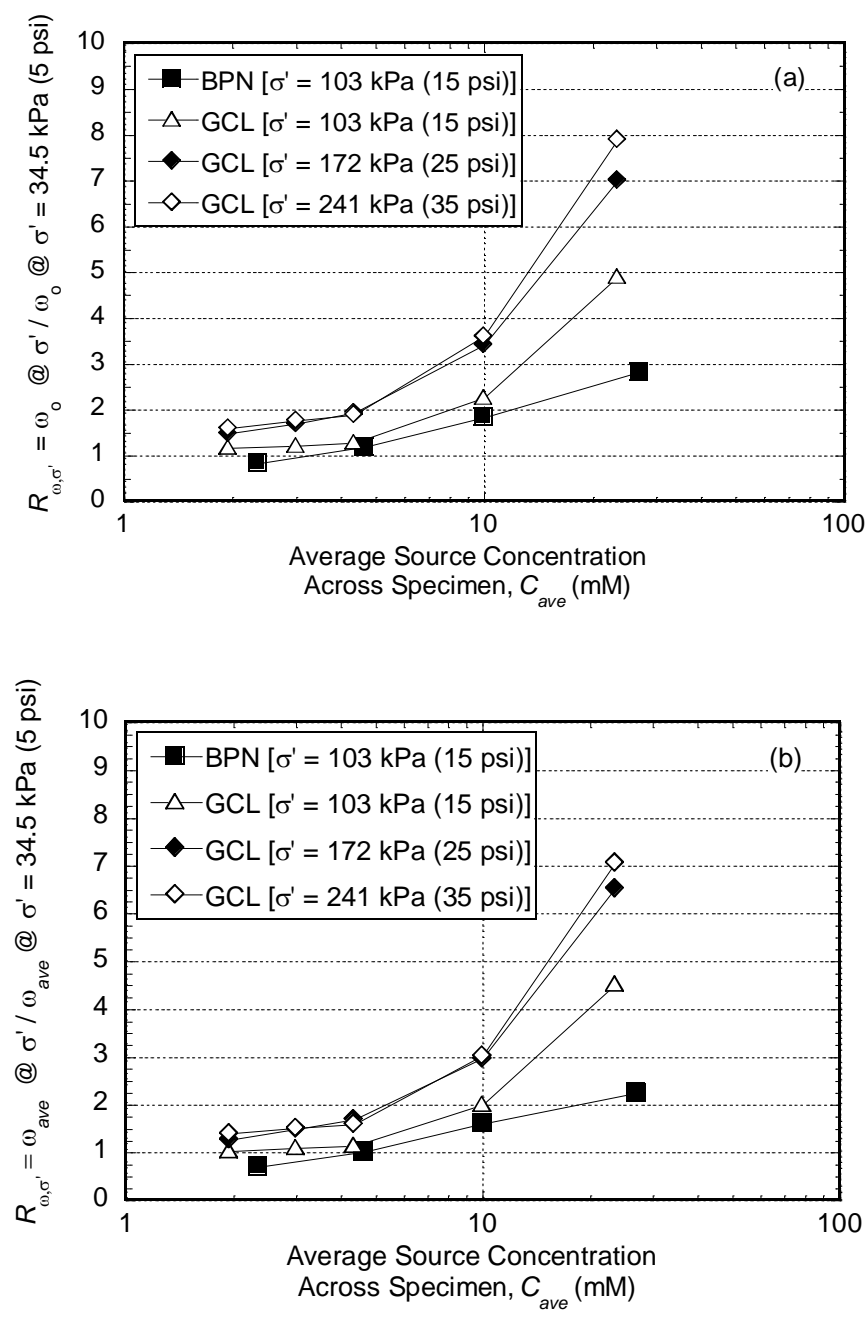


Figure 3.24. Ratio of the membrane efficiency coefficient, ω , at σ' to ω at $\sigma' = 34.5$ kPa (5 psi), versus the average salt concentration across the specimen, C_{ave} : (a) ω based on initial (source) KCl concentrations, ω_0 and (b) ω based on average KCl concentrations, ω_{ave} ($\sigma' =$ initial effective stress).

Material	σ' (kPa)	A	B	r^2
BPN	34.5	0.69	0.71	1.0
BPN	103	0.85	0.39	0.95
GCL	34.5	1.21	0.20	0.92
GCL	103	1.07	0.20	0.98

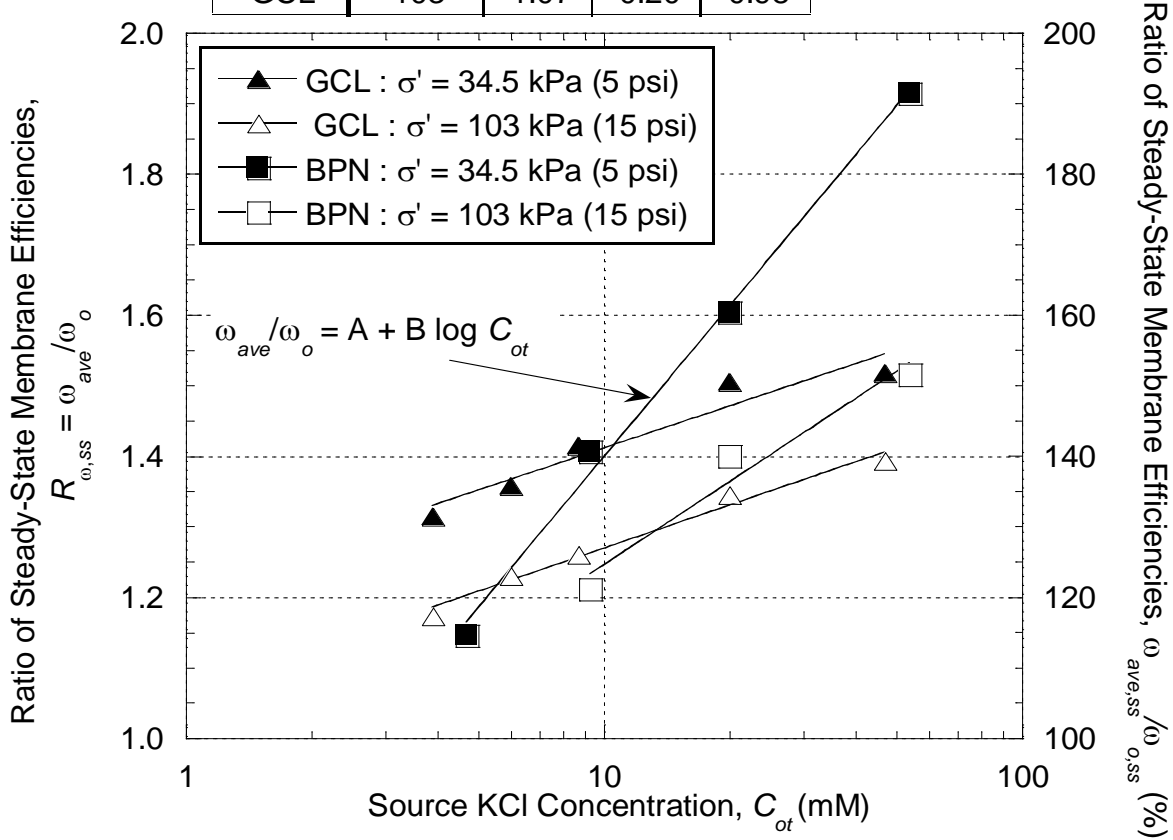


Figure 3.25. Ratio of the membrane efficiency coefficient in terms of average KCl concentrations, ω_{ave} , relative to that based on initial KCl concentrations, ω_o , or $R_{\omega_{ss}}$, versus the source KCl concentration, C_{ot} , for non-flushed BPN specimens [FW1 @ $\sigma' = 34.5$ kPa (5 psi), FW2 @ $\sigma' = 103$ kPa (15 psi)] and flushed GCL specimens (from Kang and Shackelford 2010).

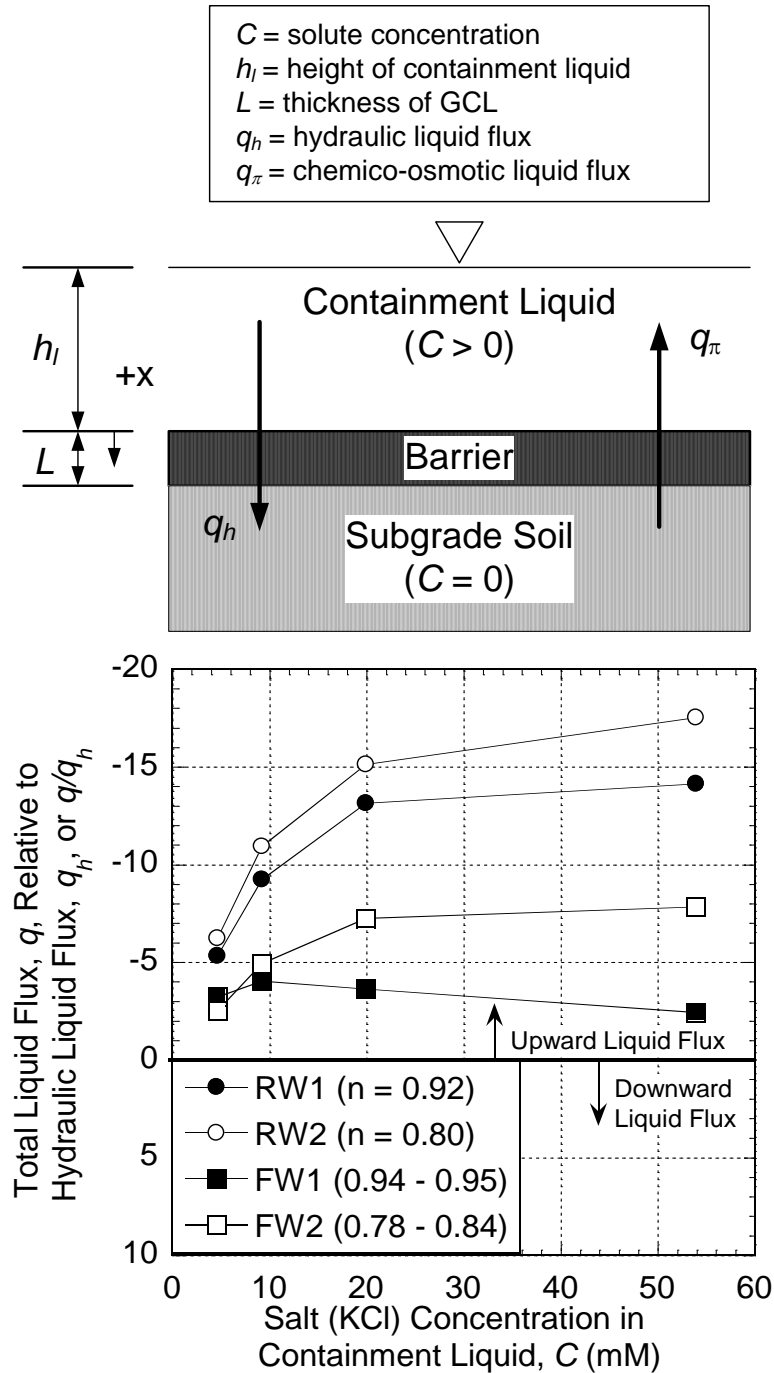


Figure 3.26. Simplified analysis depicting the effect of chemico-osmotic counterflow through BPN ($L \leq 10$ mm) used as a containment barrier as a function of the KCl concentration in containment liquid [RW1 @ $n = 0.92$, RW2 @ $n = 0.80$, FW1 @ $\sigma' = 34.5$ kPa (5 psi), and FW2 @ $\sigma' = 103$ kPa (15 psi)].

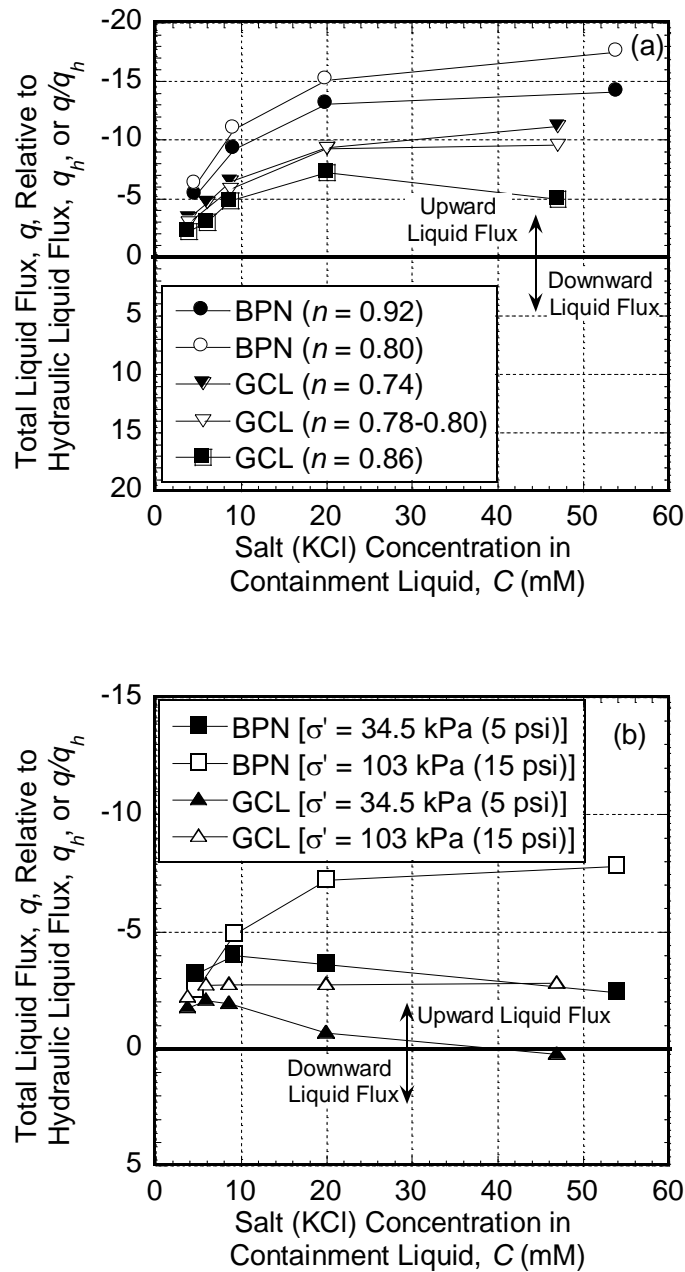


Figure 3.27. Comparison of results of a simplified analysis of the potential effect of membrane behavior on the liquid flux through BPN or a GCL containment barrier: (a) based on results of rigid-wall tests (GCL data from Malusis et al. 2003); (b) based on results of flexible-wall tests (GCL data from Kang and Shackelford 2010) [n = total porosity; σ' = initial effective stress].

References

- ATU. (1992). "ClayMax sodium bentonite liner found degraded at New Jersey site." *Aboveground Tank Update*, 3(2), 17-18.
- ASTM. (2005). "Standard test methods for liquid limit, plastic limit, and plasticity index of soils." ASTM D4318, ASTM International, West Conshohocken, PA.
- ASTM. (2006). "Standard test method for swell index of clay mineral component of geosynthetic clay liners." ASTM D5890, ASTM International, West Conshohocken, PA.
- ASTM. (2010). "Standard practice for classification of soils for engineering purposes (Unified Soil Classification System)." ASTM D2487, ASTM International, West Conshohocken, PA.
- Barbour, S. L., and Fredlund, D. G. (1989). "Mechanisms of osmotic flow and volume change in clay soils." *Canadian Geotechnical Journal*, 26(4), 551-562.
- Benson, C. H., Jo, H. Y., and Abichou, T. (2004). "Forensic analysis of excessive leakage from lagoons lined with a composite GCL." *Geosynthetics International*, 11(3), 242-252.
- Benson, C. H., and Meer, S. R. (2009). "Relative abundance of monovalent and divalent cations and the impact of desiccation on geosynthetic clay liners." *Journal of Geotechnical and Geoenvironmental Engineering*, 135(3), 349-358.
- Benson, C. H., Thorstad, P. A., Jo, H. Y., and Rock, S. A. (2007). "Hydraulic performance of geosynthetic clay liners in a landfill final cover." *Journal of Geotechnical and Geoenvironmental Engineering*, 133(7), 814-827.
- Boels, D., and van der Wal, K. "Trisoplast: New developments in soil protection." *Cagliari, Italy, Sardinia 99, CISA, Padova, Italy 77-84.*
- Bradshaw, S., Benson, C., and Scalia, J. (2012). "Cation exchange during subgrade hydration and effect on hydraulic conductivity of GCLs." *Journal of Geotechnical and Geoenvironmental Engineering*, In press.
- Buchholz, F., and Graham, A. (1998). *Modern Superabsorbent Polymer Technology*, John Wiley and Sons, New York.
- Christman, M., Benson, C. H., and Edil, T. B. (2002). "Geophysical evaluation of annular well seals." *Groundwater Monitoring and Remediation*, 22(3), 104-112.
- Di Emidio, G. (2010). *Hydraulic and Chemico-Osmotic Performance of Polymer Treated Clay*, PhD Dissertation, University of Ghent, Ghent, Belgium.

- Di Maio, C. (1996). "Exposure of bentonite to salt solution: Osmotic and mechanical effects." *Geotechnique*, 46(4), 695-707.
- Egloffstein, T. (2001). "Natural bentonites - Influence of the ion exchange and partial desiccation on permeability and self-healing capacity of bentonites used in GCLs." *Geotextiles and Geomembranes*, 19(7), 427-444.
- Estornell, P., and Daniel, D. E. (1992). "Hydraulic conductivity of 3 geosynthetic clay liners." *Journal of Geotechnical Engineering*, 118(10), 1592-1606.
- Evans, J. C. (1993). "Vertical cutoff walls." *Geotechnical Practice for Waste Disposal*, D. E. Daniel, ed., Chapman & Hall, London, 430 - 454.
- Evans, J. C., Shackelford, C. D., Yeo, S. S., and Henning, J. (2008). "Membrane behavior of soil-bentonite slurry-trench cutoff walls." *Soil & Sediment Contamination*, 17(4), 316-322.
- Fritz, S. J. (1986). "Ideality of clay membranes in osmotic processes - a review." *Clays and Clay Minerals*, 34(2), 214-223.
- Groenevelt, P. H., and Elrick, D. E. (1976). "Coupling phenomena in saturate homo-ionic montmorillonite. 2. Theoretical." *Soil Science Society of America Journal*, 40(6), 820-823.
- Gullick, R. W., and Weber, W. J. (2001). "Evaluation of shale and organoclays as sorbent additives for low-permeability soil containment barriers." *Environmental Science & Technology*, 35(7), 1523-1530.
- Heller, H., and Keren, R. (2003). "Anionic polyacrylamide polymer adsorption by pyrophyllite and montmorillonite." *Clays and Clay Minerals*, 51(3), 334-339.
- Henning, J. T., Evans, J. C., and Shackelford, C. D. (2006). "Membrane behavior of two backfills from field-constructed soil-bentonite cutoff walls." *Journal of Geotechnical and Geoenvironmental Engineering*, 132(10), 1243-1249.
- Ito, H. (2006). "Compaction properties of granular bentonites." *Applied Clay Science*, 31(1-2), 47-55.
- James, A. N., Fullerton, D., and Drake, R. (1997). "Field performance of GCL under ion exchange conditions." *Journal of Geotechnical and Geoenvironmental Engineering*, 123(10), 897-901.
- Jo, H. Y., Benson, C. H., and Edil, T. B. (2004). "Hydraulic conductivity and cation exchange in non-prehydrated and prehydrated bentonite permeated with weak inorganic salt solutions." *Clays and Clay Minerals*, 52(6), 661-679.

- Jo, H. Y., Benson, C. H., Shackelford, C. D., Lee, J. M., and Edil, T. B. (2005). "Long-term hydraulic conductivity of a geosynthetic clay liner permeated with inorganic salt solutions." *Journal of Geotechnical and Geoenvironmental Engineering*, 131(4), 405-417.
- Jo, H. Y., Katsumi, T., Benson, C. H., and Edil, T. B. (2001). "Hydraulic conductivity and swelling of nonprehydrated GCLs permeated with single-species salt solutions." *Journal of Geotechnical and Geoenvironmental Engineering*, 127(7), 557-567.
- Kajita, L. S. (1997). "An improved contaminant resistant clay for environmental clay liner applications." *Clays and Clay Minerals*, 45(5), 609-617.
- Kang, J.-B., and Shackelford, C. D. (2009). "Clay membrane testing using a flexible-wall cell under closed-system boundary conditions." *Applied Clay Science*, 44(1-2), 43-58.
- Kang, J. B., and Shackelford, C. D. (2010). "Membrane behavior of compacted clay liners." *Journal of Geotechnical and Geoenvironmental Engineering*, 136(10), 1368-1382.
- Kang, J.-B., and Shackelford, C. D. (2011). "Consolidation enhanced membrane behavior of a geosynthetic clay liner." *Geotextiles and Geomembranes*, 29(6), 544-556.
- Katsumi, T., Ishimori, H., Ogawa, A., Yoshikawa, K., Hanamoto, K., and Fukagawa, R. (2007). "Hydraulic conductivity of nonprehydrated geosynthetic clay liners permeated with inorganic solutions and waste leachates." *Soils and Foundations*, 47(1), 79-96.
- Kenney, T. C., Vanveen, W. A., Swallow, M. A., and Sungaila, M. A. (1992). "Hydraulic conductivity of compacted bentonite sand mixtures." *Canadian Geotechnical Journal*, 29(3), 364-374.
- Kolstad, D. C., Benson, C. H., and Edil, T. B. (2004). "Hydraulic conductivity and swell of nonprehydrated geosynthetic clay liners permeated with multispecies inorganic solutions." *Journal of Geotechnical and Geoenvironmental Engineering*, 130(12), 1236-1249.
- Lagaly, G., Ogawa, M., Dékány, I., Faïza Bergaya, B. K. G. T., and Gerhard, L. (2006). "Chapter 7.3 Clay Mineral Organic Interactions." *Developments in Clay Science*, Elsevier, 309-377.
- Lee, J. M., and Shackelford, C. D. (2005a). "Concentration dependency of the prehydration effect for a geosynthetic clay liner." *Soils and Foundations*, 45(4), 27-41.
- Lee, J. M., and Shackelford, C. D. (2005b). "Impact of bentonite quality on hydraulic conductivity of geosynthetic clay liners." *Journal of Geotechnical and Geoenvironmental Engineering*, 131(1), 64-77.

- Lee, J. M., and Shackelford, C. D. (2005c). "Solution retention capacity as the swell index test for sodium an alternative to bentonite." *Geotechnical Testing Journal*, 28(1), 61-70.
- Lee, J. M., Shackelford, C. D., Benson, C. H., Jo, H. Y., and Edil, T. B. (2005). "Correlating index properties and hydraulic conductivity of geosynthetic clay liners." *Journal of Geotechnical and Geoenvironmental Engineering*, 131(11), 1319-1329.
- Lin, L. C., and Benson, C. H. (2000). "Effect of wet-dry cycling on swelling and hydraulic conductivity of GCLs." *Journal of Geotechnical and Geoenvironmental Engineering*, 126(1), 40-49.
- Lo, I. M. C., Liljestrand, H. M., Khim, J., and Shimizu, Y. (1996). "Clay liner materials for land disposal of hazardous non-metal wastes." *Water Science and Technology*, 33(8), 71-77.
- Malusis, M. A., and Shackelford, C. D. (2002a). "Chemico-osmotic efficiency of a geosynthetic clay liner." *Journal of Geotechnical and Geoenvironmental Engineering*, 128(2), 97-106.
- Malusis, M. A., and Shackelford, C. D. (2002b). "Coupling effects during steady-state solute diffusion through a semipermeable clay membrane." *Environmental Science & Technology*, 36(6), 1312-1319.
- Malusis, M. A., Shackelford, C. D., and Olsen, H. W. (2001). "A laboratory apparatus to measure chemico-osmotic efficiency coefficients for clay soils." *Geotechnical Testing Journal*, 24(3), 229-242.
- Malusis, M. A., Shackelford, C. D., and Olsen, H. W. (2003). "Flow and transport through clay membrane barriers." *Engineering Geology*, 70 (3-4), 235-248.
- Manassero, M., and Dominijanni, A. (2003). "Modelling the osmosis effect on solute migration through porous media." *Geotechnique*, 53(5), 481-492.
- Meer, S. R., and Benson, C. H. (2007). "Hydraulic conductivity of geosynthetic clay liners exhumed from landfill final covers." *Journal of Geotechnical and Geoenvironmental Engineering*, 133(5), 550-563.
- Mitchell, J. K. (1976). *Fundamentals of Soil Behavior*, John Wiley & Sons, New York.
- Mitchell, J. K., and Soga, K. (2005). *Fundamentals of Soil Behavior*, 3rd Ed., John Wiley & Sons, Hoboken, N.J.
- Muzny, C. D., Butler, B. D., Hanley, H. J. M., Tsvetkov, F., and Peiffer, D. G. (1996). "Clay platelet dispersion in a polymer matrix." *Materials Letters*, 28(4-6), 379-384.
- Olsen, H. W., Yearsley, E. N., and Nelson, K. R. (1990). "Chemico-osmosis versus diffusion-osmosis." Transportation Research Board, Washington, DC, 15-22.

- Scalia, J. (2012). "Bentonite-polymer composites for containment applications," PhD Dissertation, University of Wisconsin - Madison, Madison, WI.
- Scalia, J., and Benson, C. H. (2011). "Hydraulic conductivity of geosynthetic clay liners exhumed from landfill final covers with composite barriers." *Journal of Geotechnical and Geoenvironmental Engineering*, 137(1), 1-13.
- Scalia, J., Benson, C. H., Edil, T. B., Bohnhoff, G. L., and Shackelford, C. D. "Geosynthetic clay liners containing bentonite polymer nanocomposite " *GeoFrontiers 2011: Advances in Geotechnical Engineering*, ASCE, Reston, VA, 1961-1970.
- Shackelford, C. D. (2011). "Membrane behavior in geosynthetic clay liners." *GeoFrontiers 2011: Advances in Geotechnical Engineering*, ASCE, Reston, VA, 1961-1970.
- Shackelford, C. D. (2012). "Membrane behavior of engineered clay barriers for geoenvironmental containment: State of the art." *GeoCongress 2012-State of the Art and Practice in Geotechnical Engineering*, R. D. Hryciw, A. Athanasopoulos-Zekkos, and N. Yesiller, eds., ASCE, Oakland, CA, 3419-3428.
- Shackelford, C. D., Benson, C. H., Katsumi, T., Edil, T. B., and Lin, L. (2000). "Evaluating the hydraulic conductivity of GCLs permeated with non-standard liquids." *Geotextiles and Geomembranes*, 18(2-4), 133-161.
- Shackelford, C. D., and Daniel, D. E. (1991). "Diffusion in saturated soil. 1. Background." *Journal of Geotechnical Engineering*, 117(3), 467-484.
- Shackelford, C. D., and Lee, J. M. (2003). "The destructive role of diffusion on clay membrane behavior." *Clays and Clay Minerals*, 51(2), 186-196.
- Shackelford, C. D., Malusis, M. A., and Olsen, H. W. (2003) "Clay membrane behavior for geoenvironmental containment " *Soil and Rock America Conference 2003, Proceedings of the joint 12th Panamerican Conference on Soil Mechanics and Geotechnical Engineering and the 39th U. S. Rock Mechanics Symposium*, 767-774.
- Smith, J. A., Bartelt-Hunt, S. L., and Burns, S. E. (2003). "Sorption and permeability of gasoline hydrocarbons in organobentonite porous media." *Journal of Hazardous Materials*, 96(1), 91-97.
- Sposito, G. (1989). *The Chemistry of Soils*, Oxford University Press, New York.
- Vasko, S., Jo, H. Y., Benson, C. H., Edil, T. B., and Katsumi, T. (2001). "Hydraulic conductivity of partially prehydrated geosynthetic clay liners permeated with aqueous calcium chloride solutions." *Geosynthetics 2001*, Industrial Fabrics Assoc. International, St. Paul, MN, 685-699.

Yeo, S. S., Shackelford, C. D., and Evans, J. C. (2005). "Membrane behavior of model soil-bentonite backfills." *Journal of Geotechnical and Geoenvironmental Engineering*, 131(4), 418-429.

Chapter 4

Coupled Solute Diffusion and Membrane Behavior of a Polymerized

Bentonite

SUMMARY: Bentonite is commonly used in hydraulic containment barriers to contain liquid flow and contaminant transport because of the low hydraulic conductivity to water, substantial membrane behavior, and low diffusion coefficients. However, bentonite has been shown to be affected adversely by environmental conditions that promote multivalent for monovalent cation exchange. Thus, bentonites have been modified to be more compatible with the surrounding environment. In this study, the diffusive properties of a polymerized bentonite, referred to as a bentonite polymer nanocomposite, or BPN, are determined through the simultaneous measurement of membrane efficiency coefficients and diffusion coefficients during multi-stage steady-state diffusion of potassium chloride (KCl). The diffusive properties are correlated with the membrane behavior of the BPN and compared with the properties of a traditional bentonite in the form of a geosynthetic clay liner (GCL). The diffusive properties were shown to correlate with the membrane behavior of the BPN such that that the diffusive flux decreased as the membrane efficiency of the BPN increased. For example, for a test in the rigid-wall cell, the effective diffusion coefficient for chloride or $D_{Cl^-}^*$ is 1.0×10^{-10} m²/s when the membrane efficiency coefficient, ω , is equal to 0.20; whereas, $D_{Cl^-}^*$ is 3.5×10^{-11} m²/s when ω is equal to 0.88. In contrast to previous test results, the effective diffusion coefficients for potassium, $D_{K^+}^*$, and $D_{Cl^-}^*$ were not equal at steady-state with $D_{Cl^-}^*$ generally being greater than $D_{K^+}^*$, especially at lower concentration of KCl (e.g., 4.7 mM). The existence of excess Na⁺ in the BPN prior to testing may have contributed to lower $D_{K^+}^*$ compared to $D_{Cl^-}^*$.

KEY WORDS: Chemico-osmosis; Clay membranes; Diffusion; Geosynthetic clay liner; Polymer modified bentonites; Semipermeable membrane

4.1 INTRODUCTION

Bentonite is a type of natural clay comprised primarily of the mineral montmorillonite (smectite) and is commonly used in hydraulic containment barriers to control liquid flow and contaminant transport. Example applications include *in situ* vertical cutoff walls for control of groundwater, barriers (liners) for waste containment (e.g., landfills, wastewater ponds, manure lagoons, nuclear storage, etc.), secondary containment in tank farms, and seals in monitoring and water supply wells (Estornell and Daniel 1992; Evans 1994; Kajita 1997; Christman et al. 2002; Smith et al. 2003). Sodium bentonite (Na-bentonite), where Na^+ is the dominant exchangeable cation, is used in nearly all of these applications. Na-bentonite is preferred for such applications relative to other types of bentonite, such as calcium bentonite (Ca-bentonite) or magnesium bentonite (Mg-bentonite), because Na-bentonite tends to swell to a greater extent in the presence of water leading to lower hydraulic conductivity, k , to water or dilute aqueous solutions containing inorganic or organic solutes (i.e., $k \leq 10^{-10}$ m/s). Also, Na-bentonites can exhibit substantial semipermeable membrane behavior for dilute concentrations of simple salts (Malusis et al. 2001; Malusis and Shackelford 2002a; Kang and Shackelford 2009). Both membrane behavior and low k are beneficial in hydraulic containment applications, because (1) low k results in limited advective (hydraulically driven) transport, and (2) membrane behavior promotes hyperfiltration, chemico-osmotic flow, and reduced diffusion of aqueous-phase chemicals (Shackelford et al. 2003; Shackelford 2011; Shackelford 2012).

However, the beneficial properties of bentonite can be affected adversely by environmental conditions that promote exchange of multivalent cations for monovalent cations (i.e., cation exchange). Such cation exchange can cause a collapse of the hydrated interlayer of the bentonite and limit osmotic swell, thereby potentially increasing the mass flux of aqueous soluble chemicals via advection and diffusion and decreasing hyperfiltration and chemico-osmotic counter flow (Malusis and Shackelford 2002b; Manassero and Dominijanni 2003; Kolstad et al. 2004).

This incompatibility between chemicals in solution and Na-bentonite has spurred considerable interest in modifying bentonites to be more compatible with the surrounding environment. For example, Na-bentonites have been amended with organic molecules for improved hydraulic and diffusive performance (e.g., Onikata et al. 1996, 1999; Trauger and Darlington 2000; Ashmawy et al. 2002; Di Emidio 2010; Di Emidio et al. 2010; Mazzieri et al. 2010a and b; Di Emidio et al. 2011; Mazzieri 2011). In these cases, organic molecules were intercalated to increase the potential for osmotic swell in the presence of multivalent-for-monovalent cation exchange and/or elevated solute concentrations.

The bentonite investigated in this study was modified at the nanoscale in an attempt to ensure that the swollen structure of the bentonite is retained. Organic molecules (acrylic acid) were inserted between the montmorillonite layers and then polymerized *in situ* to form an interconnected structure within the bentonite. Because this modification occurs at the nanoscale, the resulting modified material commonly is referred to as a bentonite-polymer nanocomposite or BPN (Scalia et al. 2011; Scalia 2012).

The BPN evaluated in this study is unique relative to other treated or modified bentonites, such as organobentonites, and the more typical anionic polymer modified bentonites. In the

case of the BPN, the polymerized bentonite is formed when acrylic acid molecules are polymerized after insertion into the interlayers of the montmorillonite mineral structure. In contrast, organobentonites typically are synthesized either by solution or by solid-state reactions (Lagaly et al. 2006). Also, typical anionic polymer modified bentonites employ long-chain anionic polymers, such as the anionic polyacrylimides, that are electrostatically associated with the positively charged edges of the bentonite platelets (e.g., Boels and van der Wal 1999; Heller and Keren 2003), rather than bonded in the interlayer space of the montmorillonite mineral structure as occurs in the case of the BPN evaluated in this study.

Traditional Na-bentonites in the form of manufactured hydraulic barriers known as a geosynthetic clay liners, or GCLs, have been shown to exhibit semipermeable membrane behavior (e.g., Malusis and Shackelford 2002a). The existence of this membrane behavior also has been shown experimentally to be directly correlated with solute diffusion through the Na-bentonite, whereby an increase in membrane efficiency towards that for an ideal (perfect) semipermeable membrane was shown to correlate with a decrease in the diffusive solute flux through Na-bentonite (Malusis and Shackelford 2002b). Such a decrease in solute flux also is beneficial to the containment function of hydraulic barriers (Shackelford et al. 2003; Kang and Shackelford 2011).

Accordingly, the purpose of this study was to evaluate simultaneously both the diffusive and membrane properties of the BPN, and then correlate the diffusive properties with the membrane behavior of the BPN. The hypothesis was that the diffusive and membrane properties of the BPN would be superior to those of a traditional Na-bentonite, and that the diffusive flux would decrease as the membrane efficiency of the BPN increased. This hypothesis was evaluated through the simultaneous measurement of membrane efficiency coefficients and

effective diffusion coefficients during multi-stage steady-state diffusion of potassium chloride (KCl) through the BPN over a range in source concentrations for which the BPN behaved as a semipermeable membrane. The results of this study were compared with those of a traditional (unmodified) Na-bentonite from literature. In addition, unlike previous studies wherein the Na-bentonites were permeated with de-ionized water prior to membrane testing in order to leach (flush) soluble salts from the pore waters of the Na-bentonites, thereby enhancing the measured membrane behavior, the specimens of BPN tested in this study were not flushed of soluble salts prior to membrane testing. Thus, any enhanced membrane and/or diffusion behavior of the BPN relative to that of previous studies would be under conditions that were less favorable for BPN.

4.2 MATERIALS AND METHODS

4.2.1 Materials

The BPN evaluated in this study was provided by Colloid Environmental Technologies Co. (CETCO, Hoffman Estates, IL). The BPN was created using polyacrylic acid (PAA) and methods similar to the production of polymer nanocomposites (e.g., Muzney et al. 1996). The BPN classified as a high-plasticity clay or CH according to the Unified Soil Classification System (ASTM D 2487). Mineralogical analyses conducted by Mineralogy, Inc. (Tulsa, OK) using x-ray diffraction indicated the composition of the BPN as 76 % montmorillonite, 15 % quartz, 7 % plagioclase feldspar, and 2 % illite/mica. Additional details regarding the properties of the BPN are provided in Chapter 3 and by Scalia et al. (2011) and Scalia (2012).

The liquids used in this study included de-ionized water (DIW) and solutions of DIW with potassium chloride (KCl) (certified A.C.S.; Fisher Scientific, Fair Lawn, NJ) with measured concentrations ranging from 4.7 mM to 54 mM KCl. Concentrations of all inorganic metals

(e.g., K^+ , Na^+) monitored in the study were measured using inductively coupled plasma-atomic emission spectrometry or ICP-AES (IRIS[®] Advantage/1000 ICAP Spectrometer, Thermo Jarrel Ash Co., Franklin, MA), whereas concentrations of anionic chemical species, principally chloride (Cl^-), were measured using ion chromatography or IC (Dionex[®] 4000i IC Module, Dionex Co., Sunnyvale, CA). The measured pH of the KCl solutions ranged from 5.20 to 5.31 and the measured electrical conductivity, EC , ranged from 70.7 to 661 mS/m.

4.2.2 Testing Apparatus and Procedures

The testing apparatus and procedures used in this study are similar to those described in detail by Malusis et al. (2001) and Kang and Shackelford (2009). In summary, a saturated BPN specimen is confined in either a rigid-wall cell or a flexible-wall cell. A solution with an initial concentration of KCl, $C_{o,t} (> 0)$, is circulated through a porous disk along the top of the specimen while DIW ($C_{o,b} = 0$) is circulated simultaneously through a porous disk along the base of the specimen. The system is closed during membrane testing such that no liquid flow is allowed to occur through the specimen to maintain a constant volume condition. As a result, a pressure builds up on the high concentration side (i.e., top) of the specimen during circulation of KCl to counteract the tendency for chemico-osmotic liquid flow from the bottom to the top of the specimen. The pressures in the top and bottom circulation lines are measured continuously using in-line pressure transducers (model Nos. PX181-100G5V or PX209-015G10V, Omega Engineering Inc., Stamford, CT), and the difference in pressure across the specimen, $-\Delta P (> 0)$, which represents the chemico-osmotic pressure, is monitored directly using a differential pressure transducer (model DP15-64, Validyne Engineering Corp., Northridge, CA).

If the specimen is not an ideal membrane, then solutes can and do diffuse from the top to the bottom of the specimen. In the present case, this diffusion results in concentrations of K^+ and Cl^- in the circulation outflow from the base of the specimen being greater than those in the circulation inflow to the base of the specimen ($C_b > C_{o,b}$), whereas concentrations of K^+ and Cl^- in the circulation outflow from the top of the specimen are lower than those in the circulation inflow at the top of the specimen ($C_t < C_{o,t}$). As a result, the concentrations of relevant chemical species in the circulation outflows from the bottom of the specimens were monitored as a function of time primarily for the purpose of determining diffusion coefficients as discussed subsequently (see Section 4.2.4).

4.2.3 Determination of Membrane Efficiency

Under the no-flow ($q = 0$) conditions imposed in this study, the membrane or chemico-osmotic efficiency coefficient, ω , is defined as follows (Groenevelt and Elrick 1976; Malusis et al. 2001):

$$\omega = \frac{\Delta P}{\Delta \pi} \quad (4.1)$$

where ΔP is the measured chemico-osmotic pressure difference induced across the specimen as a result of prohibiting chemico-osmotic flux of liquid, and $\Delta \pi$ is the theoretical chemico-osmotic pressure difference across an "ideal" semipermeable membrane (i.e., $\omega = 1$) subjected to an applied difference in solute (electrolyte) concentration (e.g., Olsen et al. 1990). The $\Delta \pi$ is calculated in accordance with the van't Hoff expression (Malusis et al. 2001).

4.2.4 Measurement of Transport Parameters

The concentration gradient imposed across the specimen results in solute diffusion from the higher concentration boundary at the top of the specimen to the lower concentration boundary at the base of the specimen. As long as the concentration boundaries are maintained reasonably constant, the diffusion of solutes through the specimen will eventually reach a steady state. This method of measuring effective diffusion coefficients commonly is referred to as the steady-state method, the time-lag method, or the through-diffusion method (e.g., Shackelford 1991). In this method, the concentrations typically are converted to the area normalized cumulative mass per unit area, Q_t , that has diffused through the specimen, as follows:

$$Q_t = \frac{1}{A} \sum_{i=1}^{N_s} \Delta m_i = \frac{1}{A} \sum_{i=1}^{N_s} C_{b,i} \Delta V_i \quad (4.2)$$

where A = cross-sectional area of the specimen, Δm_i = the incremental mass of the solute species collected over a time increment, Δt , $C_{b,i}$ = the mass concentration of the solute species in the incremental volume, ΔV_i , of the circulation outflow from the base of the pedestal corresponding to the Δt , and N_s = the number of incremental samples corresponding to the total elapsed time, t . An important constraint in the use of Eq. 4.2 is that all solute mass must be included, such that sampling must be continuous, although ΔV_i can vary. The data typically are plotted as Q_t versus the cumulative, elapsed time, t . The plot generally is nonlinear at the beginning or transient stage of the test, followed by a steady-state stage which is indicated by a straight line representing constant diffusive mass flux (Shackelford 1991).

For comparison, values of the effective diffusion coefficient, D^* , were determined in two ways, *viz.*, by performing a linear regression of only the steady-state portion of the data, and by

performing a non-linear regression of all of the data. As described by Shackelford and Lee (2003), for the case of simple salts, such as the KCl solutions used in this study, diffusing through specimens where the concentrations of remnant ions within the pores of the specimen are much lower than that of the diffusing salt, the charge fluxes of the anion (i.e., Cl^-) and the cation (K^+) at steady state theoretically must be the same in order to satisfy the requirement for electroneutrality in solution. Since KCl is a 1:1 salt, an equivalent charge flux is the same as an equivalent molar flux, i.e., since the magnitudes of the charges on the two ions are the same. Since the atomic weights for Cl^- and K^+ are slightly different, i.e., 35.5 versus 39.1, this requirement for equivalent molar fluxes of Cl^- and K^+ means that the mass flux of K^+ theoretically should be 1.1 (= 39.1/35.5) times greater than that for Cl^- at steady state, i.e., assuming only Cl^- and K^+ are emanating from the specimen at steady state. In contrast, during the initial transient stage of the test, the requirement for electroneutrality can be significantly more complicated than that at steady state. During this transient stage, interaction between Cl^- and K^+ and the other anions and cations initially within in the pore liquids may affect the mobility of the Cl^- and K^+ , such that any differences in the values of D^* for Cl^- and K^+ based on the transient stage data versus those based on the steady-state data should reflect, in part, the impact of solute-solute interactions.

The effective diffusion coefficient, D^* , was determined by linear regression of the steady-state portion of the Q_t versus t data based on the following equation (e.g. Shackelford 1991):

$$D^* = \left(\frac{\Delta Q_t}{\Delta t} \right) \left(\frac{L}{nw_A \Delta C} \right) \quad (4.3)$$

where $\Delta Q_t / \Delta t$ represents the slope of the linear regression, L is the specimen thickness, n is the

specimen porosity, w_A is the atomic weight of the diffusing solute, ΔC is the molar concentration difference of the solute (i.e., anion or cation) across the specimen. A sequential linear regression was conducted on the data as described in Shackelford and Lee (2003). Briefly, a linear regression was conducted on an increasing number of Q_t versus t data points until the coefficient of determination, r^2 , deviated significantly from unity. The point where this deviation occurred was assumed to be the distinction between the transient and steady-state portion of the data or time to steady-state, t_{ss} . The steady-state data was used to calculate D^* which is defined as follows (Shackelford and Daniel 1991; Malusis and Shackelford 2002b):

$$D^* = D_o \tau_a \quad (4.4)$$

where D_o is the aqueous-phase or free-solution diffusion coefficient of the solute, τ_a is an apparent tortuosity factor ($0 \leq \tau_a \leq 1$) representing the product of the actual matrix (geometric) tortuosity factor, τ_m , and a restrictive tortuosity factor, τ_r , or

$$\tau_a = \tau_m \tau_r = \tau_m \prod_{i=1}^N \tau_i = \tau_m (\tau_1 \tau_2 \cdots \tau_N) \quad (4.5)$$

where τ_r represents the product of N other factors (τ_i) that contribute to the apparent tortuosity factor by acting to reduce or restrict the diffusive solute flux through the porous medium, such as anion exclusion, increased water viscosity near the surface of clay particles, etc..

As previously noted, D^* also was determined by performing non-linear regression of the complete set of data (i.e., both the transient and the steady-state data) using the entire solution to

Fick's second law for the case of diffusion through porous media with a constant inlet concentration c_1 at $x = 0$ and outlet concentration c_2 ($c_2 \ll c_1$) at $x = L$ (e.g., Crank 1975). In this case, the cumulative mass of a solute that has diffused through the porous media at an elapsed time, t , is given as follows (e.g., Skagius and Neretnieks 1986):

$$Q_t = Lc_1 \left[\frac{D^*nt}{L^2} - \frac{R_d n}{6} - \frac{2R_d n}{\pi^2} \sum_{i=1}^{\infty} \frac{(-1)^i}{i^2} \exp\left(-\frac{D^*ni^2\pi^2t}{L^2R_d n}\right) \right] \quad (4.6)$$

where $R_d (\geq 1)$ is the retardation factor of the solute which takes into account the possibility for linear, reversible, instantaneous sorption. Equation 4.6 was fitted to the measured data via non-linear regression to determine both D^* and R_d simultaneously.

4.2.5 Testing Program

Multiple-stage membrane/diffusion tests were conducted in this study by sequentially circulating four KCl solutions (4.7, 9.3, 20, and 54 mM KCl) across the top boundary of the specimen for each test, while simultaneously circulating DIW across the bottom boundary of the specimen. A total of four tests were conducted, two using a rigid-wall (RW) cell and two using a flexible-wall (FW) cell. The rigid-wall tests, designated as RW1 and RW2, corresponded to specimen thicknesses, L , of 16.7 mm and 8.6 mm and total specimen porosities, n , of 0.92 and 0.80, respectively. The flexible-wall tests, designated as FW1 and FW2, corresponded to initial effective stresses, σ' , of 34.5 kPa (5 psi) and 103 kPa (15 psi), respectively, and initial values of n immediately after consolidation, but prior to membrane testing, of 0.95 and 0.84, respectively. The circulation liquid emanating from the top of the specimens was collected and analyzed for concentrations of cations (ICP). The circulation liquid from the bottom of the specimens was

analyzed for concentrations of anions (IC) and cations (ICP) and the concentrations were then used for determination of D^* . A detailed description of the membrane testing procedure is provided in Chapter 3.

4.3 RESULTS

4.3.1 Membrane Efficiency Coefficients

The results of the membrane efficiency coefficient measurements for the two rigid-wall tests (RW1 and RW2) and the two flexible-wall tests (FW1 and FW2) were previously presented and discussed in detail in Chapter 3. The resulting ω values are summarized in Table 4.1 and range from 0.88 for RW2 during the circulation of 4.7 mM KCl to 0.04 for FW1 during circulation of 54 mM KCl. Consistent with previous studies, the ω values decrease with increasing concentration of KCl, increase with decreasing porosity or increasing initial effective stress, and decrease for tests conducted in flexible-wall cells compared to those conducted in rigid-wall cells (Malusis et al. 2001; Malusis and Shackelford 2002a; Kang and Shackelford 2009; Kang and Shackelford 2011). Further details associated with these measured ω values can be found in Chapter 3.

4.3.2 Exit Concentrations and Charge Balances

The measured exit concentrations of cations (Ca^{2+} , K^+ , and Na^+) from the top and bottom of the cell (i.e., C_t and C_b , respectively) during testing are shown in Figs. 4.1 and 4.2. The steady-state concentrations of K^+ increased as the source concentration (C_{or}) increased with each stage of the test (e.g, from 4.7 mM to 9.3 mM KCl, from 9.3 mM to 20 mM, etc.). The concentrations of Na^+ measured in the circulation outflows from the top and bottom of the cell

represent the excess Na^+ initially present within the BPN as a result of manufacturing (Scalia 2012). The fact that Na^+ is measured in the circulation outflow from the top of the specimen indicates that diffusion of remnant Na^+ occurred from within the BPN towards both specimen boundaries. The concentrations of Na^+ exiting the bottom of the cell exceeded the concentrations of K^+ during the first two stages (4.7 mM and 9.3 mM KCl) for all four tests (refer to Fig. 4.2). However, during the last stage of the tests when 54 mM KCl was being circulated across the top of the specimens, the concentrations of K^+ in the bottom of the cell exceeded the concentrations of Na^+ , due to increased diffusion of K^+ through the BPN and a continually diminishing amount of remnant Na^+ in the BPN. Concentrations of Ca^{2+} generally were low (i.e., near the detection limit) throughout the tests.

The measured exit concentrations of anions (i.e., Cl^- , F^- , and SO_4^{2-}) from the bottom of the cell for all four membrane tests are included in Fig. 4.3. Measured Cl^- concentrations were predominant among the concentration of anions in the circulation outflows and were used to calculate diffusion coefficients for Cl^- . The steady-state concentrations of Cl^- increased with each stage of the test as the source concentrations (C_{ot}) increased. The concentrations of Cl^- reached steady state quicker than those of K^+ as a result of cation exchange, principally K^+ for Na^+ initially present on the BPN, as well as due to electroneutrality constraints resulting from the excess Na^+ in the pore water of the BPN as discussed subsequently in Section 4.4.3.

The solute concentrations measured at the bottom of the cell during testing, as well as the charge balances representing the differences between the sum of the cationic charges and the sum of the anionic charges, are shown as a function of the elapsed time in Fig. 4.4 and 4.5, respectively. The total concentration of cations includes the sum of the concentrations of Na^+ , K^+ , and Ca^{2+} , whereas the total concentrations of anions includes the sum of the concentrations

of Cl^- , F^- , and SO_4^{2-} . The concentrations of additional cations and anions also were measured, including the cations Ag, B, Ba, Be, Cd, Co, Cr, Cu, Fe, L, Mg, Mn, Mo, Ni, P, Pb, S, Si, Sr, Ti, V, Zn and the anions NO_2^- , NO_3^- , Br^- , PO_4^{3-} , but were either negligible (i.e., < 0.1 mg/L) or nondetectable. Except for the stage of the tests involving circulation of the 54 mM KCl solution, the total concentration of the cations generally were greater than that of the anions at the bottom of the cell. As a result, the charge balance generally was slightly greater than zero for the majority of the stages of all tests. In the case of the circulation of the 54 mM KCl solution, the aforementioned trend was not consistent among the different tests. For example, during circulation of the 54 mM KCl solution, the total concentration of anions exceeded those of cations for test RW1, whereas the concentrations of cations exceeded those of anions for test FW2.

The total concentration of cations may be greater than that of the anions because of an excess of soluble Na^+ in the BPN as a result of the manufacture of the BPN (Scalia et al. 2011; Scalia 2012). In addition, there may be carboxylate anions (RCOO^-) in the system also as a result of the manufacture of the BPN (Scalia et al. 2011; Scalia 2012). The concentration of carboxylate anions was neither measured nor included in the charge balance, which may lead to an erroneous charge balance indicating an excess of cation relative to anions.

4.3.3 Diffusion Results

Plots of Q_t versus time for all four tests are shown in Fig. 4.6. Since multiple-stage membrane/diffusion tests were conducted, the slope of Q_t versus time increased with increasing concentration of KCl; i.e., a greater diffusive mass flux occurred as a result of the greater concentration gradient imposed across the specimen. In order to evaluate the results for D^* , the

four stages of the test were separated and net values of Q_t and t , or Q_t' and t' , respectively, pertaining to each individual stage of the test were defined as follows:

$$Q_t' = Q_{t,x+1} - Q_{t,x} \quad (4.7)$$

$$t' = t_{x+1} - t_x \quad (4.8)$$

where $Q_{t,x}$ (a constant) represents the final value of Q_t from the previous stage of the test and $Q_{t,x+1}$ (a variable) represents the values of Q_t determined for the current stage of the test. Similarly, t_x (a constant) represents the total elapsed time corresponding to the end of the previous stage of the test, and t_{x+1} (a variable) represents the elapsed time for the current stage of the test. Essentially, the use of Q_t' and t' for each stage of the test amounts to resetting Q_t and t to zero for the evaluation of D^* for each stage of the test (i.e., during circulation of 9.3 mM, 20 mM, and 54 mM KCl).

Individual plots of Q_t' versus time, t' for each test are shown in Figs 4.7 through 4.10 for Cl^- and in Figs 4.11 through 4.14 for K^+ . The slope of $\Delta Q_t' / \Delta t'$ varied from 48.4 to 2020 $\text{mg/m}^2\text{-d}$ for Cl^- and from 2.37 to 1600 $\text{mg/m}^2\text{-d}$ for K^+ . The $\Delta Q_t' / \Delta t'$ increased as the source concentration increased, again reflecting the greater diffusive solute mass flux with increasing C_{ot} . The lower magnitudes in $\Delta Q_t' / \Delta t'$ for K^+ indicate attenuation or exchange of the K^+ and interactions due to the excess Na^+ in the BPN.

The D^* values resulting from linear regression of the steady-state portion of the data are summarized in Table 4.1 and shown in Fig. 4.15. The values of D^* resulting from non-linear regression of the full data set for each stage of the membrane test based on Eq. 4.6 also are shown in Fig. 4.15 for comparison. In general, the values of D^* estimated from the linear

regression, or D_{ss}^* , are slightly higher than those estimated from the nonlinear regression, or D_{nl}^* , with the differences in values being most evident at the lowest source concentrations (e.g., 4.7 mM KCl). The ratio of the D_{ss}^* to the D_{nl}^* (i.e., D_{ss}^*/D_{nl}^*) varies from 0.84 to 1.54 with most values (> 62.5 %) within the narrow range of 1.02 to 1.09. Thus, the values of D_{ss}^* and D_{nl}^* are similar overall, with the values of D_{ss}^* being consistently higher (conservative), albeit only slightly, relative to the values of D_{nl}^* . The slight differences in the values of D_{ss}^* relative to those of D_{nl}^* reflect, in part, the influence of the remnant anions other than Cl^- and the remnant cations other than K^+ on the diffusion of Cl^- and K^+ through the BPN. All subsequent D^* values will be those based on D_{ss}^* .

The steady-state values of D^* for the K^+ or $D_{K^+}^*$, are generally lower than those for the Cl^- , or $D_{Cl^-}^*$, with differences between $D_{Cl^-}^*$ and $D_{K^+}^*$ decreasing with increasing source concentration, C_{ot} , of KCl. For example, for test FW1, $D_{Cl^-}^*$ is 1.7×10^{-10} and $D_{K^+}^*$ is 4.3×10^{-12} m²/s during circulation of 4.7 mM KCl, whereas $D_{Cl^-}^*$ is 2.9×10^{-10} m²/s and the $D_{K^+}^*$ is 2.0×10^{-10} m²/s during circulation with 54 mM KCl. These differences also are illustrated in Fig. 4.16 in terms of the ratio of the effective diffusion coefficient of chloride relative to that of potassium, or $D_{Cl^-}^*/D_{K^+}^*$. The values of $D_{Cl^-}^*/D_{K^+}^*$ are highest at a C_{ot} of 4.7 mM KCl (e.g., 36.9 for RW1), and decrease with increasing C_{ot} , such that the values of $D_{Cl^-}^*/D_{K^+}^*$ approach unity, the theoretical diffusion coefficient ratio of Cl^- to K^+ at steady state (e.g., for example, $D_{Cl^-}^*/D_{K^+}^*$ is 1.08 for RW2 when C_{ot} of 54 mM). These differences between $D_{Cl^-}^*$ and $D_{K^+}^*$, especially at the lower values of C_{ot} , which appear to violate the aforementioned requirement for electroneutrality, can be attributed to the confounding influence of the significant concentration

of remnant Na^+ in the pore liquid of the BPN specimens (as will be discussed in the following section).

In addition, the values of $D_{\text{Cl}^-}^*/D_{\text{K}^+}^*$ for RW2 and FW2 are lower than those for RW1 and FW1. The lower values of $D_{\text{Cl}^-}^*/D_{\text{K}^+}^*$ for RW2 and FW2 compared to RW1 and FW1 may be a result of the lower porosity ($n = 0.80$ vs. $n = 0.92$ for RW2 and RW1, respectively) or the higher effective stress ($\sigma' = 103$ kPa [15 psi] vs. 34.5 kPa [5 psi]) which resulted in lower values of $D_{\text{Cl}^-}^*$ especially at lower values of C_{ot} . For example during the circulation of 4.7 mM KCl the $D_{\text{Cl}^-}^*$ for test RW1 is 1×10^{-10} m²/s whereas for test RW2 $D_{\text{Cl}^-}^*$ is 3.7×10^{-11} m²/s. The values of $D_{\text{Cl}^-}^*/D_{\text{K}^+}^*$ for FW2 also may be lower than those for FW1 as a result of drainage that occurred during consolidation of the specimen in test FW2 to a higher effective stress (i.e., $\sigma' = 103$ kPa [15 psi]). This drainage may have resulted in a reduced amount of soluble cations, Na^+ , in the pores liquid of the specimen. The effect of the Na^+ in the pore liquid is described in additional detail in the following section.

The values of D^* are plotted versus those of ω in Fig. 4.17. The values of D^* decrease with increasing ω as expected, since in the limit as the membrane behavior trends toward that of a perfect membrane (i.e., $\omega \rightarrow 1$), solute transport becomes increasingly more restricted such that no solute transport occurs when $\omega = 1$ (Malusis and Shackelford 2002b).

4.3.4 Apparent Tortuosity Factors

In general, the apparent tortuosity factor, τ_a , representing the effect of the porous media on the rate of solute diffusion, varies from zero when there are no interconnected pores corresponding to a perfect or ideal semipermeable membrane to unity when there is no porous

medium (Shackelford and Daniel 1991). That is, an increase in the value of τ_a reflects a less tortuous pathway and/or less solute restriction via membrane behavior (Malusis and Shackelford 2002b). Accordingly, values of τ_a were calculated by dividing the steady-state D^* values for Cl^- , $D_{\text{Cl}^-}^*$, by the free-solution (aqueous-phase) diffusion coefficient, D_o for KCl of $19.93 \times 10^{-10} \text{ m}^2/\text{s}$ (Shackelford and Daniel 1991), and the resulting values of τ_a are shown in Fig. 4.18.

The D_o value for KCl was used to calculate τ_a , because both K^+ and Cl^- were diffusing in the same direction during the tests which corresponds to the case of salt (mutual) diffusion (Shackelford and Daniel 1991). In this case, the self-diffusion coefficient, D_o , of K^+ ($19.6 \times 10^{-10} \text{ m}^2/\text{s}$) is lower than that of Cl^- ($20.3 \times 10^{-10} \text{ m}^2/\text{s}$), such that the diffusing K^+ tends to slow that rate of diffusion of Cl^- , whereas the diffusing Cl^- tends to speed the rate of diffusion of K^+ . As a result, the free-solution diffusion coefficient of KCl is intermediate between that for K^+ and Cl^- (Shackelford and Daniel 1991). Thus, use of the free-solution diffusion coefficient for the salt, KCl, should result in more representative values for τ_a than the more common practice of using the self-diffusion coefficient for Cl^- as D_o . In addition, the resulting τ_a values estimated using the free-solution diffusion coefficient for KCl are higher (i.e., more conservative) than those estimated using the self-diffusion coefficient for Cl^- . Regardless of this distinction, the differences in the τ_a values calculated in this study using either the D_o value for KCl or the D_o value for Cl^- were minor (< 0.001).

4.4 DISCUSSION

4.4.1 Comparison of Effective Diffusion Coefficients

The values of D^* measured in this study for BPN are compared in Fig. 4.19 versus those for a GCL reported by Malusis and Shackelford (2002b). The values of $D_{\text{Cl}^-}^*$ for the BPN are

similar to those for a GCL except for the results from RW2 where the $D_{Cl^-}^*$ values for the BPN range from 3.7×10^{-11} to 1.0×10^{-10} m²/s for C_{ot} of 4.7 and 54 mM KCl, respectively, whereas the $D_{Cl^-}^*$ values for the GCL range from 7.05×10^{-11} to 2.34×10^{-10} m²/s for C_{ot} of 3.9 to 47 mM KCl, respectively (refer to Fig. 4.19a). The lower $D_{Cl^-}^*$ for RW2 correlate with the higher ω for the BPN compared to the GCL. The lower $D_{Cl^-}^*$ and higher ω for the BPN compared with that of the GCL even when the porosities are similar (0.80 for the BPN versus 0.78 to 0.80 for the GCL) indicates that other factors are contributing to the measured ω and D^* of the BPN, such as the superabsorbent polymer (PAA) clogging the pores of the BPN (Scalia 2012).

In contrast the values of $D_{K^+}^*$ for the BPN are much lower than those for the GCL especially at lower C_{ot} (e.g., < 20 mM KCl, refer to Fig. 4.19b). The values of $D_{K^+}^*$ for the GCL vary from 4.39×10^{-11} to 1.99×10^{-10} m²/s whereas the values of $D_{K^+}^*$ for the BPN vary from 2.7×10^{-12} m²/s for RW1 to 2.0×10^{-10} m²/s for FW1. There are many potential factors contributing to the low $D_{K^+}^*$ for the BPN which are discussed in detail in Section 4.4.3.

The values of $D_{Cl^-}^*$ for both the BPN and the GCL are plotted versus ω in Fig. 4.20a. The values of $D_{Cl^-}^*$ for RW2 and FW2 are lower than those for the GCL for the range in ω measured in this study ($0.04 \leq \omega \leq 0.88$). The values of $D_{Cl^-}^*$ for the GCL are similar to the $D_{Cl^-}^*$ for tests RW1 and FW1. For both materials, BPN and GCL, the $D_{Cl^-}^*$ decrease with increasing ω such that $D_{Cl^-}^*$ trends toward zero as ω approaches unity. This result is consistent with the expected behavior of a semipermeable membrane as a perfect membrane (i.e., $\omega = 1$) restricts all solute transport.

4.4.2 Comparison of Tortuosity Factors

The resulting values of τ_a shown in Fig. 4.18a vary from 0.14 for FW1 to 0.017 for RW2. The values of τ_a are lower for RW2 and FW2 relative to those for RW1 and FW1. This difference occurs because RW2 and FW2 were conducted at lower porosities and higher σ' , respectively, resulting in more tortuous pathways. As ω approaches unity, τ_a must approach zero (see Fig. 4.18a), because, by definition, an ideal or perfect semipermeable membrane ($\omega = 1$) is one in which all solutes are restricted from migration. In addition, τ_a approaches a maximum value representing the matrix tortuosity factor, τ_m , as ω approaches zero (i.e., $\tau_a \rightarrow \tau_m$ as $\omega \rightarrow 0$, because $\tau_r \rightarrow 1$). As a result, values of τ_m were estimated by extrapolating the trends in the τ_a versus ω , and the resulting values of τ_m are summarized in Fig. 4.18a. The lowest value for τ_m of approximately 0.07 occurred for test RW2, whereas the values of τ_m for tests RW1 and FW1 are similar at 0.14 and 0.15, respectively.

As described in Section 4.2.4, τ_a also can be defined as the product of the τ_m and τ_r . Therefore, values τ_r were calculated as the ratio of τ_a relative to τ_m , or τ_a/τ_m (Malusis and Shackelford 2002b). The resulting values of τ_r are included in Fig. 4.18b, and tend to decrease as ω increases. This trend of decreasing τ_r with increasing ω is due to a more restrictive migration pathway resulting from an increase solute restriction and/or viscosity of water due to a thicker diffuse double layer (Shackelford and Daniel 1991; Malusis and Shackelford 2002b). In addition, the values of τ_r are lower for the rigid-wall tests (RW1 and RW2) and the flexible-wall test conducted at the higher σ' (FW2), indicating the migration pathways for these tests were more restrictive than those for FW1. Based largely on the results presented by Malusis and Shackelford (2002b), Manassero and Dominijanni (2003) proposed that τ_r be estimated using the

empirical correlation, $\tau_r = 1 - \omega$. The values of τ_r for this study generally follow this linear trend (refer to Fig. 4.18b).

The values of τ_m for both the BPN and the GCL are plotted versus n in Fig. 4.21. In general, the value of τ_m decreases with decreasing n for the BPN. The trend of τ_m versus n is linear over the narrow range in porosities encountered in this study (i.e., $0.84 \leq n \leq 0.95$). However, the negative y-intercept suggests that the relationship between τ_m and n is non-linear overall. The τ_m for the GCL (Malusis and Shackelford 2002b) is significantly greater than that for BPN at a similar porosity ($\tau_m = 0.12$ @ $n = 0.79$ and $\tau_m = 0.07$ @ $n = 0.80$, respectively). Since τ_m represents the component of the apparent tortuosity attributed only to the geometry of interconnected pores, a lower τ_m for the BPN at similar n indicates that the diffusive pathways of the interconnected pores for the BPN were more tortuous than those for the GCL, likely due, in part, to the presence of the superabsorbent polymer in the pores of the BPN.

4.4.3 Explanation of Diffusion Coefficients

In this study involving diffusion of K^+ and Cl^- through specimens of the BPN, the measured values of D^* for Cl^- and K^+ were not equivalent at steady state, with D^* for Cl^- , or $D_{Cl^-}^*$, generally being greater than D^* for K^+ , or $D_{K^+}^*$, with the difference between $D_{Cl^-}^*$ and $D_{K^+}^*$ decreasing with increase in the concentration of KCl used in the test. This difference between $D_{Cl^-}^*$ and $D_{K^+}^*$ at steady-state diffusion is in stark contrast to previous results showing essentially equivalency between $D_{Cl^-}^*$ and $D_{K^+}^*$ at steady-state diffusion through specimens of the GCLs containing conventional bentonites (e.g., Malusis and Shackelford 2002b). The difference between the results in this study for BPN and those for previous studies involving conventional

bentonites can be attributed, in part, to the requirement for charge flux balance at steady state (e.g., Shackelford and Lee 2003), and the difference in the specimen preparation procedures for the BPN specimens tested in this study versus the specimens of conventional bentonites tested in previous studies. Specifically, the BPN specimens in this study were not flushed (leached) of remnant soluble salts, predominantly Na^+ , existing within the pore liquid of the BPN specimens prior to membrane testing, whereas most, if not all, specimens of conventional bentonites tested in previous studies were permeated with DIW for extensive periods prior to membrane and diffusion testing for the purpose of flushing remnant soluble salts from the pores of the specimens.

For example, at steady state, electroneutrality requires charge flux balance between the anions and the cations diffusing through the system. For the current study involving primarily Cl^- , K^+ , and Na^+ , this requirement can be written as follows:

$$J_{d,\text{Cl}^-} * -z_{\text{Cl}^-} = J_{d,\text{K}^+} * z_{\text{K}^+} + J_{d,\text{Na}^+} * z_{\text{Na}^+} \quad (4.9)$$

where J_d represents the diffusive molar flux of the noted ionic species (i.e., Cl^- , K^+ , and Na^+) and z represents the charge of Cl^- , K^+ , and Na^+ (-1, +1, and +1, respectively). The J_d for the different ionic species can be written following Fick's first law for diffusion in soil as follows (e.g., Shackelford and Daniel 1991):

$$J_d = nD^*i_c \quad (4.10)$$

where n is the total porosity of the specimen, D^* is the effective diffusion coefficient, and i_c is the

molar concentration gradient of each ionic species. Since n should be constant for a given specimen, substitution of Eq. 4.10 into Eq. 4.9 for each ionic species results in the following expression:

$$D_{Cl^-}^* \cdot i_{c,Cl^-} = D_{K^+}^* \cdot i_{c,K^+} + D_{Na^+}^* \cdot i_{c,Na^+} \quad (4.11)$$

As previously noted, the membrane tests in this study were conducted by circulating solutions of KCl with concentrations C_o across the top of the specimen and DIW along the base of the specimen (refer to Fig. 4.22a). Therefore, at steady-state diffusive molar flux, $i_{c,Cl^-} = i_{c,K^+} = i_c$. However, the value of i_{c,Na^+} results from the existence of excess Na^+ in the BPN prior to testing, and varies as a function of time and location within the specimen due to diffusion of Na^+ from within the specimen to both the top and bottom boundaries of the specimen during testing (refer to illustration in Fig. 4.22b). Thus, if the ratio of i_c to i_{c,Na^+} is defined as I_c , then Eq. 4.11 can be reduced to:

$$D_{Cl^-}^* = D_{K^+}^* + D_{Na^+}^* \cdot I_c \quad (4.12)$$

In accordance with Eq. 4.12, the equivalency between $D_{Cl^-}^*$ and $D_{K^+}^*$ will depend on the value of I_c . That is, for values of $I_c > 0$, $D_{Cl^-}^* > D_{K^+}^*$, whereas, in the limit as I_c approaches zero, $D_{K^+}^*$ approaches $D_{Cl^-}^*$ (i.e., $D_{K^+}^* \rightarrow D_{Cl^-}^*$ as $I_c \rightarrow 0$).

As suggested by the measured concentrations of Cl^- , K^+ , and Na^+ in the circulation outflows from the bottom of the test specimens shown in Fig. 4.2 and 4.3, the value of i_{c,Na^+}

likely is significantly greater than the value of i_c during circulation of the relatively dilute solutions of KCl (i.e., 4.7 and 9.3 mM), such that the value of I_c in Eq. 4.12 likely was significantly greater than zero, resulting in the values of $D_{K^+}^*$ being significantly lower than the values of $D_{Cl^-}^* > D_{K^+}^*$ in accordance with Eq. 4.12 and as indicated in Fig. 4.15 and 4.16. However, as the duration of the tests extended, the amount of Na^+ remaining in the specimens diminished, and the concentrations of KCl used in the tests increased, such that the value of I_c decreased with time (i.e., $I_c \downarrow$ as $t \uparrow$). As a result, the measured values of $D_{K^+}^*$ increased and approached those of $D_{Cl^-}^*$, which remained relative constant throughout the tests, as the concentrations KCL applied in the test increased.

4.5 CONCLUSIONS

The results of multiple-stage membrane/diffusion tests conducted on a bentonite polymer nanocomposite (BPN) with varying concentrations of KCl were presented and discussed. The effective diffusion coefficients, D^* , for the BPN were determined over a range in source concentrations for which the BPN behaved as a semipermeable membrane. The diffusive properties of the BPN were correlated with the membrane behavior of the BPN. In general, the values of D^* decrease with increasing membrane efficiency coefficient, ω , as expected. For example, for test RW2, the value of $D_{Cl^-}^*$ is $1.0 \times 10^{-10} \text{ m}^2/\text{s}$ with a ω of 0.20 during the circulation of 54 mM KCl versus $3.7 \times 10^{-11} \text{ m}^2/\text{s}$ with a ω of 0.88 during the circulation of 4.7 mM KCl. In addition, as ω approached unity, the D^* for the BPN approached zero, which is consistent with theory since an ideal membrane (i.e., $\omega = 1$) restricts all solute migration.

The values of D^* measured in this study for BPN were compared with the values of D^* for a GCL reported by Malusis and Shackelford (2002b). In general, the values of $D_{Cl^-}^*$ were similar for the BPN and the GCL with the exception of test RW2 where the values of $D_{Cl^-}^*$ were lower for the BPN than the GCL (e.g., $3.7 \times 10^{-11} \text{ m}^2/\text{s}$ versus $7.05 \times 10^{-10} \text{ m}^2/\text{s}$, respectively). However, the values of $D_{K^+}^*$ were much lower for the BPN than the GCL with the $D_{K^+}^*$ for the BPN as low as $2.7 \times 10^{-12} \text{ m}^2/\text{s}$. These differences are likely a result of the excess remnant Na^+ initially in the pores of the BPN and superabsorbent polymer clogging the pores of the BPN.

The apparent, matrix, and restrictive tortuosity factors (τ_a , τ_m , and τ_r , respectively) also were determined for the BPN. The values of τ_a were lower for the tests conducted at lower porosities or higher effective stresses. Consistent with theory, the value of τ_a decreased with increasing ω for all four tests on the BPN. The τ_a is expected to trend towards zero as ω approaches unity because a perfect membrane restricts all solute migration. The values of τ_m were plotted versus the porosity for the BPN and for a GCL (from Malusis and Shackelford 2002b). The τ_m for the BPN was lower than the GCL at a similar porosity indicating that the interconnected pores of the BPN were more tortuous than the GCL, likely, as a result of superabsorbent polymer in the pores of the BPN.

The values of $D_{Cl^-}^*$ were generally higher than the values of $D_{K^+}^*$ for the BPN with the difference between the two increasing with a decrease in the concentration of KCl. However, previous tests showed equivalency between $D_{Cl^-}^*$ and $D_{K^+}^*$ for steady-state diffusion through a GCL. The existence of excess Na^+ in the BPN prior to testing may have contributed to the lower values of $D_{K^+}^*$ compared to $D_{Cl^-}^*$ especially during the circulation of low concentrations of KCl (e.g., 4.7 mM KCl). When the concentrations of KCl increased and the duration of the test

increased (resulting in decreased concentration of excess Na^+ in the pores), the difference between the two D^* decreased.

Table 4.1. Results of membrane testing and diffusion analysis for bentonite polymer nanocomposite using rigid-wall (RW) and flexible-wall (FW) cells.

Test No.	Porosity, n	Initial Effective Stress, σ' [kPa (psi)]	Source KCl Concentration, C_{ot} (mM)	Membrane Efficiency Coefficient, $\omega^{(a)}$	Solute	Effective Diffusion Coefficient, D^* (m^2/s)	
						Linear	Non-linear
RW1	0.92	NA	4.7	0.80	Cl^-	1.0×10^{-10}	9.7×10^{-11}
					K^+	2.7×10^{-12}	2.2×10^{-12}
			9.3	0.65	Cl^-	1.5×10^{-10}	1.4×10^{-10}
					K^+	5.1×10^{-12}	4.8×10^{-12}
			20	0.43	Cl^-	1.4×10^{-10}	1.4×10^{-10}
					K^+	2.0×10^{-11}	1.8×10^{-11}
			54	0.17	Cl^-	2.2×10^{-10}	2.2×10^{-10}
					K^+	7.0×10^{-11}	6.6×10^{-11}
RW2	0.80	NA	4.7	0.88	Cl^-	3.7×10^{-11}	3.0×10^{-11}
					K^+	1.5×10^{-11}	1.3×10^{-11}
			9.3	0.73	Cl^-	5.5×10^{-11}	5.5×10^{-11}
					K^+	2.2×10^{-11}	1.8×10^{-11}
			20	0.46	Cl^-	6.8×10^{-11}	6.8×10^{-11}
					K^+	5.1×10^{-11}	4.5×10^{-11}
			54	0.20	Cl^-	1.0×10^{-10}	9.3×10^{-11}
					K^+	9.5×10^{-11}	8.9×10^{-11}

Table 4.1. Results of membrane testing and diffusion analysis for bentonite polymer nanocomposite using rigid-wall (RW) and flexible-wall (FW) cells (continued).

Test No.	Porosity, n	Initial Effective Stress, σ' [kPa (psi)]	Source KCl Concentration, C_{ot} (mM)	Membrane Efficiency Coefficient, $\omega^{(a)}$	Solute	Effective Diffusion Coefficient, D^* (m^2/s)	
						Linear	Non-linear
FW1	0.94 – 0.95	34.5 (5)	4.7	0.55	Cl^-	1.7×10^{-10}	1.7×10^{-10}
					K^+	4.3×10^{-12}	2.8×10^{-12}
			9.3	0.32	Cl^-	2.2×10^{-10}	2.2×10^{-10}
					K^+	3.5×10^{-11}	3.5×10^{-11}
			20	0.14	Cl^-	2.7×10^{-10}	2.7×10^{-10}
					K^+	1.2×10^{-10}	1.1×10^{-10}
			54	0.04	Cl^-	2.9×10^{-10}	2.8×10^{-10}
					K^+	2.0×10^{-10}	1.8×10^{-10}
FW2	0.78 – 0.84	103 (15)	4.7	0.46	Cl^-	7.3×10^{-11}	8.7×10^{-11}
					K^+	8.0×10^{-12}	--
			9.3	0.38	Cl^-	9.9×10^{-11}	1.0×10^{-10}
					K^+	1.9×10^{-11}	1.7×10^{-11}
			20	0.25	Cl^-	1.4×10^{-10}	1.3×10^{-10}
					K^+	5.1×10^{-11}	4.7×10^{-11}
			54	0.10	Cl^-	1.6×10^{-10}	1.5×10^{-10}
					K^+	1.0×10^{-10}	9.5×10^{-11}

(a) steady-state membrane efficiency coefficient based on initial (source) salt concentrations

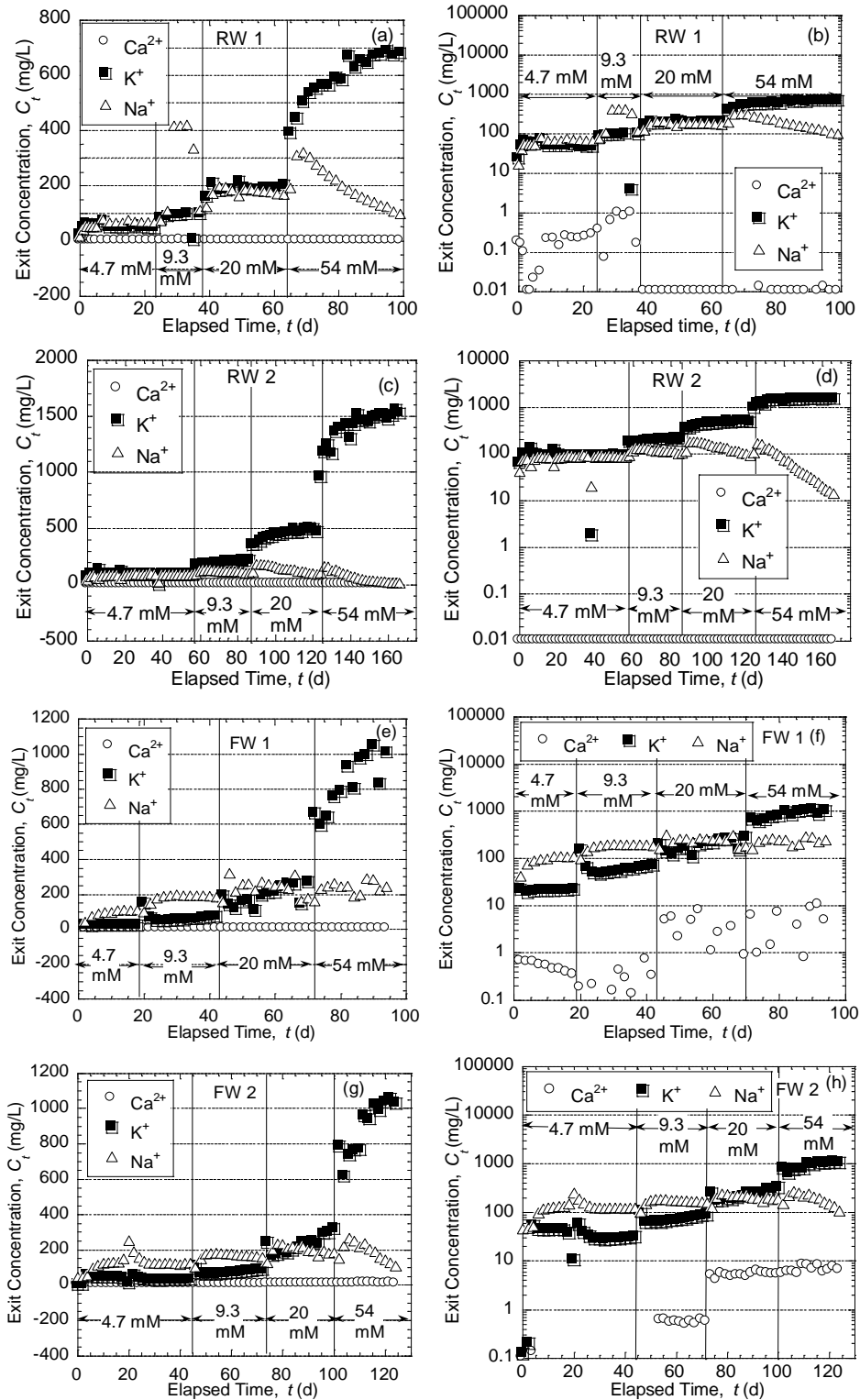


Figure 4.1. Measured exit concentrations of cations as a function of time at the top of the cell during membrane testing with KCl; (a & b) RW1 @ $n = 0.92$, (c & d) RW2 @ $n = 0.80$, (e & f) FW1 @ $\sigma' = 34.5$ kPa (5 psi), (g & h) FW2 @ $\sigma' = 103$ kPa (15 psi).

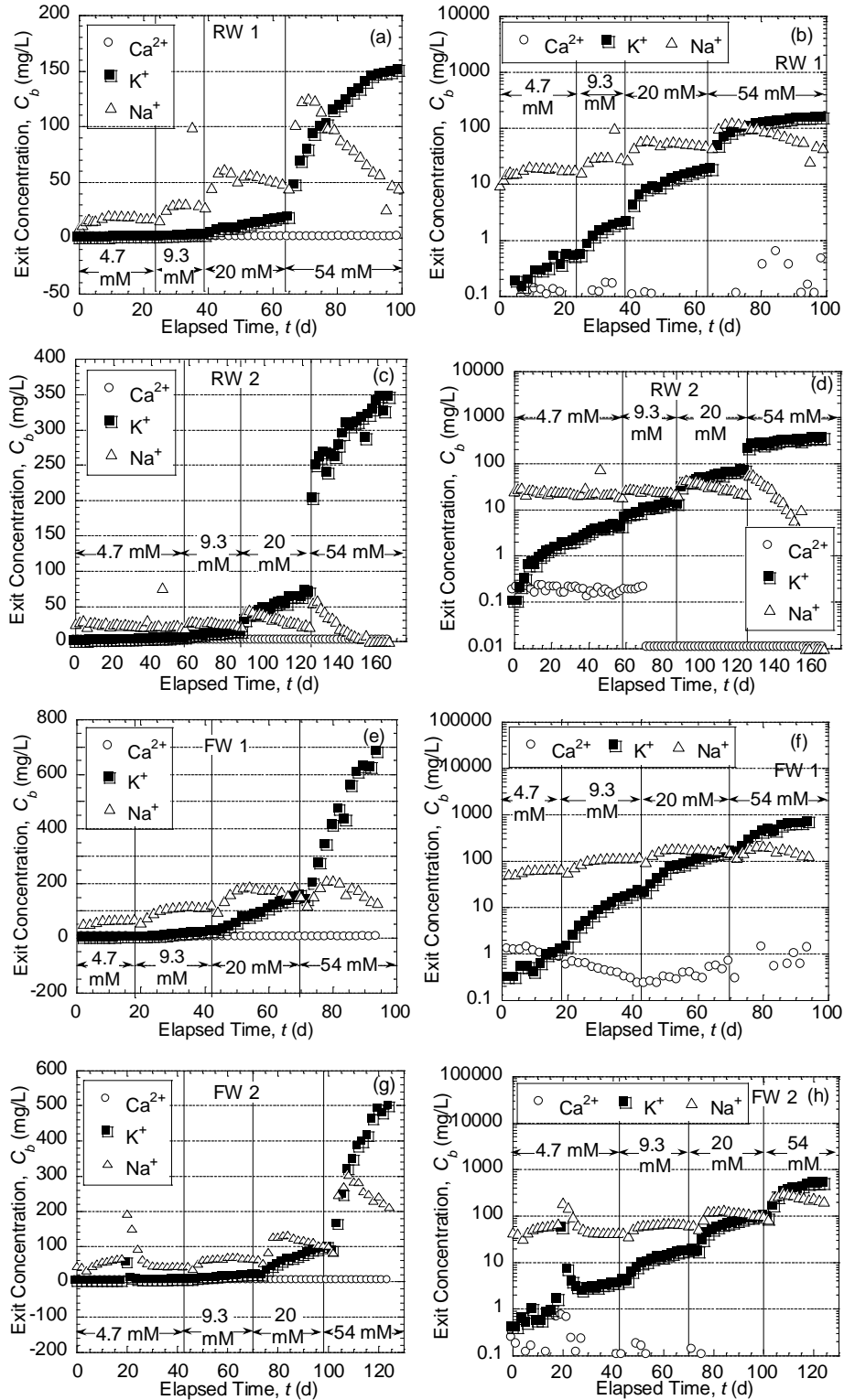


Figure 4.2. Measured exit concentrations of cations as a function of time at the bottom of the cell during membrane testing; (a & b) RW1 @ $n = 0.92$, (c & d) RW2 @ $n = 0.80$, (e & f) FW1 @ $\sigma' = 34.5$ kPa (5 psi), (g & h) FW2 @ $\sigma' = 103$ kPa (15 psi).

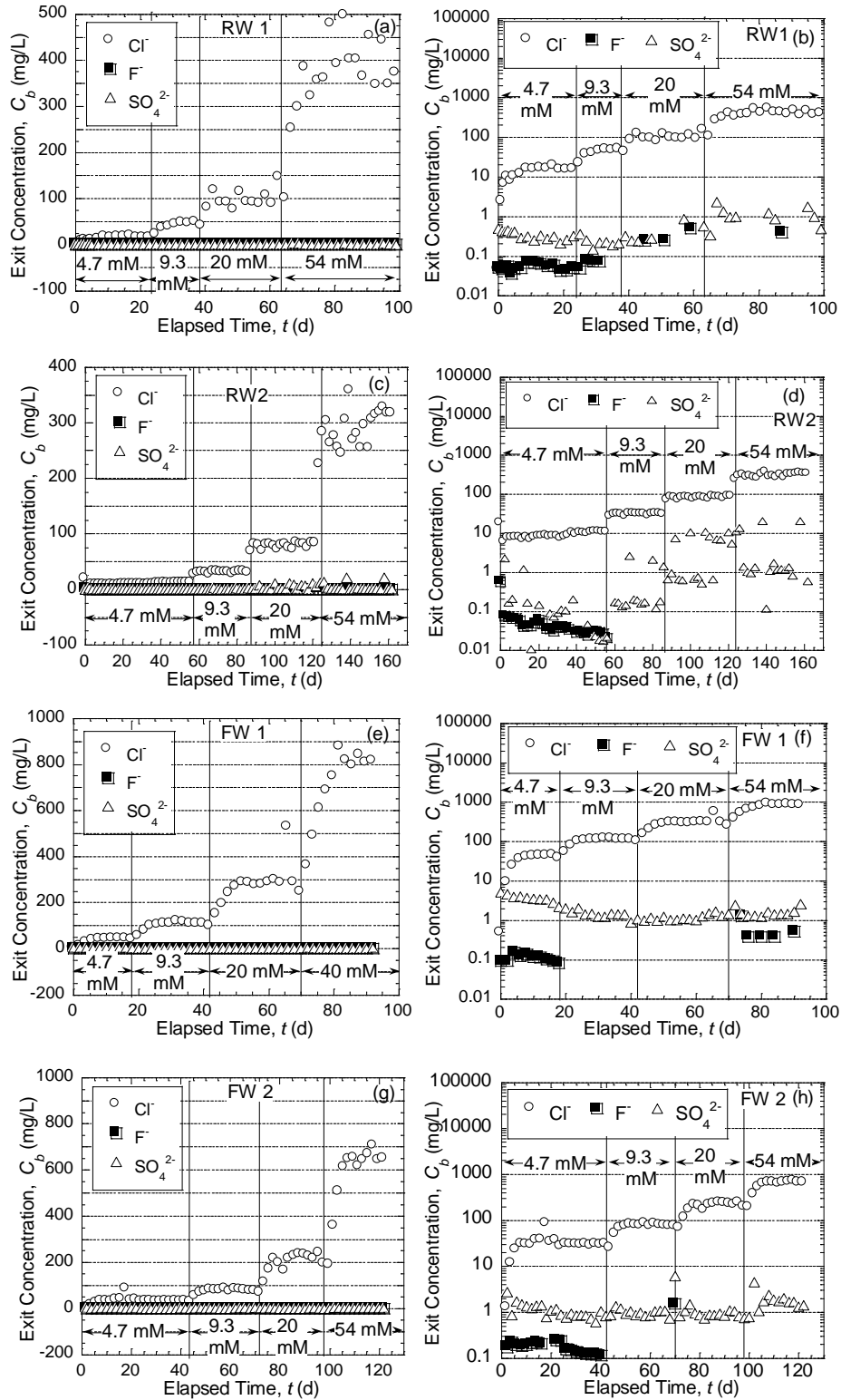


Figure 4.3. Measured exit concentrations of anions as a function of time at the bottom of the cell during membrane testing in a rigid-wall cell; (a & b) RW1 @ $n = 0.92$, (c & d) RW2 @ $n = 0.80$, (e & f) FW1 @ $\sigma' = 34.5$ kPa (5 psi), (g & h) FW2 @ $\sigma' = 103$ kPa (15 psi).

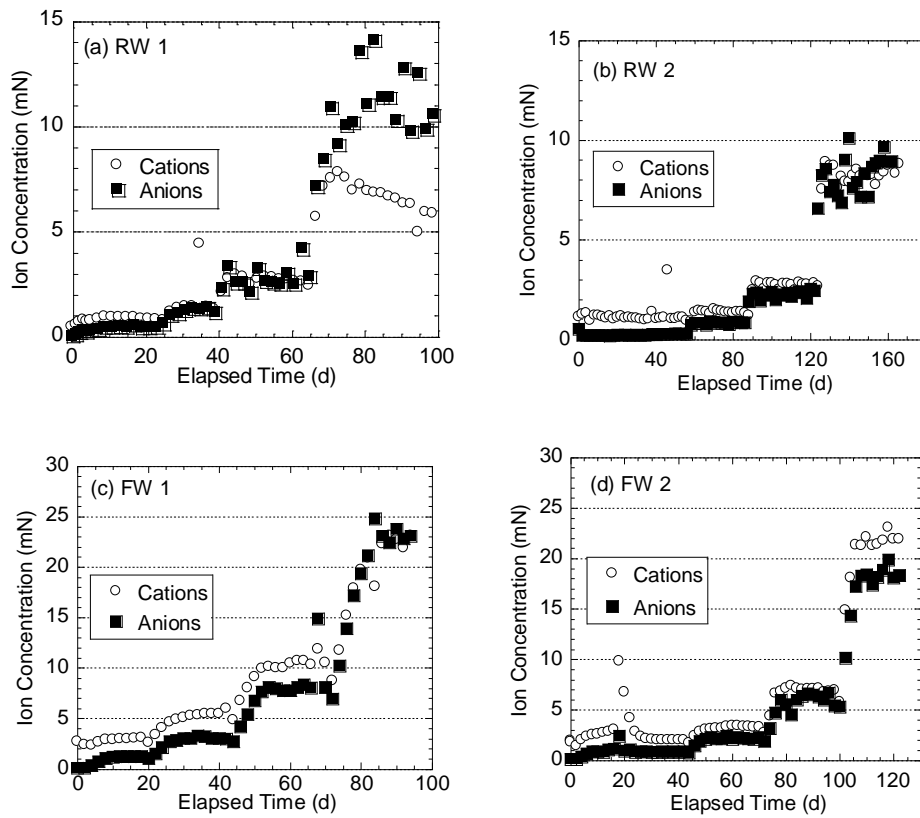


Figure 4.4. Concentrations of anions and cations at the bottom of the testing cell during membrane testing of the bentonites polymer nanocomposite as a function of time: (a) Test RW 1 ($n = 0.92$); (b) Test RW2 ($n = 0.80$); (c) Test FW1 ($\sigma' = 34.5$ kPa (5 psi)); (d) Test FW2 ($\sigma' = 103$ kPa (15 psi)).

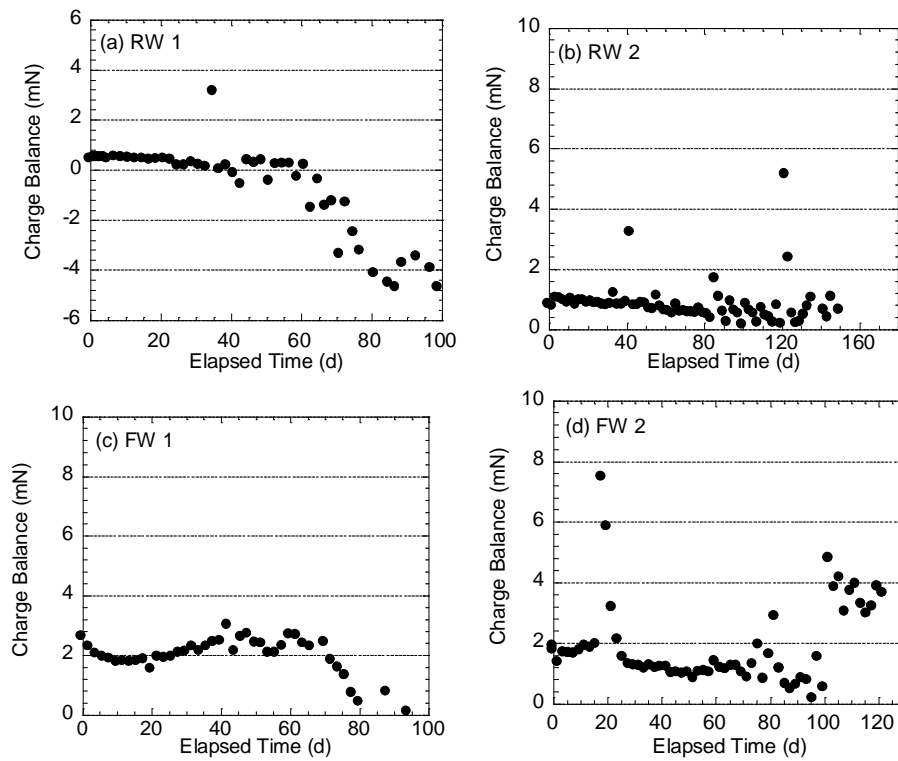


Figure 4.5. Charge balance at the bottom of the testing cell during membrane testing of the bentonites polymer nanocomposite as a function of time: (a) Test RW 1 ($n = 0.92$); (b) Test RW2 ($n = 0.80$); (c) Test FW1 ($\sigma' = 34.5$ kPa (5 psi)); (d) Test FW2 ($\sigma' = 103$ kPa (15 psi)).

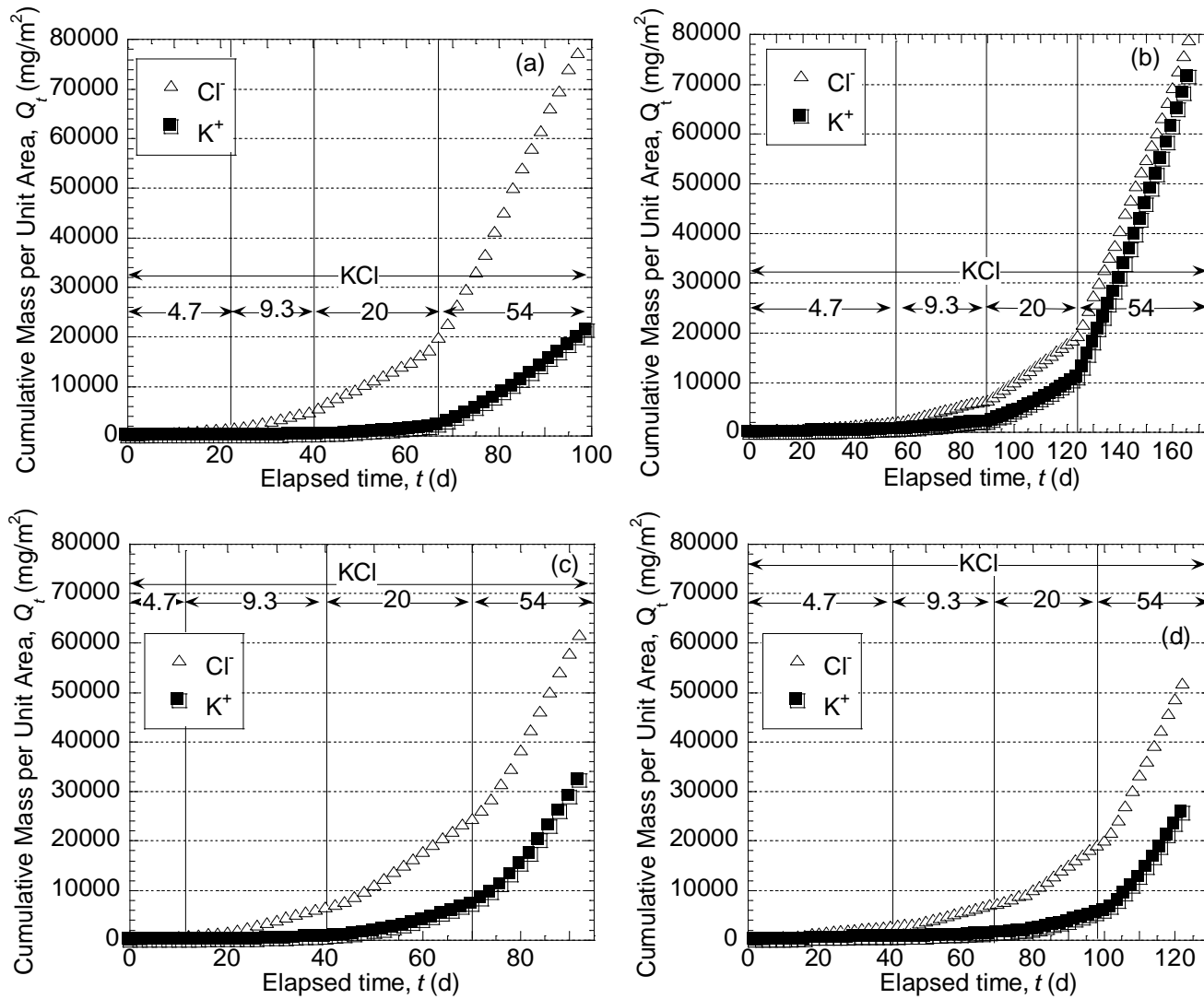


Figure 4.6. BPN diffusion test results with chloride and potassium in terms of cumulative mass per unit area, Q_t , versus elapsed time, t for (a) RW1 @ $n = 0.92$, (b) RW2 @ $n = 0.80$, (c) FW1 @ $\sigma' = 34.5$ kPa (5 psi), (d) FW2 @ $\sigma' = 103$ kPa (15 psi).

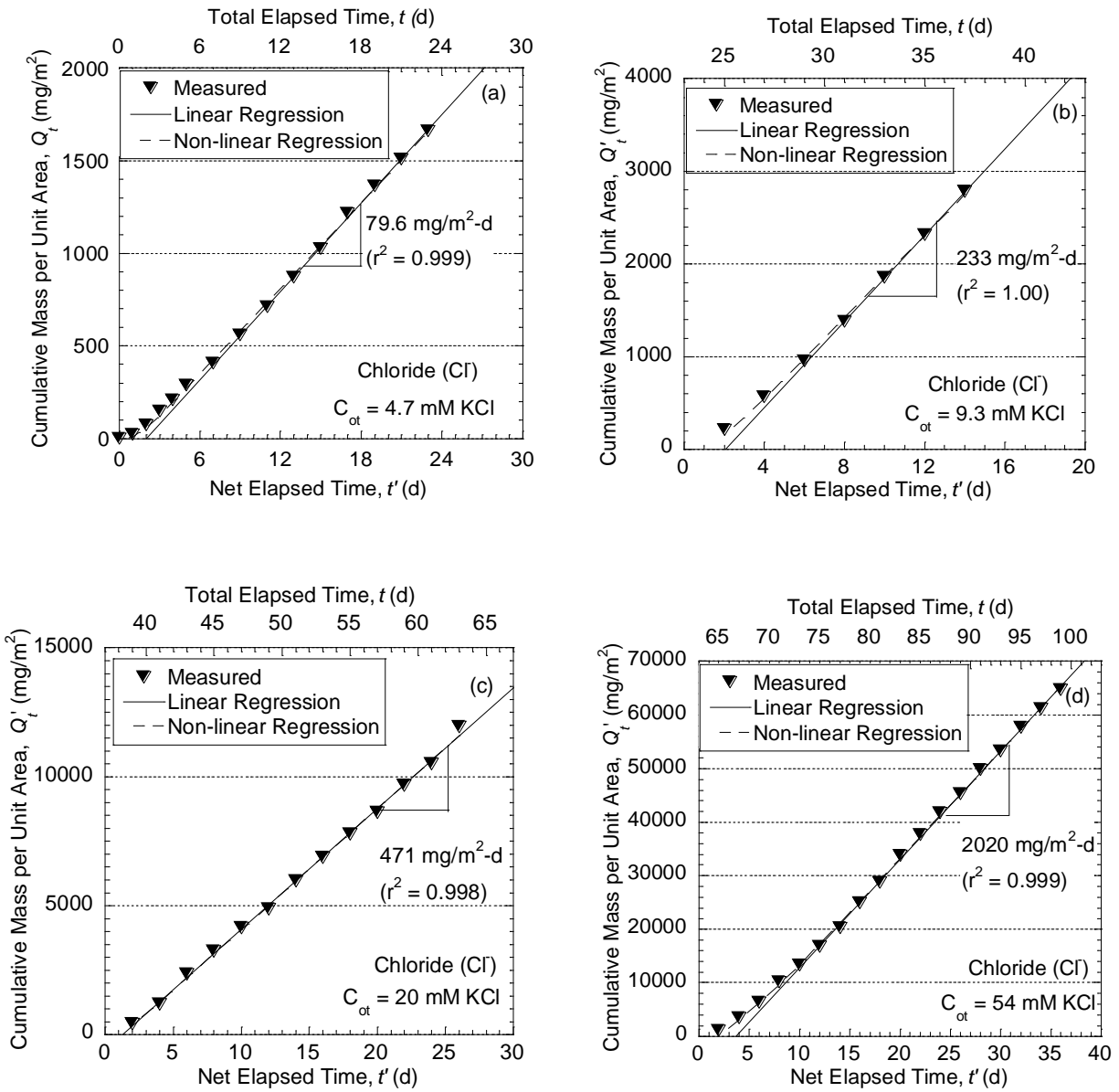


Figure 4.7. Diffusion test results from Test RW1 ($n = 0.92$) for chloride. Linear regression of steady-state data and non-linear regression of all data.

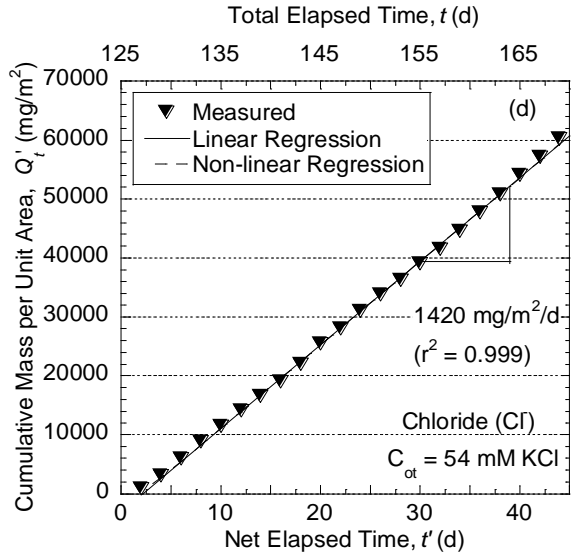
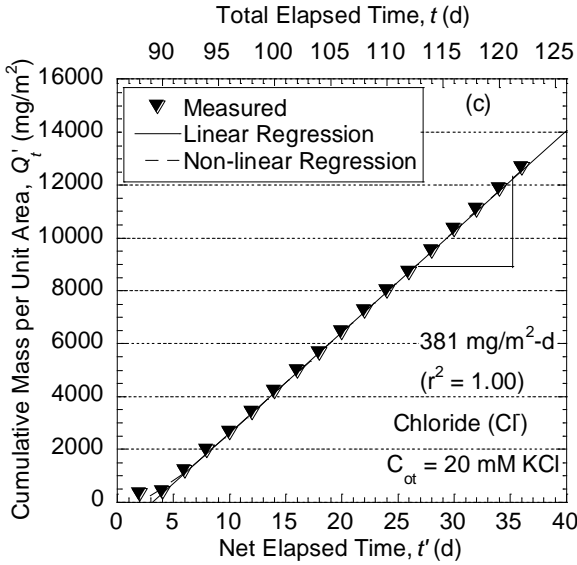
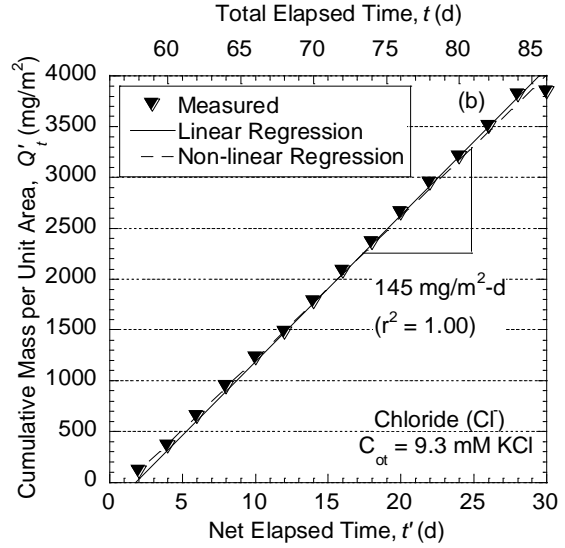
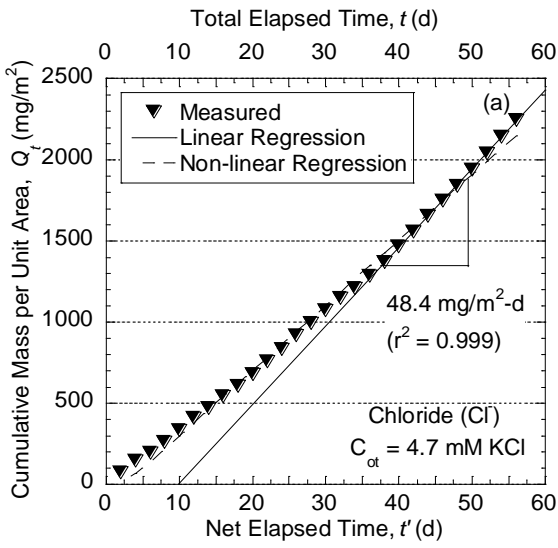


Figure 4.8. Diffusion test results from Test RW2 ($n = 0.80$) for chloride. Linear regression of steady-state data and non-linear regression of all data.

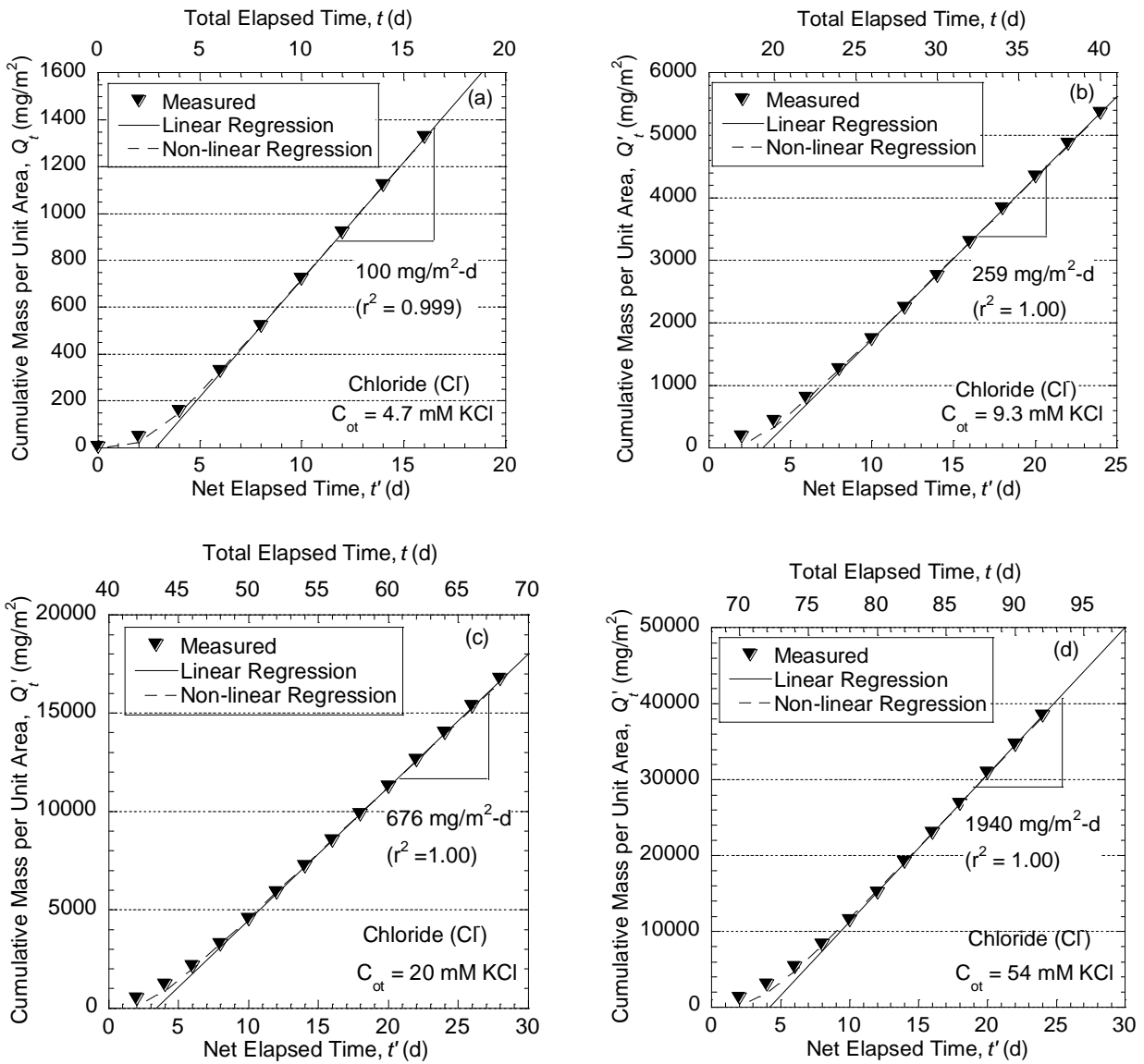


Figure 4.9. Diffusion test results from Test FW1 for chloride. Linear regression of steady-state data and non-linear regression of all data.

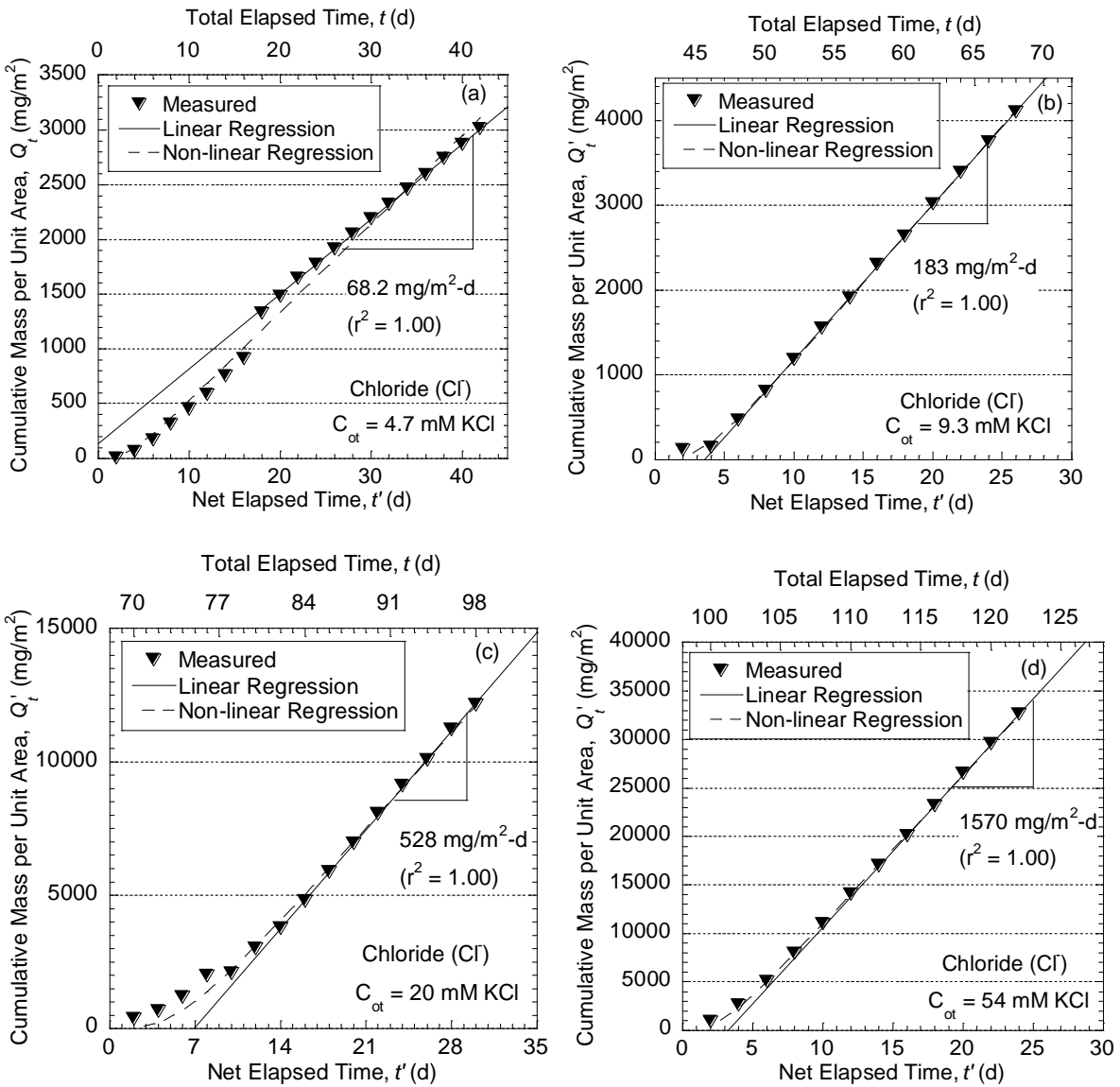


Figure 4.10. Diffusion test results from Test FW2 for chloride. Linear regression of steady-state data and non-linear regression of all data.

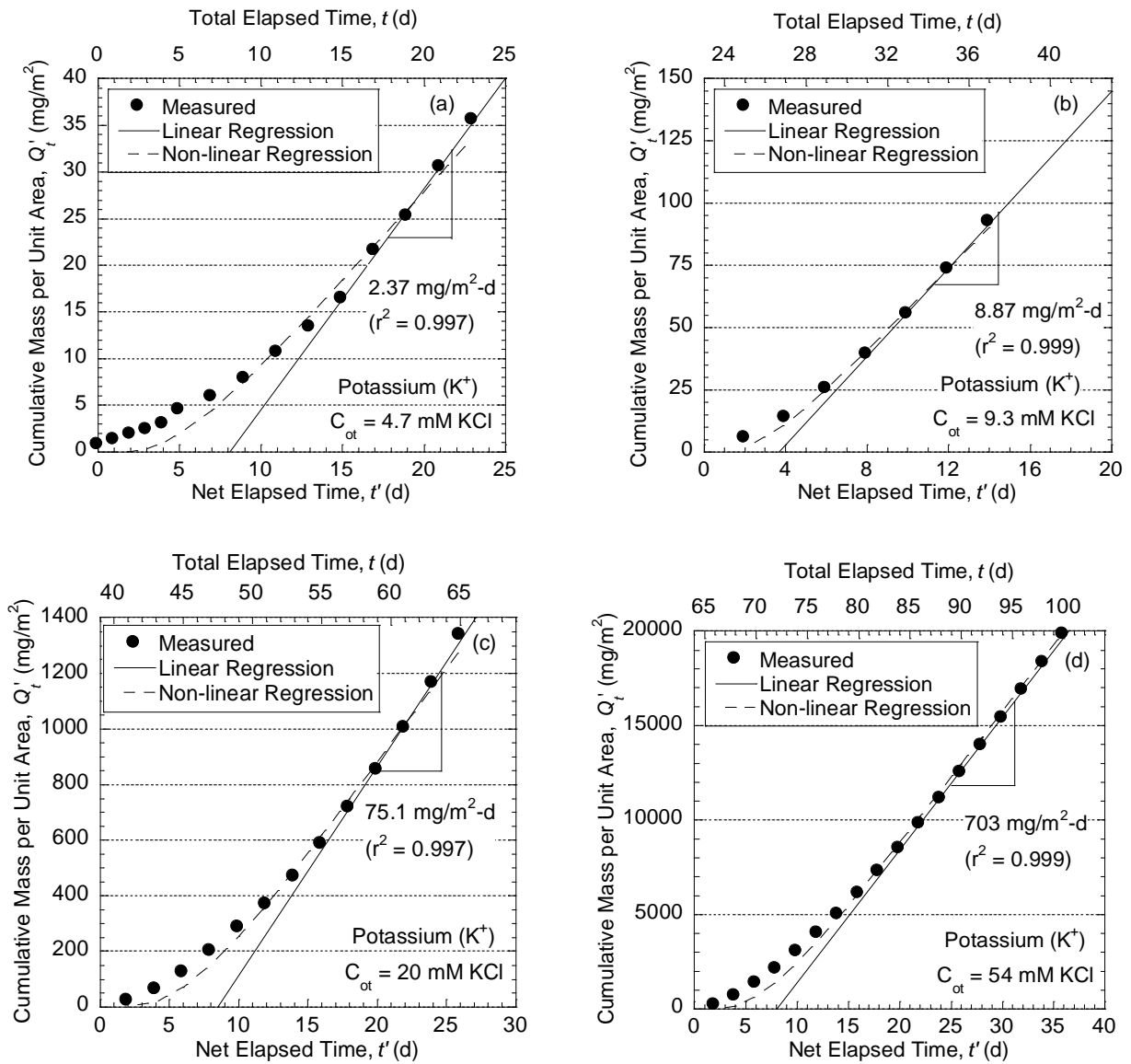


Figure 4.11. Diffusion test results from Test RW1 for potassium. Linear regression of steady-state data and non-linear regression of all data.

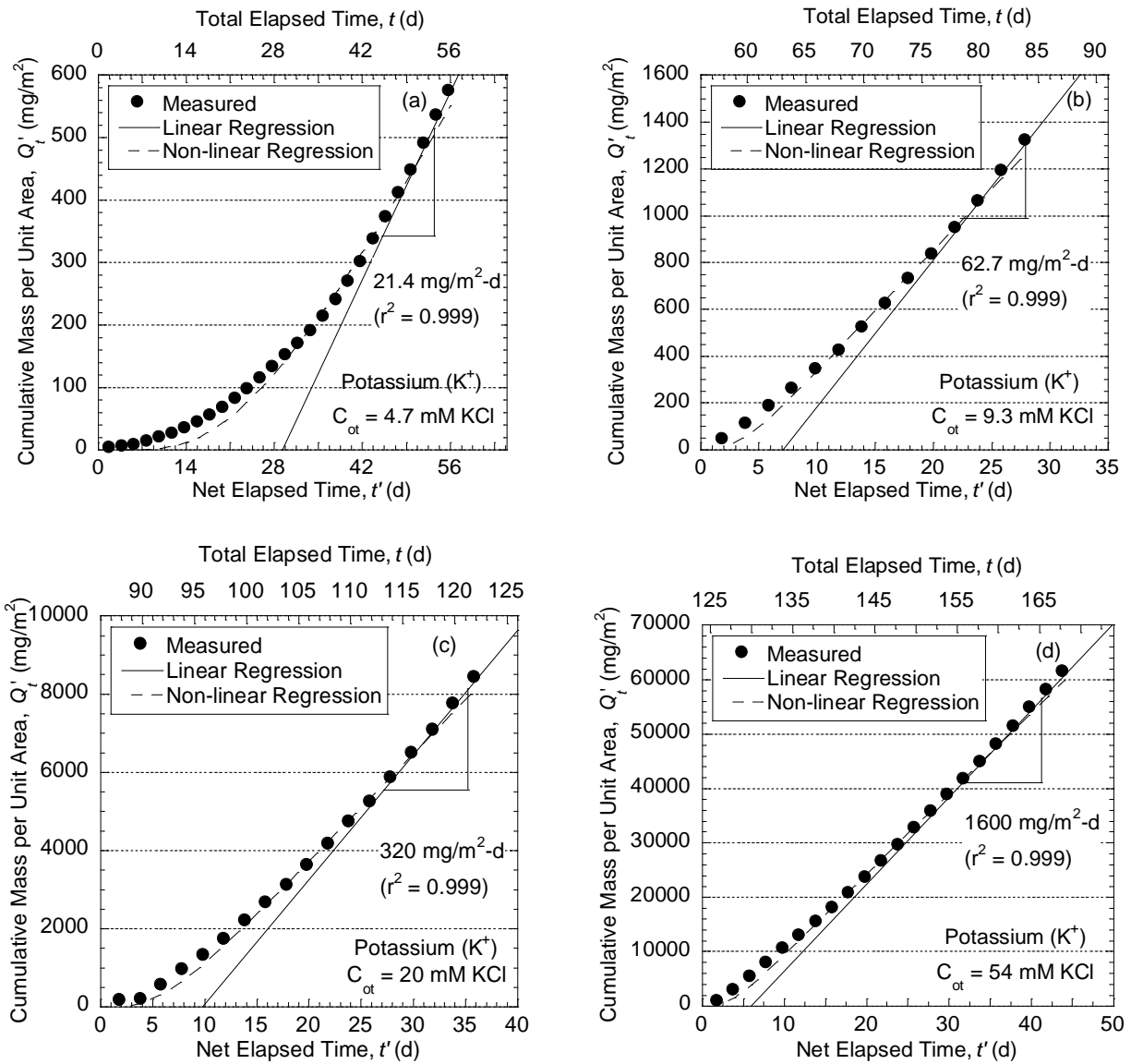


Figure 4.12. Diffusion test results from Test RW2 for potassium. Linear regression of steady-state data and non-linear regression of all data.

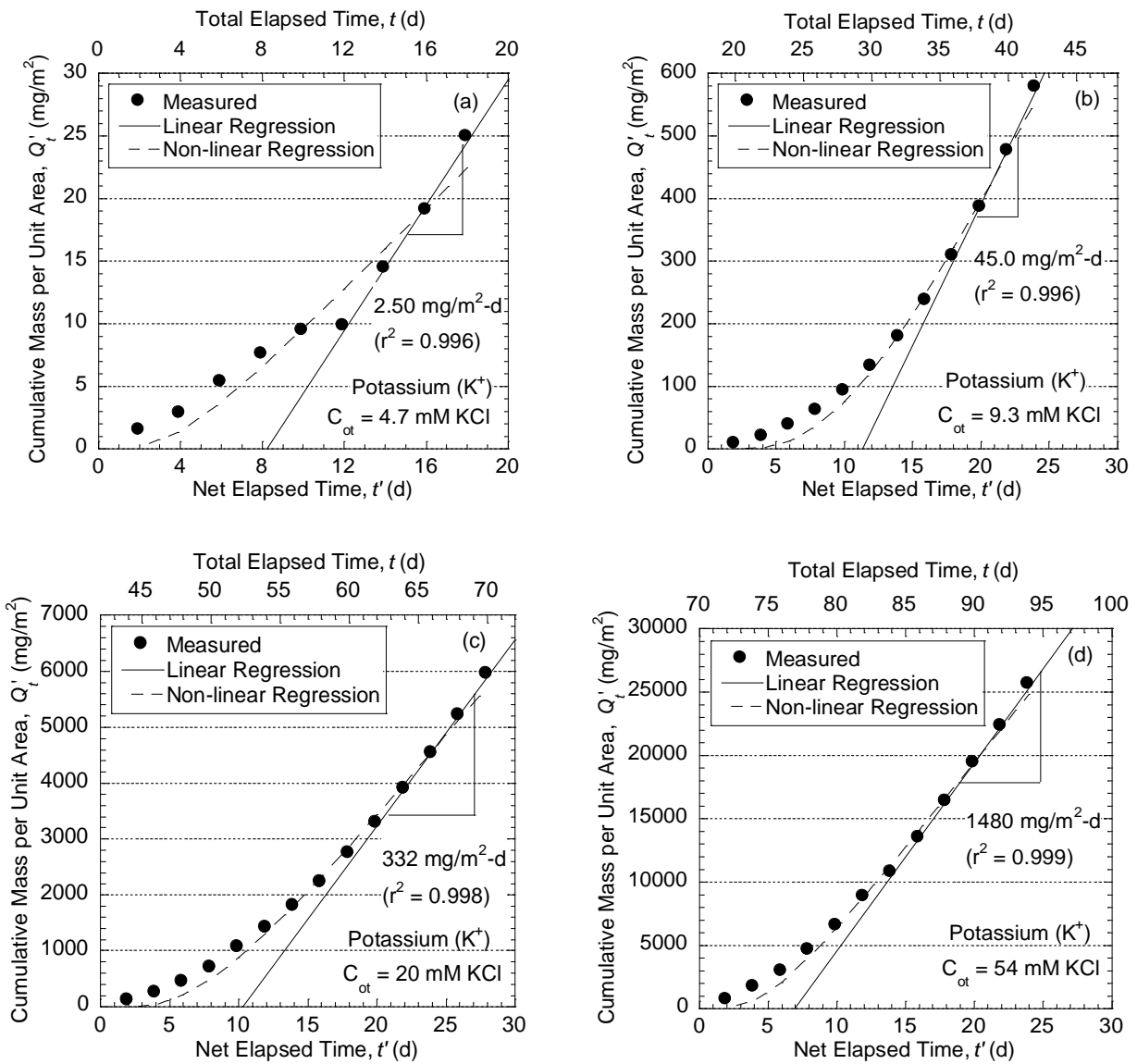


Figure 4.13. Diffusion test results from Test FW1 for potassium. Linear regression of steady-state data and non-linear regression of all data.

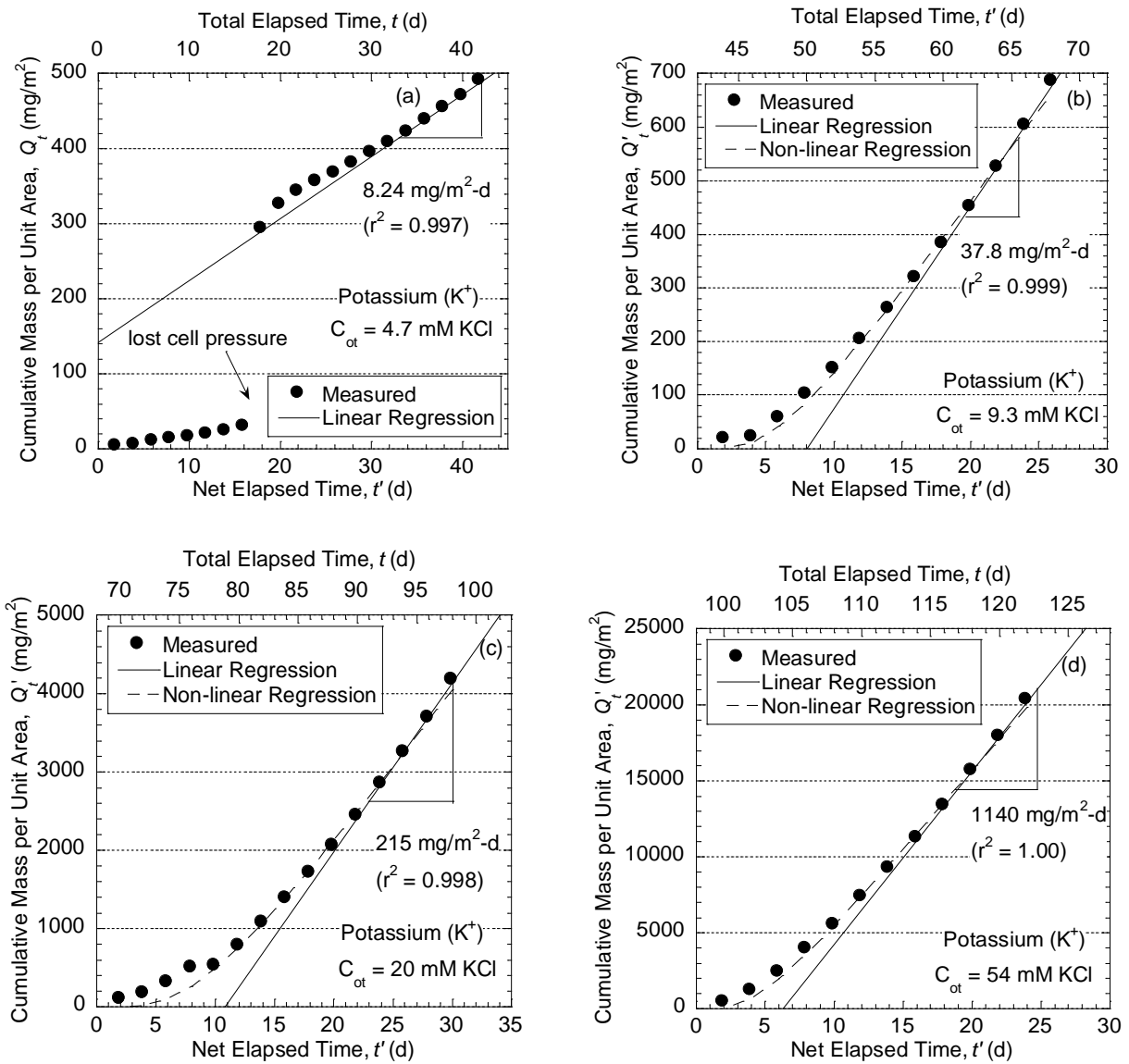


Figure 4.14. Diffusion test results from Test FW2 for potassium. Linear regression of steady-state data and non-linear regression of all data.

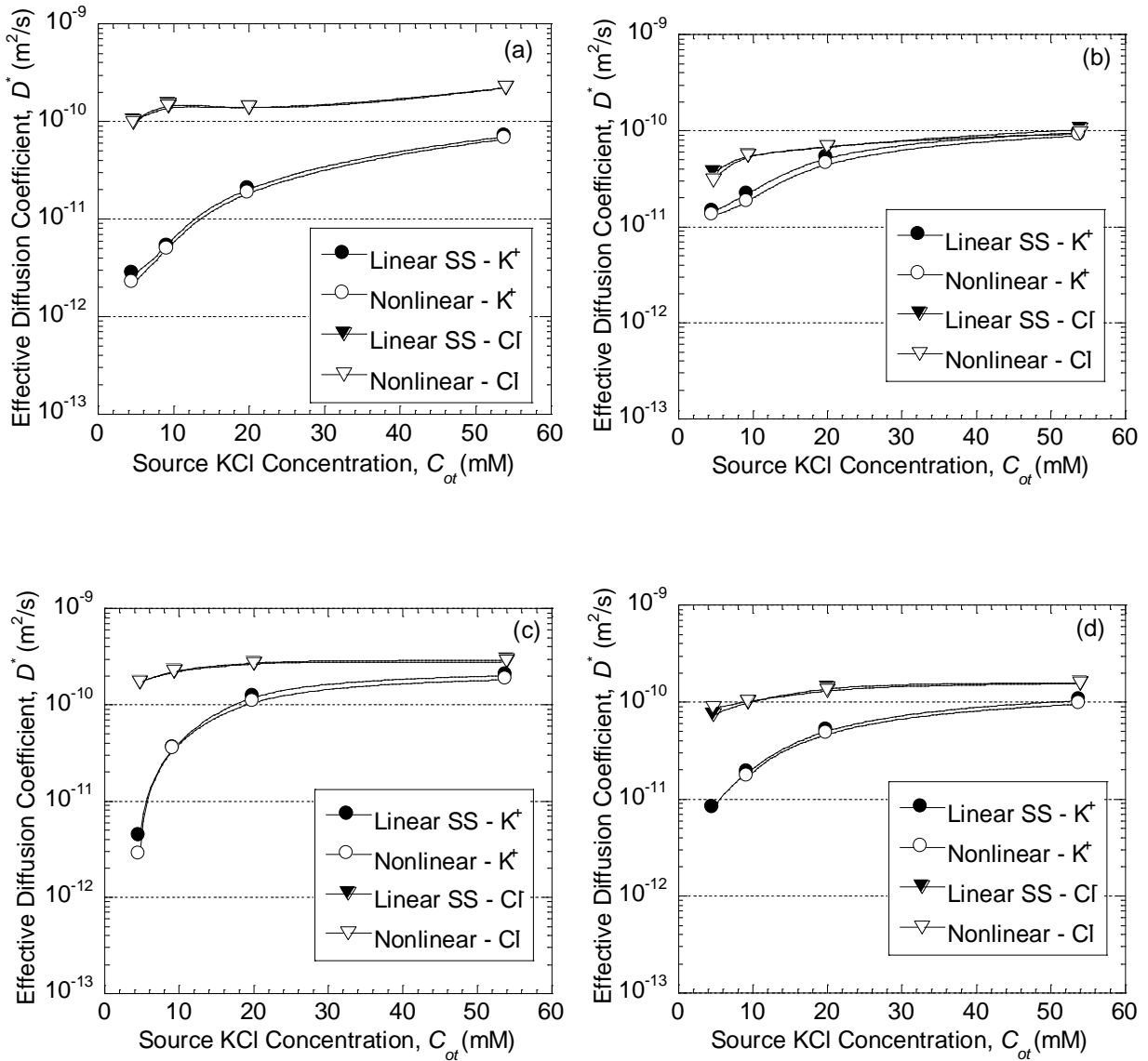


Figure 4.15. Effective diffusion coefficient (D^*) versus potassium chloride source concentration (C_{ot}) for bentonite polymer nanocomposite (BPN) for tests (a) RW1 @ $n = 0.92$, (b) RW2 @ $n = 0.80$, (c) FW1 @ $\sigma' = 34.5$ kPa (5 psi), (d) FW2 @ $\sigma' = 103$ kPa (15 psi). The D^* for the BPN was estimated using a steady state (SS) linear regression and using a non-linear regression.

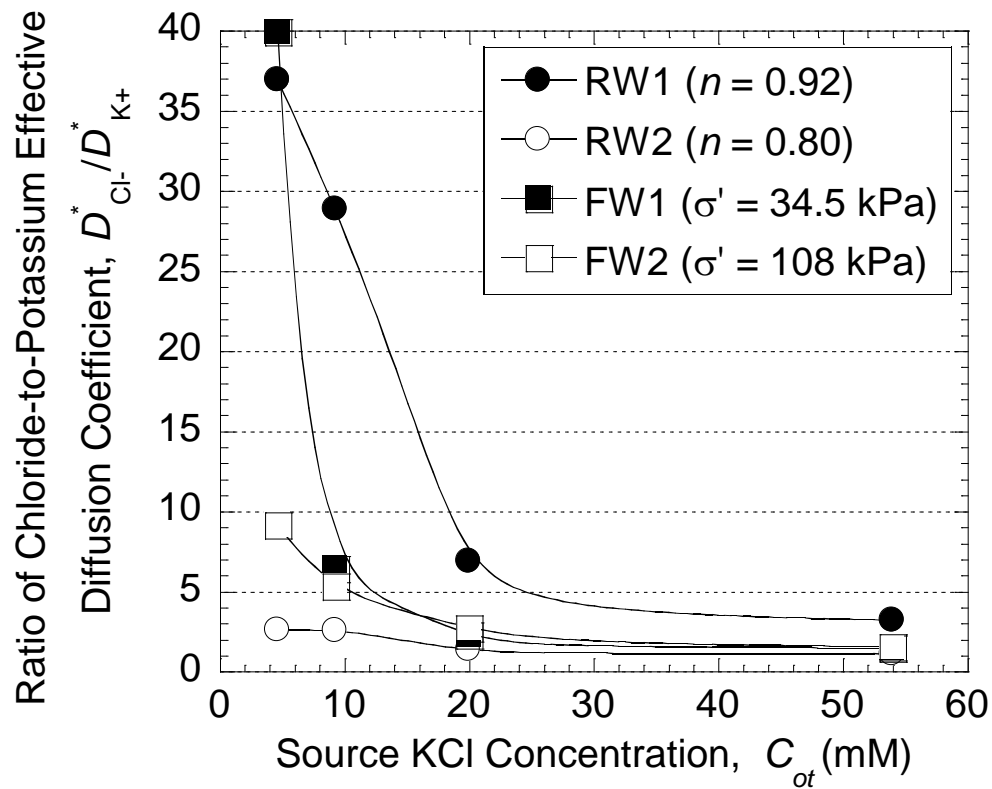


Figure 4.16. Ratio of chloride-to-potassium effective diffusion coefficient ratio at steady state versus source KCl concentration (C_{ot}) for bentonite polymer nanocomposite (BPN) for both rigid-wall (RW) and flexible-wall (FW) tests [Note: n = specimen porosity; σ' = initial effective stress in specimen].

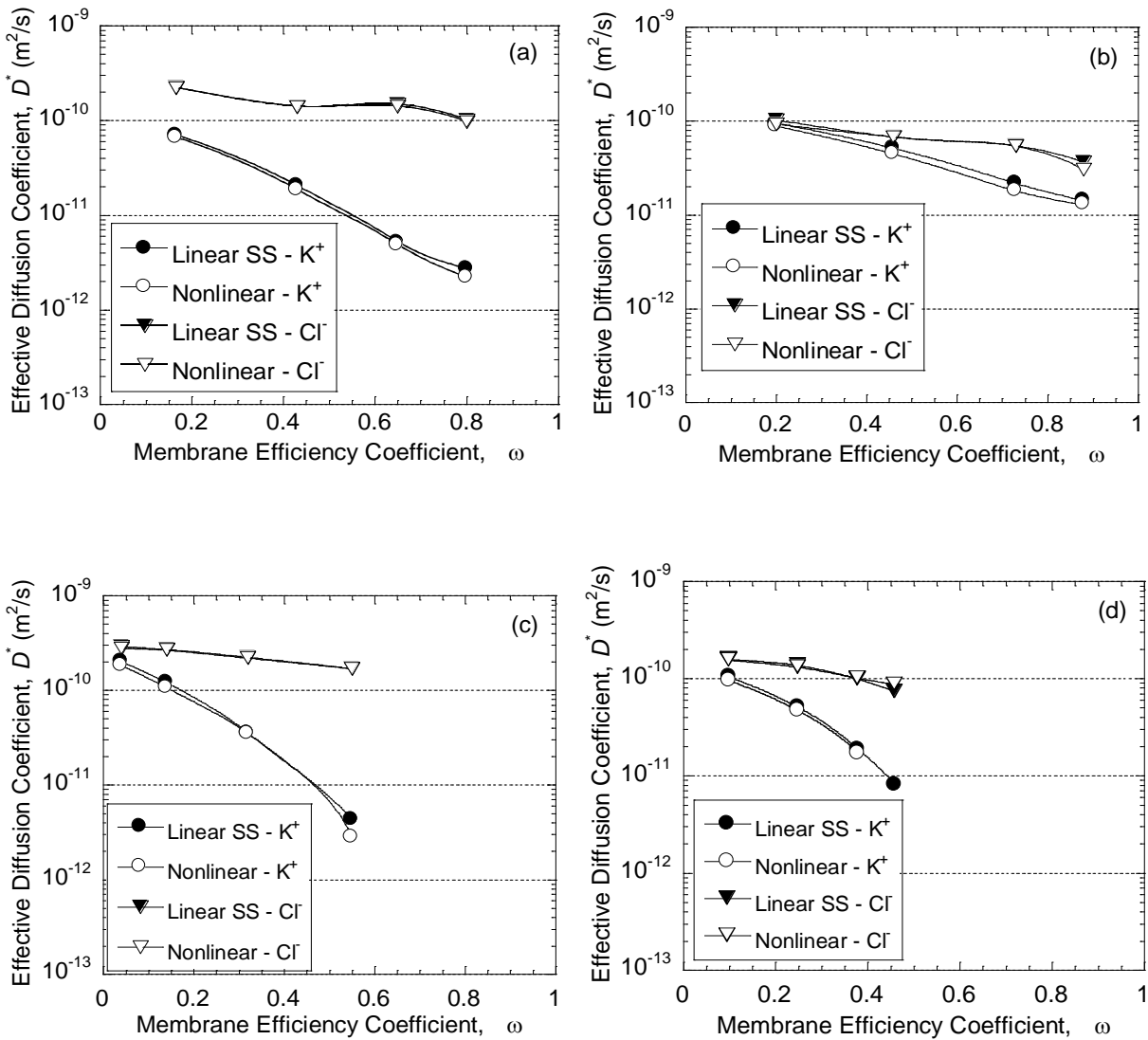


Figure 4.17. Effective diffusion coefficient (D^*) based on both linear regression of steady-state data and non-linear regression of all data as a function of the membrane efficiency coefficient for a bentonite polymer nanocomposite: (a) Test RW1 @ $n = 0.92$; (b) Test RW2 @ $n = 0.80$; (c) Test FW1 @ $\sigma' = 34.5$ kPa (5 psi); (d) Test FW2 @ $\sigma' = 103$ kPa (15 psi).

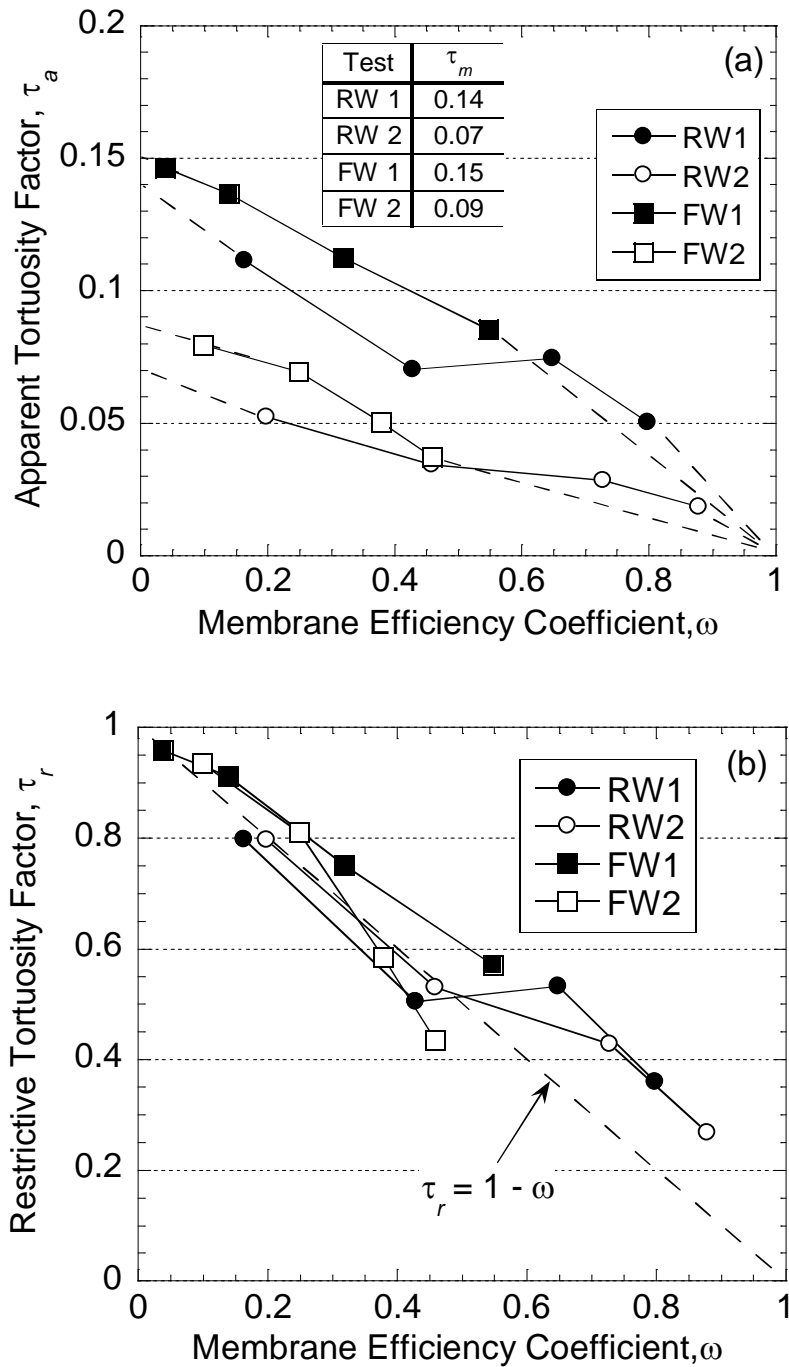


Figure 4.18. Tortuosity factors of a bentonite polymer nanocomposite based on rigid-wall (RW) and flexible-wall (FW) test results for chloride (Cl^-) as a function of membrane efficiency: (a) apparent tortuosity factor; (b) restrictive tortuosity factor, τ_r . [Note: τ_m = matrix tortuosity factor].

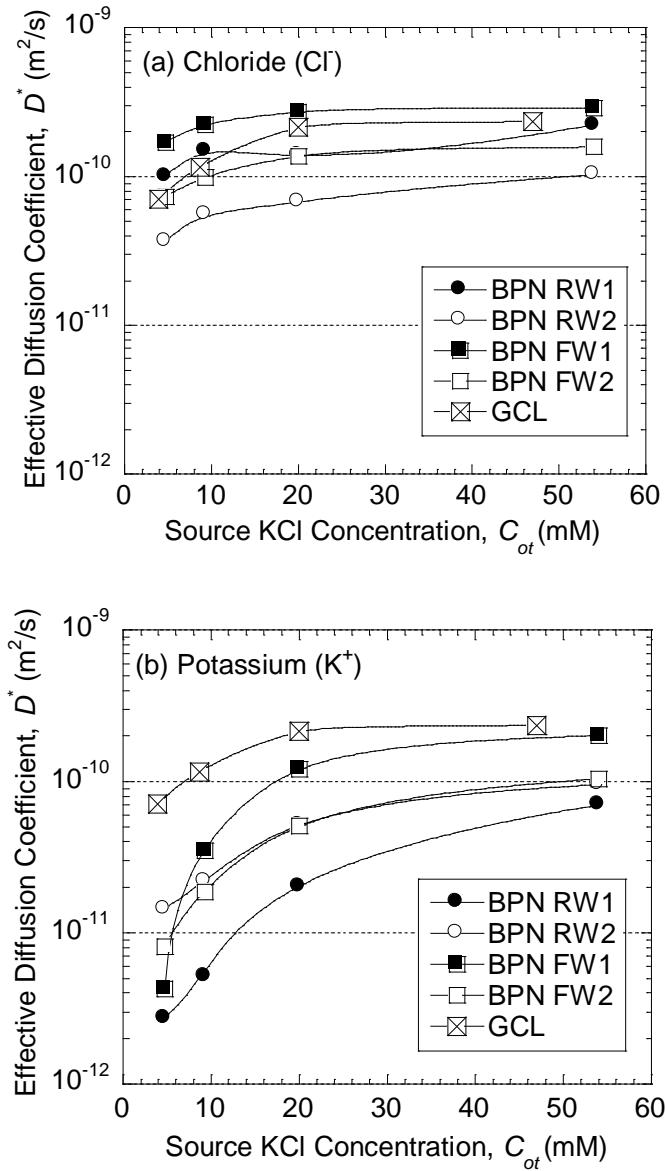


Figure 4.19. Effective diffusion coefficient (D^*) for chloride or potassium versus potassium chloride source concentration (C_{ot}) for bentonite polymer nanocomposite (BPN) and GCL (from Malusis and Shackelford 2002b). The D^* for the BPN was estimated using a steady state (SS) linear regression. BPN RW1, $n = 0.92$; BPN RW2, $n = 0.80$; BPN FW1, $n_i = 0.95$; BPN FW2, $n_i = 0.84$; GCL $n = 0.78 - 0.80$.

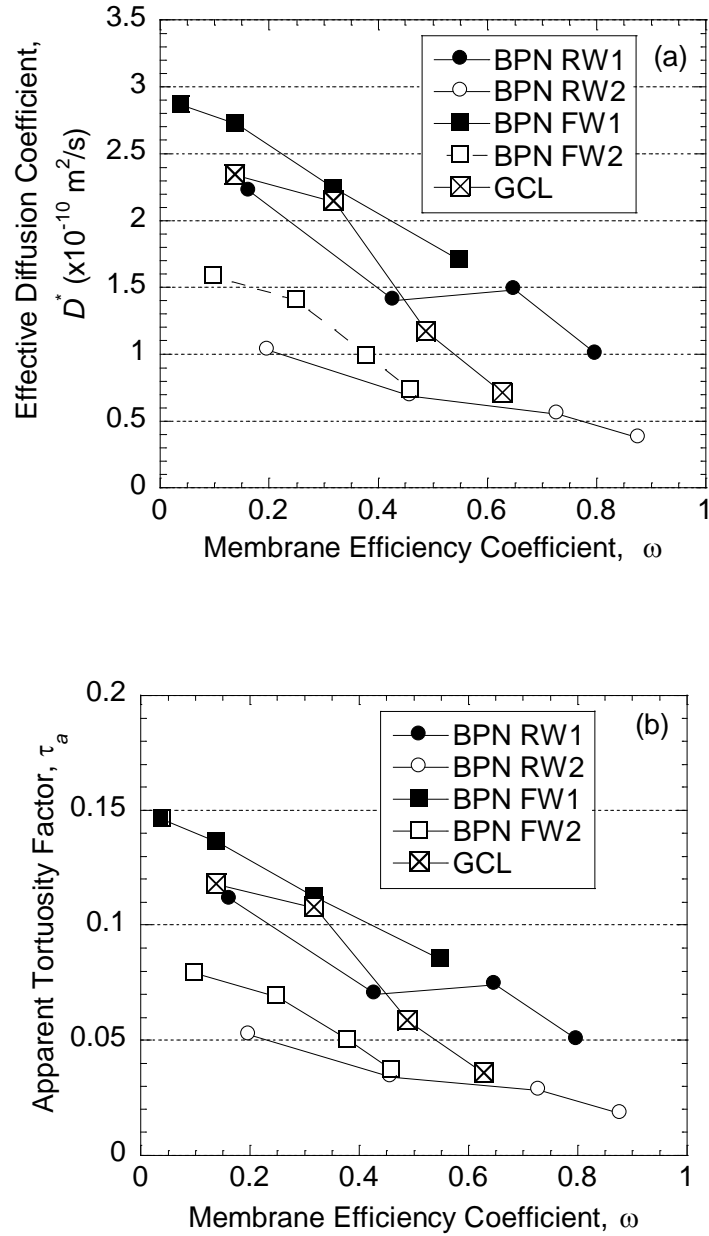


Figure 4.20. Comparison of results for a bentonite polymer nanocomposite (BPN) versus those for a geosynthetic clay liner (GCL) from Malusis and Shackelford (2002b) as a function of membrane efficiency: (a) effective diffusion coefficients for chloride; (b) apparent tortuosity factors. [Note: RW = rigid-wall cell; FW = flexible-wall cell].

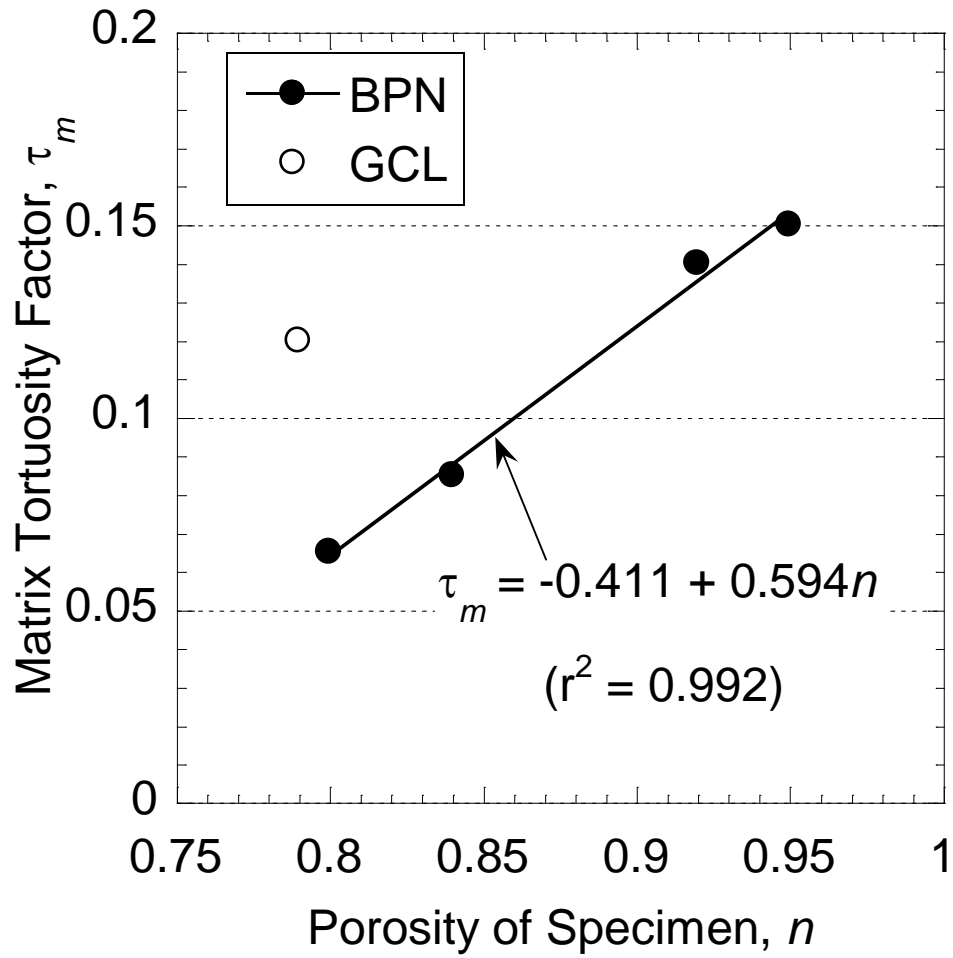


Figure 4.21. Matrix tortuosity factor versus specimen porosity for the bentonites polymer nanocomposite (BPN) evaluated in this study versus that for a geosynthetic clay liner (GCL) as reported by Malusis and Shackelford (2002b).

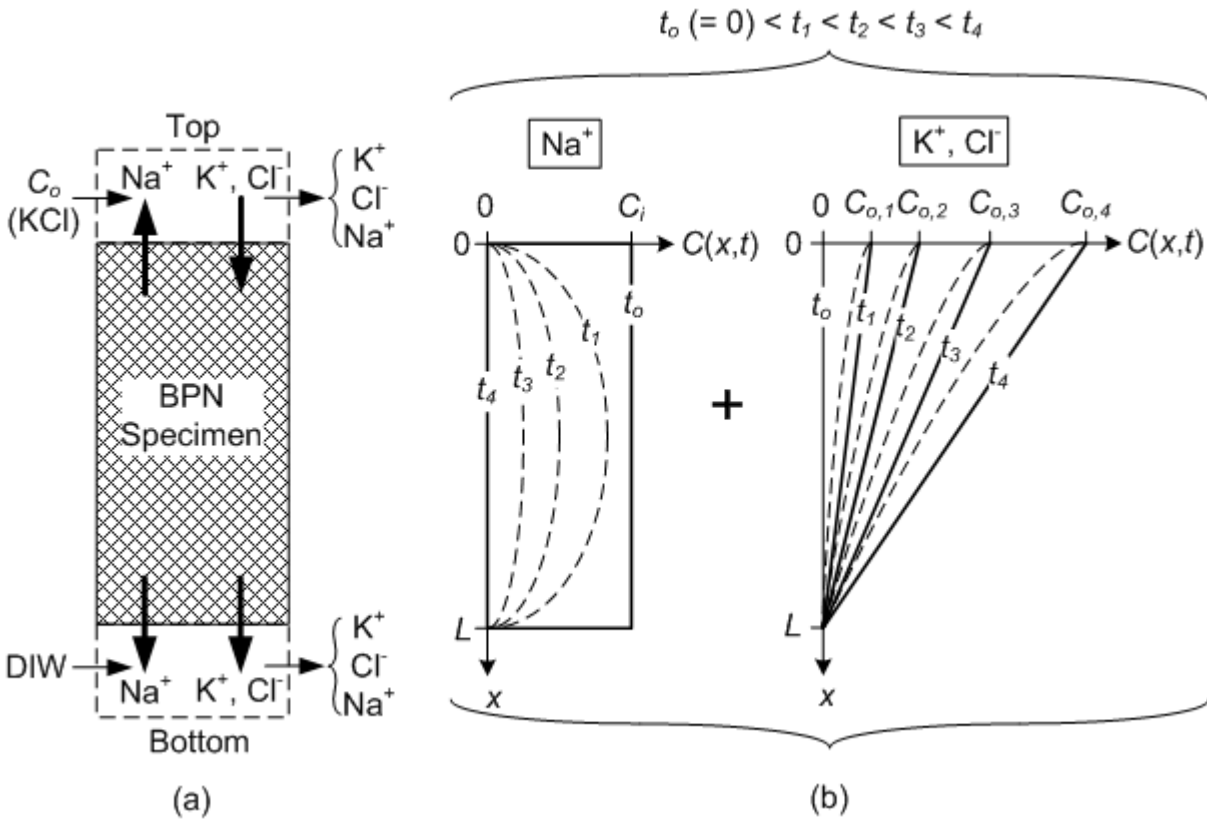


Figure 4.22. Schematic illustration of diffusion of dominant ionic species in test specimens of bentonite polymer nanocomposite (BPN): (a) directions of diffusion at top and bottom boundaries; (b) time-dependent concentration profiles.

References

- Ashmawy, A. K., Darwish, E. H., Sotelo, N., and Muhammad, N. (2002). "Hydraulic performance of untreated and polymer-treated bentonite in inorganic landfill leachates." *Clays and Clay Minerals*, 50(5), 546-552.
- Boels, D., and van der Wal, K. (1999). "Trisoplast: New developments in soil protection." Sardinia 99, CISA, Caligari, Italy, 77-84.
- Christman, M., Benson, C., and Edil, T. (2002). "Geophysical evaluation of annular well seals." *Ground Water Monitoring and Remediation*, 22(3), 104-112.
- Crank, J. (1975). *The mathematics of diffusion, 2nd Edition*, Clarendon Press, Oxford, England.
- Di Emidio, G. (2010). "Hydraulic and Chemico-Osmotic Performance of Polymer Treated Clay," PhD Dissertation, University of Ghent, Ghent, Belgium.
- Di Emidio, G., van Impe, P. O., and Flores, V. (2011). "Advances in geosynthetic clay liners: polymer enhanced clays." *Geo-Frontiers 2011: Advances in Geotechnical Engineering*, J. Han and D. Alzamora, eds., ASCE, Reston, VA, 1931-1940.
- Di Emidio, G., van Impe, P. O., and Mazzieri, F. "A polymer enhanced clay for impermeable geosynthetic clay liners." *Sixth International Conference on Environmental Geotechnics*, New Delhi, India, 963-967.
- Estornell, P., and Daniel, D. E. (1992). "Hydraulic conductivity of 3 geosynthetic clay liners." *Journal of Geotechnical Engineering-Asce*, 118(10), 1592-1606.
- Evans, J. C. (1994). "Hydraulic Conductivity of Vertical Cutoff Walls." *Hydraulic Conductivity and Waste Contaminant Transport in Soil*, STP 1142, D. E. Daniel and S. Trautwein, eds., ASTM, West Conshohocken, PA, 79-94.
- Groenevelt, P. H., and Elrick, D. E. (1976). "Coupling Phenomena in Saturated Homo-ionic Montmorillonite: II. Theoretical." *Soil Society of America Journal*, 40(6), 820-823.
- Heller, H., and Keren, R. (2003). "Anionic polyacrylamide polymer adsorption by pyrophyllite and montmorillonite." *Clays and Clay Minerals*, 51(3), 334-339.
- Kajita, L. S. (1997). "An improved contaminant resistant clay for environmental clay liner applications." *Clays and Clay Minerals*, 45(5), 609-617.
- Kang, J.-B., and Shackelford, C. D. (2009). "Clay membrane testing using a flexible-wall cell under closed-system boundary conditions." *Applied Clay Science*, 44(1-2), 43-58.
- Kang, J.-B., and Shackelford, C. D. (2011). "Consolidation enhanced membrane behavior of a geosynthetic clay liner." *Geotextiles and Geomembranes*, 29(6), 544-556.

- Kolstad, D. C., Benson, C. H., and Edil, T. B. (2004). "Hydraulic conductivity and swell of nonprehydrated geosynthetic clay liners permeated with multispecies inorganic solutions." *Journal of Geotechnical and Geoenvironmental Engineering*, 130(12), 1236-1249.
- Lagaly, G., Ogawa, M., and Dékány, I. (2006). "Clay Mineral Organic Interactions." *Developments in Clay Science*, F. Bergaya, B. K. G. Theng, and G. Lagaly, eds., Elsevier, 309-377.
- Malusis, M. A., and Shackelford, C. D. (2002a). "Chemico-osmotic efficiency of a geosynthetic clay liner." *Journal of Geotechnical and Geoenvironmental Engineering*, 128(2), 97-106.
- Malusis, M. A., and Shackelford, C. D. (2002b). "Coupling effects during steady-state solute diffusion through a semipermeable clay membrane." *Environmental Science & Technology*, 36(6), 1312-1319.
- Malusis, M. A., Shackelford, C. D., and Olsen, H. W. (2001). "A laboratory apparatus to measure chemico-osmotic efficiency coefficients for clay soils." *Geotechnical Testing Journal*, 24(3), 229-242.
- Manassero, M., and Dominijanni, A. (2003). "Modelling the osmosis effect on solute migration through porous media." *Geotechnique*, 53(5), 481-492.
- Mazzieri, F. (2011). "Impact of desiccation and cation exchange on the hydraulic conductivity of factory-prehydrated GCLs." *GeoFrontiers 2011: Advances in Geotechnical Engineering*, J. Han and D. Alzamora, eds., ASCE, Reston, VA, 976-985.
- Mazzieri, F., Di Emidio, G., and Van Impe, P. O. (2010a). "Diffusion of calcium chloride in a modified bentonite: impact on osmotic efficiency and hydraulic conductivity." *Clays and Clay Minerals*, 58(3), 351-363.
- Mazzieri, F., Pasqualini, E., and Di Emidio, G. (2010b). "Migration of heavy metals through conventional and factory-prehydrated GCL materials." *Sixth International Conference on Environmental Geotechnics*, New Delhi, Delhi, India, 963-967.
- Muzny, C. D., Butler, B. D., Hanley, H. J. M., Tsvetkov, F., and Peiffer, D. G. (1996). "Clay platelet dispersion in a polymer matrix." *Materials Letters*, 28(4-6), 379-384.
- Olsen, H. W., Yearsley, E. N., and Nelson, K. R. (1990). "Chemico-osmosis versus diffusion-osmosis." *Transportation Research Record No. 1288*, Transportation Research Board, Washington D.C., 15-22.
- Onikata, M., Kondo, M., Hayashi, N., and Yamanaka, S. (1999). "Complex formation of cation-exchanged montmorillonites with propylene carbonate: Osmotic swelling in aqueous electrolyte solutions." *Clays and Clay Minerals*, 47(5), 672-677.

- Onikata, M., Kondo, M., and Kamon, M. (1996). "Development and characterization of a multiswellable bentonite." 2nd International Congress on Environmental Geotechnics, M. Kamon, ed., A A Balkema, Rotterdam, Netherlands, 587-590.
- Scalia, J. (2012). "Bentonite-polymer composites for containment applications," PhD Dissertation, University of Wisconsin - Madison, Madison, WI.
- Scalia, J., Benson, C. H., Edil, T. B., Bohnhoff, G. L., and Shackelford, C. D. (2011). "Geosynthetic clay liners containing bentonite polymer nanocomposite." *Geo-Frontiers 2011*, J. Han and D. Alzamora, eds., ASCE, Reston, VA, 2001-2009.
- Shackelford, C. D. (1991). "Laboratory diffusion testing for waste disposal -- A review." *Journal of Contaminant Hydrology*, 7(3), 177-217.
- Shackelford, C. D. (2011). "Membrane behavior in geosynthetic clay liners." *GeoFrontiers 2011: Advances in Geotechnical Engineering*, J. Han and D. Alzamora, eds., ASCE, Reston, VA, 1961-1970.
- Shackelford, C. D. (2012). "Membrane behavior of engineered clay barriers for geoenvironmental containment: State of the art." *GeoCongress 2012-State of the Art and Practice in Geotechnical Engineering*, R. D. Hryciw, A. Athanasopoulos-Zekkos, and N. Yesiller, eds., ASCE, Oakland, CA, 3419-3428.
- Shackelford, C. D., and Daniel, D. E. (1991). "Diffusion in saturated soil. 1. Background." *Journal of Geotechnical Engineering-Asce*, 117(3), 467-484.
- Shackelford, C. D., and Lee, J. M. (2003). "The destructive role of diffusion on clay membrane behavior." *Clays and Clay Minerals*, 51(2), 186-196.
- Shackelford, C. D., Malusis, M. A., and Olsen, H. W. "Clay membrane behavior for geoenvironmental containment." *Soil and Rock America Conference 2003, Proceedings of the joint 12th Panamerican Conference on Soil Mechanics and Geotechnical Engineering and the 39th U. S. Rock Mechanics Symposium*, 767-774.
- Skagius, K., and Neretnieks, I. (1986). "Porosities and diffusivities of some nonsorbing species in crystalline rocks." *Water Resources Research*, 22(3), 389-398.
- Smith, J. A., Bartelt-Hunt, S. L., and Burns, S. E. (2003). "Sorption and permeability of gasoline hydrocarbons in organobentonite porous media." *Journal of Hazardous Materials*, 96(1), 91-97.
- Trauger, R., and Darlington, J. "Next generation geosynthetic clay liners for improved durability and performance." *14th GRI Conference, Geosynthetic Institute*, Folsom, PA, USA, 255-267.

Chapter 5

Polymerized Bentonite for Enhanced Resistance to Membrane Degradation

SUMMARY: Traditional bentonite contained in geosynthetic clay liners (GCLs) has been shown to exhibit semipermeable membrane behavior, which is beneficial in terms of the containment function of these materials. However, membrane behavior of non ideal (imperfect) clay membranes also has been shown to degrade due to the diffusion of cations into the bentonite, and this degradation has been shown to increase with increasing salt concentration and increasing valence (charge) of the principle salt cation (e.g., Ca^{2+} vs. K^+). In this study, the membrane behavior and diffusive properties of a polymerized bentonite, referred to as a bentonite polymer nanocomposite, or BPN, were determined through the simultaneous measurement of membrane efficiency coefficients and diffusion coefficients during multi-stage steady-state diffusion of calcium chloride (CaCl_2) and compared with the results taken from the literature for both traditional (unmodified) and modified bentonites. In contrast to previously reported results, the observed membrane behavior of the BPN was not destroyed during exposure to 5 mM CaCl_2 . In addition, the membrane efficiency coefficients, ω , were higher and the effective diffusion coefficients were lower for the BPN compared to those of traditional and modified bentonites. For example, the value of ω for the BPN tested in a rigid-wall cell with 5 mM CaCl_2 was 0.95, whereas the ω values for an anionic polymer modified bentonite (Hyper clay) and a GCL were 0.13 and 0, respectively. However, exposure of specimens of the BPN to 10 mM CaCl_2 for a test conducted in a rigid-wall cell and 20 mM CaCl_2 for a test conducted in a flexible-wall cell did ultimately result in complete destruction of the membrane behavior. The destruction of the membrane behavior of the specimen in the rigid-wall test was attributed to

short-circuiting along the side-walls of the rigid cell after shrinkage of the BPN specimen, whereas destruction of the membrane behavior in the flexible-wall cell correlated with the time required to reach steady-state diffusion of calcium (Ca^{2+}). The increase in Ca^{2+} concentration within the BPN specimens likely resulted in shrinkage or collapse of the interlayers within the montmorillonite component of the BPN as well as the diffuse-double layers surrounding individual clay particles, and in over-cross-linking of the polymer chains in the pores of the BPN causing the polymer to coil up and thereby increasing the diffusively active porosity. Thus, although the BPN did offer enhanced resistance to membrane degradation relative to that previously shown to exist for traditional (unmodified) and other modified bentonites, the enhanced membrane behavior was only incremental with respect to CaCl_2 solutions, and was affected by the type of cell (rigid-wall vs. flexible-wall) in which the membrane behavior was evaluated.

KEY WORDS: Chemico-osmosis; Clay membranes; Diffusion; Geosynthetic clay liner; Membrane efficiency; Polymer modified bentonites; Semipermeable membrane

5.1 INTRODUCTION

Bentonite is a clay comprised primarily of the mineral montmorillonite (smectite) and is commonly used to control liquid flow and contaminant transport for a variety of hydraulic containment barriers used to control liquid flow and contaminant transport. Bentonite has been used in *in situ* vertical cutoff walls for control of groundwater, in barriers (liners) for waste containment (e.g., landfills, wastewater ponds, anaerobic animal waste lagoons, nuclear storage, etc.) and secondary containment in tank farms, and as seals in monitoring and water supply wells

(Estornell and Daniel 1992; Evans 1994; Kajita 1997; Christman et al. 2002; Smith et al. 2003). Sodium bentonite (Na-bentonite), where Na^+ is the dominant exchangeable cation, is preferred for such applications relative to other types of bentonite, such as calcium bentonite (Ca-bentonite) or magnesium bentonite (Mg-bentonite), because Na-bentonite tends to swell to a greater extent in the presence of water leading to lower hydraulic conductivity, k , to water or dilute aqueous solutions containing inorganic or organic solutes (i.e., $k \leq 10^{-10}$ m/s) and increased semipermeable membrane behavior for dilute concentrations of simple salts (Shackelford et al. 2000; Malusis et al. 2001; Malusis and Shackelford 2002a; Kang and Shackelford 2009). Therefore, Na-bentonites are beneficial in hydraulic containment applications because (1) low k results in limited advective (hydraulically driven) contaminant transport, and (2) membrane behavior promotes hyperfiltration, chemico-osmotic counter flow, and reduced diffusion of aqueous-phase chemicals (Shackelford et al. 2003; Shackelford 2011; Shackelford 2012).

Unfortunately, most naturally occurring pore waters in earthen materials contain multivalent cations, such that Na-bentonite is thermodynamically unstable in the natural condition. In these environments, multivalent cations (e.g., Ca^{2+} and Mg^{2+}) gradually replace monovalent cations (e.g., Na^+ and K^+), originally dominating the exchange sites, thereby reducing or eliminating osmotic swelling of the bentonite and the ability of the bentonite to function effectively (Vasko et al. 2001; Kolstad et al. 2004; Lee and Shackelford 2005a; Scalia and Benson 2011; Bradshaw et al. 2012). The Ca^{2+} typically is derived from surrounding soils, and migrates into the bentonite portion of geosynthetic clay liners (GCLs), or thin (~ 5- to 10-mm-thick), manufactured barriers comprised of bentonite sandwiched between two geotextiles, usually in response to hydraulic (e.g., suction) and/or diffusive (chemical) gradients. Several field studies have shown that Ca^{2+} -for- Na^+ exchange in GCLs can result in reduced swelling

capability of the bentonite upon hydration, and ultimately to poor hydraulic performance (ATU 1992; James et al. 1997; Shackelford et al. 2000; Egloffstein 2001; Jo et al. 2001; Benson et al. 2004; Benson et al. 2007; Meer and Benson 2007; Scalia and Benson 2011; Bradshaw et al. 2012).

In addition, laboratory studies have illustrated the detrimental effects of long-term cation exchange on both k and membrane behavior (Lin and Benson 2000; Egloffstein 2001; Jo et al. 2001; Shackelford and Lee 2003; Kolstad et al. 2004; Jo et al. 2005; Lee and Shackelford 2005a; Lee et al. 2005; Di Emidio 2010; Mazzieri et al. 2010a). Partial or complete destruction of membrane behavior in bentonite has been correlated with diffusion of invading salt cations into the bentonite (Malusis and Shackelford 2002a; Shackelford and Lee 2003; Di Emidio 2010). The membrane efficiency of clay has been shown to decrease when the clay is subjected to an electrolyte solution with increasing valence (charge) and/or concentration (Malusis et al. 2001; Malusis and Shackelford 2002a). For example, Malusis et al. (2001) and Malusis and Shackelford (2002a) observed partial decreases in membrane efficiency of a GCL upon exposure to solutions of KCl. The maximum chemico-osmotic pressure difference, $-\Delta P$ (> 0), upon exposure of a specimen of the GCL to 47 mM KCl was approximately 40 kPa, but $-\Delta P$ eventually decreased to a steady-state value of 32 kPa. This behavior has been attributed to the collapse of the interlayers within individual clay particles and the diffuse-double layers (DDLs) surrounding individual clay particles, resulting from the diffusion of ions into the pores of the clay.

At a much larger scale, chemico-osmotic flow has been postulated to be a source of elevated pressures, or overpressures, in shale sedimentary basins (Neuzil 2000; Neuzil and Provost 2009). However, models based on laboratory measured material properties have been

shown to over predict the overpressures compared to those that have been reported based on field measurements, i.e., >10 MPa vs. 0.1 to 1 MPa, respectively (Marine and Fritz 1981; Neuzil and Provost 2009; Rousseau-Gueutin et al. 2009). A potential cause of this apparent disparity is the more complex composition of natural pore waters that include both monovalent and divalent cations relative to the laboratory tests that typically have been conducted using electrolyte solutions comprised of on a simple salt, such as KCl. A relatively recent assessment of this effect by Tremosa et al. (2012) has shown that more accurate overpressures are predicted when the electrolyte solutions both monovalent and divalent cations.

Shackelford and Lee (2003) demonstrated the correlation between diffusion of Ca^{2+} and the destruction of membrane behavior. Tests were conducted on a GCL using a 5 mM CaCl_2 solution. The hypothesis was that if diffusion was the cause of reduced membrane efficiency, then the membrane efficiency coefficient, ω , where $0 \leq \omega \leq 1$, should decrease to a steady-state value at the same time as the commencement of steady-state diffusion, or t_{ss} . The measured ω of the GCL reached a peak of 0.52 after 9 d, decreased to 0.016 after 35 d, and then decreased to zero after approximately 48 d. Based on a regression analysis, t_{ss} for the Ca^{2+} was 35 ± 2 d. Thus, the times to reach $\omega \sim 0$ and t_{ss} for Ca^{2+} correlated very well, indicating that the diffusion of solutes can completely destroy membrane behavior (Shackelford and Lee 2003).

Laboratory membrane tests conducted on specimens of an untreated bentonite, multi-swelling bentonite (MSB), a bentonite modified with propylene carbonate, an anionic polymer modified bentonite known as Hyper clay, and a dense pre-hydrated GCL (DPH-GCL) were conducted with dilute solutions of CaCl_2 (i.e., 1 mM and 5 mM CaCl_2) by Di Emidio (2010). The untreated bentonite initially exhibited membrane behavior with the 1 mM CaCl_2 ($\omega = 0.29$). However, as with the bentonite in the GCL from Shackelford and Lee (2003), the membrane

behavior of the untreated bentonite eventually was destroyed completely with the 5 mM CaCl₂. During the circulation of 1 mM CaCl₂, the ω for DPH-GCL was 0.27 whereas the MSB did not exhibit membrane behavior ($\omega = 0$). In contrast to the untreated bentonite, the membrane behavior of the Hyper clay was not destroyed by the dilute CaCl₂ solutions, indicating that the polymer treatment improved the performance of the Hyper clay (Di Emidio 2010). However, the Hyper clay was exposed only to 1 mM and 5 mM CaCl₂ solutions, such that stronger CaCl₂ solutions may have led to a destruction of the membrane behavior.

Cation exchange can cause collapse of the hydrated interlayer of the bentonite and limit osmotic swell, thereby potentially increasing the mass flux of aqueous soluble chemicals via advection and diffusion and decreasing hyperfiltration and chemico-osmotic counter flow (Malusis and Shackelford 2002b; Manassero and Dominijanni 2003; Kolstad et al. 2004). However, methods exist to chemically modify bentonite so that the bentonite properties are compatible with the surrounding environment. For example, Na-bentonites have been amended with organic molecules for improved hydraulic and diffusive performance (e.g., Onikata et al. 1996; Trauger and Darlington 2000; Ashmawy et al. 2002; Di Emidio 2010; Di Emidio et al. 2010; Mazzieri et al. 2010a and b; Di Emidio et al. 2011; Mazzieri 2011). In these cases, organic molecules were intercalated to increase the potential for osmotic swell in the presence of multivalent-for-monovalent cation exchange and/or elevated solute concentrations.

The bentonite investigated in this study was modified at the nanoscale in an attempt to ensure that the swollen structure of the bentonite is maintained. Organic molecules (acrylic acid) were inserted between the montmorillonite layers and then polymerized *in situ* to form an interconnected structure within the bentonite. Because this modification occurs at the nanoscale,

the resulting modified material commonly is referred to as a bentonite-polymer nanocomposite or BPN (Scalia et al. 2011; Scalia 2012).

The purpose of this study was to evaluate simultaneously both the diffusive and membrane properties of the BPN to electrolyte solutions containing CaCl_2 , and then correlate the diffusive properties with the membrane behavior of the BPN. The hypothesis is that the diffusive and membrane properties of the BPN when exposed to divalent cations (i.e., Ca^{2+}) would be superior to those of a traditional (unmodified) Na-bentonite. This hypothesis was evaluated through the simultaneous measurement of membrane efficiency coefficients and effective diffusion coefficients during multi-stage, steady-state diffusion of chloride (Cl^-) and calcium (Ca^{2+}) through the BPN over a range in source CaCl_2 concentrations for which the BPN behaved as a semipermeable membrane. The results of this study were compared with those previously reported in the literature for tests conducted to evaluate a traditional (unmodified) Na-bentonite and treated bentonites (i.e., MSB, Hyper clay, and DPH-GCL).

5.2 MATERIALS AND METHODS

5.2.1 Liquids

The liquids used in this study included de-ionized water (DIW) and solutions of DIW and calcium chloride dihydrate (CaCl_2) (certified A.C.S.; Fisher Scientific, Fair Lawn, NJ). Solutions were prepared and stored in 20-L carboys (Nalgene[®]; Thermo Fisher Scientific, Rochester, NY). The *pH* and electrical conductivity, *EC*, of the solutions were measured using a *pH* meter (Accumet[®] AB15 meter; Fisher Scientific Co., Pittsburgh, PA or Ross Ultra Triode, Thermo Scientific Orion, Waltham, MA) and an *EC* probe (150 A+ Conductivity Meter; Thermo Orion, Beverly, MA or DuraProbe Conductivity Cell; Thermo Scientific Orion, Waltham, MA),

respectively. Ion chromatography (Dionex[®] ICS-2100, Dionex Co., Sunnyvale, CA) was used to measure chloride (Cl⁻) concentrations, and inductively coupled plasma-atomic emission spectrometry, or ICP-AES (IRIS[®] Advantage/1000 ICAP Spectrometer, Thermo Jarrel Ash Co., Franklin, MA), was used to measure calcium (Ca²⁺) concentrations. The measured *EC* and *pH* of the CaCl₂ solutions are given in Table 5.1.

5.2.2 Soil

The BPN evaluated in this study was provided by Colloid Environmental Technologies Co. (CETCO, Hoffman Estates, IL). The BPN was created using polyacrylic acid (PAA) and methods similar to the production of polymer nanocomposites (e.g., Muzney et al. 1996). The BPN classified as CH for high-plasticity clay according to the Unified Soil Classification System (ASTM D 2487) (ASTM 2010). Mineralogical analyses conducted by Mineralogy, Inc. (Tulsa, OK) using x-ray diffraction indicated the composition of the BPN as 76 % montmorillonite, 15 % quartz, 7 % plagioclase feldspar, and 2 % illite/mica. Additional details regarding the properties of the BPN are provided in Scalia et al. (2011), Scalia (2012), and Chapter 3.

Tests to measure both the swell index, *SI*, and the solution retention capacity, *SRC*, were conducted using both DIW and aqueous solutions containing concentrations of CaCl₂ ranging from 5 mM to 500 mM to provide an indirect indication of the quality of the bentonite and the potential for adverse interaction (i.e., incompatibility) between the bentonite and the permeant liquids (e.g., Lee and Shackelford 2005b; Lee et al. 2005). The tests to measure *SI* were conducted in general accordance with ASTM D 5890 (ASTM 2006). Briefly, two grams of oven dried bentonite were dusted over the test solution in 0.1-g increments. The *SI* (mL/2g) was monitored after 16 h and then every 4 h up to 48 h until swelling had ceased. The tests to

measure *SRC* were conducted following the procedures described in Lee and Shackelford (2005c). However, the centrifuge speed was set at 3000 rotations per minute (RPM) rather than the 5000 RPM specified by Lee and Shackelford (2005c) to allow for an increased sensitivity of the resulting measurements.

The resulting values of *SI* and *SRC* are summarized in Tables 5.2 and 5.3, respectively, and are plotted as a function of CaCl_2 concentration in Fig. 5.1. The *SI* and *SRC* values for a "higher quality bentonites" or HQB and a "lower quality bentonites" or LQB reported by Lee and Shackelford (2005b) also are shown in Tables 5.2 and 5.3 for comparison.

As indicated by the data in Tables 5.2 and 5.3, the values of *SI* and *SRC* for the BPN are similar to but noticeably higher than those of the HQB and LQB, except for the results involving 500 mM CaCl_2 . In addition, the differences between the *SI* and *SRC* values for BPN versus those for the LQB and HQB tend to decrease with increasing concentration, as shown in Fig. 5.2. Thus, although the *SI* and the *SRC* of the BPN also decreases with increasing CaCl_2 concentration, the higher values of *SI* and *SRC* for the BPN at the lower CaCl_2 concentrations suggest that the BPN would be more resistant to chemical attack at these lower concentrations relative to the LQB and HQB (Lee and Shackelford 2005b; Lee et al. 2005).

5.2.3 Membrane Testing

The testing apparatuses and procedure are similar to those described by Malusis et al. (2001) and by Kang and Shackelford (2009) as described in Chapter 3. The BPN specimen is tested in a rigid or flexible-wall cell. The rigid-wall cell is used to test specimens under constant-volume conditions throughout the test. As explained by Kang and Shackelford (2009), the flexible-wall cell also maintains constant specimen volume during the stages of the test

devoted to measuring membrane behavior. However, volume change generally does occur during the brief (< 5 min) liquid refilling and sampling periods that are required periodically between the longer (typically 48 h) membrane testing stages. Also, the flexible-wall cell allows for back-pressure saturation of the specimen prior to membrane testing, for control of the stress conditions imposed on the specimen, and for monitoring of volume change during the refilling and sampling period (Kang and Shackelford 2009).

In general, chemical solutions are circulated across both the top and bottom boundaries of the specimen contained in the cell at the same, constant displacement rate (Malusis et al. 2001; Kang and Shackelford 2009). A solution with an initial concentration of CaCl_2 , $C_{o,t} (> 0)$, is circulated through a porous disk (GenPore porous sheet TO-6, General Polymer Corp., Reading, PA) along the top of the specimen while DIW ($C_{o,b} = 0$) is circulated simultaneously through a porous disk along the base of the specimen such that a constant concentration difference (ΔC) is maintained across the specimen. The system is closed during testing such that no liquid flow is allowed to occur. As a result, the volume change in the circulation system during circulation is zero, i.e., at least during the periods of the test devoted to measurement of the membrane behavior of the specimen. Two in-line pressure transducers (model Nos. PX181-100G5V or PX209-015G10V, Omega Engineering Inc., Stamford, CT) and a differential pressure transducer (model DP15-64, Validyne Engineering Corp., Northridge, CA) are used to measure the boundary water pressures at the top and bottom of the specimen, or u_{Top} and u_{Bottom} , respectively, and the chemico-osmotic pressure, $-\Delta P (= u_{Bottom} - u_{Top} > 0)$ across the specimen due to specimen membrane behavior. The circulation rate was adjusted to mimic "perfectly flushing" boundary conditions such that a steady-state $-\Delta P$ was achieved during the circulation period, i.e., the time between the sampling and refilling periods (e.g., see Malusis et al. 2001). The

circulation rate used in this study was $2.3 \times 10^{-10} \text{ m}^3/\text{s}$, which amounted to a circulation of approximately 40 mL every two days, after which the syringes were sampled and refilled before the start of a new circulation cycle. During the brief ($< 5 \text{ min}$) sampling and refilling periods, the outflow liquids were collected and stored for subsequent analysis (e.g., *EC* and solute concentration, *C*).

As described in Chapter 3, the BPN specimens tested in this study essentially represent specimens that were not flushed of soluble salts prior to membrane testing. In contrast, most if not all previous tests conducted on specimens of bentonite-based barriers were permeated with DIW prior to membrane testing for extensive periods ($\geq 80 \text{ d}$) in an attempt to enhance the potential for significant membrane behavior by reducing the soluble salt content in the pores of the specimens (Malusis et al. 2001; Malusis and Shackelford 2002a; Shackelford and Lee 2003; Kang and Shackelford 2009; Kang and Shackelford 2010; Kang and Shackelford 2011). In all these previous tests, the *EC* values in the permeated effluent at the end of this leaching or flushing stage, and prior to membrane testing, were all less than 70.2 mS/m. In contrast, BPN specimens were permeated for periods from weeks to months. Despite those durations of permeation, little effluent was collected due to the affinity of the BPN for water, the low k ($< 3 \times 10^{-10} \text{ m/s}$) of the BPN, and the presence of excess low molecular weight polymer clogging the system (Scalia 2012). Therefore, the specimens of BPN evaluated in this study were evaluated under initial conditions that were far less favorable towards the existence of significant semipermeable membrane behavior than had previous been evaluated for most bentonites-based specimens.

The membrane testing procedure involved multi-stage testing. First, an initial baseline pressure difference, $-\Delta P$ (> 0), was established by simultaneously circulating DIW across both

the top and bottom boundaries of the specimen (i.e., $C_{ot} = C_{ob} = 0$). Once this baseline pressure difference had been established, the liquid being circulated across the top boundary was switched from DIW to the electrolyte solution containing the lowest concentration of CaCl_2 (i.e., $C_{ot} = 5$ mM CaCl_2), and the generated chemico-osmotic pressure difference, $-\Delta P$, was recorded continuously until a steady-state condition with respect to this pressure difference was achieved. This procedure was repeated for additional stages using electrolyte solutions with progressively higher concentrations of CaCl_2 (i.e., 10 mM and 20 mM CaCl_2) until the test was terminated.

If a specimen is not an ideal or perfect membrane, then solutes can and do diffuse through the specimen. In the present case, this diffusion results in concentrations of Ca^{2+} and Cl^- in the circulation outflow from the base of the specimen being greater than those in the circulation inflow to the base of the specimen (i.e., $C_b > C_{o,b}$), whereas concentrations of Ca^{2+} and Cl^- in the circulation outflow from the top of the specimen are lower than those in the circulation inflow at the top of the specimen (i.e., $C_t < C_{o,t}$). As a result, the concentrations of relevant chemical species in the circulation outflows from the bottom of the specimens were monitored as a function of time for the purpose of determining diffusion coefficients (e.g., see Malusis et al. 2001).

5.2.4 Membrane Efficiency Coefficient

Under the closed or no-flow conditions imposed in this study (i.e., $q = 0$), the membrane or chemico-osmotic efficiency coefficient, ω , is defined as follows (Groenevelt and Elrick 1976; Malusis et al. 2001):

$$\omega = \frac{\Delta P}{\Delta \pi} = \frac{\Delta P}{vRT\Delta C} = \frac{\Delta P}{vRT(C_{ob} - C_{ot})} = \frac{\Delta P}{-vRTC_{ot}} \quad (5.1)$$

where $\Delta\pi$ is the theoretical chemico-osmotic pressure difference across an "ideal" semipermeable membrane (i.e., $\omega = 1$) subjected to an applied difference in solute (electrolyte) concentration, v is the number of ions per molecule of the salt ($= 3$ for CaCl_2), R is the universal gas constant [$8.314 \text{ J mol}^{-1}\text{K}^{-1}$], T is the absolute temperature (293 K in this study corresponding to 20 °C), and C_{ot} (> 0) and C_{ob} ($= 0$) are the initial concentrations of CaCl_2 (M) in the source solutions introduced across the top and bottom specimen boundaries, respectively. Previous studies (e.g., Malusis and Shackelford 2002a; Kang and Shackelford 2009, 2010, 2011) also have evaluated the membrane efficiency coefficient based on the average salt concentrations at each boundary of the specimen. However, only the initial, source concentrations of the CaCl_2 were used in estimating ω in this study for three reasons: (1) estimates of the ω based on source concentrations are more conservative (lower) than estimates of ω based on average concentrations, i.e., for the same measured ΔP ; (2) measurement of Ca^{2+} concentrations in the circulation outflow from the top of the specimen via calibration with *EC*, as has been done in other studies involving *KCl* circulation for flushed specimen (e.g., Kang and Shackelford 2009) was deemed to be unreliable based on the large amount of remnant Na^+ contained in the non-flushed BPN specimens evaluated in this study (e.g., see Chapter 4); and (3) measurement of Ca^{2+} concentrations in samples of the circulation outflow from the top was considered to be too costly given reason (1).

5.2.5 Determination of Diffusion Coefficients

In the case of non-ideal specimens, some solute diffusion of salt cations and anions in the circulation inflow still occurs through the specimen as a result of the concentration gradient imposed across the specimen during the membrane tests. Since the concentrations at the

specimen boundaries are maintained reasonably constant during membrane testing, the diffusion of solutes through the specimen eventually reaches a steady state. The boundary conditions are consistent with those associated the steady-state or through-diffusion method for measuring effective diffusion coefficients (e.g., Shackelford 1991). In this method, the concentrations of solutes that have diffused through the specimen typically are converted to the cumulative mass per unit area of a specimen, Q_t , as follows:

$$Q_t = \frac{1}{A} \sum_{i=1}^{N_s} \Delta m_i = \frac{1}{A} \sum_{i=1}^{N_s} C_{b,i} \Delta V_i \quad (5.2)$$

where A is the cross-sectional area of the specimen, Δm_i is the incremental mass of the solute species collected over a time increment, Δt , $C_{b,i}$ is the mass concentration of the solute species in the incremental volume, ΔV_i , of the circulation outflow from the base of the pedestal corresponding to the Δt , and N_s is the number of incremental samples corresponding to the total elapsed time, t . The data typically are plotted as Q_t versus the cumulative, elapsed time, t . The plot generally is nonlinear at the beginning or transient stage of the test, followed by a steady-state stage which is indicated by a straight line representing constant diffusive mass flux (Shackelford 1991). The effective diffusion coefficient, D^* , is determined with a linear regression from the steady-state portion of the data with a slope $\Delta Q_t / \Delta t$ based on the following equation:

$$D^* = \left(\frac{\Delta Q_t}{\Delta t} \right) \left(\frac{L}{nw_A \Delta C} \right) \quad (5.3)$$

where L is the specimen thickness, n is the specimen porosity, w_A is the atomic weight of the diffusing solute, and ΔC is the molar concentration difference of the solute (i.e., anion or cation) across the specimen. A sequential linear regression was conducted on the data as described in Shackelford and Lee (2003). Briefly, a linear regression was conducted on an increasing number of Q_t versus t data points until the coefficient of determination, r^2 , deviated significantly from unity. The point where this deviation occurred was assumed to be the distinction between the transient and steady-state portion of the data or the time to reach steady-state, t_{ss} .

5.2.6 Testing Program

Two membrane/diffusion tests were conducted in this study, with one test conducted using a rigid-wall (RW) cell and another test conducted using a flexible-wall (FW) cell. The thickness, L , of the specimen contained within the RW cell was 10.4 mm, and the total specimen porosity, n , was 0.87. The specimen in the FW cell was confined at an initial effective stresses, σ' , of 103 kPa (15 psi) corresponding to an initial n (i.e., immediately after consolidation, but prior to membrane testing) of 0.94. The circulation liquid emanating from the bottom boundary of the specimen was collected and saved for analysis for concentrations of cations (ICP) and anions (IC) for the primary purpose of determining diffusion coefficients in accordance with Eq. 5.3.

5.3 RESULTS

5.3.1 Electrical Conductivity

The EC of the circulation outflow liquids versus time for the two tests are presented in Fig. 5.3. The expected temporal trends in these measured boundary EC values have been

established in several previous studies (e.g., Malusis et al. 2001; Malusis and Shackelford 2002a,b; Shackelford and Lee 2003; Yeo et al. 2005; Kang and Shackelford 2009; 2010, 2011; Chapter 3). In general, the values of EC increased with time in response to an increase in the EC of the source solution, EC_o , when the concentration of circulation liquid at the top of the cell (C_{ot}) increased. The EC of the circulation outflow from the top boundary of the cell, EC_{Top} , was lower than EC_o of the source solution ($EC_{Top} < EC_o$) as a result of diffusion of solute into the specimen at this boundary. In contrast, the EC of the circulation outflow from the bottom boundary of the cell, EC_{Bottom} , increased with time as a result of solute diffusing out from the specimen.

The EC at the top and bottom boundaries eventually stabilized indicating establishment of steady-state conditions with respect to EC . However, the time required to reach this steady-state EC value was longer in some stages relative to other stages. For example, during circulation of 10 mM $CaCl_2$ in the RW cell, the EC_{Bottom} continued to increase until approximately day 182 (or approximately 100 d after the start of circulation of 10 mM $CaCl_2$). In contrast, during the circulation of 10 mM $CaCl_2$ in the FW cell, the EC_{Bottom} leveled off in less than 14 days. One possible explanation for the behavior of the RW test could be gradual changes in the fabric of the BPN after exposure to stronger concentrations of the divalent cation Ca^{2+} resulting in gradual shrinkage of the specimen away from the rigid side-walls of the cell.

Another anomalous behavior is a second increase in the value of EC_{Bottom} and decrease in the value of EC_{Top} during the circulation of 20 mM $CaCl_2$ in the FW test. This apparent sudden increase in EC corresponds to other changes in the test (i.e., $\Delta P \rightarrow 0$) and will be discussed in additional detail in Section 5.4.2.

5.3.2 Boundary Water Pressures

The boundary water pressures, u_{top} and u_{bottom} , measured in the cell with in-line pressure transducers during membrane testing on the BPN are presented in Fig. 5.4. For the rigid-wall (RW) test, the boundary water pressures were essentially the same (i.e., $u_{top} \approx u_{bottom}$) during the circulation of DIW across both the top and bottom specimen boundaries. However during circulation of DIW for the flexible-wall (FW) test, the boundary water pressures were slightly different resulting in a minor baseline pressure difference, $-\Delta P_o$, of -1.3 kPa. Upon commencement of circulating CaCl_2 solutions, the u_{top} increased relative to u_{bottom} for both tests (i.e., $u_{top} > u_{bottom}$). For the RW test, u_{bottom} decreased relative to the backpressure, u_{bp} , and exceeded the limit of the in-line pressure transducer. However, for the FW test, u_{bottom} initially was less than u_{bp} but slowly increased to a value greater than u_{bp} after 28 d [i.e., $u_{bottom} > u_{bp} = 68.9$ kPa (10 psi)]. Both u_{top} and u_{bottom} continued to increase until, during the third stage of the FW test, the boundary water pressures converged (i.e., $u_{top} \approx u_{bottom}$) and gradually decreased until u_{top} and u_{bottom} were equal to u_{bp} . This decrease in u_{top} and u_{bottom} correlates with the loss in membrane behavior and will be discussed in additional detail in Section 5.4.2.

For the FW test, the confining stress, σ_c , was held constant at 172 kPa (25 psi). However, throughout the test, the boundary water pressures (i.e., u_{top} and u_{bottom}) changed with time leading to changes in the effective stresses at the top, σ'_{top} ($= \sigma_c - u_{top}$), and the bottom, σ'_{bottom} ($= \sigma_c - u_{bottom}$), of the specimen (refer to Fig. 5.5a). As a result, the average effective stress, σ'_{ave} , based on these boundary effective stress (i.e., $\sigma'_{ave} = (\sigma'_{top} + \sigma'_{bottom})/2$) also was not constant (refer to Fig. 5.5b). In general, the σ'_{ave} decreased from greater than 128 kPa during circulation of DIW to less than 41.3 kPa during circulation of 20 mM CaCl_2 . Since the boundary water pressures

trended toward the backpressure during the circulation of 20 mM CaCl₂ (i.e., $u_{top} \approx u_{bottom} \approx u_{bp}$), σ'_{ave} increased from less than 41.3 kPa to the confining stress [$\sigma'_{ave} \approx \sigma_c = 103$ kPa (15 psi)].

5.3.3 Chemico-Osmotic Pressures and Membrane Efficiency Coefficients

The measured chemico-osmotic pressure differences, $-\Delta P$ (> 0) are presented in Fig. 5.6. The baseline differential pressure, $-\Delta P_o$, induced during the circulation of DIW across both the top and bottom boundary was approximately equal to zero for the RW test, but approximately -1.3 kPa (-0.2 psi) for the FW test. Therefore, corrected or effective values of the pressure difference, $-\Delta P_e$ [$= -\Delta P_{ss} - (-\Delta P_o)$], as summarized in Table 5.4, were used to calculate ω shown in Table 5.4. Possible explanations for this non-zero baseline differential pressure include slight differences in the hydraulic resistance of the porous disks along the top and bottom of the specimen resulting in slightly different head losses within the disks or slight differences in the syringes that circulate liquid across the top and bottom of the specimen resulting in slightly different flow rates across the specimen (e.g., Malusis et al. 2001). The values of ω were calculated using Eq. 5.1, the measured chemico-osmotic pressure differences, and values for $\Delta\pi$ of 36.6, 73.1, or 146 kPa for the CaCl₂ concentrations of 5 mM, 10 mM, and 20 mM, respectively.

Immediately after the circulation liquid was switched from DIW to 5 mM CaCl₂, $-\Delta P_e$ began to increase. For the RW test (Fig. 5.6a), $-\Delta P_e$ increased from zero to 20 kPa in less than three days and then gradually increased to the maximum value, $-\Delta P_{e,max}$, of 37.0 kPa after approximately 50 d. The steady-state value, $-\Delta P_{e,ss}$, was approximately 34.5 kPa, which corresponds with a steady-state membrane efficiency coefficient, ω_{ss} , of 0.95. During the second stage of the RW test (i.e., circulation of 10 mM CaCl₂), $-\Delta P_e$ reached a maximum value of 47.9

kPa after two days, leveled off at approximately 33 kPa for several weeks, and then started to decrease after 143 d, ultimately to value of zero (i.e., $\omega_{ss} = 0$) after approximately 154 d, or 74 d after the start of the second stage.

The ultimate destruction of the observed membrane behavior for the RW tests can be attributed to at least three possible mechanisms. First, as has previously been shown with respect to the destruction of membrane behavior in a conventional bentonites (Shackelford and Lee 2003), the increase in concentration of a divalent calcium, Ca^{2+} , in the pore water results in progressively greater shrinkage or collapse of the interlayers within the montmorillonite component of the bentonites particles as well as the diffuse double layers surrounding individual clay particles. Second, the superabsorbent polymer (PAA) within the BPN is sensitive to the cations in the pore water, such that the Ca^{2+} ions may have caused over cross-linking of the polymer chains in the pores of the BPN to causing the polymer to coil up increasing the hydraulically and diffusive active porosity (Buchholz and Graham 1998; Scalia et al. 2011; Scalia 2012). Third, the aforementioned shrinkage of the polymer may have resulted in the shrinkage of the BPN, such that short-circuiting occurred along the side-walls of the specimen. The decrease in $-\Delta P_e$ occurred rather quickly, dropping 20 kPa in two days which is in contrast to the gradual decrease in $-\Delta P_e$ over 26 days reported by Shackelford and Lee (2003), implying that the second and third mechanisms may be the primary factors leading to the destruction of membrane behavior for the BPN in the RW cell.

To test this third mechanism, rhodamine dye was added to the CaCl_2 reservoir on day 160 to stain the diffusive pathways through or around the specimen. The results was that dye was visible along the side-walls of the cell and, after the test was broken down, the specimen was cut open and the dye was observed to have traveled only through the top half of the specimen (see

Figs. 5.7 and 5.8). Shrinkage of the specimen also was visible. Thus, short-circuiting may have caused or contributed to the loss of a measured $-\Delta P$ in the RW test.

During the circulation of 5 mM CaCl_2 for the FW test (refer to Fig. 5.6b), the $-\Delta P_e$ quickly increased to approximately 6 kPa in less than three days and then gradually increased to a $-\Delta P_e$ of 14.4 kPa. The value for $-\Delta P_{e,max}$ of 14.8 kPa was only slightly higher than the value for $-\Delta P_{e,ss}$ of 14.4. Similarly, the values of ω_{max} and ω_{ss} were close at 0.41 and 0.39, respectively. After the solution had been switched to 10 mM CaCl_2 , the value for $-\Delta P_{e,max}$ of 20.4 kPa was achieved within two days, followed by a decrease in $-\Delta P_e$ to 8.3 kPa. This post-peak degradation in $-\Delta P$ is similar to that previously reported by others (e.g., Malusis and Shackelford 2002a; Shackelford and Lee 2003), and can be attributed to diffusion of the solutes into the BPN and subsequent shrinkage or collapse of the interlayers within the montmorillonite component of the bentonites particles, the diffuse double layers surrounding individual bentonite particles, as well as the polymer within the BPN as a result of an increase in pore-water concentration of Ca^{2+} . The value of $-\Delta P_{e,ss}$ for this stage was approximately 8.3 kPa with a calculated value for ω_{ss} of 0.11.

The fact that the observed membrane behavior in the FW test was not completely destroyed after circulation of 10 mM CaCl_2 during the second stage of the test, as was the case with the RW test, lends further credence that shrinkage of the BPN specimen in the RW test caused short-circuiting of the membrane behavior in that test. i.e., since such shrinkage in the FW test would not be expected to result in separation of the specimen from the side walls. Since, the membrane behavior for the FW test was not completely destroyed after the second stage of the FW test, a third stage involving circulation of 20 mM CaCl_2 across the top of the specimen was conducted for the FW test. During this third stage, the value of $-\Delta P_e$ increased slightly to a

maximum, $-\Delta P_{e,max}$, of 9.75 kPa corresponding to a calculated value for ω_{max} of 0.07, but then continued to decrease until at 285 d when the $-\Delta P_e$ was less than 0.5 kPa, at which the values for both $-\Delta P_{e,ss}$ and ω_{ss} were approximately zero.

5.3.4 Volume Change

As described in Kang and Shackelford (2009) and in Chapter 3, although drainage was not allowed to occur during the circulation stages of the membrane tests, drainage from the specimen did occur during the brief (< 5 min) refilling and sampling periods successive electrolyte circulation stages. Kang and Shackelford (2009) attributed the drainage to an increment in effective stress resulting from physico-chemico interactions between the pore water in the bentonite and the individual particles of bentonite, commonly referred to as the R – A effect of osmotic consolidation (e.g., Mitchell 1976; Barbour and Fredlund 1989; Di Maio 1996). As described in Chapter 3, the R – A effect likely was the dominant mechanism in terms of volume change of the specimens. In addition, the brief increase in σ' to the initial value of 103 kPa (15 psi) when the back pressure was re-established during the sampling/refilling intervals also could have caused specimen compression during the refilling and sampling stages. An additional volume change mechanism specific to the BPN is related to the interaction of the superabsorbent polymer portion of the BPN with the divalent cation, Ca^{2+} . This interaction may result in over-cross-linking within the polymer leading to “catastrophic” collapse of the BPN as a result of bridging between clay platelets and the polymer and the polymer stitching together (Buchholz and Graham 1998).

The resulting measured values of incremental volume change, $-\Delta V (> 0)$ and cumulative volume change, $\sum(-\Delta V)$, are presented in Fig. 5.9, and the resulting changes in bulk specimen

porosities are summarized in Table 5.5. The ΔV values generally were negative, indicating that the volume of the specimen decreased during the test (i.e., a final volume less than the initial volume). The magnitude of $-\Delta V$ increased with increasing concentration of CaCl_2 , until half way through the last stage of the test (during the circulation of 20 mM CaCl_2) when the volume change trended toward zero. The value of $-\Delta V$ was generally less than 0.5 mL during the circulation of 5 mM CaCl_2 , whereas $-\Delta V$ was as much as 1.3 mL during the circulation of 20 mM CaCl_2 . The value of $\sum(-\Delta V)$ was 85.7 mL, which corresponds to a cumulative volumetric strain, $\sum(-\Delta V)/V_o$, of 71 % (see Fig. 5.10). The incremental volumetric strains, $(-\Delta V)/V_o$, were generally less than 0.4 % during the circulation of 5 mM CaCl_2 , but increased to as much as 1.1 % during the circulation of 20 mM CaCl_2 , which is consistent with an increasing R – A effect with increasing salt concentration. A pictorial view of the volume change is included in Fig. 5.11. Photographs of the specimen in the cell at several stages of the test, i.e., before circulation of DIW (Fig. 5.11a), after circulation of DIW (Fig. 5.11b), during circulation of 10 mM CaCl_2 (Fig. 5.11c) after circulation of 20 mM CaCl_2 (Fig. 5.11d), and after termination of the test (Fig. 5.11e) are depicted.

The eventual stabilization of the volume change during the last stage of the test coincides with EC increasing suddenly, u_{top} and u_{bottom} converging and trending toward u_{bp} , and $-\Delta P_e$ reaching zero. The simultaneous occurrence of all of these factors implies that the loss of membrane behavior was correlated with the cessation in the swelling and subsequent shrinkage of the BPN (see Fig. 5.11e) resulting in larger pores and/or establishment of preferential pathways within the specimen. Additional discussion in this regard is included in Section 5.4.1.

5.3.5 Exit Concentrations

The measured exit concentrations of cations (Ca^{2+} , K^+ , Na^+) emanating from the bottom of the cell (i.e., C_b) are shown in Fig. 5.12. The concentrations of Ca^{2+} increased as the source concentration, C_{ot} , increased (e.g., from 5 mM to 10 mM CaCl_2). The concentrations of Na^+ measured in the circulation outflows from the bottom of the cell are due to diffusion of the excess Na^+ initially present within the BPN as a result of manufacturing (Scalia 2012), and are similar to the trends in Na^+ concentrations described in Chapter 4. The concentrations of Na^+ exiting the bottom of the cell exceeded the concentrations of Ca^{2+} during the first stage of the RW test (i.e., 5 mM CaCl_2) and during the first two stages of the FW test (i.e., 5 mM and 10 mM CaCl_2) (refer to Fig. 5.12c and d). However, during the last stage of both tests, when 10 mM and 20 mM CaCl_2 was being circulated across the top of the specimens for the RW test and the FW test, respectively, the concentrations of Ca^{2+} in the bottom of the cell exceeded the concentrations of Na^+ , due to increased diffusion of Ca^{2+} through the BPN, a continually diminishing amount of remnant Na^+ in the BPN, and the previously discussed potential short-circuiting of Ca^{2+} along the rigid side walls for the RW test. Finally, in contrast to both Na^+ and Ca^{2+} concentrations, concentrations of K^+ generally were low (i.e., near the detection limit) throughout the tests.

The measured exit concentrations of anions (i.e., Cl^- , F^- , and SO_4^{2-}) from the bottom of the cell for both tests are shown in Fig. 5.13. Measured Cl^- concentrations were predominant among the concentration of anions in the circulation outflows and, therefore, were used to calculate diffusion coefficients for Cl^- .

For the RW test, the steady-state concentrations of Cl^- not only increased with each stage of the test as the source concentration (C_{ot}) increased, but also increased during the circulation of

10 mM CaCl₂ as a likely result of the factors described in Section 5.3.3 (i.e., compression of the double layer, increase in active porosity, and/or short-circuiting). For the FW test, the steady-state concentrations of Cl⁻ generally increased with each stage of the test as the source concentrations (C_{ot}) increased (e.g., from 5 mM to 10 mM CaCl₂, and from 10 mM to 20 mM CaCl₂). During the circulation of 10 mM CaCl₂, the concentrations of Cl⁻ in the circulation outflow from the bottom of the specimen in the FW test ranged from 50 to 60 mg/L (1.4 to 1.7 mM Cl⁻) throughout the test duration, whereas those in the RW test ranged from 40 to 50 mg/L (1.1 to 1.4 mM Cl⁻) for the first 50 d and then suddenly increased to as high as 116 mg/L (3.27 mM Cl⁻). This sudden increase in Cl⁻ concentrations for the RW test relative to the FW test again suggests that short-circuiting occurred during the circulation of 10 mM CaCl₂ for the RW test.

5.3.6 Diffusion Results

Plots of Q_t versus time for both tests are shown in Fig. 5.14. The slope of Q_t versus time increased with increasing concentration of CaCl₂. When a greater concentration gradient was imposed across the specimen, a greater diffusive mass flux occurred, resulting in an increase in the slope of Q_t versus time. As described in Chapter 4, in order to evaluate the results for D^* , the multiple stages of the tests were separated and net values of Q_t and t , or Q_t' and t' , respectively, pertaining to each individual stage of the test. Essentially, the use of Q_t' and t' for each stage of the test amounts to resetting Q_t and t to zero for each stage of the test (i.e., during circulation of 5 mM, 10 mM, and 20 mM CaCl₂) in order to evaluate D^* independently for each stage.

Individual plots of Q_t' versus time, t' for each test are shown in Figs. 5.15 and 5.16. The slope, or $\Delta Q_t' / \Delta t'$, varied from 45.8 to 478 mg/m²-d for Cl⁻ and from 2.60 to 361 mg/m²-d for Ca²⁺. The value of $\Delta Q_t' / \Delta t'$ increased as the source concentration, C_{ot} , increased, again

reflecting the greater diffusive solute mass flux with increasing C_{ot} . The lower magnitudes in $\Delta Q_i' / \Delta t'$ for Ca^{2+} reflect attenuation or exchange of the Ca^{2+} and interactions due to the excess Na^+ in the BPN. Finally, the resulting D^* values resulting from linear regression of the steady-state portion of the data are summarized in Table 5.4 and shown in Fig. 5.17a.

The steady-state values of D^* for the Ca^{2+} , or $D_{\text{Ca}^{2+}}^*$ are lower than those for the Cl^- , or $D_{\text{Cl}^-}^*$, with differences between $D_{\text{Cl}^-}^*$ and $D_{\text{Ca}^{2+}}^*$ generally decreasing with increasing source concentration, C_{ot} , of CaCl_2 . For example, for test FW, $D_{\text{Cl}^-}^*$ is 9.8×10^{-12} and $D_{\text{Ca}^{2+}}^*$ is 2.3×10^{-12} during circulation of 5 mM KCl, whereas $D_{\text{Cl}^-}^*$ is 4.3×10^{-11} and the $D_{\text{Ca}^{2+}}^*$ is 1.7×10^{-11} during circulation with 20 mM CaCl_2 . These differences also are illustrated in Fig. 5.17b in terms of the ratio of the effective diffusion coefficient of chloride relative to that of calcium, or $D_{\text{Cl}^-}^* / D_{\text{Ca}^{2+}}^*$. The values of $D_{\text{Cl}^-}^* / D_{\text{Ca}^{2+}}^*$ are highest at a C_{ot} of 5 mM CaCl_2 for the RW test (e.g., 14 for RW), and generally decrease with increasing C_{ot} , such that the values of $D_{\text{Cl}^-}^* / D_{\text{Ca}^{2+}}^*$ approach unity, the theoretical diffusion coefficient ratio of Cl^- to Ca^{2+} at steady state (e.g., for example, $D_{\text{Cl}^-}^* / D_{\text{Ca}^{2+}}^*$ is 2.5 for FW when C_{ot} of 20 mM). However, the $D_{\text{Cl}^-}^* / D_{\text{Ca}^{2+}}^*$ for 10 mM CaCl_2 is slightly higher than the $D_{\text{Cl}^-}^* / D_{\text{Ca}^{2+}}^*$ for 5 mM CaCl_2 for the FW test (6.1 versus 4.3, respectively). These differences between $D_{\text{Cl}^-}^*$ and $D_{\text{Ca}^{2+}}^*$, especially at the lower values of C_{ot} , which appear to violate the electroneutrality requirement, can be attributed to the confounding influence of the significant concentration of remnant Na^+ in the pore liquid of the BPN specimens (as was discussed in Chapter 4). In contrast, the $D_{\text{Cl}^-}^* / D_{\text{Ca}^{2+}}^*$ of 0.75 for the RW test with 10 mM CaCl_2

is slightly less than unity. However, the D^* values for this test are suspect because of the aforementioned likelihood of short-circuiting during this stage of the test.

The values of D^* are plotted versus those of ω in Fig. 5.18. The values of D^* for both the RW test and the FW test and for both Ca^{2+} and Cl^- (i.e., $D_{\text{Ca}^{2+}}^*$ and $D_{\text{Cl}^-}^*$, respectively) decrease with increasing ω such that D^* trends toward zero as ω approaches unity. This result is consistent with the expected behavior of a semipermeable membrane as a perfect membrane (i.e., $\omega = 1$) restricts all solute transport.

5.4 DISCUSSION

5.4.1 Destruction of Membrane Behavior

The time to reach steady-state diffusion for chloride, t_{ss,Cl^-} , and for calcium, $t_{ss,\text{Ca}^{2+}}$, were determined based on the time to reach a linear ΔQ versus Δt as described in Shackelford and Lee (2003). The time to reach steady state for the FW test can be correlated with the time at which the ΔP and, thus, the ω approached zero. In addition, the time at which the volume change stabilized occurred at nearly the same time as the destruction of membrane behavior (refer to Fig. 5.19a). The volume changes in the FW specimen can be attributed to the interaction of the BPN with CaCl_2 , likely the exchange of Na^+ for Ca^{2+} . Test results indicated that the volume change stabilized when the diffusion of Ca^{2+} reached steady state, indicating that cation exchange was complete, and the membrane behavior approached zero. This observation is consistent with that reported by Shackelford and Lee (2003), who found that the time to reach steady-state diffusion of Ca^{2+} through a specimen of a GCL contained in a rigid-wall cell was identical to the time at which the membrane behavior of the GCL was destroyed (i.e., ω reached zero).

In contrast, the time required to reach steady-state diffusion for the test performed in the rigid-wall cell did not correlate as well with the time at which the membrane behavior was destroyed (refer to Fig. 5.19b). In fact, for this test, steady-state diffusion occurred after $-\Delta P$ reached zero ($t'_{ss,Cl^-} = 82$ d, $t'_{ss,Ca^{2+}} = 94$ d, $t_{\Delta P \rightarrow 0} = 76$ d), indicating that the ability of the BPN specimen in this test to restrict solute migration was destroyed prior to the principal salt ions (Cl^- and Ca^{2+}) having achieved steady-state diffusion. This lack of correlation between steady-state diffusion and membrane destruction represents additional evidence that short-circuiting lead to the loss of semipermeable membrane behavior in the rigid-wall test.

5.4.2 Comparison of Membrane Efficiencies

The measured values of ω from this study are compared in Fig. 5.20 with those previously reported for tests conducted using a GCL from Shackelford and Lee (2003), and tests conducted using untreated bentonite, Hyper clay, multi-swellable bentonite (MSB), and dense-prehydrated GCL (DPH-GCL) from Di Emidio (2010). Previous studies have shown destruction of membrane behavior when GCLs are exposed to $CaCl_2$ (e.g., Shackelford and Lee 2003). In contrast to these previous studies, the membrane behavior of the BPN was not destroyed during the circulation of lower, 5 and 10 mM (FW test only), concentrations of $CaCl_2$. For example, for the RW and FW tests performed using the BPN and the 5 mM $CaCl_2$ solution, the resulting values for ω of 0.95 and 0.30, respectfully, are higher than those previously reported for the GCL ($\omega = 0$), Hyper clay ($\omega = 0.13$), and untreated bentonite ($\omega = 0$) based on the results of rigid-wall tests using a 5 mM $CaCl_2$ solution. Di Emidio (2010) also reported results of tests conducted in rigid-wall cells using 1 mM $CaCl_2$ and specimens of Hyper clay, untreated sodium bentonite, DPH-GCL and MSB. The resulting values of ω from these tests were greater than zero for all of

the materials except the MSB, which did not exhibit membrane behavior (refer to Table 5.6 and Fig. 5.20). Although the tests involving specimens of BPN in this study were not conducted with 1 mM CaCl₂, based on the typical trends of increasing ω with decreasing C_{ot} , the expected values of ω for the BPN specimens would be similar to or greater than the ω values reported by Di Emidio (2010) for Hyper clay, untreated bentonite, and DPH-GCL. No previous studies have been conducted with 10 mM and 20 mM CaCl₂ solutions.

5.4.3 Comparison of Diffusion Coefficients

The effective diffusion coefficients from this study also are compared with those previously reported by Shackelford and Lee (2003) and Di Emidio (2010) in Fig. 5.21 and summarized in Table 5.6. The values of $D_{Cl^-}^*$ and $D_{Ca^{2+}}^*$ for the BPN at a C_{ot} of 5 mM CaCl₂ are lower than those for a GCL, untreated bentonite, MSB, and Hyper clay. The values of $D_{Cl^-}^*$ and $D_{Ca^{2+}}^*$ for each of the materials varied in the order: untreated bentonite > MSB > Hyper clay > GCL > BPN-RW > BPN-FW. The lower D^* for the BPN-RW and BPN-FW compared to the other materials correlates with the higher ω for the BPN. However, the trend between lower D^* and higher ω is not consistent between the two BPN tests (i.e., RW test and FW test) at the C_{ot} of 5 mM CaCl₂. At this source concentration, the value of $D_{Cl^-}^*$ based on the RW test was higher than that for the FW test (3.3×10^{-11} vs. 9.8×10^{-12} m²/s, respectively), whereas the value of ω based on the RW test was higher than that based on the FW test (0.95 vs. 0.39, respectively). The reason for this inconsistency is not readily apparent, but may be related, in part, to the different conditions in the flexible-wall cell versus the rigid-wall cell, specifically, the fact that

significant volume change (compression) of the specimen occurred in the FW test but not in the RW test, leading to differences in the fabric of the two specimens.

5.5 CONCLUSIONS

Multi-stage chemico-osmotic/diffusion tests were conducted on a polyacrylic polymerized bentonite known as a bentonite polymer nanocomposite, or BPN, with varying concentrations of CaCl_2 . The membrane efficiency coefficient, ω , and the effective diffusion coefficient, D^* , were determined for the BPN and compared with results from literature for untreated bentonite and treated bentonites. The results of index properties of the BPN, including the swell index and solution retention capacity, performed using CaCl_2 solutions implied that the BPN would be more resistant to chemical attack than untreated or traditional bentonite when exposed to dilute solutions of CaCl_2 .

In contrast to previously reported results from membrane tests performed on specimens of traditional (unmodified) bentonite, the membrane behavior of specimens of the BPN contained in both rigid-wall (RW) and flexible-wall (FW) cells was sustained at CaCl_2 concentrations exceeding 5 mM. For example, the values of ω for the BPN specimens subjected to 5 mM CaCl_2 and contained in RW and FW cells were 0.95 and 0.30, respectfully. In addition, these values of ω were greater than that the value for ω of 0.13 previously reported for a anionic polymer modified clay known as Hyper clay that was tested in a rigid-wall cell and subjected to 5 mM CaCl_2 . Thus, the BPN evaluated in this study exhibited greater resistance to chemical degradation relative to both traditional (unmodified) and a polymer modified bentonite tested under the same or similar conditions.

The generated chemico-osmotic pressure difference, $-\Delta P (> 0)$, of the BPN in the RW test trended to zero when the specimen was exposed to 10 mM CaCl_2 . This apparent destruction of the membrane behavior was attributed to the possibility of several factors *viz.*, (1) shrinkage and collapse of the BPN as a result of increased concentrations of Ca^{2+} in the pore water, (2) over-cross-linking of the polymer within the pores of the BPN as a result of Ca^{2+} in the pore water resulting in an increase in the diffusively active porosity, and/or (3) short-circuiting of CaCl_2 along the rigid side-wall of the RW cell. At least two lines of evidence indicated that factor (3) was the dominant mechanism resulting in a destruction of membrane behavior, including rhodamine dye staining the short-circuiting pathway along the outer surface of the specimen and the fact that the membrane behavior was not destroyed in the FW test during circulation of 10 mM CaCl_2 . Short-circuiting in the FW cell is not expected, since separation of the specimen from the flexible side-walls is unlikely. However, exposure of the BPN specimen contained in the FW cell to a higher concentration (20 mM) of CaCl_2 also resulted in complete destruction of membrane behavior, which was attributed to an increase in pore sizes resulting from diffusion of Ca^{2+} into the pores of the BPN. Also, for the test conducted in the FW cell, the time at which the membrane behavior approached zero correlated with the time required for steady-state diffusion of Ca^{2+} , which is consistent with the findings of a previous study based on membrane testing of a traditional bentonite contained within a RW cell. Thus, although the BPN evaluated in this study exhibited greater resistance to chemical degradation than had previously been reported, this increased resistance was not unbounded with increasing CaCl_2 concentration.

Values of the effective diffusion coefficient, D^* , measured in this study for the BPN were compared with those previously reported in literature for a GCL, an untreated bentonite, Hyper clay, and multiswellable bentonite (MSB). At a source concentration of 5 mM CaCl_2 , the values

of $D_{Cl^-}^*$ and $D_{Ca^{2+}}^*$ for the BPN were the lowest among the various bentonites, with the values of $D_{Cl^-}^*$ and $D_{Ca^{2+}}^*$ varying in the order: untreated bentonite > MSB > Hyper clay > GCL > BPN-RW > BPN-FW. The lower D^* values for the the BPN specimens are consistent with with the higher ω for the BPN specimens relative to those for the other bentonites, and the lower D^* values for the BPN-FW specimen relative to the BPN-RW specimen are consistent with the higher ω of the BPN-FW specimen relative to the BPN-RW specimen.

Table 5.1. Chemical properties of liquids used in study.

Liquid	Concentration		<i>pH</i>	Electrical Conductivity, <i>EC</i> (mS/m), @ 25°C
	(mM)	(mg/L)		
De-ionized Water (DIW)	0	0	7.35	0.06
CaCl ₂ Solutions	5	555	5.33	104.5
	10	1110	6.66	182.4
	20	2220	6.33	317
	50	5550	5.54	830
	500	55500	5.35	6430

Table 5.2. Results of swell index tests for lower quality bentonite (LQB), higher quality bentonite (HQB), and BPN.

CaCl ₂ Concentration (mM)	Swell Index, <i>SI</i> (mL/2g)		
	LQB ⁽¹⁾	HQB ⁽¹⁾	BPN
0 (DIW)	27.4	30.0	67
5	26.9	29.8	50
10	19.0	20.9	-
20	14.2	15.2	-
50	10.5	10.8	13
100	8.7	8.5	-
500	7.6	7.5	7

⁽¹⁾ From Lee and Shackelford (2005c).

Table 5.3. Results of solution retention capacity tests for lower quality bentonite (LQB), higher quality bentonite (HQB), and BPN.

CaCl ₂ Concentration (mM)	Solution Retention Capacity, <i>SRC</i> (mL/g)		
	LQB ⁽¹⁾	HQB ⁽¹⁾	BPN ⁽²⁾
0 (DIW)	5.7	7.2	11.0
5	2.9	4.2	9.0
10	2.5	2.7	-
20	2.4	2.3	-
50	2.0	2.0	4.3
100	1.8	1.7	-
500	1.8	1.7	1.4

⁽¹⁾ From Lee and Shackelford (2005c) with centrifuge speed at 5000 rpm.

⁽²⁾ Based on procedure from Lee and Shackelford (2005c) with centrifuge speed at 3000 rpm.

Table 5.4. Membrane/diffusion test results for BPN.

Type of Cell	Source CaCl ₂ Concentration, C _{ot} (mM)	Maximum Effective Chemico-Osmotic Pressure Difference, -ΔP _{e,max} (kPa)	Maximum Membrane Efficiency Coefficient, ω _{max}	Steady-State Effective Chemico-Osmotic Pressure Difference, -ΔP _{e,ss} (kPa)	Steady-State Membrane Efficiency Coefficient, ω _{ss}	Stage Duration (days)	Effective Diffusion Coefficient, D* (m ² /s)	
							Cl ⁻	Ca ²⁺
Rigid-wall	5	37.0	1.0	34.5	0.95	80	3.3 x 10 ⁻¹¹	2.3 x 10 ⁻¹²
	10	47.9	0.66	~0	0	186	9.4 x 10 ⁻¹¹⁽¹⁾	1.3 x 10 ⁻¹⁰⁽¹⁾
Flexible-wall	5	14.8	0.41	14.4	0.39	104	9.8 x 10 ⁻¹²	2.3 x 10 ⁻¹²
	10	20.4	0.28	8.3	0.11	102	2.1 x 10 ⁻¹¹	3.5 x 10 ⁻¹²
	20	9.75	0.07	~0	0	100	4.3 x 10 ⁻¹¹	1.7 x 10 ⁻¹¹

⁽¹⁾Values for the rigid-wall test conducted using 10 mM CaCl₂ are suspect because of the potential for short-circuiting in the test.

Table 5.5. Bulk porosities of test specimen during membrane testing in a flexible-wall cell.

Stage of Test	Porosity, n [$\sigma' = 103 \text{ kPa (15 psi)}$]
After Consolidation	0.94
After DIW Circulation	0.94
After 5 mM CaCl_2 Circulation	0.94
After 10 mM CaCl_2 Circulation	0.90
After 20 mM CaCl_2 Circulation	0.78

Table 5.6. Membrane/diffusion test results from literature for untreated and treated bentonites.

Type of Material or Barrier	Source CaCl ₂ Concentration, C _{ot} (mM)	Maximum Effective Chemico-Osmotic Pressure Difference, -ΔP _{e,max} (kPa)	Maximum Membrane Efficiency Coefficient, ω _{max}	Steady-State Effective Chemico-Osmotic Pressure Difference, -ΔP _{e,ss} (kPa)	Steady-State Membrane Efficiency Coefficient, ω _{ss}	Stage Duration (days)	Effective Diffusion Coefficient, D* (m ² /s)	
							Cl ⁻	Ca ²⁺
GCL ⁽¹⁾	5	19.3	0.52	0	0	75	1.2 x 10 ⁻¹⁰	1.1 x 10 ⁻¹⁰
Untreated bentonite ⁽²⁾	1	4.1	0.56	2.1	0.29	60	4.0 x 10 ⁻¹¹	4.1 x 10 ⁻¹¹
	5	4.4	0.12	0	0	~20	2.2 x 10 ⁻¹⁰	2.2 x 10 ⁻¹⁰
MSB ⁽²⁾	5	6.1	0.17	0	0	~40	1.8 x 10 ⁻¹⁰	1.6 x 10 ⁻¹⁰
Hyper clay ⁽²⁾	1	4.7	0.65	4.7	0.65	~40	4.4 x 10 ⁻¹¹	3.9 x 10 ⁻¹¹
	5	4.8	0.13	4.8	0.13	~80	1.7 x 10 ⁻¹⁰	1.4 x 10 ⁻¹⁰
Dense Prehydrated GCL ⁽²⁾	1	6.6	0.91	2.0	0.27	40	--	--

⁽¹⁾ From Lee and Shackelford (2005c).

⁽²⁾ From Di Emidio (2010).

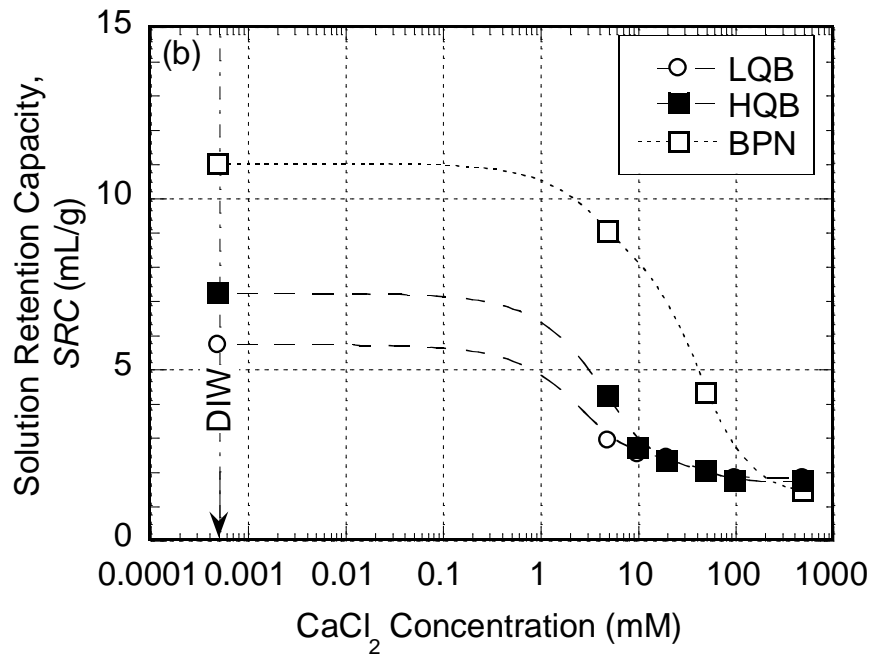
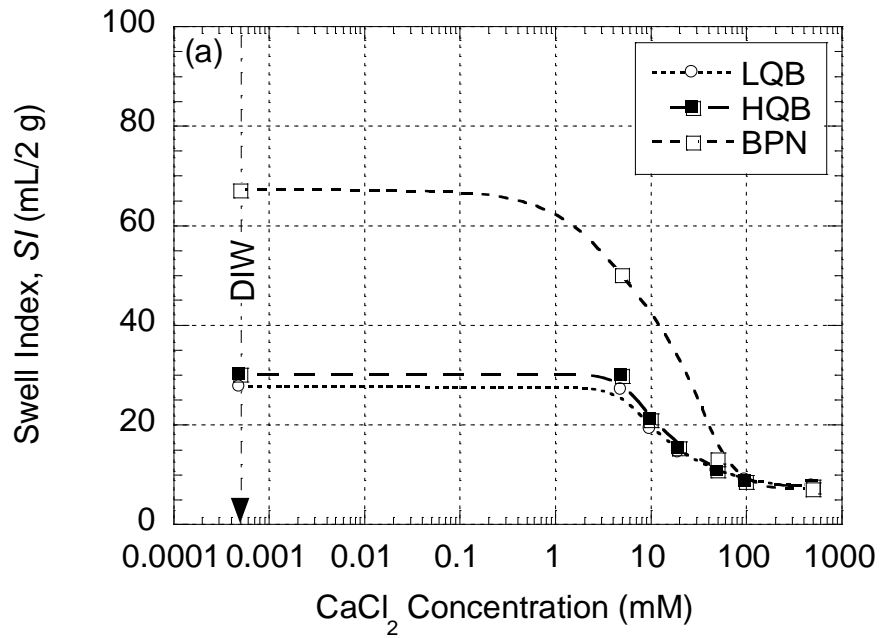


Figure 5.1. Index test results for lower quality bentonite (LQB), higher quality bentonite (HQB) from Lee and Shackelford (2005c) and BPN versus CaCl₂ concentration of solution: (a) swell index; (b) solution retention capacity.

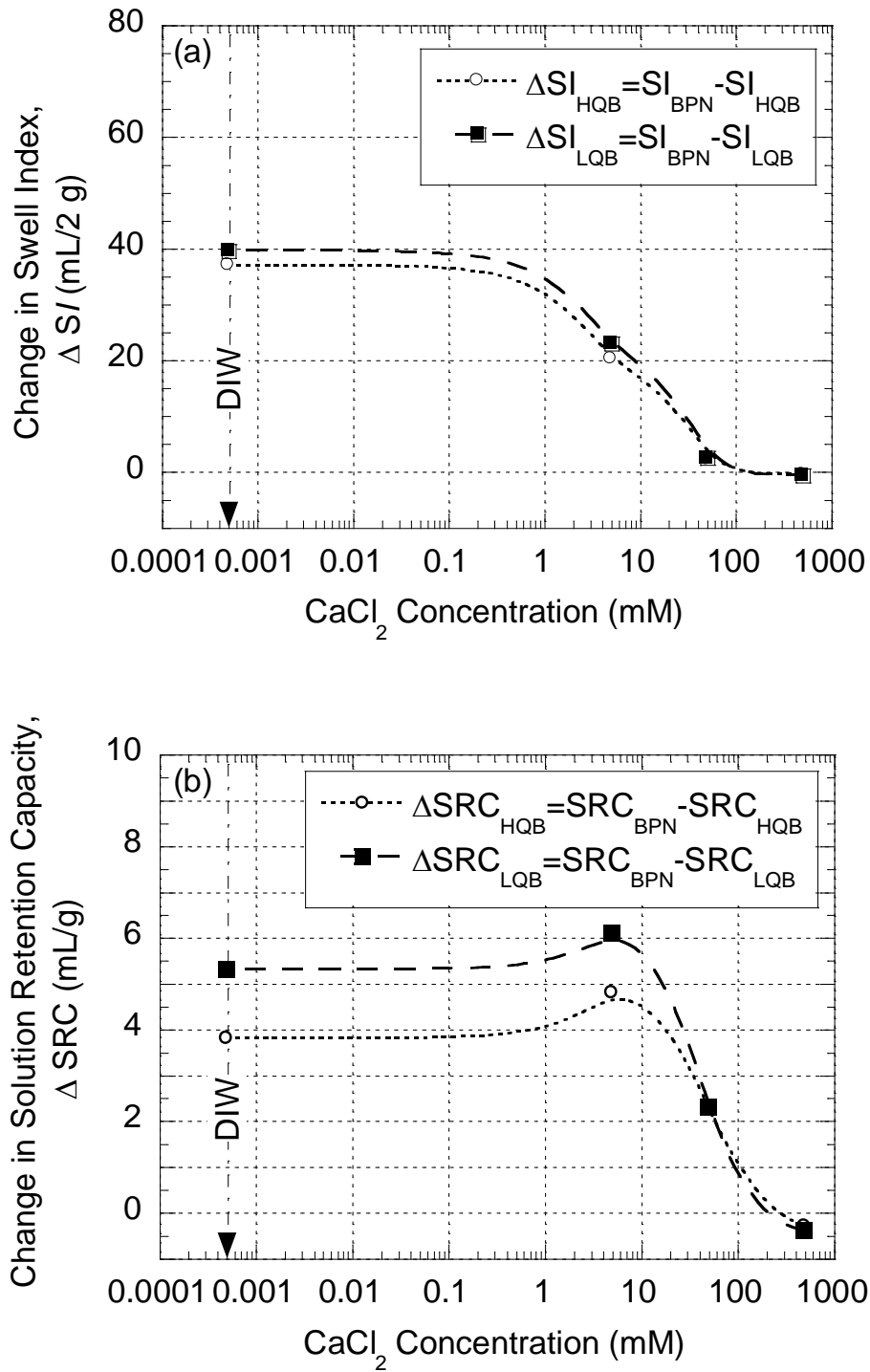


Figure 5.2. Change in (a) swell index, SI , and (b) solution retention capacity, SRC , for higher quality bentonites (HQB) and lower quality bentonites (LQB) (from Lee and Shackelford 2003b) relative to the SRC of the BPN (PN) versus CaCl_2 concentration of solution.

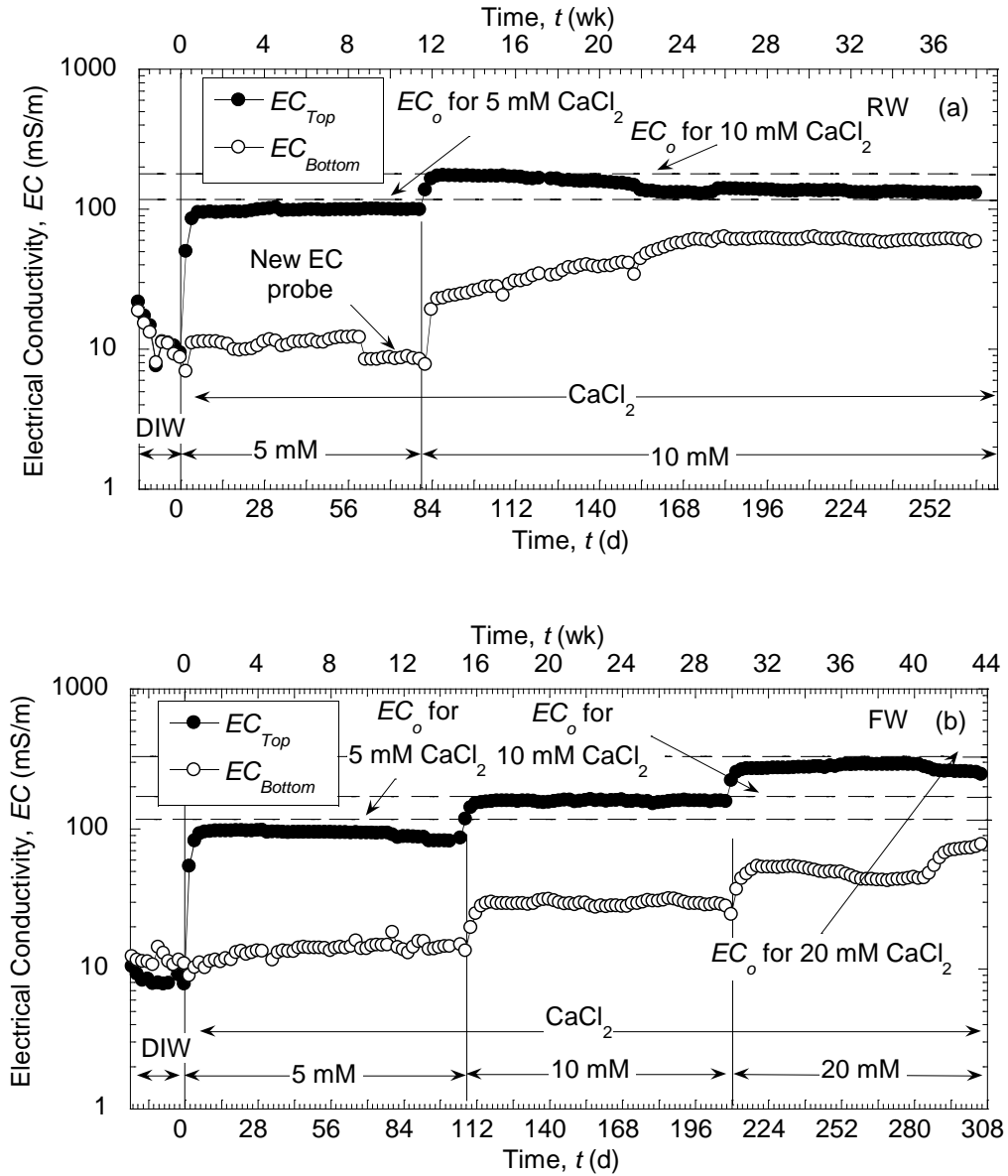


Figure 5.3. Measured electrical conductivity across top and bottom boundaries during membrane testing of BPN specimens in rigid-wall cell (a) RW @ $n = 0.87$ and a flexible-wall cell (b) FW @ $\sigma' = 103$ kPa (15 psi).

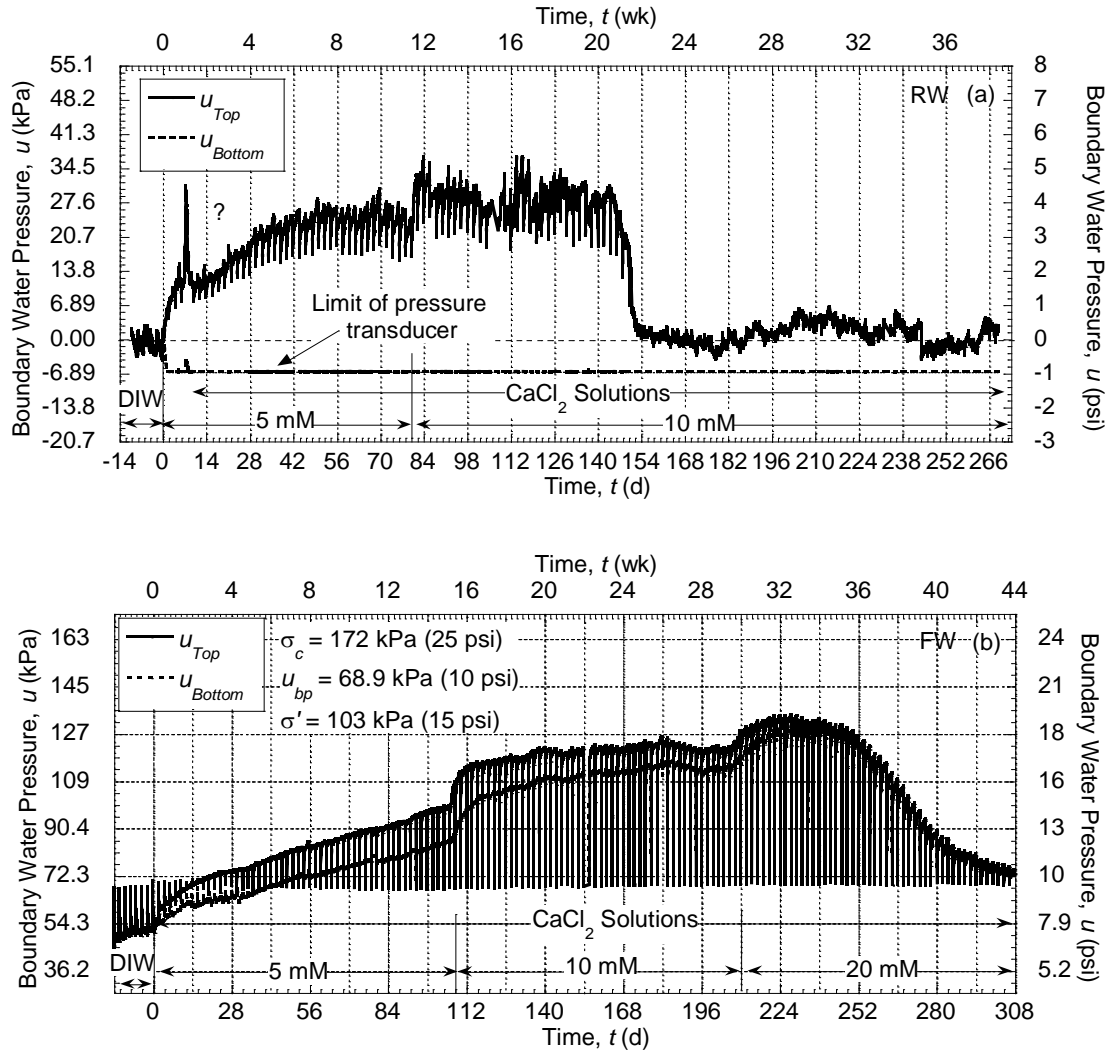


Figure 5.4. Boundary water pressures for BPN specimens during membrane testing in a rigid-wall cell (a) RW @ $n = 0.87$ and a flexible-wall cell (b) FW @ $\sigma' = 103$ kPa (15 psi).

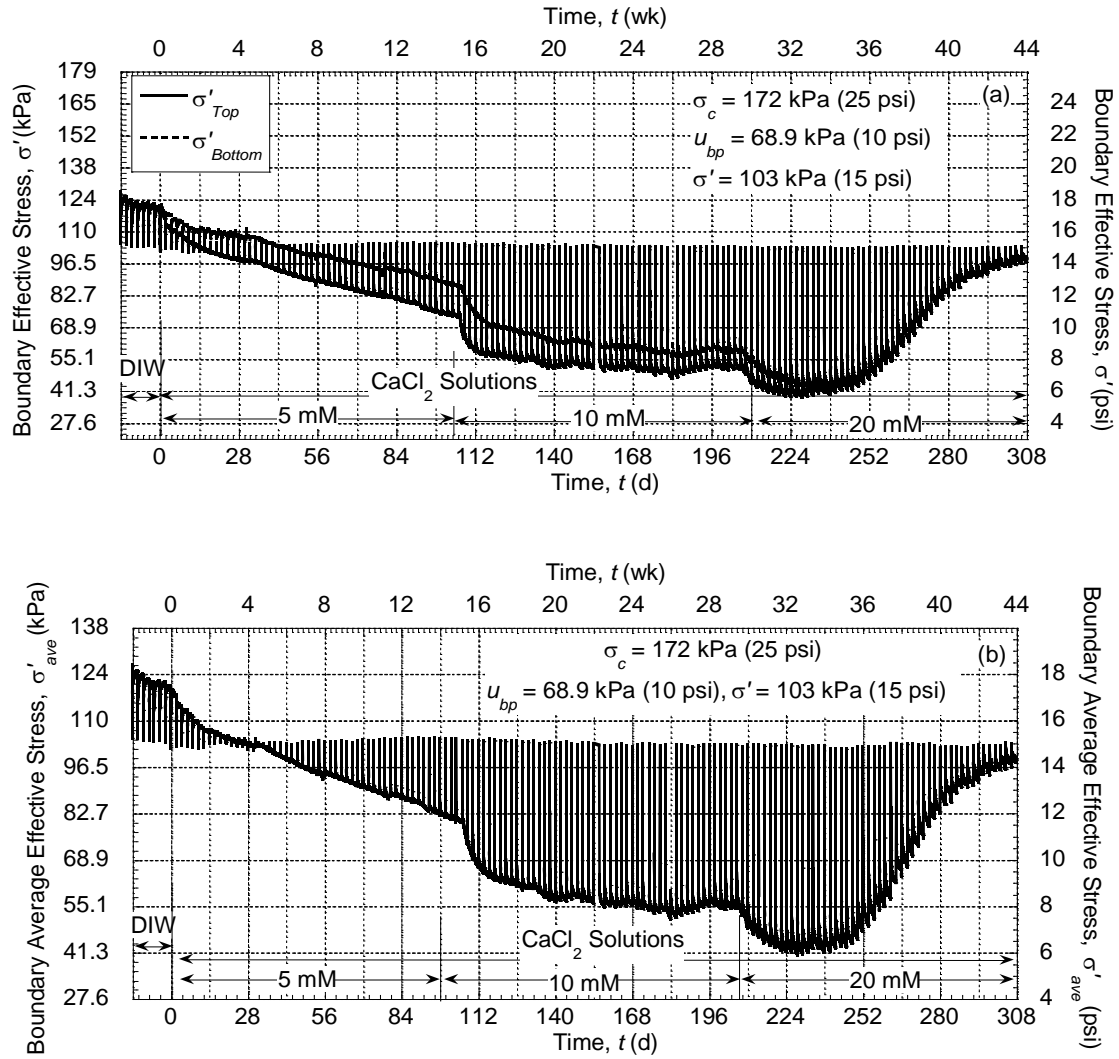


Figure 5.5. Boundary effective stresses in BPN during membrane testing in flexible-wall cell (a) boundary effective stress at the top and bottom of the specimen, σ'_{Top} and σ'_{Bottom} , respectively; (b) average boundary effective stress, σ'_{ave} .

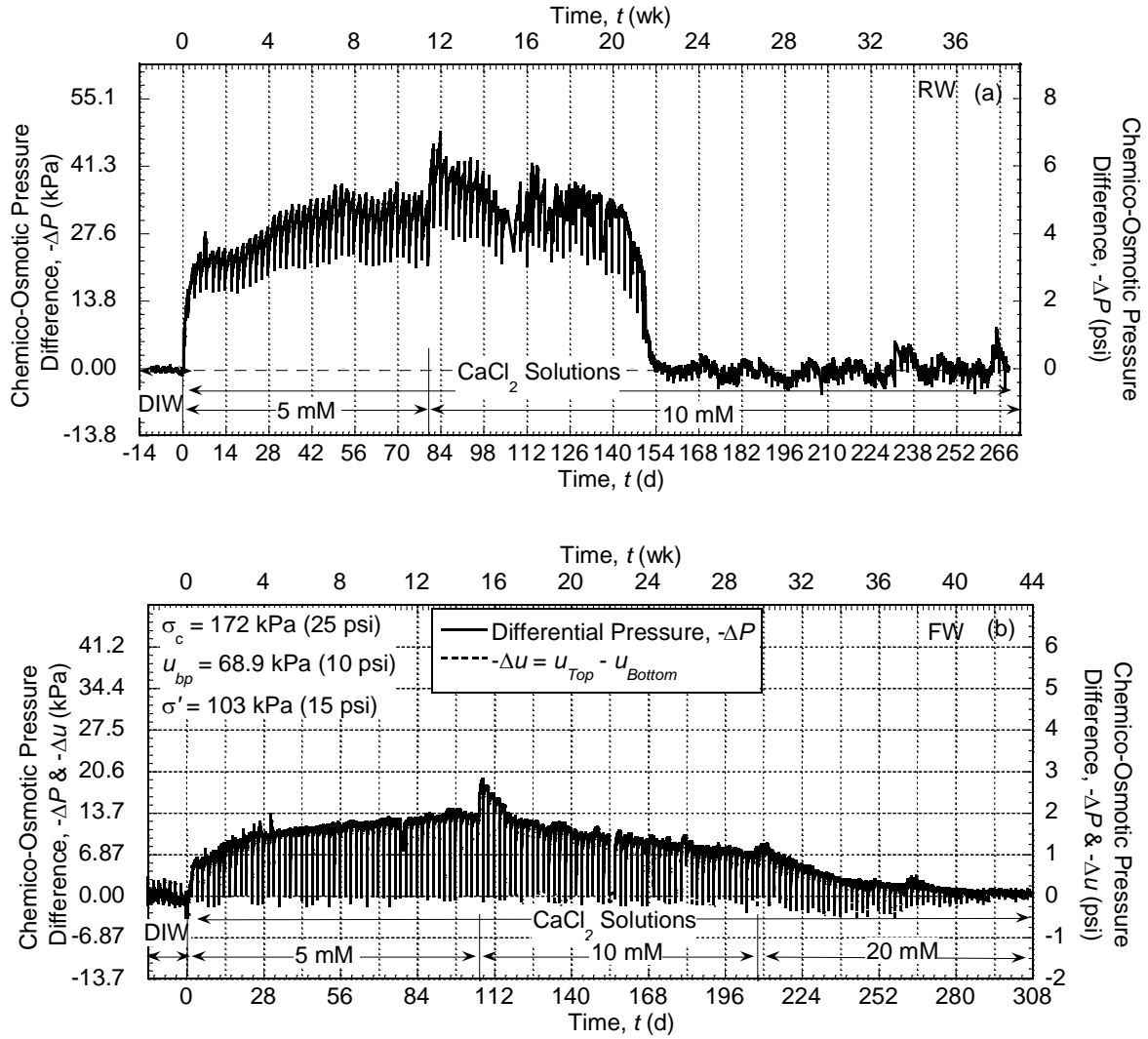


Figure 5.6. Measured chemico-osmotic pressure differences across BPN specimens during membrane testing in a rigid-wall cell (a) RW @ $n = 0.87$ and a flexible-wall cell (b) FW @ $\sigma' = 103 \text{ kPa (15 psi)}$.

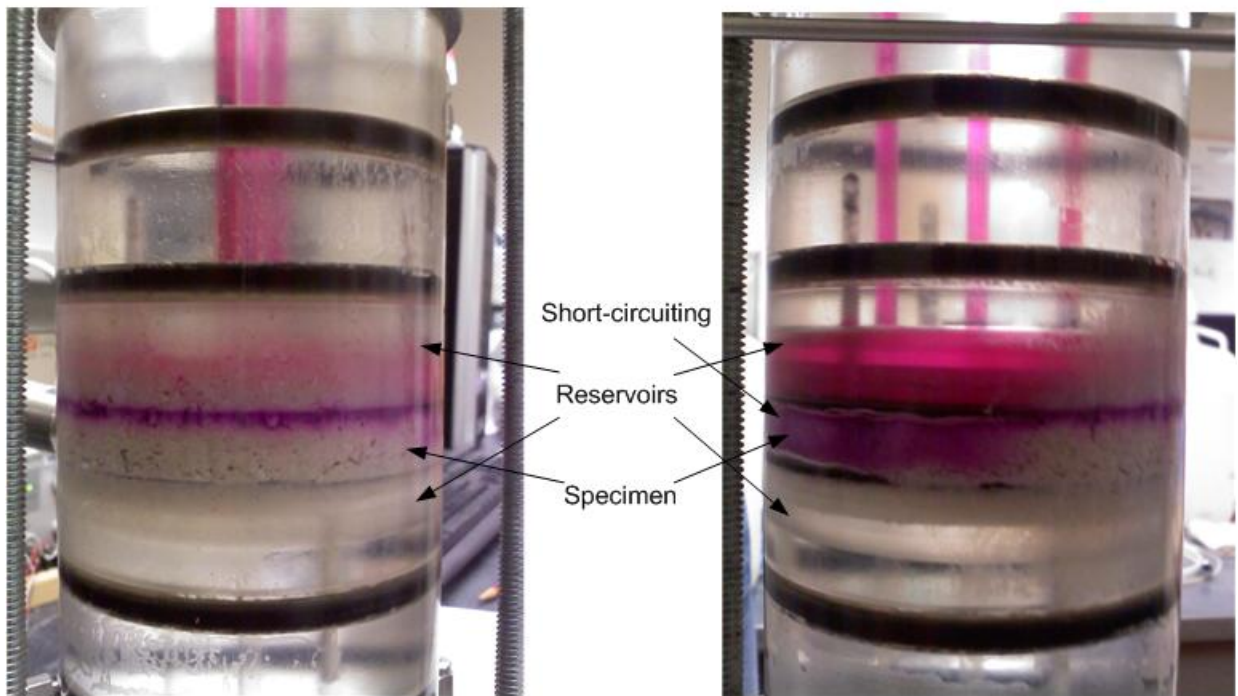
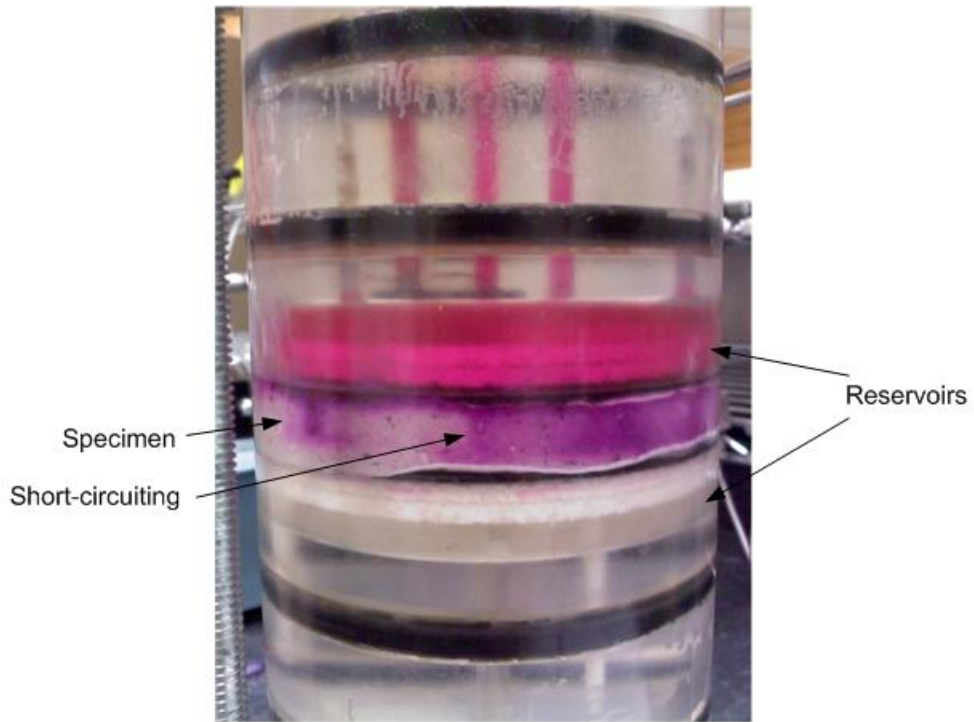


Figure 5.7. Photographs of potential short-circuiting of 10 mM CaCl_2 during membrane testing of BPN in rigid-wall cell, RW @ $n = 0.87$. Rhodamine dye (pink color) was added to top reservoir to indicate migration pathways.

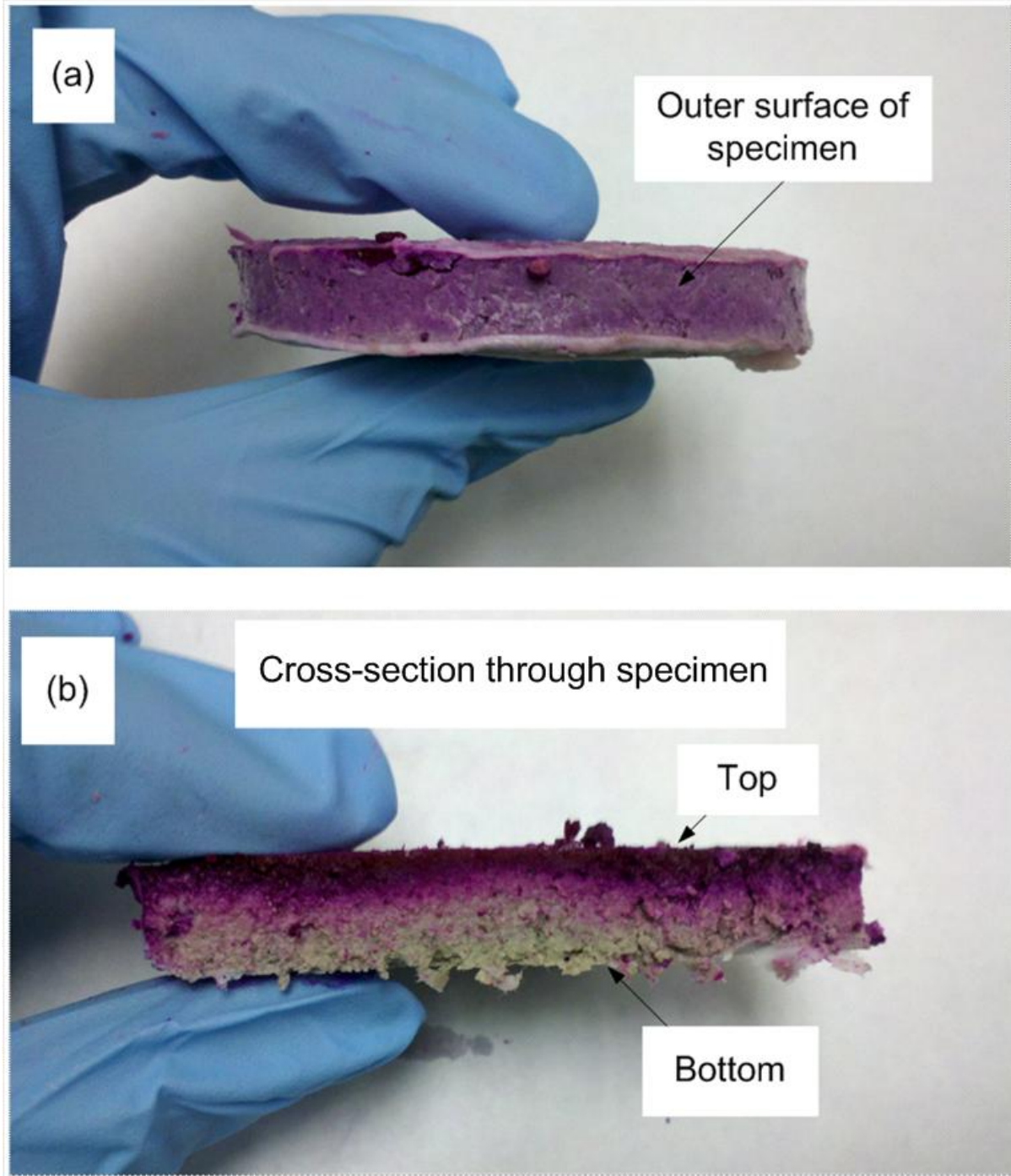


Figure 5.8. Photographs of BPN specimen after circulation of 10 mM CaCl_2 with rhodamine dye during membrane testing of BPN in rigid-wall cell, RW @ $n = 0.87$. (a) Showing stained outer surface of the BPN specimen and (b) showing the cross-section through the specimen where only the upper surface is stained.

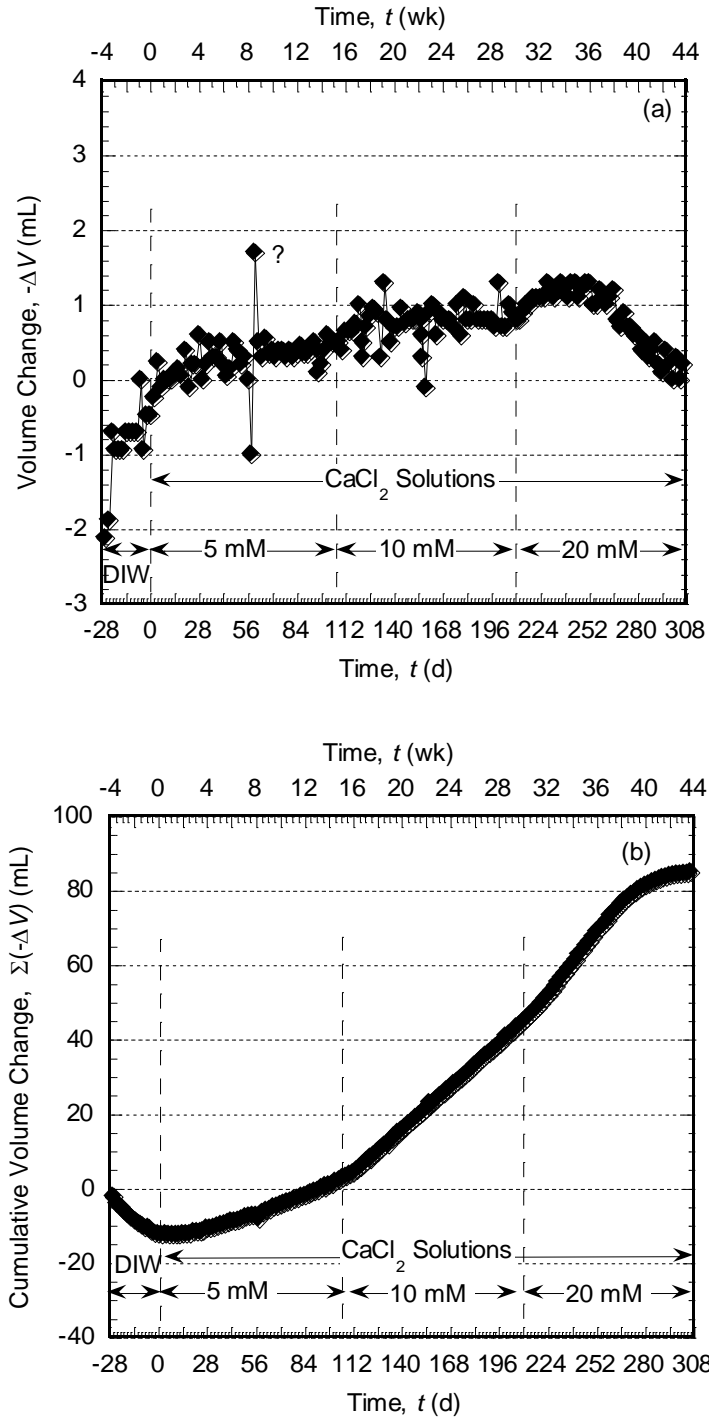


Figure 5.9. Volume change versus time (a) and cumulative volume change versus time (b) during membrane testing on BPN in a flexible-wall cell @ $\sigma' = 103$ kPa (15 psi).

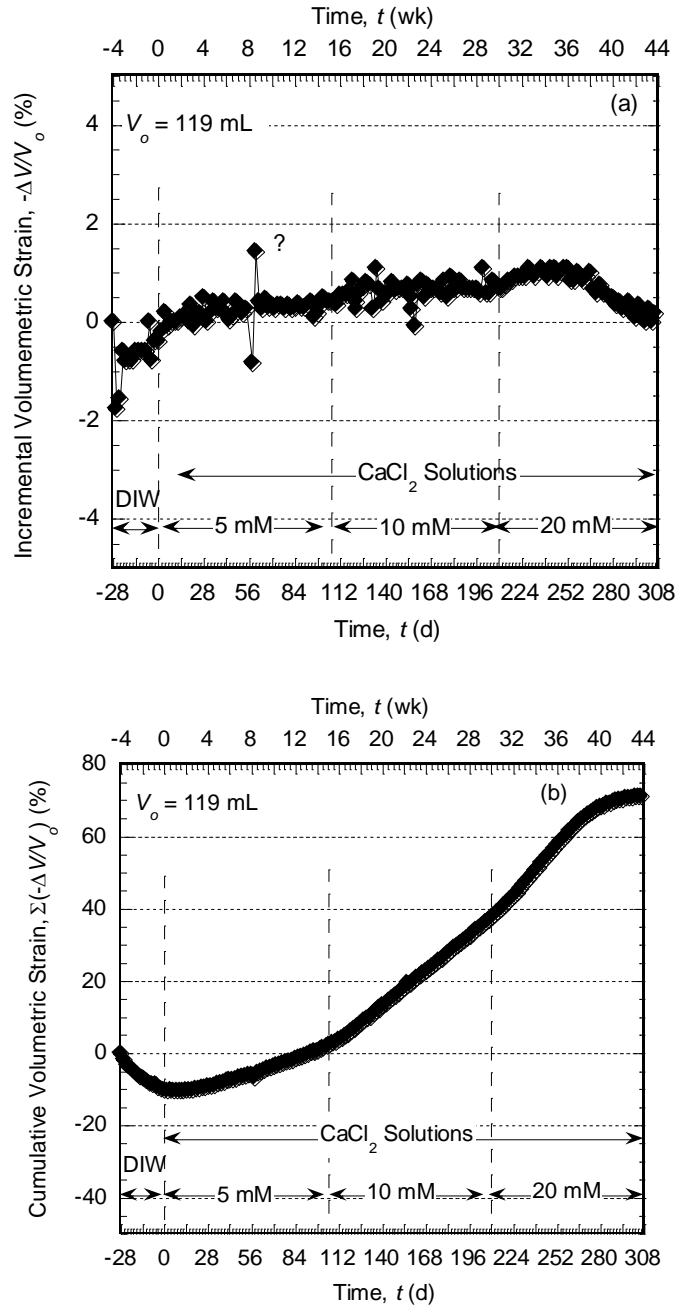


Figure 5.10. Volumetric strain versus time (a) and cumulative volumetric strain versus time (b) during membrane testing on BPN in a flexible-wall cell @ $\sigma' = 103$ kPa (15 psi).



Figure 5.11. Photographs depicting BPN specimen volume change during membrane testing in a flexible-wall cell: (a) before circulation of DIW; (b) after circulation of DIW but before circulation of 5 mM CaCl_2 ; (c) during circulation of 10 mM CaCl_2 ; (d) after circulation of 20 mM CaCl_2 ; (e) after termination of test.

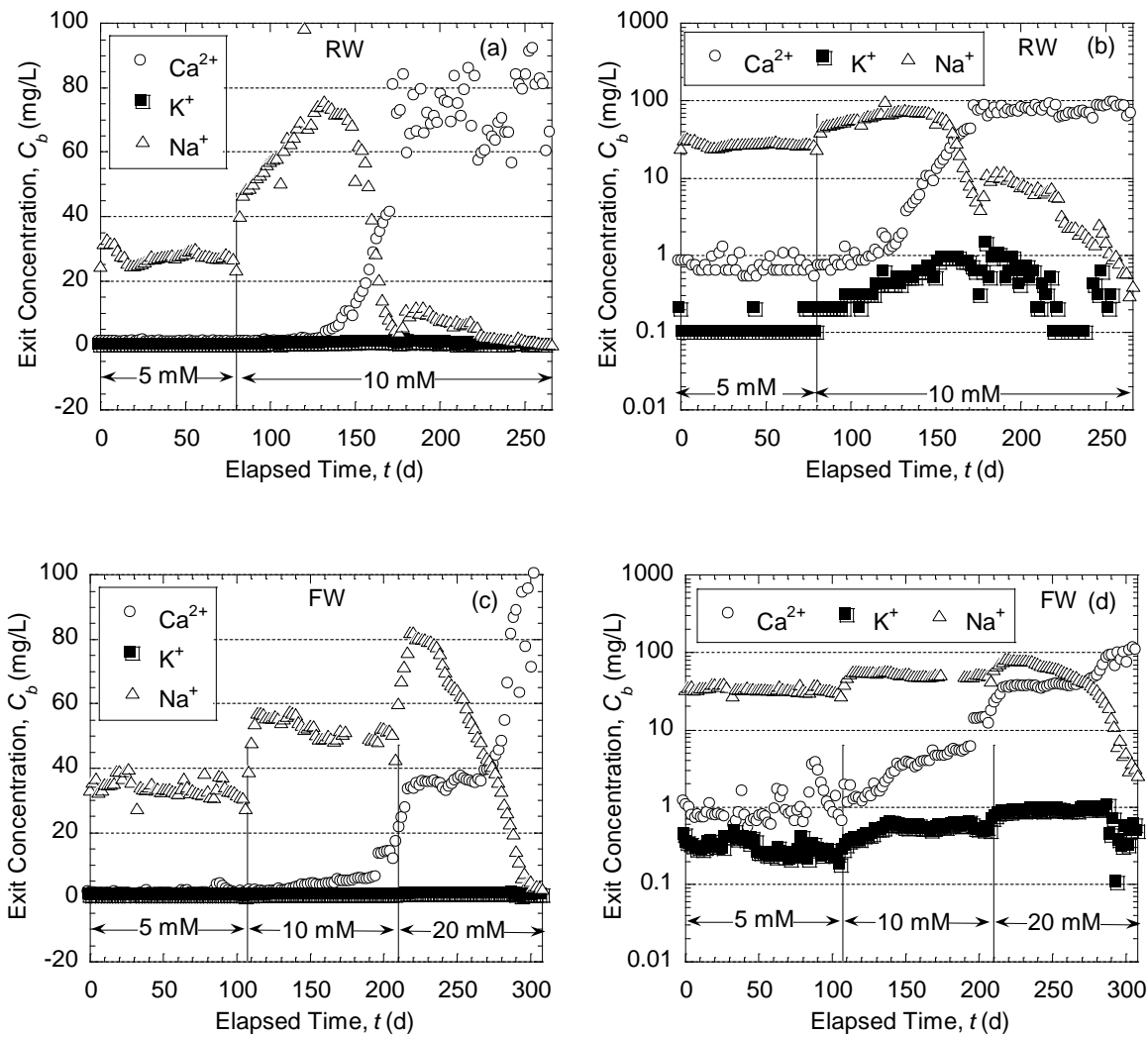


Figure 5.12. Measured exit concentrations of cations as a function of time at the bottom of the cell during membrane testing with CaCl_2 ; (a & b) RW @ $n = 0.87$ and (c & d) FW @ $\sigma' = 103$ kPa (15 psi).

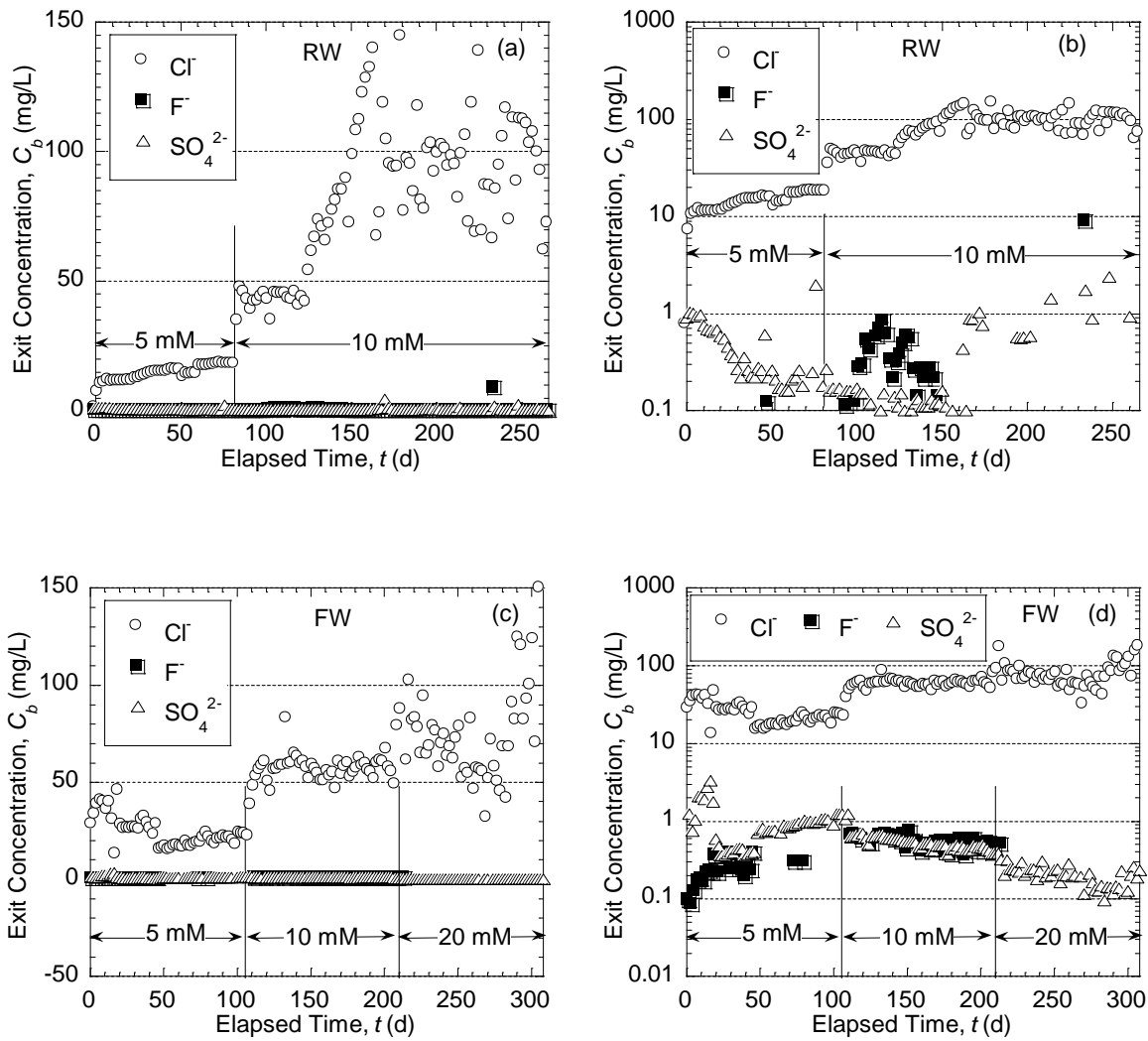


Figure 5.13. Measured exit concentrations of anions as a function of time at the bottom of the cell during membrane testing with CaCl₂; (a & b) RW @ $n = 0.87$ and (c & d) FW @ $\sigma' = 103$ kPa (15 psi).

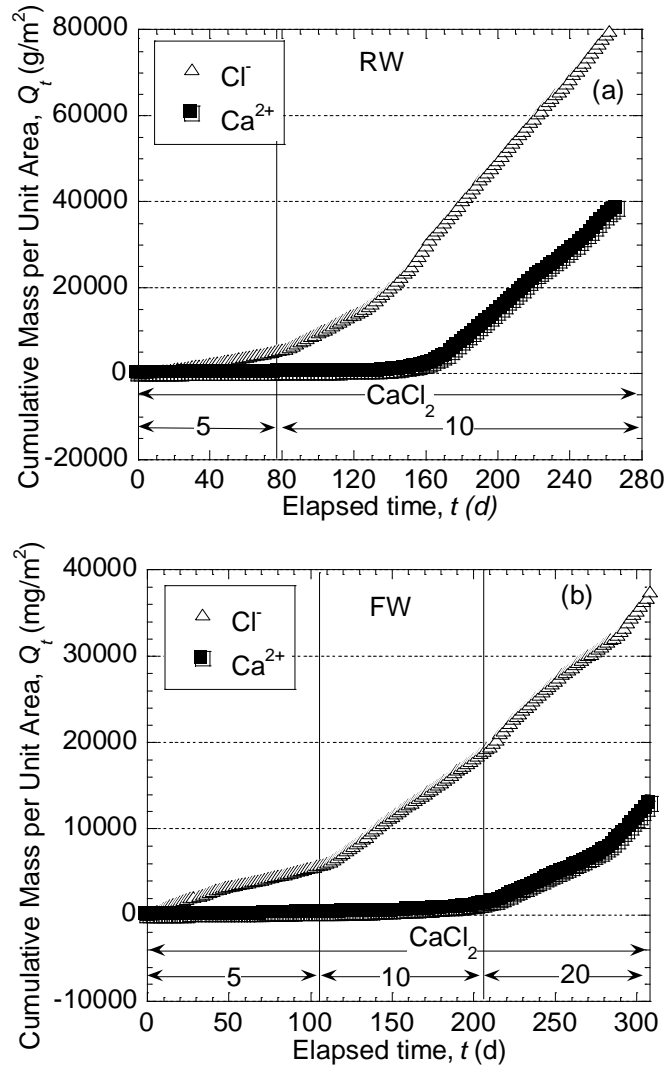


Figure 5.14. BPN diffusion test results with chloride and calcium in terms of cumulative mass per unit area, Q_t , versus elapsed time, t for (a) RW @ $n = 0.87$ and (b) FW @ $\sigma' = 103$ kPa (15 psi).

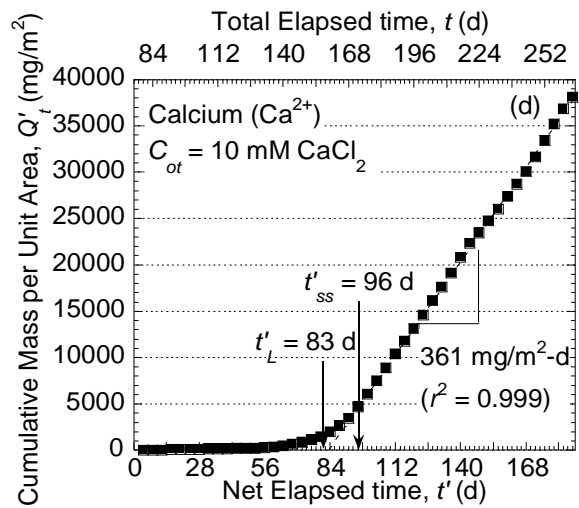
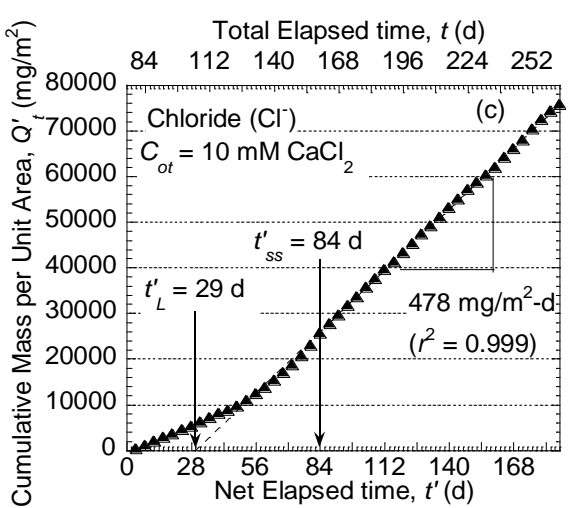
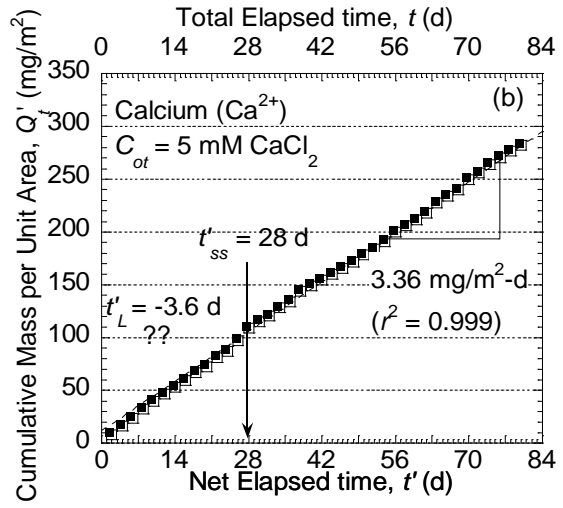
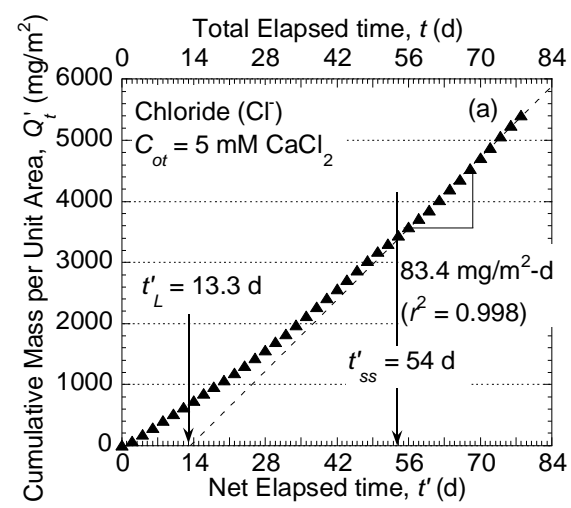


Figure 5.15. Diffusion results for chloride (a, c) or calcium (b, d) for test conducted in the rigid-wall cell.

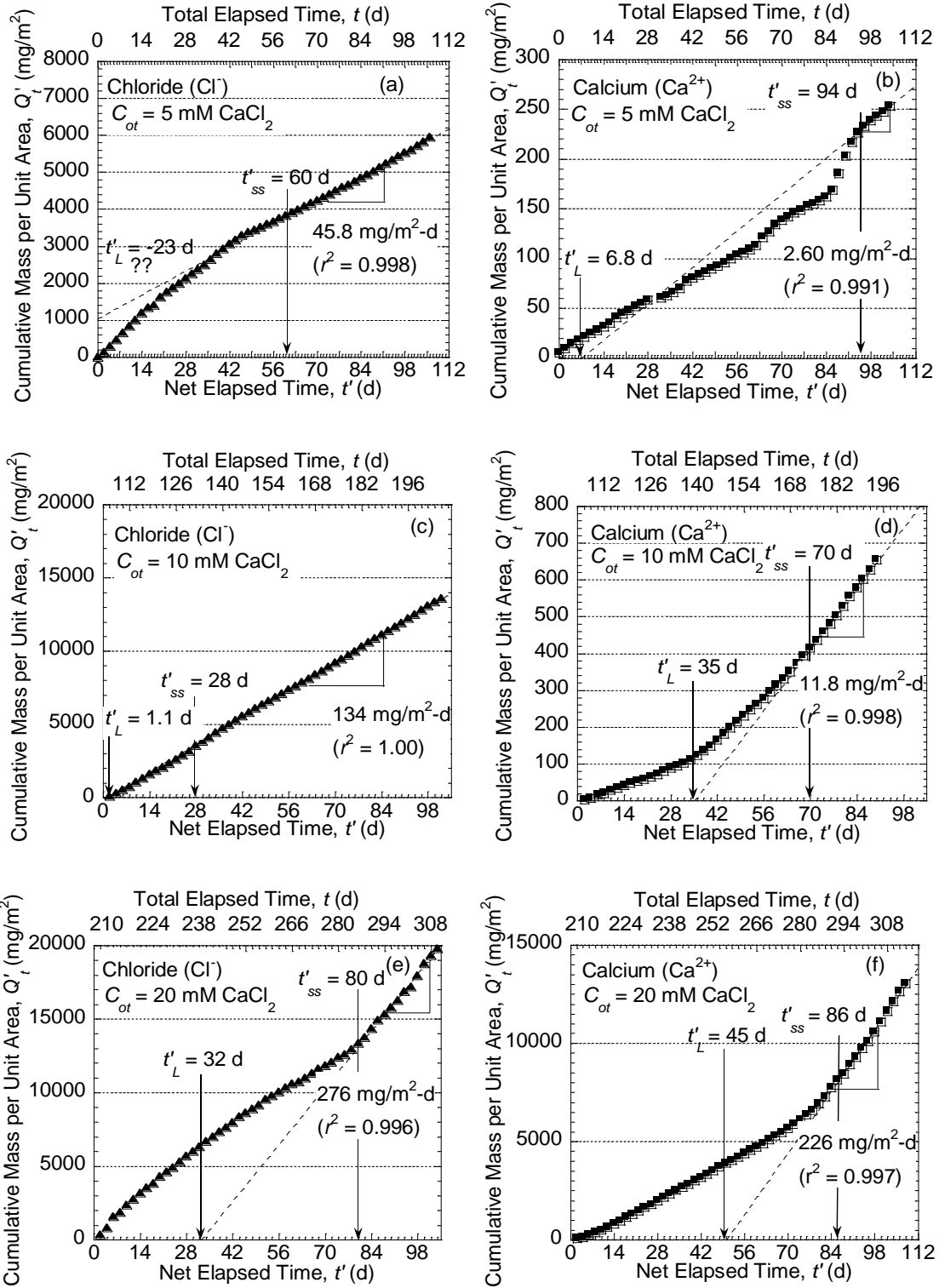


Figure 5.16. Diffusion results for chloride (a, c, e) or calcium (b, d, f) for test conducted in the flexible-wall cell.

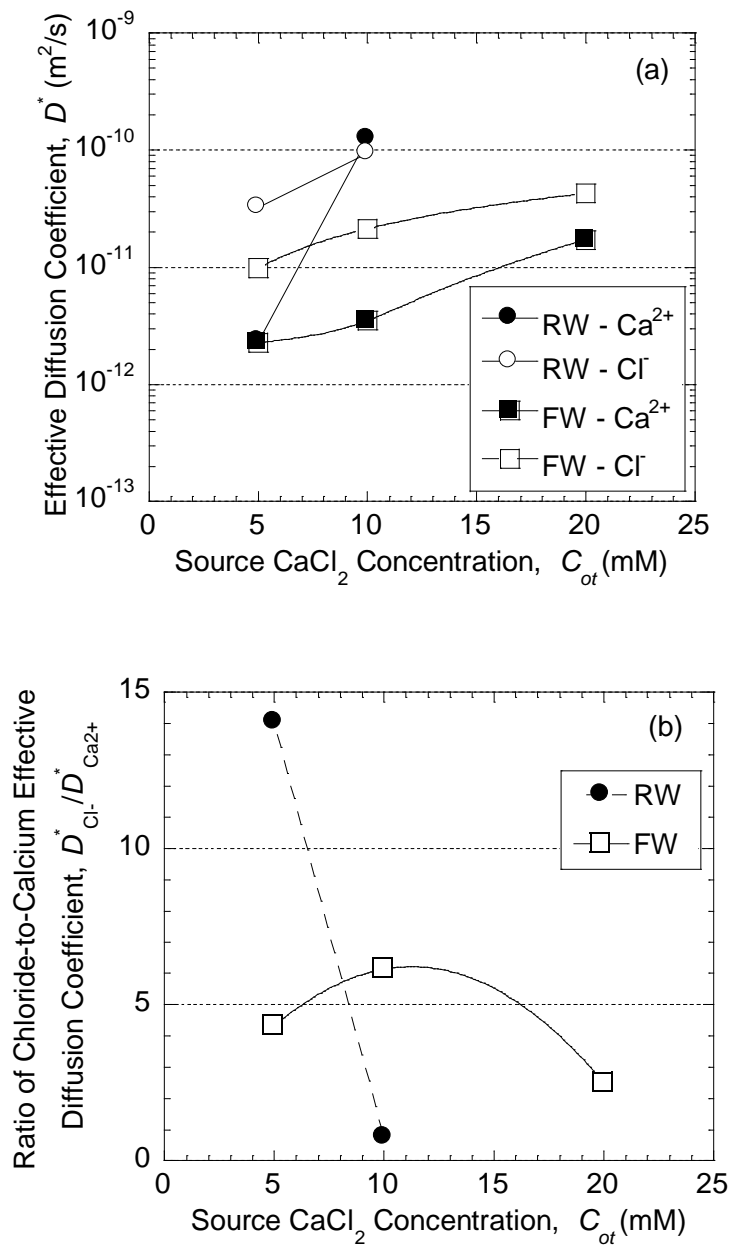


Figure 5.17. Effective diffusion coefficient (a) and ratio of chloride-to-calcium effective diffusion coefficient (b) versus calcium chloride source concentration (C_{ot}) for bentonite polymer nanocomposite (BPN) for tests RW @ $n = 0.87$ and FW @ $\sigma' = 103$ kPa (15 psi).

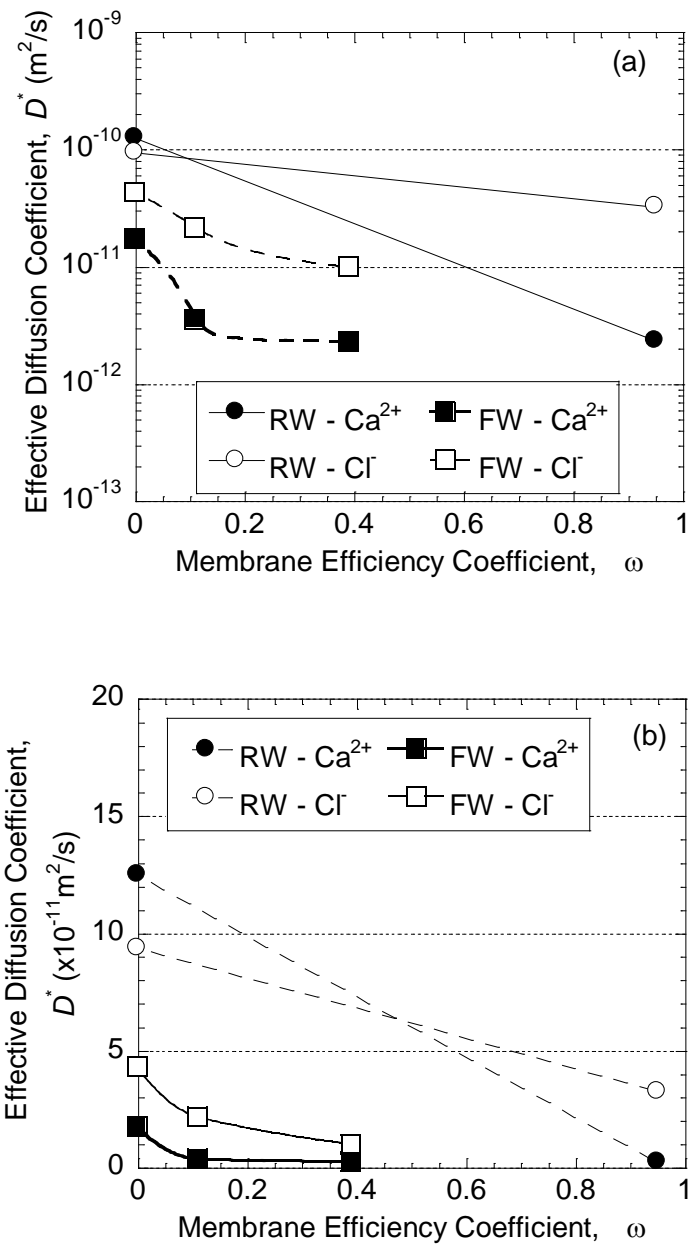


Figure 5.18. Effective diffusion coefficient (D^*) as a function of the membrane efficiency coefficient for a bentonite polymer nanocomposite: RW @ $n = 0.87$; FW @ $\sigma' = 103 \text{ kPa}$ (15 psi).

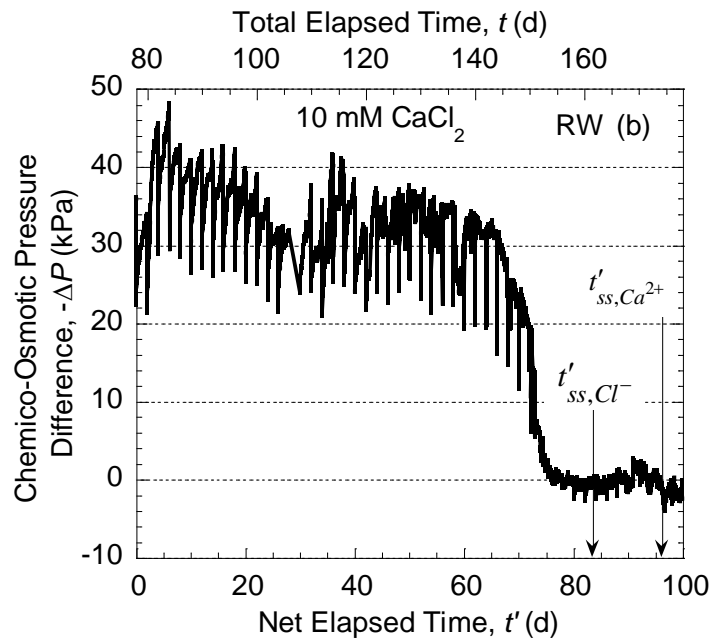
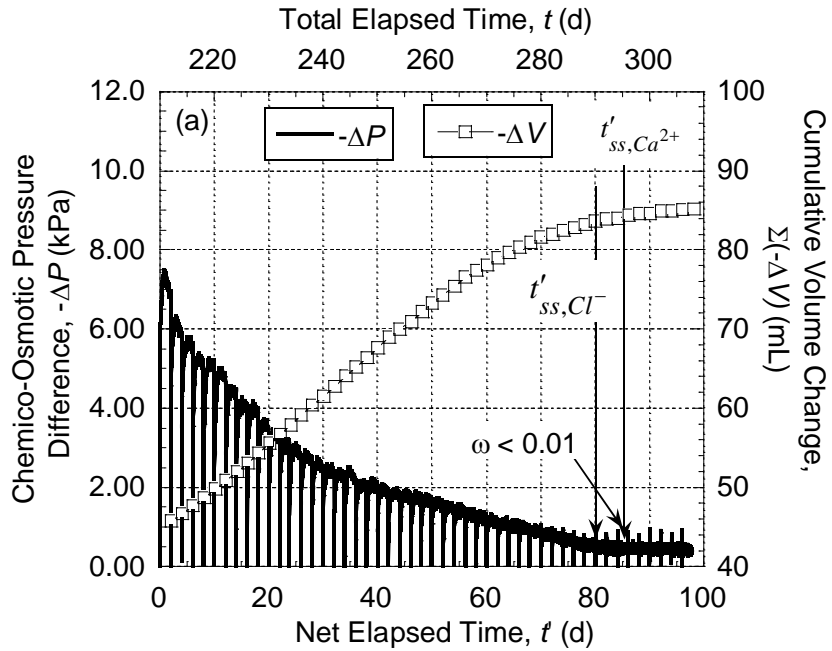


Figure 5.19. Measured chemico-osmotic pressure differences versus time for membrane testing of bentonite polymer nanocomposite: (a) flexible-wall test at 20 mM $CaCl_2$ with $t'_{ss,Cl^-} = 80$ d and $t'_{ss,Ca^{2+}} = 86$ d; (b) rigid-wall tests at 10 mM $CaCl_2$ with $t'_{ss,Cl^-} = 84$ d and $t'_{ss,Ca^{2+}} = 96$ d.

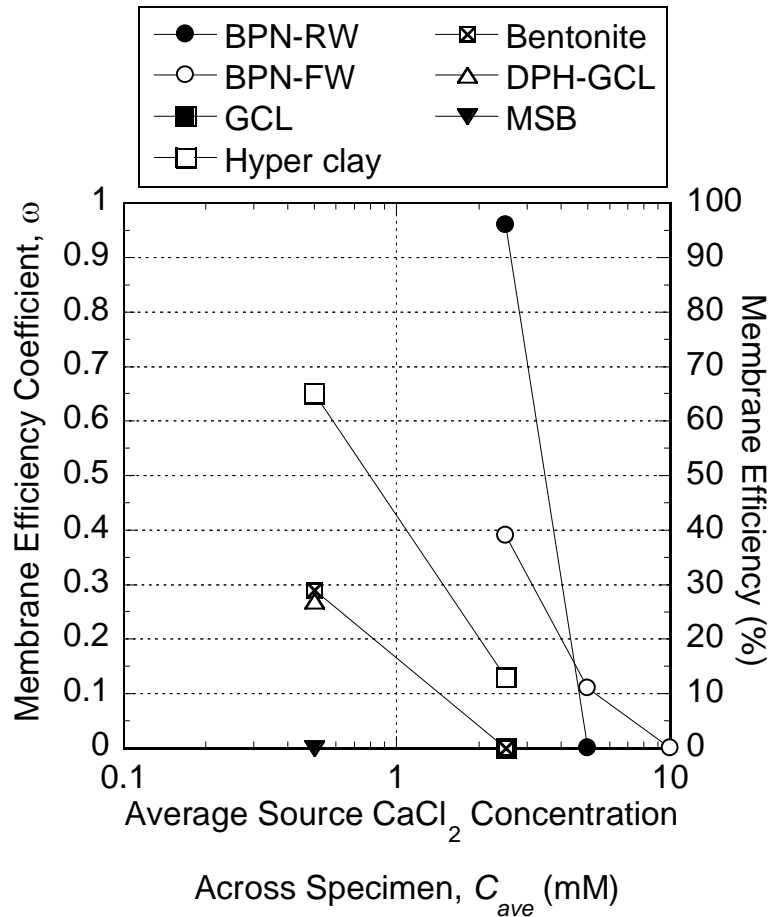


Figure 5.20. Results of steady-state membrane efficiency coefficients for specimens of bentonite polymer nanocomposite tested in rigid-wall and flexible-wall cells (BPN-RW, BPN-FW), a GCL from Shackelford and Lee (2003), and untreated bentonite, multi-swellable bentonite (MSB), and Hyper clay from Di Emidio (2010) as a function of average salt concentration across the specimen.

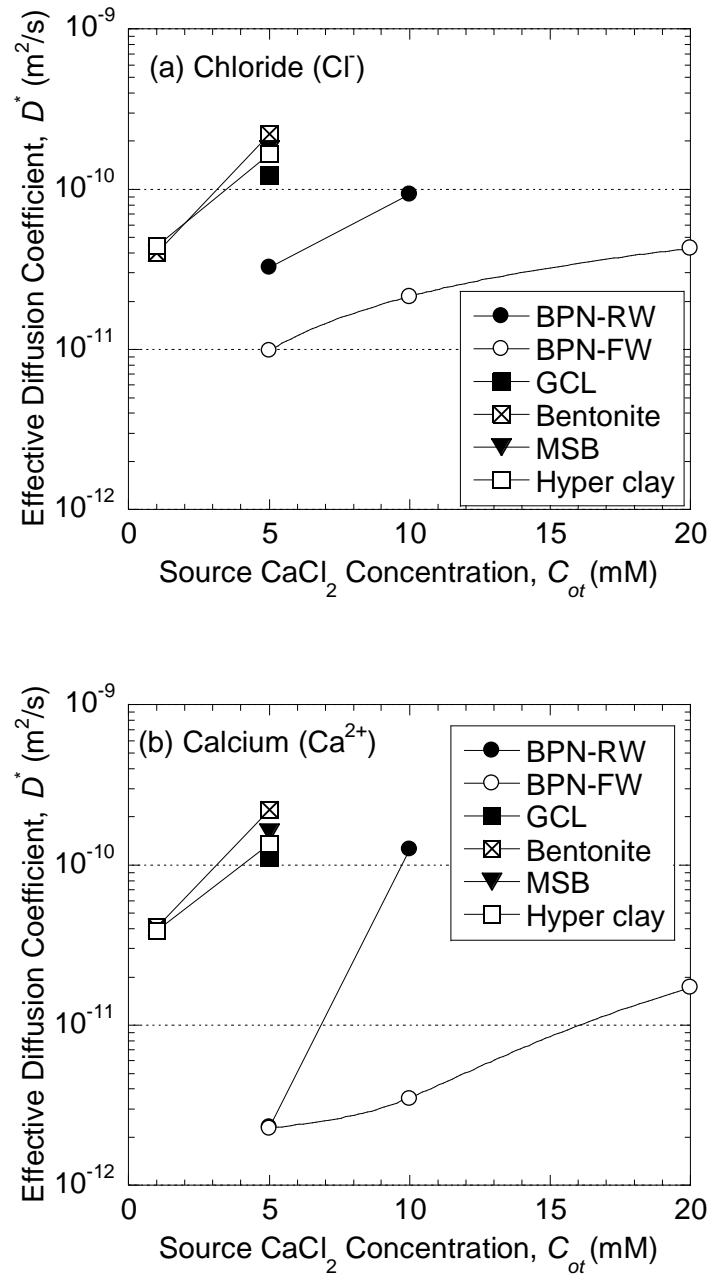


Figure 5.21. Effective diffusion coefficient for (a) chloride and (b) calcium versus source concentration of calcium chloride for bentonite polymer nanocomposite tested in rigid-wall and flexible-wall cells (BPN-RW, BPN-FW), a GCL from Shackelford and Lee (2003), and untreated bentonite, multi-swellable bentonite (MSB), and Hyper clay from Di Emidio (2010) as a function of average salt concentration across the specimen.

References

- Ashmawy, A. K., Darwish, E. H., Sotelo, N., and Muhammad, N. (2002). "Hydraulic performance of untreated and polymer-treated bentonite in inorganic landfill leachates." *Clays and Clay Minerals*, 50(5), 546-552.
- ASTM. (2006). "Standard test method for swell index of clay mineral component of geosynthetic clay liners." ASTM D5890 ASTM International, West Conshohocken, PA.
- ASTM. (2010). "Standard practice for classification of soils for engineering purposes (Unified Soil Classification System)." ASTM D2487, ASTM International, West Conshohocken, PA.
- ATU. (1992). "ClayMax sodium bentonite liner found degraded at New Jersey site." *Aboveground Tank Update*, 3(2), 17-18.
- Barbour, S. L., and Fredlund, D. G. (1989). "Mechanisms of osmotic flow and volume change in clay soils." *Canadian Geotechnical Journal*, 26(4), 551-562.
- Benson, C. H., Jo, H. Y., and Abichou, T. (2004). "Forensic analysis of excessive leakage from lagoons lined with a composite GCL." *Geosynthetics International*, 11(3), 242-252.
- Benson, C. H., Thorstad, P. A., Jo, H. Y., and Rock, S. A. (2007). "Hydraulic performance of geosynthetic clay liners in a landfill final cover." *Journal of Geotechnical and Geoenvironmental Engineering*, 133(7), 814-827.
- Bradshaw, S., Benson, C., and Scalia, J. (2012). "Cation exchange during subgrade hydration and effect on hydraulic conductivity of GCLs." *Journal of Geotechnical and Geoenvironmental Engineering*, In press.
- Buchholz, F., and Graham, A. (1998). *Modern Superabsorbent Polymer Technology*, Wiley, New York.
- Christman, M., Benson, C., and Edil, T. (2002). "Geophysical evaluation of annular well seals." *Ground Water Monitoring and Remediation*, 22(3), 104-112.
- Di Emidio, G. (2010). "Hydraulic and Chemico-Osmotic Performance of Polymer Treated Clay," PhD Dissertation, University of Ghent, Ghent, Belgium.
- Di Emidio, G., van Impe, P. O., and Flores, V. (2011). "Advances in geosynthetic clay liners: polymer enhanced clays." *Geo-Frontiers 2011: Advances in Geotechnical Engineering*, J. Han and D. Alzamora, eds., ASCE, Reston, VA, 1931-1940.
- Di Emidio, G., van Impe, P. O., and Mazzieri, F. "A polymer enhanced clay for impermeable geosynthetic clay liners." *Sixth International Conference on Environmental Geotechnics*, New Delhi, India, 963-967.

- Di Maio, C. (1996). "Exposure of bentonite to salt solution: Osmotic and mechanical effects." *Geotechnique*, 46(4), 695-707.
- Egloffstein, T. A. (2001). "Natural bentonites influence of the ion exchange and partial desiccation on permeability and self-healing capacity of bentonites used in GCLs." *Geotextiles and Geomembranes*, 19(7), 427-444.
- Estornell, P., and Daniel, D. E. (1992). "Hydraulic conductivity of 3 geosynthetic clay liners." *Journal of Geotechnical Engineering-Asce*, 118(10), 1592-1606.
- Evans, J. C. (1994). "Hydraulic Conductivity of Vertical Cutoff Walls." *Hydraulic Conductivity and Waste Contaminant Transport in Soil*, STP 1142, D. E. Daniel and S. Trautwein, eds., ASTM, West Conshohocken, PA, 79-94.
- Groenevelt, P. H., and Elrick, D. E. (1976). "Coupling phenomena in saturated homo-ionic montmorillonite: II. Theoretical." *Soil Society of America Journal*, 40(6), 820-823.
- James, A. N., Fullerton, D., and Drake, R. (1997). "Field performance of GCL under ion exchange conditions." *Journal of Geotechnical and Geoenvironmental Engineering*, 123(10), 897-901.
- Jo, H. Y., Benson, C. H., Shackelford, C. D., Lee, J. M., and Edil, T. B. (2005). "Long-term hydraulic conductivity of a geosynthetic clay liner permeated with inorganic salt solutions." *Journal of Geotechnical and Geoenvironmental Engineering*, 131(4), 405-417.
- Jo, H. Y., Katsumi, T., Benson, C. H., and Edil, T. B. (2001). "Hydraulic conductivity and swelling of nonprehydrated GCLs permeated with single-species salt solutions." *Journal of Geotechnical and Geoenvironmental Engineering*, 127(7), 557-567.
- Kajita, L. S. (1997). "An improved contaminant resistant clay for environmental clay liner applications." *Clays and Clay Minerals*, 45(5), 609-617.
- Kang, J.-B., and Shackelford, C. D. (2009). "Clay membrane testing using a flexible-wall cell under closed-system boundary conditions." *Applied Clay Science*, 44(1-2), 43-58.
- Kang, J.-B., and Shackelford, C. D. (2011). "Consolidation enhanced membrane behavior of a geosynthetic clay liner." *Geotextiles and Geomembranes*, 29(6), 544-556.
- Kang, J. B., and Shackelford, C. D. (2010). "Membrane Behavior of Compacted Clay Liners." *Journal of Geotechnical and Geoenvironmental Engineering*, 136(10), 1368-1382.
- Kolstad, D. C., Benson, C. H., and Edil, T. B. (2004). "Hydraulic conductivity and swell of nonprehydrated geosynthetic clay liners permeated with multispecies inorganic solutions." *Journal of Geotechnical and Geoenvironmental Engineering*, 130(12), 1236-1249.

- Lee, J. M., and Shackelford, C. D. (2005a). "Concentration dependency of the prehydration effect for a geosynthetic clay liner." *Soils and Foundations*, 45(4), 27-41.
- Lee, J. M., and Shackelford, C. D. (2005b). "Impact of bentonite quality on hydraulic conductivity of geosynthetic clay liners." *Journal of Geotechnical and Geoenvironmental Engineering*, 131(1), 64-77.
- Lee, J. M., and Shackelford, C. D. (2005c). "Solution retention capacity as the swell index test for sodium an alternative to bentonite." *Geotechnical Testing Journal*, 28(1), 61-70.
- Lee, J. M., Shackelford, C. D., Benson, C. H., Jo, H. Y., and Edil, T. B. (2005). "Correlating index properties and hydraulic conductivity of geosynthetic clay liners." *Journal of Geotechnical and Geoenvironmental Engineering*, 131(11), 1319-1329.
- Lin, L. C., and Benson, C. H. (2000). "Effect of wet-dry cycling on swelling and hydraulic conductivity of GCLs." *Journal of Geotechnical and Geoenvironmental Engineering*, 126(1), 40-49.
- Malusis, M. A., and Shackelford, C. D. (2002a). "Chemico-osmotic efficiency of a geosynthetic clay liner." *Journal of Geotechnical and Geoenvironmental Engineering*, 128(2), 97-106.
- Malusis, M. A., and Shackelford, C. D. (2002b). "Coupling effects during steady-state solute diffusion through a semipermeable clay membrane." *Environmental Science & Technology*, 36(6), 1312-1319.
- Malusis, M. A., Shackelford, C. D., and Olsen, H. W. (2001). "A laboratory apparatus to measure chemico-osmotic efficiency coefficients for clay soils." *Geotechnical Testing Journal*, 24(3), 229-242.
- Manassero, M., and Dominijanni, A. (2003). "Modelling the osmosis effect on solute migration through porous media." *Geotechnique*, 53(5), 481-492.
- Marine, I. W., and Fritz, S. J. (1981). "Osmotic model to explain anomalous hydraulic heads." *Water Resources Research*, 17(1), 73-82.
- Mazzieri, F. (2011). "Impact of desiccation and cation exchange on the hydraulic conductivity of factory-prehydrated GCLs." *GeoFrontiers 2011: Advances in Geotechnical Engineering*, J. Han and D. Alzamora, eds., ASCE, Reston, VA, 976-985.
- Mazzieri, F., Di Emidio, G., and Van Impe, P. O. (2010a). "Diffusion of calcium chloride in a modified bentonite: impact on osmotic efficiency and hydraulic conductivity." *Clays and Clay Minerals*, 58(3), 351-363.
- Mazzieri, F., Pasqualini, E., and Di Emidio, G. (2010b). "Migration of heavy metals through conventional and factory-prehydrated GCL materials." *Sixth International Conference on Environmental Geotechnics*, New Delhi, Delhi, India, 963-967.

- Meer, S. R., and Benson, C. H. (2007). "Hydraulic conductivity of geosynthetic clay liners exhumed from landfill final covers." *Journal of Geotechnical and Geoenvironmental Engineering*, 133(5), 550-563.
- Mitchell, J. K. (1976). *Fundamentals of soil behavior*, Wiley, New York.
- Muzny, C. D., Butler, B. D., Hanley, H. J. M., Tsvetkov, F., and Peiffer, D. G. (1996). "Clay platelet dispersion in a polymer matrix." *Materials Letters*, 28(4-6), 379-384.
- Neuzil, C. E. (2000). "Osmotic generation of 'anomalous' fluid pressures in geological environments." *Nature*, 403(6766), 182-184.
- Neuzil, C. E., and Provost, A. M. (2009). "Recent experimental data may point to a greater role for osmotic pressures in the subsurface." *Water Resources Research*, 45, 14.
- Onikata, M., Kondo, M., Hayashi, N., and Yamanaka, S. (1999). "Complex formation of cation-exchanged montmorillonites with propylene carbonate: Osmotic swelling in aqueous electrolyte solutions." *Clays and Clay Minerals*, 47(5), 672-677.
- Onikata, M., Kondo, M., and Kamon, M. (1996). "Development and characterization of a multiswellable bentonite." 2nd International Congress on Environmental Geotechnics, M. Kamon, ed., A A Balkema, Rotterdam, Netherlands, 587-590.
- Rousseau-Gueutin, P., de Greef, V., Goncalves, J., Violette, S., and Chanchole, S. (2009). "Experimental device for chemical osmosis measurement on natural clay-rock samples maintained at in situ conditions: Implications for formation pressure interpretations." *Journal of Colloid and Interface Science*, 337(1), 106-116.
- Scalia, J. (2012). "Bentonite-polymer composites for containment applications," PhD Dissertation, University of Wisconsin - Madison, Madison, WI.
- Scalia, J., and Benson, C. H. (2011). "Hydraulic conductivity of geosynthetic clay liners exhumed from landfill final covers with composite barriers." *Journal of Geotechnical and Geoenvironmental Engineering*, 137(1), 1-13.
- Scalia, J., Benson, C. H., Edil, T. B., Bohnhoff, G. L., and Shackelford, C. D. (2011). "Geosynthetic clay liners containing bentonite polymer nanocomposite." *Geo-Frontiers 2011: Advances in Geotechnical Engineering*, J. Han and D. Alzamora, eds., ASCE, Reston, VA, 2001-2009.
- Shackelford, C. D. (1991). "Laboratory diffusion testing for waste disposal -- A review." *Journal of Contaminant Hydrology*, 7(3), 177-217.
- Shackelford, C. D. (2011). "Membrane behavior in geosynthetic clay liners." *GeoFrontiers 2011: Advances in Geotechnical Engineering*, J. Han and D. Alzamora, eds., ASCE, Reston, VA, 1961-1970.

- Shackelford, C. D. (2012). "Membrane behavior of engineered clay barriers for geoenvironmental containment: State of the art." *GeoCongress 2012-State of the Art and Practice in Geotechnical Engineering*, R. D. Hryciw, A. Athanasopoulos-Zekkos, and N. Yesiller, eds., ASCE, Oakland, CA, 3419-3428.
- Shackelford, C. D., Benson, C. H., Katsumi, T., Edil, T. B., and Lin, L. (2000). "Evaluating the hydraulic conductivity of GCLs permeated with non-standard liquids." *Geotextiles and Geomembranes*, 18(2-4), 133-161.
- Shackelford, C. D., and Lee, J. M. (2003). "The destructive role of diffusion on clay membrane behavior." *Clays and Clay Minerals*, 51(2), 186-196.
- Shackelford, C. D., Malusis, M. A., and Olsen, H. W. (2003). "Clay membrane behavior for geoenvironmental containment." *Soil and Rock America Conference 2003, Proceedings of the joint 12th Panamerican Conference on Soil Mechanics and Geotechnical Engineering and the 39th U. S. Rock Mechanics Symposium*, 767-774.
- Smith, J. A., Bartelt-Hunt, S. L., and Burns, S. E. (2003). "Sorption and permeability of gasoline hydrocarbons in organobentonite porous media." *Journal of Hazardous Materials*, 96(1), 91-97.
- Trauger, R., and Darlington, J. (2000). "Next generation geosynthetic clay liners for improved durability and performance." 14th GRI Conference, Geosynthetic Institute, Geosynthetic Institute, Folsom, PA, USA, 255-267.
- Tremosa, J., Goncalves, J., and Matray, J. M. (2012). "Natural conditions for more limited osmotic abnormal fluid pressures in sedimentary basins." *Water Resources Research*, 48, 1-14.
- Vasko, S., Jo, H. Y., Benson, C. H., Edil, T. B., and Katsumi, T. (2001). "Hydraulic conductivity of partially prehydrated geosynthetic clay liners permeated with aqueous calcium chloride solutions." *Geosynthetics 2001, Industrial Fabrics Assoc. International*, St. Paul, MN, 685-699.
- Yeo, S. S., Shackelford, C. D., and Evans, J. C. (2005). "Membrane behavior of model soil-bentonite backfills." *Journal of Geotechnical and Geoenvironmental Engineering*, 131(4), 418-429.

Chapter 6

Polymerized Bentonite Amended Backfills for Vertical Cutoff Walls

SUMMARY: The potential for incompatibility between soil-bentonite (SB) backfills of vertical cutoff walls comprised of conventional bentonite (CB) and contaminated groundwater has led to evaluation of chemically modified bentonites for improved chemical resistance. Accordingly, the hydraulic conductivity (k) to tap water, consolidation behavior, and chemical compatibility (Δk) based on permeation with CaCl_2 solutions of SB backfills amended with a polymerized bentonite known as bentonite polymer nanocomposite (BPN) were evaluated and compared with those for a backfill comprised of CB. The BPN was considered for use both as a dry amendment and as the constituent in the bentonite slurry. Slurry comprised of only 2 % BPN was found to possess essentially the same rheological properties (e.g., viscosity, filtrate loss) typically associated with traditional slurries requiring 5 % CB. As a result, the three backfills that were evaluated included clean silica sand amended with either 2 or 5 % dry BPN and mixed with 2 % BPN slurry (i.e., 2BPN2 and 5BPN2, respectively), and the same sand amended with 5 % dry CB and mixed with 5 % CB slurry (5CB5). For all bentonite backfills, the k to water decreased with increasing effective stress, σ' . The ranges in the measured k values for each of the three backfills varied in the order: 2BPN2 backfill ($3.0 \times 10^{-7} \geq k \geq 1.4 \times 10^{-10}$ m/s) > 5CB5 backfill ($1.8 \times 10^{-10} \geq k \geq 7.4 \times 10^{-11}$ m/s) > 5BPN2 backfill ($9.3 \times 10^{-11} \geq k \geq 1.3 \times 10^{-11}$ m/s). Also, the BPN backfills displayed bi-linear stress-strain curves (semi-logarithmic scale) and were more sensitive to stress conditions than the CB backfill. For example, the values of the coefficient of compression, C_c , for the 5BPN2 backfill in the stress range $5 \text{ kPa} \leq \sigma' \leq 46 \text{ kPa}$ were 2.6 times greater relative to those in the stress range $46 \text{ kPa} \leq \sigma' \leq 1485 \text{ kPa}$. The C_c of the 5CB5 backfill

and the 5BPN2 backfill for $5 \text{ kPa} \leq \sigma' \leq 46 \text{ kPa}$ (0.13 and 0.12, respectively) are sufficiently close to suggest that both backfills have similar compression behaviors under low stress conditions. However, for $46 \text{ kPa} \leq \sigma' \leq 1485 \text{ kPa}$, C_c for the 5BPN2 backfill decreases significantly to a value of 0.046, whereas that for the 5CB5 backfill remains the same. Finally, even though the chemical resistance of the BPN backfills in terms of Δk upon permeation with CaCl_2 solutions was not better than that of the CB backfill, the final k of the 5BPN2 backfill after permeation with 50 mM CaCl_2 was almost two orders of magnitude lower than that of the 5CB5 backfill permeated with 50 mM CaCl_2 ($3.2 \times 10^{-11} \text{ m/s}$ versus $2.5 \times 10^{-9} \text{ m/s}$, respectively). Thus, the overall hydraulic performance of the backfill containing 5 % dry BPN was significantly better than that of the backfill containing 5 % dry CB.

Key Words: Backfills; Compatibility; Consolidation; Hydraulic Conductivity; Polymerized bentonite

6.1 INTRODUCTION

Soil-bentonite (SB) vertical cutoff walls have been used since the early 1940s to control seepage into excavations and through earthen dams, as barriers to salt-water intrusion along coastal regions, and more recently to control contaminant migration in groundwater (Xanthakos 1979; D'Appolonia 1980; USEPA 1984; Ressi and Cavalli 1985; USEPA 1992; LaGrega et al. 2001; Yeo et al. 2005; Evans et al. 2008; Malusis et al. 2009; Hong et al. 2012). Vertical cutoff walls typically are constructed by first excavating a trench from 0.6 to 1.5 m in width typically through relatively high permeable soils to depths up to 30 m (100 ft) (Xanthakos 1979; D'Appolonia 1980; Ressi and Cavalli 1985). The trench is held open by placing bentonite slurry

consisting of a mixture of water and about 5 % of a conventional sodium bentonite (Na-bentonite) by dry weight into the open excavation, usually to a level that is somewhat higher than the surrounding groundwater, resulting in an outward hydraulic gradient for flow of the slurry into the surrounding soil. The penetration of the slurry into the surrounding soil results in the formation of thin (e.g., several mm) filter cake with a low hydraulic conductivity, k (i.e., $< 10^{-11}$ m/s), that serves to both minimize slurry loss from the trench and maintain sufficient lateral pressure for trench stability (Ressi and Cavalli 1985). Trenches up to 300-m long have stayed open as long as the slurry extends to the top of the trench and the groundwater level is sufficiently lower than the slurry level (D'Appolonia 1980). The trench then is backfilled with the trench spoils typically combined with bentonite slurry to impart the necessary rheological properties, and additional dry bentonite in cases where the trench spoils do not include a fines content sufficient to impart a suitably low hydraulic conductivity (D'Appolonia 1980; USEPA 1984).

Detailed methods of slurry trench construction depend on site conditions. Backhoes, clamshells, and/or draglines may be used to excavate the trench depending on the required depth. The bentonite slurry is mixed on site using ponds or large vortex or propeller type mixers. The target Marsh viscosity of the slurry is approximately 40 s. A lower viscosity (i.e., < 36 s) may lead to trench stability problems and lack of filter cake formation (D'Appolonia 1980; Evans 1993). The SB backfill, consisting of trench spoils, bentonite slurry, and additional bentonite for clean coarse-grained spoils, is mixed adjacent to the trench. The ideal consistency of the backfill material for placement purposes corresponds to a water content that produces a slump ranging from 100 mm to 150 mm (D'Appolonia 1980; Evans 1993; LaGrega et al. 2001). The unit weight of the backfill material should be approximately 2.35 kN/m^3 (15 lb/ft^3) greater than the

unit weight of the slurry to ensure displacement of the slurry by the backfill (D'Appolonia 1980; Evans 1993).

The k , compressibility, and strength of the backfill are important considerations for the proper performance of SB cutoff walls (D'Appolonia 1980). The k of the backfill depends on the soil gradation and the amount of bentonite added to the backfill. In general, greater than 1 % bentonite and greater than 20 % fines are recommended for the backfill in order to reach the desired k for the completed wall, which typically is lower than 1×10^{-9} m/s. In coarse-grained formations, such as a clean sand, a minimum of 5 % bentonite has been recommended to achieve a k less than 1×10^{-9} m/s (Yeo et al. 2005). However, increasing the amount of fines not only decreases k but also increases the compressibility of the backfill (D'Appolonia 1980; Yeo et al. 2005).

A potential for incompatibility between the soil-bentonite cutoff wall and the surrounding contaminated groundwater typically exists when such cutoff walls are used for environmental containment applications (e.g., USEPA 1984; Ryan 1987; Beirck and Chang 1994; Katsumi et al. 2008). Such incompatibility typically is reflected by an increase in k (i.e., $\Delta k > 0$) due to physico-chemico interactions between the permeant liquid and the backfill. Incompatibility also can lead to piping failure in scenarios involving granular backfill soils and small amounts of bentonite (D'Appolonia 1980; USEPA 1984; USEPA 1992).

The potential for such incompatibility has led to evaluation of replacing conventional (unmodified) Na-bentonites with modified bentonites for improved chemical resistance. For example, Malusis and McKeehan (2012) evaluated the use of multi-swellable bentonite (MSB) in place of conventional untreated bentonite and a commercially available treated bentonite for SB cutoff walls. The MSB is treated with propylene carbonate for improved chemical resistance

and has been shown to swell in 0.6 M NaCl solutions, suggesting that the material may be less susceptible to chemical attack and incompatibility (Onikata et al. 1999). The SB backfills were permeated with solutions of CaCl₂ with concentrations ranging from 10 to 1000 mM. Of the backfills studied, those with MSB exhibited the lowest increases in k when permeated with solutions of CaCl₂. For example, the k of the MSB increased a maximum 2.1 times when permeated with CaCl₂ solutions relative to the k to tap water, whereas the k of the untreated Na-bentonite backfills increased as much as 3.1 times. However, none of the SB backfills exhibited more than a five-fold increase in k when permeated with CaCl₂ solutions.

The objective of this study was to evaluate the potential use of an acrylic acid polymerized bentonite, known as a bentonite polymer nanocomposite or BPN, as a substitute for conventional bentonite (CB) in SB backfills for the purpose of improving resistance to chemical incompatibility. The BPN previously has been evaluated for improved hydraulic performance in geosynthetic clay liners (Scalia et al. 2011). The evaluation conducted in this study consisted of measuring the k based on permeation with tap water, the consolidation (compressibility) behavior, and the chemical compatibility (i.e., Δk) of backfills amended with dry BPN and prepared using BPN slurry, and comparing the results with those based on the use of a traditional backfill amended with dry CB and prepared using CB slurry.

6.2 MATERIALS AND METHODS

6.2.1 Constituent Soils

Three constituent soils were used in this study: silica sand, a CB, and the BPN. The silica sand, with a specific gravity of solids, G_s , of 2.65, was available commercially from U.S. Silica (Grade F-35 foundry sand, Ottawa, IL). Both bentonites were supplied by Colloid

Environmental Technologies Co. (CETCO, Hoffman Estates, IL). The CB is a commercially available product (VOLCLAY[®] CG-50), whereas the BPN was specially produced with polyacrylic acid (PAA) using methods similar to those used for the production of polymer nanocomposites (e.g., Muzney et al. 1996). In brief, the BPN was formed by polymerizing PAA molecules after insertion into the interlayers of the montmorillonite mineral structure. The PAA bonds with sodium ions initially in the interlayer region and the surface of the individual bentonite particles. These bonds are expected to prevent the PAA from leaching out during permeation. The polymerized bentonite is referred to as a nanocomposite, because the modifications to the bentonite are expected to occur at the nanoscale (Scalia et al. 2011; Scalia 2012). Additional details regarding the preparation of the BPN are given in Chapter 3 and by Scalia et al. (2011) and Scalia (2012).

The particle-size distributions and classifications [ASTM D 2487 (2010a)] for the constituent soils are shown in Fig. 6.1, and the index properties of the CB and the BPN are summarized in Table 6.1. Both the CB and the BPN classify as high-plasticity clays (CH), whereas the silica sand classifies as poorly graded sand (SP).

6.2.2 Permeant Liquids

The permeant liquids used in this study included tap water and solutions of de-ionized water (DIW) and calcium chloride dihydrate ($\text{CaCl}_2 \cdot 2\text{H}_2\text{O}$) (certified A.C.S.; Fisher Scientific, Fair Lawn, NJ). The CaCl_2 solutions were used as permeant liquids in hydraulic conductivity tests to allow for comparison of results with previous hydraulic conductivity tests conducted on SB backfills (Malusis and McKeehan 2012). Solutions were prepared and stored in 20-L carboys (Nalgene[®]; Thermo Fisher Scientific, Rochester, NY). The *pH* and electrical

conductivity, EC , of the solutions were measured using a pH meter (Accumet[®] AB15 meter; Fisher Scientific Co., Pittsburgh, PA) and an EC probe (150 A+ Conductivity Meter; Thermo Orion, Beverly, MA), respectively. Ion chromatography (Dionex[®] 4000i IC Module, Dionex Co., Sunnyvale, CA) was used to measure chloride (Cl^-) concentrations, and inductively coupled plasma-atomic emission spectrometry, or ICP-AES (IRIS[®] Advantage/1000 ICAP Spectrometer, Thermo Jarrel Ash Co., Franklin, MA), was used to measure calcium (Ca^{2+}) concentrations. The measured EC and pH of the $CaCl_2$ solutions are given in Table 6.2.

6.2.3 Slurries

Slurries with from 2 to 5 % by weight of either CB or BPN suspended in water were evaluated for use in preparing backfills. The slurries were mixed in a high-speed blender for 5 min and allowed to hydrate for a minimum of 24 h. The density and viscosity of the slurries were measured using a mud balance (Model 140, Fann Instrument Company, Houston, TX) and a Marsh Funnel Viscometer (Model 201, Fann Instrument Company, Houston, TX), respectively, following API recommended practice 13B-1 (API 2003). The slurries were tested in a filter press (300 APT Filter Press, Fann Instrument Company, Houston, TX) to determine if the material had sufficient fines to produce a filter cake and to measure the filtrate loss. The filtrate loss was measured following API Recommended Practice 13B-1 (API 2003). In addition, the pH of the slurries was measured using the aforementioned pH meter.

The resulting measured properties of the slurries are shown in Fig. 6.2 as a function of the content of bentonite (i.e., either CB or BPN). Desirable properties of the slurry included a target viscosity of 40 s, a filtrate loss less than 25 mL, and $6.5 \leq pH \leq 10$ (e.g., Evans 1993).

As shown in Fig. 6.2, the viscosity and density of slurries containing both the CB and the BPN increased substantially with increasing percentage of CB or BPN. For example, the viscosity of a slurry containing 2 % CB was only 29 s, whereas that of a slurry containing 5 % CB was 38 s. In contrast, the viscosity of a slurry containing 2 % BPN was 39 s, whereas that of a slurry containing 5 % BPN was 97 s. The density of both the CB and BPN slurries also increased, albeit only slightly, with increasing bentonite content. The densities of the slurries containing either 2 % CB or 2 % BPN were both approximately 1.01 g/cm³, whereas those of the slurries containing 5 % CB or 5 % BPN were both approximately 1.03 g/cm³.

As expected, the filtrate losses of slurries containing either the CB or the BPN decreased as the respective bentonites content increased from 2 to 5 %. However, the overall range in filtrate losses of the BPN slurries was substantially lower than that of the CB slurries, i.e., from 6 to 10.5 mL versus from 15 to 26.8, respectively. The differences in filtrate losses of the BPN slurries relative to those of the CB slurries are consistent with the differences in the aforementioned viscosities of the resulting slurries (i.e., the viscosities of the BPN slurries are substantially higher than those of the CB slurries).

The values of *pH* for all BPN slurries were approximately neutral (*pH*~7). A nearly neutral *pH* is consistent with what would be expected for this material, because the addition of the PAA is neutralized by an addition of sodium hydroxide during the polymerization process (Scalia et al. 2011). In contrast, the values of *pH* for all CB slurries were more basic and ranged from 9.2 to 9.4, which is similar to that reported by Malusis et al. (2010) for an untreated sodium bentonite.

Since only the viscosity of 39 s for the 2 % BPN-water slurry was close to the target viscosity of 40 s, whereas all the other slurry criteria were achieved, only the 2 % BPN-water

slurry was selected for use in preparing the backfills amended with either 2 % or 5 % dry BPN. In contrast and as expected, the 5 % CB-water slurry satisfied all of the aforementioned criteria and, therefore, was used in the preparation of the traditional backfill prepared using the CB.

6.2.4 Slump Tests

The relationships between slump, $-\Delta H$ (> 0), and gravimetric water content for each backfill, w_B , were measured according to ASTM C143 (ASTM 2009). However, because a limited quantity of BPN was available for this study, the mini-slump cone described in Malusis et al. (2008) was used for the slump tests to minimize the amount of BPN required.

Three backfills were prepared for evaluation by mixing either dry CB or dry BPN with the silica sand. Based on the results reported by Yeo et al. (2005), who found that the addition of 5 % dry bentonite to an otherwise clean sand was required to achieve a suitably low k value (i.e., $\leq 1 \times 10^{-9}$ m/s) for SB backfills, two backfills were prepared by adding either 5 % dry CB or 5 % dry BPN to silica sand. A third backfill prepared by adding only 2 % dry BPN also was evaluated. This 2 % BPN backfill was justified on the basis that lower BPN contents are more desirable in terms of cost, and lower BPN contents may be adequate on the basis of the inherently better hydraulic performance expected for the BPN relative to the CB (e.g., Scalia et al. 2011). The respective slurries (i.e., 5 % CB slurry for sand-CB backfill and 2 % for the two sand-BPN backfills) described above were added incrementally to all three backfills to determine the relationships between $-\Delta H$ and w_B .

The resulting measured slump curves are presented in Fig. 6.3. Linear regressions of the $-\Delta H$ versus w_B are also included in Fig. 6.3. The target slump of each backfill was 125 mm. The values of w_B at $-\Delta H = 125$ mm ranged from 21.5 % for the sand-BPN backfill with 2 % dry

BPN to 40.9 % for the sand-CB backfill with 5 % dry CB (refer to Table 6.3).

6.2.5 Preparation of Backfills for Testing

Bulk volumes of the three different backfills used to prepare specimens for consolidation and hydraulic conductivity testing were prepared by combining the sand, the dry CB (5 %) or dry BPN (2 % or 5 %), and the necessary amount of either the 5 % CB slurry or the 2 % BPN slurry required to achieve a slump of 125 mm. The water contents and final bentonite contents for these backfills are summarized in Table 6.3. In order to simplify the presentation, the backfill designations identified in Table 6.3 (i.e., 5CB5, 2BPN2, and 5BPN2), which indicate the percentage of dry bentonite added to the sand (first number), the type of bentonite (letters), and the percentage of the bentonite in the slurry (last number), will be used in all subsequent descriptions.

As indicated in Table 6.3, the final contents of bentonite in the prepared backfills, B_B , varied as a result of the variable amount of respective slurry that was added to the dry backfill to achieve the desired slump of 125 mm. Thus, the values of B_B for the prepared 2BPN2, 5BPN2, and 5CB5 backfills were actually 2.4 %, 5.5 %, and 7.1 %, respectively. Thus, the two backfills prepared with BPN contained less overall bentonite than the backfill prepared using the CB.

6.2.6 Consolidation

The compressibility of the prepared backfills was measured according to conventional consolidation testing procedures, ASTM D 2435 (ASTM 2004). In addition, after primary consolidation had been achieved for each load increment, k also was measured as described by Olsen and Daniel (1981).

Specimens were prepared in fixed-ring consolidometers. The backfill was placed in the cell, rodded to eliminate large voids, and loaded with a small seating load to an initial stress of 5 kPa for 24 h. Consolidation of the specimen commenced immediately thereafter by applying incremental loads such that each subsequent load was doubled relative to the previous load up to a maximum stress of 1485 kPa (215 psi). Each loading stage was maintained for a minimum of 24 h. Following the loading stage of the test, the specimens were unloaded by reducing the applied loads incrementally by a factor of four relative to the previous load. Again, each unloading stage was maintained for a minimum of 24 h.

At the end of each loading stage, and prior to the subsequent loading, the specimens were permeated with tap water using the falling head procedure to measure the k of the backfills as a function of applied stress (e.g., Yeo et al. 2005; Malusis et al. 2009; Hong et al. 2012). The permeation was continued until the termination criteria specified in ASTM D 5084 (ASTM 2010b) were satisfied. These termination criteria include at least four consecutive k values with an outflow-to-inflow ratio of 1.00 ± 0.25 and steady k . The k was considered steady when at least four consecutive values of k were within $\pm 25\%$ of the average k for $k \geq 10^{-10}$ m/s or within $\pm 50\%$ for $k \leq 1 \times 10^{-10}$ m/s, and there was no upward or downward trend in a plot of k versus time. Because of the particularly low values of k (i.e., $\leq 10^{-10}$ m/s) measured for the specimens of the 5BPN2 backfill, the testing durations required to measure k using this approach were all ≥ 48 h for this backfill.

6.2.7 Flexible-Wall Hydraulic Conductivity Tests

The k of the backfills also was measured using the falling-head system in flexible-wall cells for comparison with the measured k values obtained from the consolidation testing. The

backfill specimens for flexible-wall testing were prepared and permeated in general accordance with the procedures described in Malusis et al. (2009) and Hong et al. (2012). Test specimens of the backfill were assembled in 102-mm (4-in) diameter flexible-wall permeameters. A conventional latex membrane then was attached to the base pedestal with o-rings. Then, *in lieu* of porous stones and filter paper, a 0.75-kg/m² non-woven, needle-punched GT was placed on the base pedestal followed by a heat-bonded, non-woven GT. Next, a 1.68-mm (66-mil)-thick high density, polyethylene (HDPE) geomembrane (GM) was shaped into a cylinder and placed around the latex membrane of the permeameter to provide lateral support for the soft, unconsolidated backfill. The cylinder of HDPE GM was secured around the latex membrane using o-rings, and the top of the latex membrane was stretched over the top of the cylinder. The specimen was placed within the latex membrane in three lifts, rodded to remove large voids, and leveled off using a plastic top cap to create a flat surface. The two GTs were placed above the specimen followed by a top pedestal. The top pedestal was secured to the latex membrane with o-rings. The final thickness of the specimens varied from 71.4 to 96.4 mm.

After assembling the cell, the cell was connected to the hydraulic control system, and the backfill specimens initially were hydrated with the permeant liquid (i.e., tap water or solutions of CaCl₂) by leaving the influent lines open for 48 h under an effective confining stress of approximately 20 kPa. Prior to permeation of the specimen, the hydraulic lines were flushed with the permeant liquid to remove air bubbles that may have migrated out of the specimen during hydration.

After this hydration stage, falling head *k* tests were conducted in general accordance with ASTM D 5084 (ASTM 2010b). The testing methods were similar to those described in Lee and Shackelford (2005), Jo et al. (2005) and Scalia (2012). Specimens were permeated from the

bottom to the top under an average effective stress of approximately 20 kPa with an average hydraulic gradient of approximately 20. Reservoirs containing tap water under the sole influence of gravity were used to provide the cell and influent pressures (see Fig. 6.4). Because of the expected low k for the BPN backfills, inclined influent burettes were used to limit the change in the head, and, therefore, change in the effective stresses, during the test. The k was calculated using the standard equation for a falling head test, or

$$k = \frac{aL}{At} \ln \frac{h_o}{h_l} \quad (6.1)$$

where a is the cross-sectional area of the influent burette, L is the length of the specimen (thickness in the direction of flow), A is the total cross-sectional area of the soil specimen, h_o is the initial head, h_l is the final head, and t is the time between h_o and h_l . However, because of the inclined burette, the values of h were calculated as follows:

$$h = H + y = H + x \sin \alpha \quad (6.2)$$

where H is the vertical distance between the bottom of the inclined burette and the sample bag, α is the inclination of the burette, x is the location of water along the height of the inclined burette, and y is the height of water in the inclined burette relative to the bottom of the inclined burette (see Fig. 6.4). Also, because of a concern for evaporation of what was expected to be small volumes of outflow, the outflow was collected in fluorinated ethylene propylene (FEP) sample bags (Jensen Inert Products, Coral Springs, FL).

Permeation began by opening the effluent line, and monitoring the level of the influent liquid and the mass of the effluent sample bag versus time. The mass of the effluent sample bag was used to calculate the volume of the outflow (V_{out}) assuming a density of liquid of 1 Mg/m^3 . The outflow was collected from the sample bags in approximately 30-mL intervals and the pH and EC were monitored. The majority of the specimens were permeated until achieving the following criteria (Shackelford et al. 2000; Jo et al. 2005): (1) outflow within $\pm 25 \%$ of inflow; (2) a steady-state k (four or more measurements within $\pm 50 \%$ of the mean k and no temporal trend in k); (3) an outflow-to-inflow ratio of EC , or EC_o/EC_i , of 1.0 ± 0.05 (i.e., for specimens permeated with CaCl_2 solutions); and (4) a minimum of two pore volumes of flow (PVF). However, because of the extremely low k of the specimens of the 5BPN2 backfill (i.e., $k \leq 3.2 \times 10^{-11} \text{ m/s}$) permeated with either tap water or 50 mM CaCl_2 and the associated extremely low volumes of flow, the tests involving these specimens were terminated after 313 and 403 d of permeation, but prior to achieving two PVF and the EC ratio criterion. In addition, the specimens of 2BPN2 backfill were terminated after 1 d, before achieving 2 PVF, because of the extremely high k of the specimens ($k \geq 1.3 \times 10^{-7} \text{ m/s}$).

Both one-stage and two-stage k tests were conducted (e.g., Lee and Shackelford 2005). Two-stage tests were conducted on the CB backfills and one-stage tests were conducted on the BPN backfills. For the one-stage tests, the specimens were permeated directly with a CaCl_2 solution. However, for the two-stage tests, the specimens were first permeated with tap water until the aforementioned termination criteria were achieved, and then the permeant liquid was changed to a CaCl_2 solution. Malusis and McKeehan (2012) compared the results of one-stage tests and two-stage tests on CB backfills, and reported that, because the bentonite in the CB backfill is hydrated during the creation of the backfill mixtures, any effect due to prehydration is

minimal. As a result, and because of the expected low k of the BPN backfills, only one-stage tests were performed using specimens of the backfills containing BPN.

6.3 RESULTS AND DISCUSSION

6.3.1 Stress-Strain Behavior

Results of the consolidation tests conducted on each backfill are presented in Fig. 6.5. The consolidation results are plotted in terms of void ratio, e , versus logarithm of effective consolidation stress, $\log \sigma'$, or e - $\log \sigma'$ curves, and in terms of strain, ε , versus $\log \sigma'$, or ε - $\log \sigma'$ curves. Values of the compression index, C_c , and the swell index, C_s , representing the slopes of loading and unloading portions of the e - $\log \sigma'$ curves, respectively, are summarized in Fig. 6.5a, whereas values of the compression ratio, R_c , and the swell ratio, R_s , representing the slopes of the loading and unloading portions of the ε - $\log \sigma'$ curves, respectively, and are summarized in Fig. 6.5b.

Both the loading and unloading portions of the stress-strain curves for the tests conducted with the 5BPN2 backfill were bi-semilog linear, with slopes at lower σ' being greater than those at higher σ' . For example, the ratio of the C_c values for $5 \text{ kPa} \leq \sigma' \leq 46 \text{ kPa}$ relative to those for $46 \text{ kPa} \leq \sigma' \leq 1485 \text{ kPa}$ was 2.6, whereas the ratio of the C_s values for $5 \text{ kPa} \leq \sigma' \leq 23 \text{ kPa}$ relative to those for $23 \text{ kPa} \leq \sigma' \leq 1485 \text{ kPa}$ was 32.5. Similarly, the ratio of the R_c values for $5 \text{ kPa} \leq \sigma' \leq 46 \text{ kPa}$ relative to those for $46 \text{ kPa} \leq \sigma' \leq 1485 \text{ kPa}$ was 2.7, whereas the ratio of the R_s values for $5 \text{ kPa} \leq \sigma' \leq 23 \text{ kPa}$ relative to those for $23 \text{ kPa} \leq \sigma' \leq 1485 \text{ kPa}$ was 13.5. This atypical behavior likely is the result of the polymer content of the BPN. Superabsorbent polymers, such as the polyacrylate in the BPN, are sensitive to stress conditions (Buchholz and Graham 1998), such that the BPN exhibited both greater compression and swell at lower σ' .

The values of C_c and C_s for the 2BPN2 backfill were 0.015 and 0.003, respectively. This relatively low C_c reflects a relatively incompressible backfill, probably the result of the low bentonite content for this particular backfill and the dominance of the sand matrix in terms of compressibility. For example, the void ratio of the 2BPN2 backfill decreased during compression from 0.74 to 0.69. In contrast, the void ratio of the backfill containing conventional bentonite (i.e., the 5CB5 backfill) decreased during compression from 1.07 to 0.69, corresponding to C_c and C_s of 0.13 and 0.007, respectively, values of which are similar to those reported by others for similarly comprised backfills (e.g., Yeo et al. 2005). Finally, the fact that the 2BPN2 backfill did not display the same behavior as the 5BPN2 backfill suggests that the 2BPN2 backfill did not contain sufficient amount of polymer in the form of the BPN to result in a similar behavior as that observed for the 5BPN2 backfill.

The values for coefficient of compression, C_c , of 0.13 for the 5CB5 backfill and 0.12 for the 5BPN2 backfill under low stress conditions ($5 \text{ kPa} \leq \sigma' \leq 46 \text{ kPa}$) are sufficiently close to suggest that both backfills have similar compression behaviors under low stress conditions. However, under higher stress conditions ($46 \text{ kPa} \leq \sigma' \leq 1485 \text{ kPa}$), C_c for the 5BPN2 backfill decreases significantly to a value of 0.046, whereas that for the 5CB5 backfill remains the same. This reduction in C_c for the 5BPN2 backfill at higher stresses suggests that the compression behavior of this backfill at these higher stresses is controlled primarily by the sand matrix comprising the bulk of the backfill.

In contrast, although the value of 0.004 for the swell index, C_s , of the 5BPN2 backfill under the higher stress conditions ($46 \text{ kPa} \leq \sigma' \leq 1485 \text{ kPa}$) is reasonably close to that of 0.007 for the 5CB5, the C_s value for the 5BPN2 backfill increases significantly to 0.13 under the lower stress conditions ($5 \text{ kPa} \leq \sigma' \leq 46 \text{ kPa}$), indicating a much greater swelling potential for this

backfill at the lower stresses. This increase in C_s can be attributed to the dominance of the superabsorbent polymer portion of the BPN in controlling the swell behavior at the lower stress conditions.

6.3.2 Coefficients of Volume Change, Compressibility, and Consolidation

The coefficients of volume change, m_v , and coefficients of compressibility, a_v , were determined from the slopes of ε versus σ' and e versus σ' , respectively, for the loading stages of the consolidation test. The m_v and a_v values are summarized in Table 6.4 and plotted versus average σ' in Fig. 6.6. In general, the values of m_v and a_v decrease with increasing σ' and varied in the order: 5CB5 backfill > 5BPN2 backfill > 2BPN2 backfill.

The coefficients of consolidation, c_v , were determined using both the logarithm-of-time (Casagrande) and the square-root-of-time (Taylor) methods for the loading stages of the consolidation tests. The c_v values are summarized in Table 6.5 and plotted versus average σ' in Fig. 6.7. The c_v for the 5CB5 and 5BPN2 backfills varied between 10^{-6} and 10^{-9} m²/s and generally increased with increasing σ' . The c_v for the 2BPN2 backfill also varied from 10^{-6} to 10^{-9} m²/s; however, there was no consistent trend in the c_v versus σ' . This inconsistent behavior in c_v is similar to that previously described in terms of the C_c and C_s values for the 2BPN2 backfill, and again implies that the consolidation behavior of this 2BPN2 backfill is being controlled more by the sand matrix than by the bentonite content of the backfill.

The ratios of the c_v based on Taylor method to the c_v based on Casagrande method, c_v (Taylor)/ c_v (Casagrande), also are included in Table 6.5 and plotted in Figure 6.7. In general, the value of c_v based on the Taylor method is greater than that based on the Casagrande method (i.e., a ratio greater than unity). For the 5CB5 backfill and the 5BPN2 backfill, the ratios of c_v values

are generally lower than three; however, for the 2BPN2 backfill, the ratios of c_v values are as high as 54. The magnitudes of the ratios of c_v values for the 5CB5 and 5BPN2 backfills are similar to those reported by Yeo et al. (2005) and Duncan (1993), which reported c_v ratios generally in the range of one to three. The value of c_v based on the Taylor method generally is greater than that based on the Casagrande method because of several factors including the rate of strain at different σ' and secondary compression during primary consolidation (Duncan 1993; Olson 1998; Yeo et al. 2005). The reasons for the significantly higher ratios of c_v values for the 2BPN2 backfill are not entirely clear, but are undoubtedly related, in part, to the effect of insufficient bentonite content in this backfill on the k and compressibility of the backfill.

The trends in c_v versus average effective stress for the 5CB5 and 5BPN2 backfills also are similar to those reported by (a) Yeo et al. (2005) for backfills comprised of sand and conventional bentonite (CB) (b) Malusis et al. (2009) for sand-CB backfills amended with low amounts ($< 10\%$) of two types of activated carbon, and (c) Hong et al. (2012) for sand-CB backfills amended with low amounts ($\leq 10\%$) of three types of zeolites. Yeo (2005) reported that an increase in c_v with an increase in σ' is likely a result of the greater decrease in the coefficient of volume compressibility, m_v , relative to the decrease in k for increasing σ' . Despite the similarity in trends, the values of c_v for this study are generally lower than those reported by Yeo et al. (2005) as shown in Fig. 6.8, which was expected for the 5BPN2 backfill as a result of the extremely low k for this backfill. In addition, the sand used in this study is slightly finer (i.e., smaller particle size) than that used by Yeo et al. (2005) which resulted in lower k and thus a lower c_v for the 5CB5 backfill compared to 5% bentonite backfill for Yeo et al. (2005).

6.3.3 Hydraulic Conductivity to Water

The values of hydraulic conductivity to water, k , measured during consolidation testing are plotted as a function of σ' in Fig. 6.9. As expected, the values of k generally decreased with increasing σ' . The k for all three backfills was less than the typical regulatory limit of 10^{-9} m/s, i.e., except in the case of the 2BPN2 backfill at the low σ' of 23 kPa (3.3 psi). In this case, the k value of 3.0×10^{-7} m/s can be attributed to the combination of the low bentonite content and relatively low stress condition (i.e., relatively high void ratio). Overall, the ranges in the measured k values for each of the three backfills varied in the order: 2BPN2 backfill ($3.0 \times 10^{-7} \geq k \geq 1.4 \times 10^{-10}$ m/s) > 5CB5 backfill ($1.8 \times 10^{-10} \geq k \geq 7.4 \times 10^{-11}$ m/s) > 5BPN2 backfill ($9.3 \times 10^{-11} \geq k \geq 1.3 \times 10^{-11}$ m/s). Since the bentonite content of the 5CB5 backfill was greater than that of the 5BPN2 backfill (Table 6.3), the lower range in k values associated with the 5BPN2 backfill can be attributed to the differences in the type of bentonite (i.e., BPN vs. CB).

The values of k measured during consolidation testing are plotted as a function of the void ratio, e , in Fig. 6.10. The k of the 5BPN2 backfill was more sensitive to changes in e than the k of the 5CB5 backfill. The values for the slopes of the e -log k curves, or c_k , were 0.53 for the 5CB5 backfill, 0.11 for the 5BPN2 backfill, and 0.0057 for the 2BPN2 backfill. A steeper slope, i.e., greater c_k , indicates lesser sensitivity in k based on changes in e . Since the 5BPN2 backfill actually contained less bentonite than the 5CB5 backfill, this greater sensitivity in k due to changes in e of the 5BPN2 backfill can be attributed to the difference in the types of the backfills (i.e., BPN vs. CB).

The k of the backfill was estimated using the relationship between m_v and c_v in accordance with the following expression (e.g., Lambe and Whitman 1969):

$$k = c_v m_v \gamma_w \quad (6.3)$$

where γ_w is the unit weight of water and the values of c_v were based on the logarithm-of-time method. The estimated values of k , or k_e , are compared with the k values measured in the consolidometer for the three backfills in Fig. 6.11. The ratios of k_e to k generally range from 0.9 to 4 for the 5CB5 backfill and 0.1 to 10 for the 5BPN2 backfill as shown in Fig. 6.11. However, for the 2BPN2 backfill, the ratios vary between 10^{-3} and unity, likely as a result of the low content of BPN and the predominance of the sand matrix.

The values of k measured in the flexible-wall cells are presented in Fig. 6.12 and compared with k values measured in the consolidometer for the three backfills in Fig. 6.13. The best agreement between the two methods for measuring k occurred for the 5CB5 backfill. In contrast, the k for the 5BPN2 backfill measured with the consolidometer was greater than the k measured in the flexible-wall cell. This difference likely reflects, in part, the greater effect of the different stress conditions existing in the two types of permeameters on the BPN, since the superabsorbent polymer portion of the BPN is sensitive to stress conditions (Buchholz and Graham 1998). For the 2BPN2 backfill, all of the k values measured in the consolidometer except one were lower than those measured in the flexible-wall cell, again reflecting a significant effect of the different stress conditions existing in the two types of permeameters on this backfill.

The values of k for specimens the three backfills evaluated in this study are plotted versus the backfill bentonite content (B_B) in Fig. 6.14 along with the results for the SB backfill

specimens from Malusis and McKeehan (2012). The k values to water of the specimens with 2.44 % BPN (i.e., 2BPN2), 4.6 % NaturalGel (NG), and 4.5 % MSB were greater than the typical regulatory limit of 10^{-9} m/s. The specimen with 5.5 % BPN (5BPN2) exhibited the lowest k to water of all of the specimens tested (2.0×10^{-12} m/s). The k values to water of the specimens with 7.1 % CB (5CB5) were similar to those of the specimens with 4.6 % SW101 (a modified “contaminant resistant” bentonite), 5.6 % MSB, and 5.7 % NG (1.8×10^{-10} m/s $< k < 4.4 \times 10^{-10}$ m/s). The low k of the 5BPN2 backfill to water would be expected based on the swell index, SI , of the BPN in water compared to the SI of these different bentonites (refer to Fig. 6.15). The SI , which can be correlated with the k of the bentonite to water (Shackelford et al. 2000; Egloffstein 2001; Jo et al. 2001; Kolstad et al. 2004; Lee et al. 2005), is highest for the BPN at 73 mL/2g, whereas, the next highest SI is for the SW-101 at 43 mL/2g. The SI of the CB is similar to that of the NG investigated by Malusis and McKeehan (2012) as would be expected on the basis that both materials are unmodified Na-bentonites.

6.3.4 Hydraulic Conductivity to CaCl_2 Solutions

Values of k measured in flexible-wall cells based on permeation with water, k_w , and CaCl_2 solutions, k_c , are plotted in Figs. 6.16 and 6.17 and summarized in Table 6.6. For the two-stage tests performed using the 5CB5 backfill, the value of k_c based on permeation with the relatively dilute 5 mM CaCl_2 solution for 170 d remained essentially unchanged relative to the value of k_w for the same specimen (i.e. $k_c/k_w = 0.96$). However, permeation of specimens of the 5CB5 backfill with the stronger 50 mM CaCl_2 and 500 mM CaCl_2 solutions resulted in increases in k from an initial k_w values of 2.2×10^{-10} m/s and 2.0×10^{-10} m/s to final k_c values of 2.5×10^{-9} ($k_c/k_w = 11.4$) and 2.2×10^{-9} m/s ($k_c/k_w = 11.0$), respectively.

The one-stage tests using the 5BPN2 backfill exhibited lower values of k_c than those with 5CB5 backfill (see Fig. 6.18). For example, the value of k_c for the 5BPN2 backfill based on permeation with 50 mM CaCl_2 was almost two orders of magnitude lower than that for the 5CB5 backfill (i.e., 3.2×10^{-11} m/s vs. 2.5×10^{-9} m/s, respectively), despite the fact that the 5CB5 backfill was prehydrated by permeation with water whereas the 5BPN2 specimen was not prehydrated. Thus, even though the value of k_c for the 5BPN2 backfill based on permeation with 50 mM CaCl_2 was 15 times greater than the value of k_w for the 5BPN2 backfill (i.e., $k_c/k_w = 15$), the final k_c for the 5BPN2 backfill still was well below the typical regulatory limit of 10^{-9} m/s. In contrast, the value of k_c for the 2BPN2 backfill permeated with 50 mM CaCl_2 increased only slightly relative to the value of k_w for 2BPN2 ($k_c/k_w = 3.5$), but both the values of k_w and k_c for the 2BPN2 backfill were greater than 10^{-9} m/s. These high values of k_c and k_w for the 2BPN2 backfill as well as the relatively minor incompatibility in the 2BPN2 backfill can be attributed to an insufficient amount of BPN in the backfill, which not only reduces the susceptibility of the backfill to chemical attack, but also reduces the ability of the backfill to achieve a suitably low hydraulic conductivity.

The lower values of k for the 5BPN2 backfill are expected based on previous tests conducted on specimens containing the BPN (Scalia 2012). In these tests, GCLs containing either CB or BPN were permeated with various solutions of CaCl_2 (e.g., 5, 50, 500 mM) and the k was monitored over time. For the BPN GCLs, the values of k were lower than 9.0×10^{-11} m/s regardless of the permeant liquid, whereas with the CB GCLs, the k was as much as five orders of magnitude greater than that of the BPN GCL (i.e., 4.5×10^{-7} m/s for the CB compared to 6.5×10^{-13} m/s for the BPN when permeated with 500 mM CaCl_2). The possible mechanisms for this low k with the BPN include sorption of the Ca^{2+} by the polymer, polymer clogging the

hydraulically active pores, and "stitching" together of the granules by the in-situ polymerized chains of PAA (Scalia 2012). Despite the differences in the amounts of bentonite contained in GCLs (i.e., 100 %) versus the amounts of bentonite contained in the backfills evaluated in this study, these same mechanisms (i.e., sorption, clogging, and stitching) likely are responsible for the lower k of the 5BPN2 backfill compared to the 5CB5 backfill when permeated with solutions of CaCl_2 .

The final values of k_c for the 5CB5 backfill based on permeation with 50 mM or 500 mM CaCl_2 were greater than the typical regulatory limit of 10^{-9} m/s. These results are in contrast to the results of similar tests reported by Malusis and McKeehan (2012). The k of bentonite backfills permeated with tap water and then solutions of CaCl_2 (10 to 1000 mM) did not increase more than five-fold regardless of the concentration of CaCl_2 . The difference in these results can be attributed to at least two factors, viz., the slightly lower effective stress conditions (20 kPa versus 34.5 kPa) and the larger primary particle size in the sand used in this study versus that used by Malusis and McKeehan (2012). The mortar sand used by Malusis and McKeehan also classified as a poorly graded sand (SP), however, the mortar sand contained smaller particles which may contribute to the lower k of sand-bentonite backfill as the amount of fines has been shown to affect the k of backfill material (e.g., Yeo et al. 2005).

6.3.5 Intrinsic Permeability to CaCl_2 Solutions

The effects of changes in k , Δk , due to differences in the chemical properties of the permeant liquids versus those due to physico-chemical interactions between the permeant liquid and the soil can be ascertained by comparing the values of intrinsic permeability, K , of the specimens to the different permeant liquids where K is related to k using the following equation

(Shackelford 1994; Shackelford et al. 2000):

$$K = k \frac{\mu}{\gamma} \quad (6.4)$$

where μ is the absolute viscosity and γ is the unit weight of the permeant liquid. The use of K for comparison is advantageous in that the changes in K are due only to changes in the fabric of the soil (i.e., effects of changes in the μ and γ of the permeant liquid are removed). The intrinsic permeability values of the CB and BPN backfills are summarized in Table 6.6.

Values for the intrinsic permeability ratio, representing the ratio of K based on permeation with CaCl_2 solutions relative to K based on permeation with water, or K_c/K_w , are shown in Fig. 6.19 along with the ratios for SB backfills from Malusis and McKeehan (2012), a compacted sand-attapulgate-bentonite (S-A-B) mixture from Stern and Shackelford (1998), and a geosynthetic clay liner (GCL) containing 100 % bentonite from Lee and Shackelford (2005) and Shackelford et al. (2000). The K_c/K_w for the MSB was the lowest over the range in CaCl_2 investigated (10 – 1000 mM CaCl_2), whereas the K_c/K_w for the GCL was the highest. The K_c/K_w for the CB backfill (i.e., 5CB5) is higher than that for the NG backfill. For example, the K_c/K_w for the CB specimen permeated with 500 mM CaCl_2 [5CB5(3)] is 11 whereas the K_c/K_w for NG backfill permeated with 500 mM CaCl_2 is 3.1. These differences are likely as result of the different test conditions described above (i.e., different σ' and gradation of sand). The K_c/K_w for the 5% BPN backfill was high at 16 indicating a significant interaction between the permeant liquid (i.e., 50 mM CaCl_2) and the soil matrix.

As indicated in Fig. 6.19, the chemical resistance of the 5BPN2 backfill in terms of a change in K (or k) was not improved relative to that of both the 5CB5 backfill evaluated in this

study and the backfills investigated by Malusis and McKeehan (2012), which, in fact, were slightly better. However, because the k_w for the 5BPN2 backfill was more than two orders of magnitude (110 times) lower than that for the 5CB5 backfill, the final k_c for the 5BPN2 backfill to 50 mM CaCl₂ of 3.2×10^{-11} m/s was substantially lower than that for the 5CB5 backfill to 50 mM CaCl₂ of 2.5×10^{-9} m/s, and also substantially lower than the typical regulatory maximum k value of 1.0×10^{-9} m/s. Thus, the overall hydraulic performance of the 5BPN2 backfill was considerably better than that of the 5CB5 backfill.

6.4 SUMMARY AND CONCLUSIONS

The objective of this study was to evaluate the potential for the use of an acrylic acid polymerized bentonite, referred to as a bentonite polymer nanocomposite, or BPN, in soil-bentonite (SB) vertical cutoff walls for hydraulic containment applications. Three backfills were evaluated including two BPN backfills that consisted of clean silica sand amended with either 2 or 5 % dry BPN mixed with 2 % BPN slurry (i.e., 2BPN2 and 5BPN2, respectively), and one conventional (unmodified) bentonite, or CB, backfill that consisted of the same sand amended with 5 % dry CB mixed with a 5 % CB slurry (5CB5). The hydraulic conductivity (k) to tap water, consolidation behavior, and chemical compatibility (Δk) based on permeation with CaCl₂ solutions of the BPN backfills were evaluated and compared with those for a backfill comprised of CB.

In general, the two BPN backfills (5BPN2 and 2BPN2) were more sensitive to stress conditions than the CB backfill (5CB5). The stress-strain behavior of the 5BPN2 backfill was bi-semi-log linear. The slopes at lower effective stresses, σ' , were higher than those at higher σ' , likely as a result of the superabsorbent polymer portion of the BPN which is sensitive to stress

conditions. For example, the values of the coefficient of compression, C_c , for the 5BPN2 backfill in the stress range $5 \text{ kPa} \leq \sigma' \leq 46 \text{ kPa}$ were 2.6 times greater than those in the stress range $46 \text{ kPa} \leq \sigma' \leq 1485 \text{ kPa}$. The low C_c of 2BPN2 backfill suggests that the sand matrix dominated the compressibility of the backfill.

The values for the coefficient of consolidation, c_v , of both the 5CB5 and 5BPN2 backfills ranged from $10^{-6} \text{ m}^2/\text{s}$ to $10^{-9} \text{ m}^2/\text{s}$, and the c_v values generally increased with increasing σ' . This trend of increasing c_v with increasing σ' is consistent with the results of previous studies evaluating the consolidation properties of backfills comprised of conventional bentonite (e.g., Yeo et al. 2005), and is attributed to a greater decrease in compressibility with increasing σ' relative to decrease in hydraulic conductivity, k , with increasing σ' . In contrast, no consistent trend in c_v versus σ' was observed for the 2BPN2 backfill. The lack of a trend in c_v versus σ' for the 2BPN2 backfill was likely a result of insufficient BPN in the backfill, such that the sand matrix rather than the BPN controlled the overall behavior of the backfill.

For all backfills, the k to water decreased with increasing σ' , as expected. However, the ranges in the measured k values for each of the three backfills varied in the order: 2BPN2 backfill ($3.0 \times 10^{-7} \geq k \geq 1.4 \times 10^{-10} \text{ m/s}$) > 5CB5 backfill ($1.8 \times 10^{-10} \geq k \geq 7.4 \times 10^{-11} \text{ m/s}$) > 5BPN2 backfill ($9.3 \times 10^{-11} \geq k \geq 1.3 \times 10^{-11} \text{ m/s}$). Also, the agreement in k values measured in the consolidometer versus those measured on separate specimens in a flexible-wall permeameter was better in the case of the 5CB5 backfill than in the two backfills comprised of BPN. This relatively poorer agreement for the BPN backfills implies a greater effect of the different stress conditions in the two types of permeameters for the BPN backfills, which likely is a consequence, in part, of the sensitivity of superabsorbent polymer portion of the BPN to stress conditions.

Based on the results of flexible-wall hydraulic conductivity tests using CaCl₂ solutions, the chemical resistance of the 5BPN2 backfill was better than that of the CB backfill. For example, the k for the 5BPN2 backfill permeated with 50 mM CaCl₂ of 3.2×10^{-11} m/s was almost two orders of magnitude lower than that for the 5CB5 backfill permeated with 50 mM CaCl₂ of 2.5×10^{-9} m/s. In addition, the final values of k measured for the 5CB5 permeated with 50 and 500 mM CaCl₂ were greater than the typical regulatory limit of 10^{-9} m/s, whereas those for the 5BPN2 backfill were not. The ultimately lower k values for the 5BPN2 backfill can be attributed, in part, to the possibility of sorption of the Ca²⁺ by the polymer, polymer clogging the hydraulically active pores, and/or "stitching" together of the granules by the in-situ polymerized chains of polyacrylic acid.

Table 6.1. Index properties of two bentonites evaluated in this study.

Property	Standard	Average Value or Type [No. trials]	
		Conventional Bentonite (CB)	Bentonite Polymer Nanocomposite (BPN)
Specific Gravity	ASTM D 854 (ASTM 2006b)	2.71 [2]	2.67 [2]
Soil Classification	ASTM D 2487 (ASTM 2010a)	CH [3]	CH [3] ^a
Percent Clay (%)	ASTM D 422 (ASTM 2007)	90 [3]	96 [3]
Liquid Limit, <i>LL</i> (%)	ASTM D 4318 (ASTM 2005)	420 [4]	255 [2]
Plasticity Index, <i>PI</i> (%)	ASTM D 4318 (ASTM 2005)	381 [4]	NA
Swell Index, <i>SI</i> (mL/2g)	ASTM D 5890 (ASTM 2006a)	32 [5]	73 [5]
Solution Retention Capacity, <i>SRC</i> (mL/1g)	b	7.7 [6]	11.0 [6]

^a Based on grain-size distribution.

^b Based on procedures in Lee and Shackelford (2005) with centrifuge speed adjusted to 3000 rpm.

NA = Not applicable

Table 6.2. Chemical properties of liquids used in study.

Liquid	CaCl ₂ Concentration		Absolute Viscosity, μ (mPa-s) ^a	Unit Weight, γ (kN/m ³) ^a	<i>pH</i>	Electrical Conductivity, <i>EC</i> (mS/m) @ 25°C
	(mM)	(mg/L)				
Tap Water	--	--	1.01	9.81	7.30	8.99
CaCl ₂ Solutions	5	560	1.01	9.81	5.33	104.5
	50	5600	1.01	9.95	5.54	830
	500	56000	1.17	10.1	5.35	6430

^aFrom Malusis and McKeehan (2012).

Table 6.3. Compositions, designations, and characteristics at a slump, $-\Delta H$, of 125 mm for sand-bentonite backfills containing conventional bentonite (CB) or bentonite polymer nanocomposite (BPN).

Backfill Composition			Backfill Designation	Backfill Characteristics @ Slump, $-\Delta H$, of 125 mm	
Type of Bentonite	Amount of Bentonite Added to Sand (% by dry weight)	Amount of Bentonite in Slurry (% by dry weight)		Backfill Water Content, w_B (%)	Backfill Bentonite Content, B_B (%)
CB	5	5	5CB5	40.9	7.1
BPN	5	2	5BPN2	24.2	5.5
BPN	2	2	2BPN2	22.3	2.4

Table 6.4. Coefficients of volume change and compressibility for sand-bentonite backfills with 5 % conventional bentonite (CB) mixed with 5 % CB slurry (5CB5), 2 % bentonite polymer nanocomposite (BPN) mixed with 2 % BPN slurry (2BPN2), and 5% BPN mixed with 2 % BPN slurry (5BPN2).

Effective Stress, σ' (kPa)			Coefficient of Volume Change, m_v (1/kPa)			Coefficient of Compressibility, a_v (1/kPa)		
Initial	Final	Average	5CB5	2BPN2	5BPN5	5CB5	2BPN2	5BPN5
15	23	19	2.5×10^{-3}	8.5×10^{-4}	6.3×10^{-3}	4.9×10^{-3}	4.0×10^{-4}	1.1×10^{-2}
23	46	34.5	1.6×10^{-3}	3.1×10^{-4}	1.1×10^{-3}	3.0×10^{-3}	1.3×10^{-3}	1.9×10^{-3}
46	93	69.5	3.7×10^{-4}	3.0×10^{-5}	2.2×10^{-4}	7.1×10^{-4}	4.7×10^{-4}	3.3×10^{-4}
93	186	139.5	2.3×10^{-4}	4.6×10^{-5}	1.2×10^{-4}	4.3×10^{-4}	NR	1.7×10^{-4}
186	371	278.5	9.6×10^{-5}	2.8×10^{-5}	5.5×10^{-5}	1.7×10^{-4}	4.4×10^{-5}	7.3×10^{-5}
371	742	556.5	3.5×10^{-5}	1.5×10^{-5}	2.2×10^{-5}	6.1×10^{-5}	1.5×10^{-5}	3.0×10^{-5}
742	1485	1114	1.6×10^{-5}	8.5×10^{-6}	1.2×10^{-5}	2.9×10^{-5}	1.5×10^{-5}	1.3×10^{-5}

Table 6.5. Coefficients of consolidation for sand-bentonite backfills with 5 % conventional bentonite (CB) mixed with 5 % CB slurry (5CB5), 2 % bentonite polymer nanocomposite (BPN) mixed with 2 % BPN slurry (2BPN2), and 5% BPN mixed with 2 % BPN slurry (5BPN2).

Effective Stress, σ' (kPa)			Coefficient of Consolidation, c_v ($\times 10^{-9}$ m ² /s)						c_v (Taylor) / c_v (Casagrande)		
			Casagrande Method			Taylor Method					
Initial	Final	Average	5CB5	2BPN2	5BPN5	5CB5	2BPN2	5BPN5	5CB5	2BPN2	5BPN5
15	23	19	6.9	25	5.4	5.8	280	5.0	0.8	11	0.9
23	46	34.5	9.0	35	6.1	30	450	5.8	3.3	13	1.0
46	93	69.5	32	6.4	5.0	94	230	5.0	2.9	36	1.0
93	186	139.5	38	2.4	25	45	130	160	1.2	54	6.4
186	371	278.5	180	160	69	170	510	120	0.9	3.2	1.7
371	742	556.5	190	23	140	190	17	190	1.0	0.74	1.4
742	1485	1114	620	15	1000	450	130	530	0.7	8.7	0.5

Table 6.6. Results of flexible-wall hydraulic conductivity tests on sand-bentonite backfills containing conventional bentonite (CB) or bentonite polymer nanocomposite (BPN).

Backfill Designation ^(a)	Test of Test	Permeant Liquid(s)	Hydraulic Conductivity ^(b)			Intrinsic Permeability ^(c)		
			k_w (m/s)	k_c (m/s)	k_c/k_w	K_w (m ²)	K_c (m ²)	K_c/K_w
5CB5	2-Stage	Water/5 mM CaCl ₂	2.1×10^{-10}	2.0×10^{-10}	0.96	2.2×10^{-17}	2.1×10^{-17}	0.96
5CB5	2-Stage	Water/50 mM CaCl ₂	2.2×10^{-10}	2.5×10^{-9}	11	2.3×10^{-17}	2.5×10^{-16}	11
5CB5	2-Stage	Water/500 mM CaCl ₂	2.0×10^{-10}	2.2×10^{-9}	11	2.0×10^{-17}	2.5×10^{-16}	13
2BPN2	1-Stage	Water	1.3×10^{-7}	NA	3.4	1.3×10^{-13}	NA	3.5
2BPN2	1-Stage	50 mM CaCl ₂	NA	4.3×10^{-7}		NA	4.4×10^{-14}	
5BPN2	1-Stage	Water	2.0×10^{-12}	NA	16	2.1×10^{-19}	NA	15
5BPN2	1-Stage	50 mM CaCl ₂	NA	3.2×10^{-11}		NA	3.3×10^{-18}	

^(a) Sand-bentonite backfills with 5 % CB mixed with 5 % CB slurry (5CB5), 2 % BPN mixed 2 % BPN slurry (2BPN2), and 5 % BPN mixed with 2 % BPN slurry (5BPN2).

^(b) k_w and k_c are the hydraulic conductivities of the backfill to tap water and to solutions of CaCl₂, respectively

^(c) K_w and K_c are the intrinsic permeabilities of the backfill to tap water and to solutions of CaCl₂, respectively

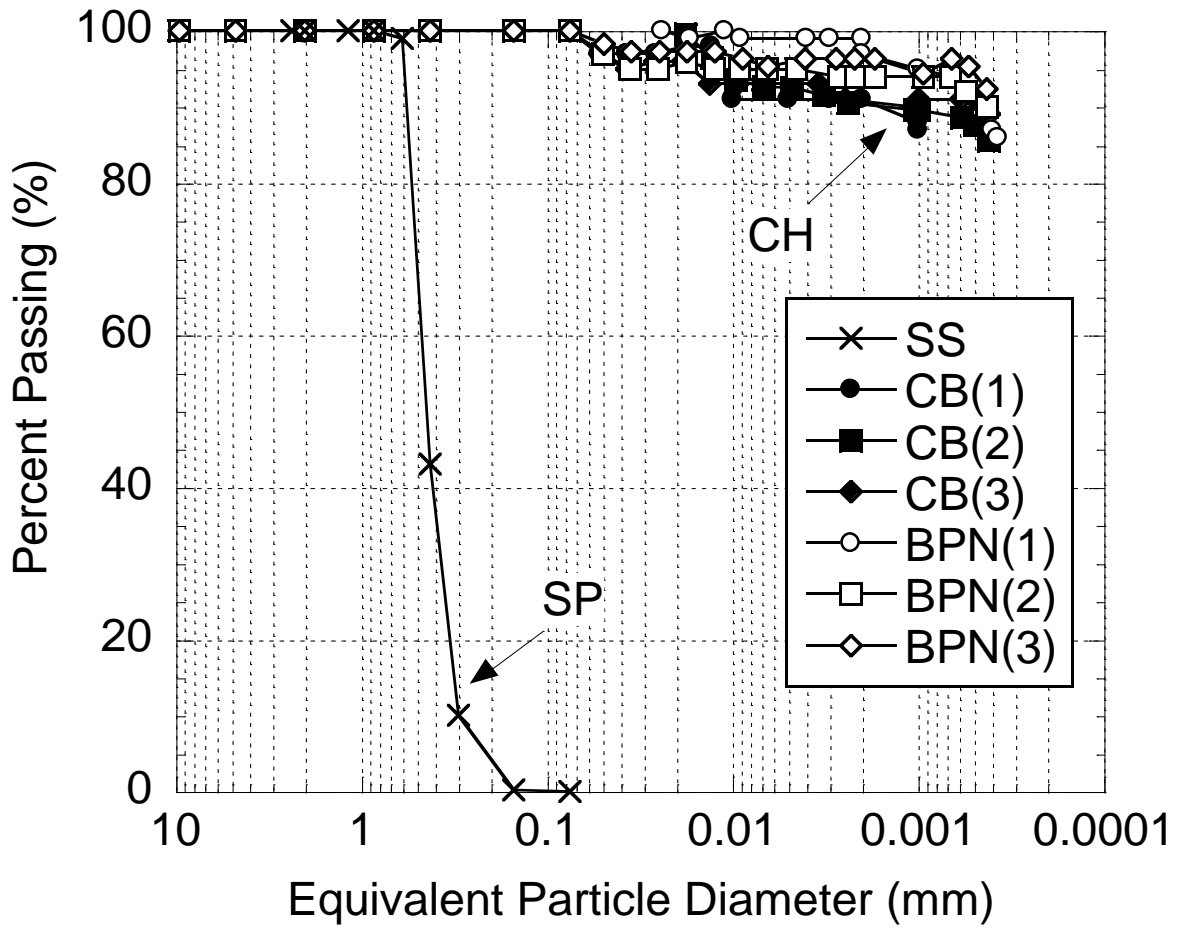


Figure 6.1. Particle-size distributions, ASTM D 422 (ASTM 2007), for silica sand (SS) and replicated samples of conventional bentonite (CB), bentonite polymer nanocomposite (BPN), and. [Notes: number in () is the sample number; SP = poorly graded sand and CH = high plasticity clay according to ASTM D 2487 (ASTM 2010a)].

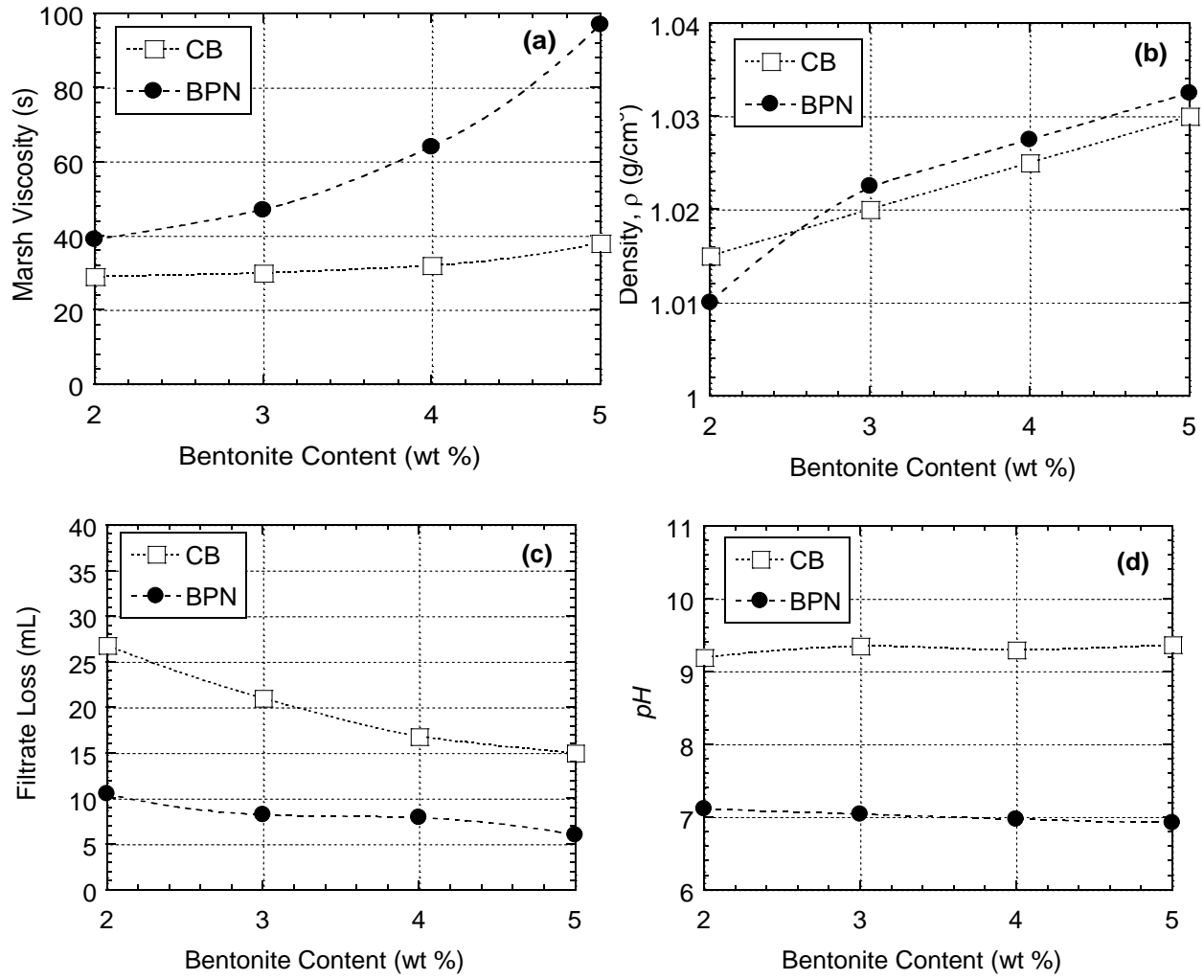


Figure 6.2. Properties of slurries of conventional bentonite (CB) and bentonite polymer nanocomposite (BPN) as a function of bentonite content: (a) Marsh viscosity; (b) density; (c) filtrate loss; (d) pH .

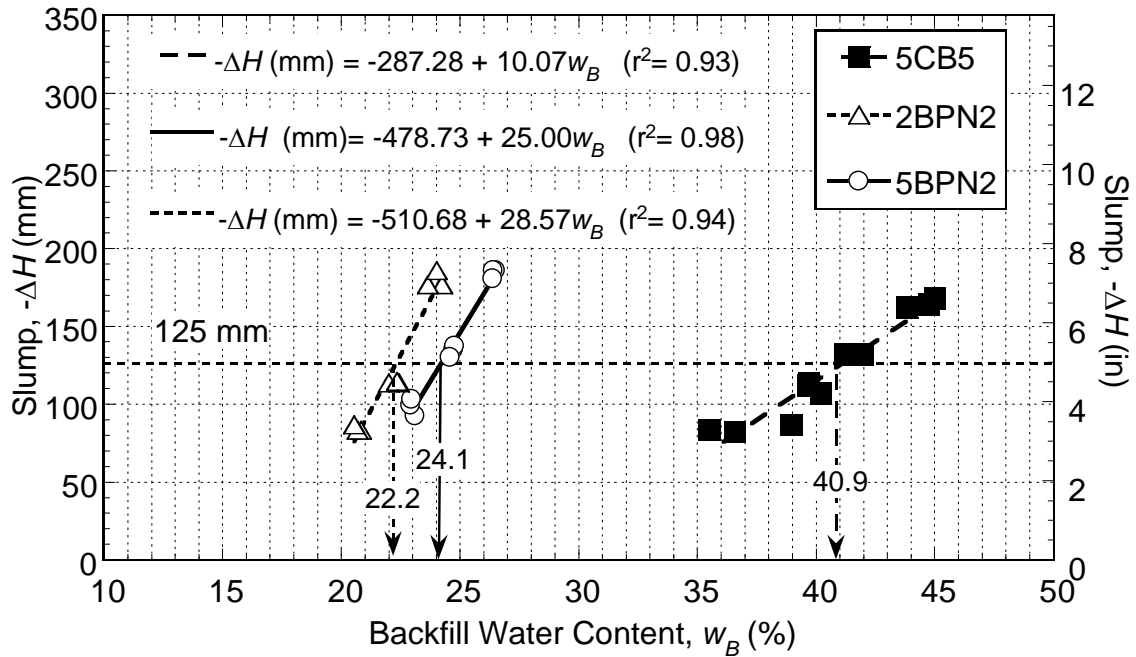


Figure 6.3. Backfill slump versus backfill gravimetric water content for sand-bentonite backfills with 5 % conventional bentonite (CB) mixed with 5 % CB slurry (5CB5), 2 % bentonite polymer nanocomposite (BPN) mixed with 2 % BPN slurry (2BPN2), and 5% BPN mixed with 2 % BPN slurry (5BPN2).

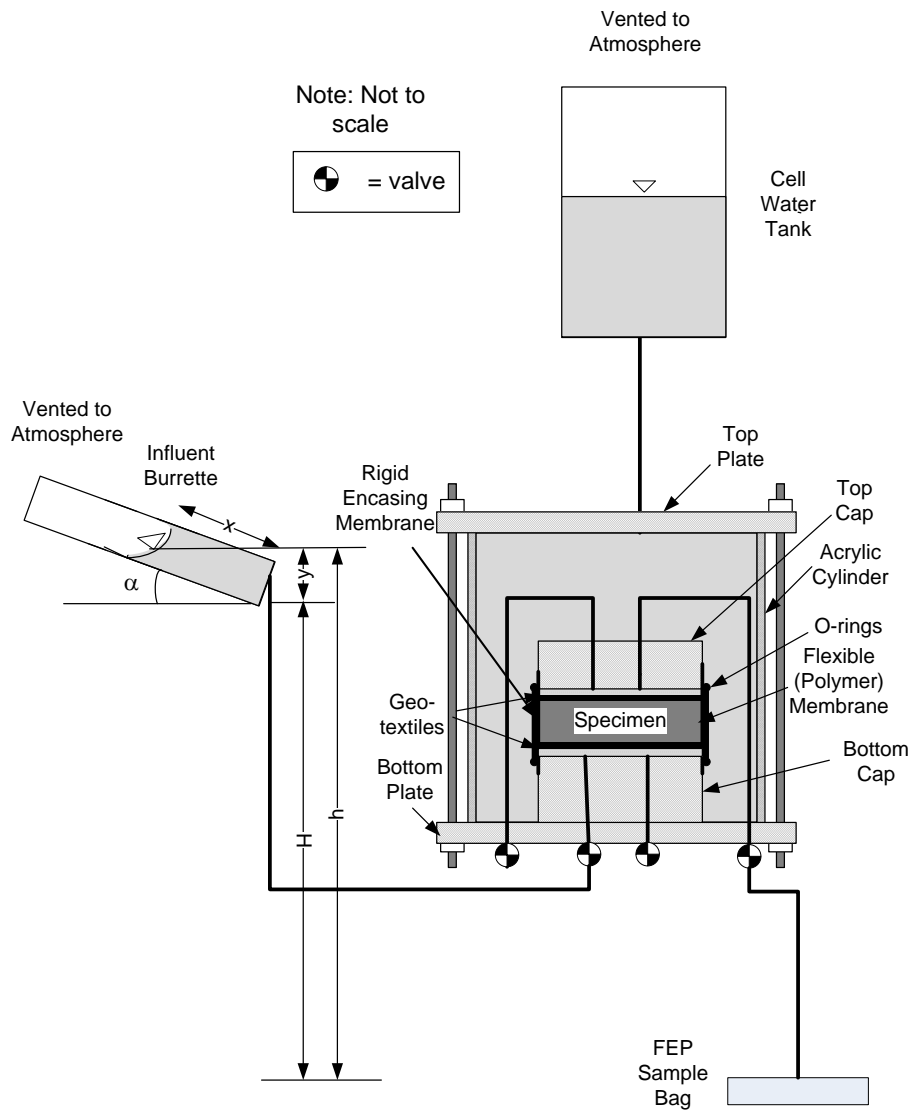


Figure 6.4. Schematic diagram illustrating falling headwater-constant tailwater permeation system for measuring hydraulic conductivity.

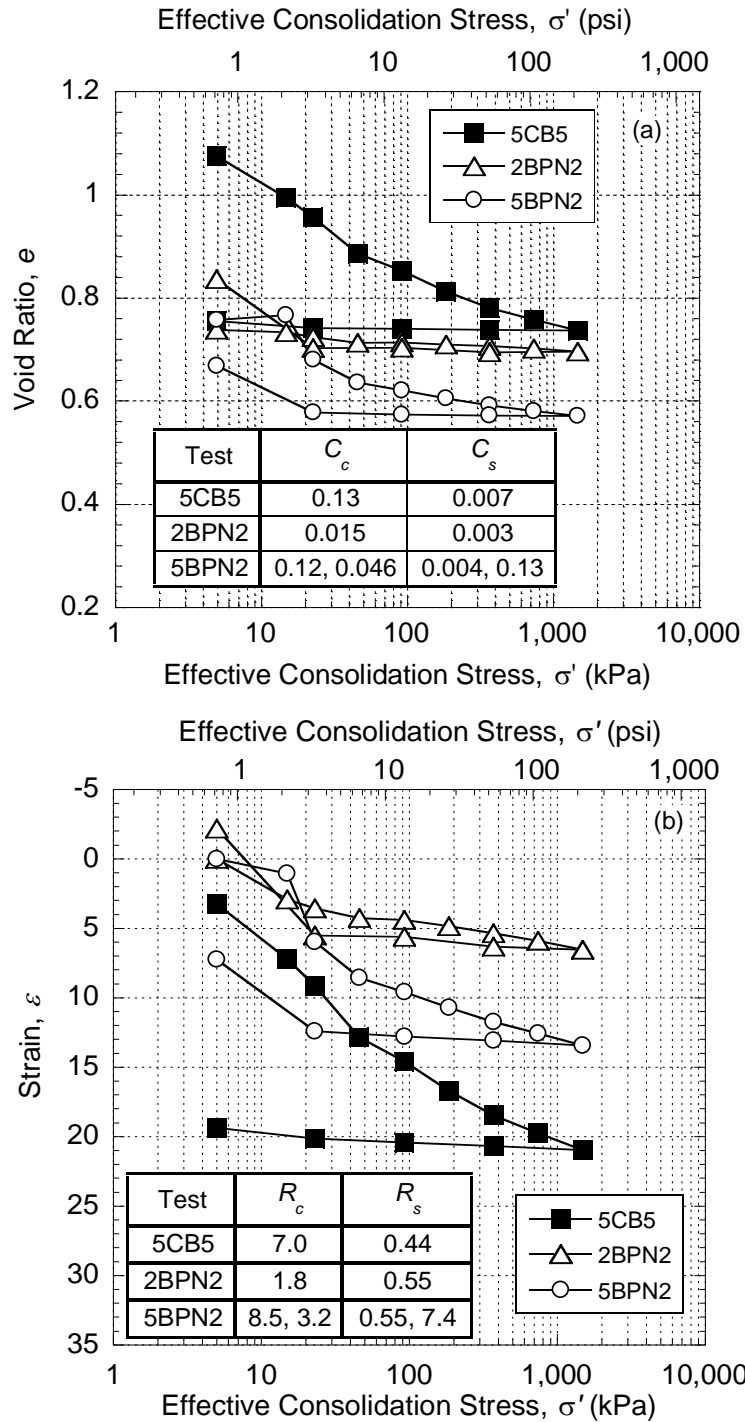


Figure 6.5. Effective consolidation stress versus (a) void ratio and (b) strain for sand-bentonite backfills with 5 % conventional bentonite (CB) mixed with 5 % CB slurry (5CB5), 2 % bentonite polymer nanocomposite (BPN) mixed with 2 % BPN slurry (2BPN2), and 5% BPN mixed with 2 % BPN slurry (5BPN2).

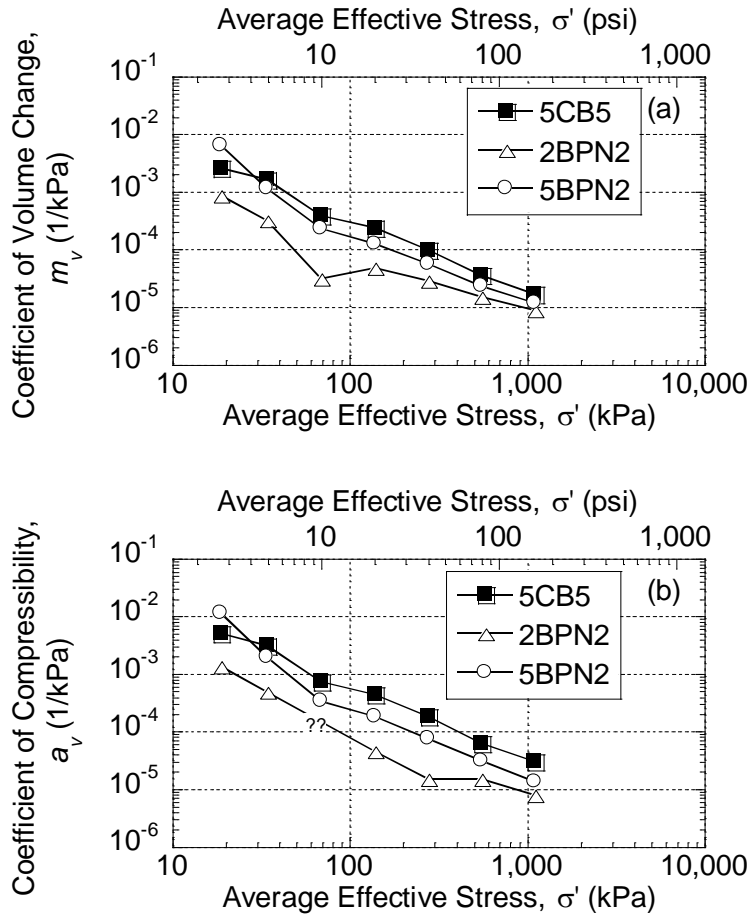


Figure 6.6. Coefficient of volume change (a) and coefficient of compressibility (b) as a function of average effective stress during loading for sand-bentonite backfills with 5 % conventional bentonite (CB) mixed with 5 % CB slurry (5CB5), 2 % bentonite polymer nanocomposite (BPN) mixed with 2 % BPN slurry (2BPN2), and 5% BPN mixed with 2 % BPN slurry (5BPN2).

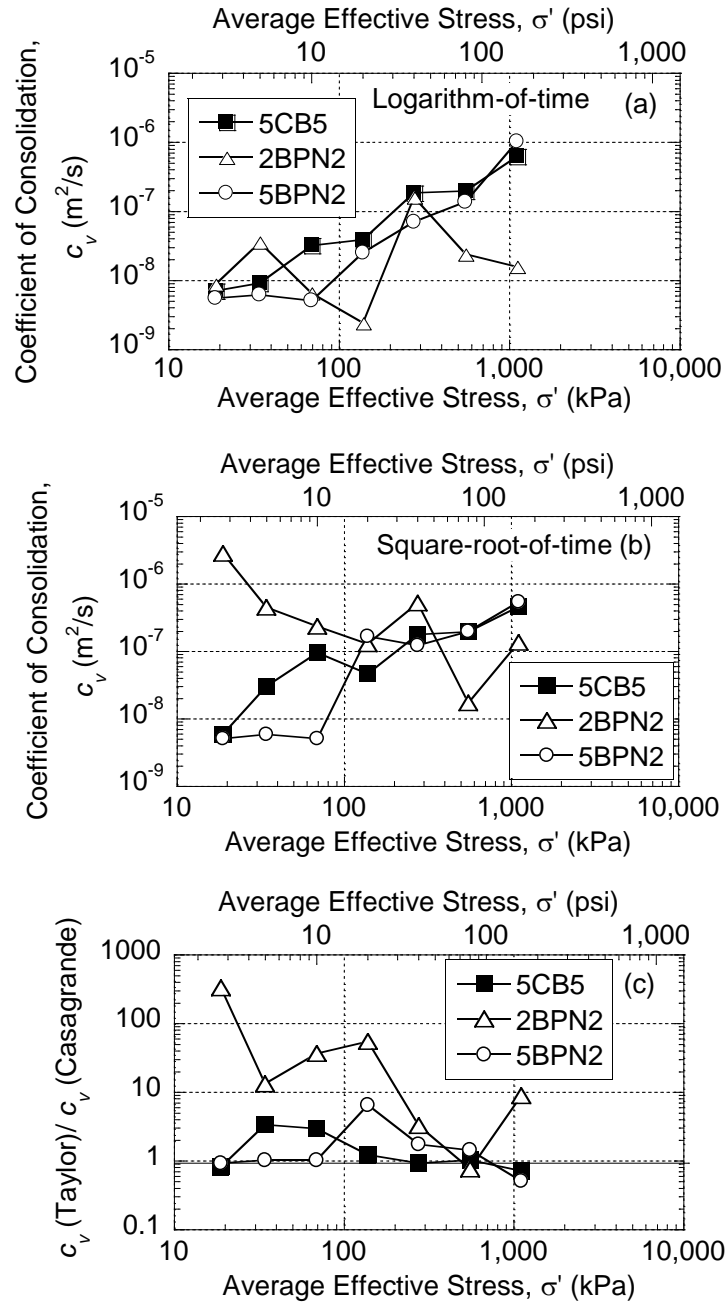


Figure 6.7. Coefficient of consolidation based on (a) Casagrande's method (b) Taylor's method and (c) a ratio of Taylor's method to Casagrande's method as a function of average effective stress during loading for sand-bentonite backfills with 5 % conventional bentonite (CB) mixed with 5 % CB slurry (5CB5), 2 % bentonite polymer nanocomposite (BPN) mixed with 2 % BPN slurry (2BPN2), and 5% BPN mixed with 2 % BPN slurry (5BPN2).

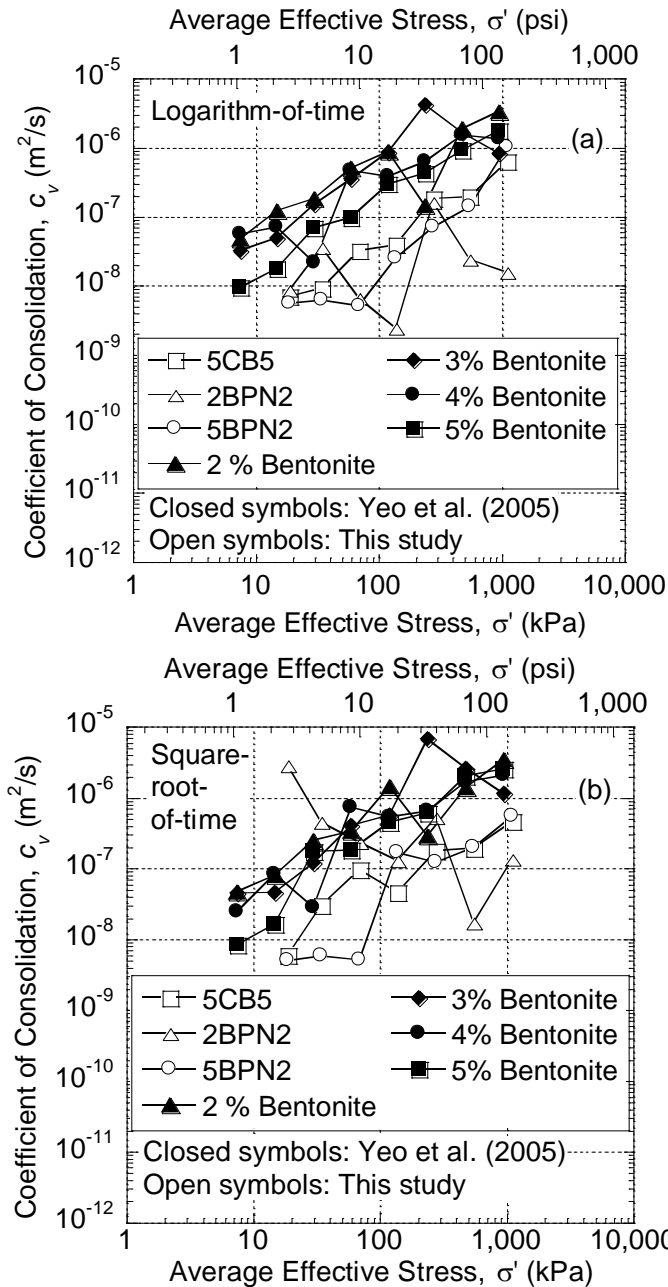


Figure 6.8. Comparisons of coefficient of consolidation based on (a) Casagrande's method (b) Taylor's method as a function of average effective stress during loading for sand-bentonite backfills with 5 % conventional bentonite (CB) mixed with 5 % CB slurry (5CB5), 2 % bentonite polymer nanocomposite (BPN) mixed with 2 % BPN slurry (2BPN2), and 5% BPN mixed with 2 % BPN slurry (5BPN2) and backfill mixtures with 2 to 5 % bentonite by dry weight from Yeo et al. (2005).

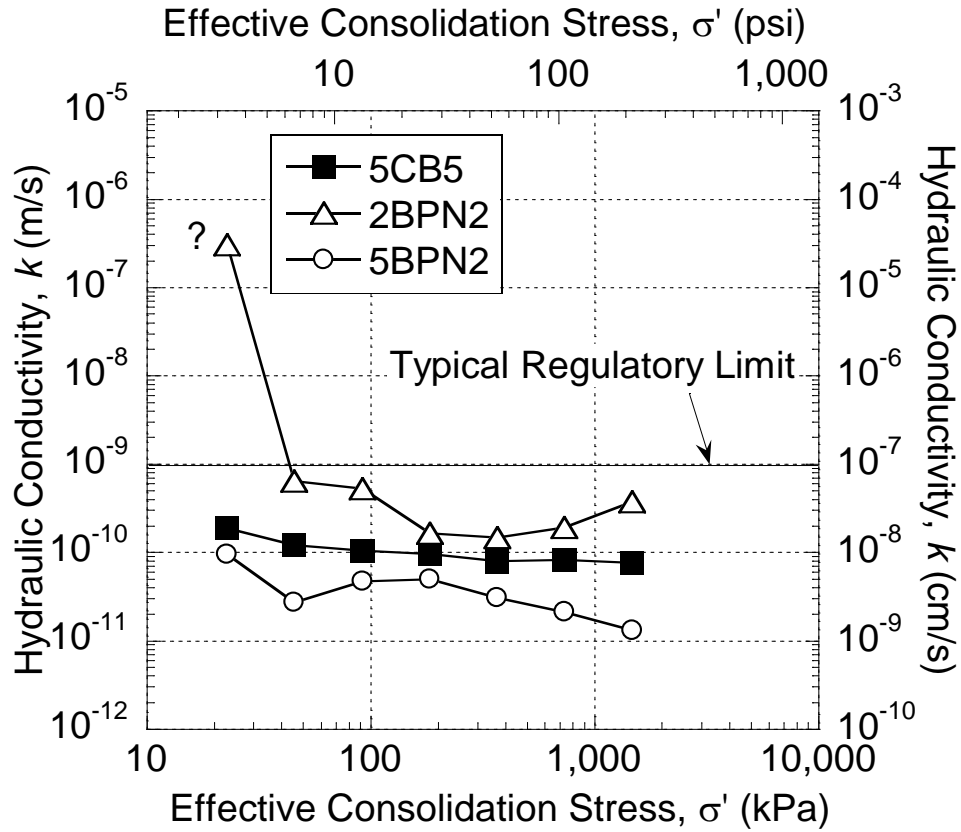


Figure 6.9. Effective consolidation stress versus measured hydraulic conductivity for sand-bentonite backfills with 5 % conventional bentonite (CB) mixed with 5 % CB slurry (5CB5), 2 % bentonite polymer nanocomposite (BPN) mixed with 2 % BPN slurry (2BPN2), and 5% BPN mixed with 2 % BPN slurry (5BPN2).

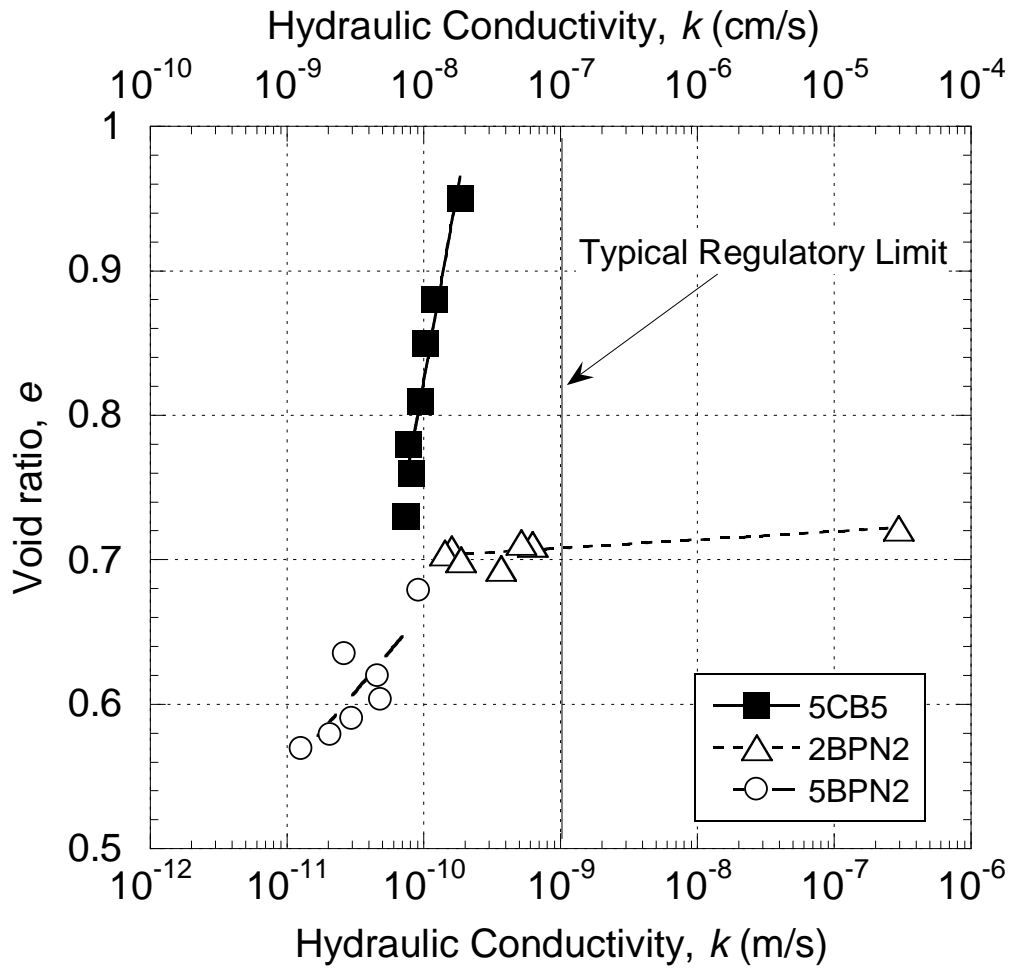


Figure 6.10. Measured hydraulic conductivity versus void ratio for sand-bentonite backfills with 5 % conventional bentonite (CB) mixed with 5 % CB slurry (5CB5), 2 % bentonite polymer nanocomposite (BPN) mixed with 2 % BPN slurry (2BPN2), and 5% BPN mixed with 2 % BPN slurry (5BPN2).

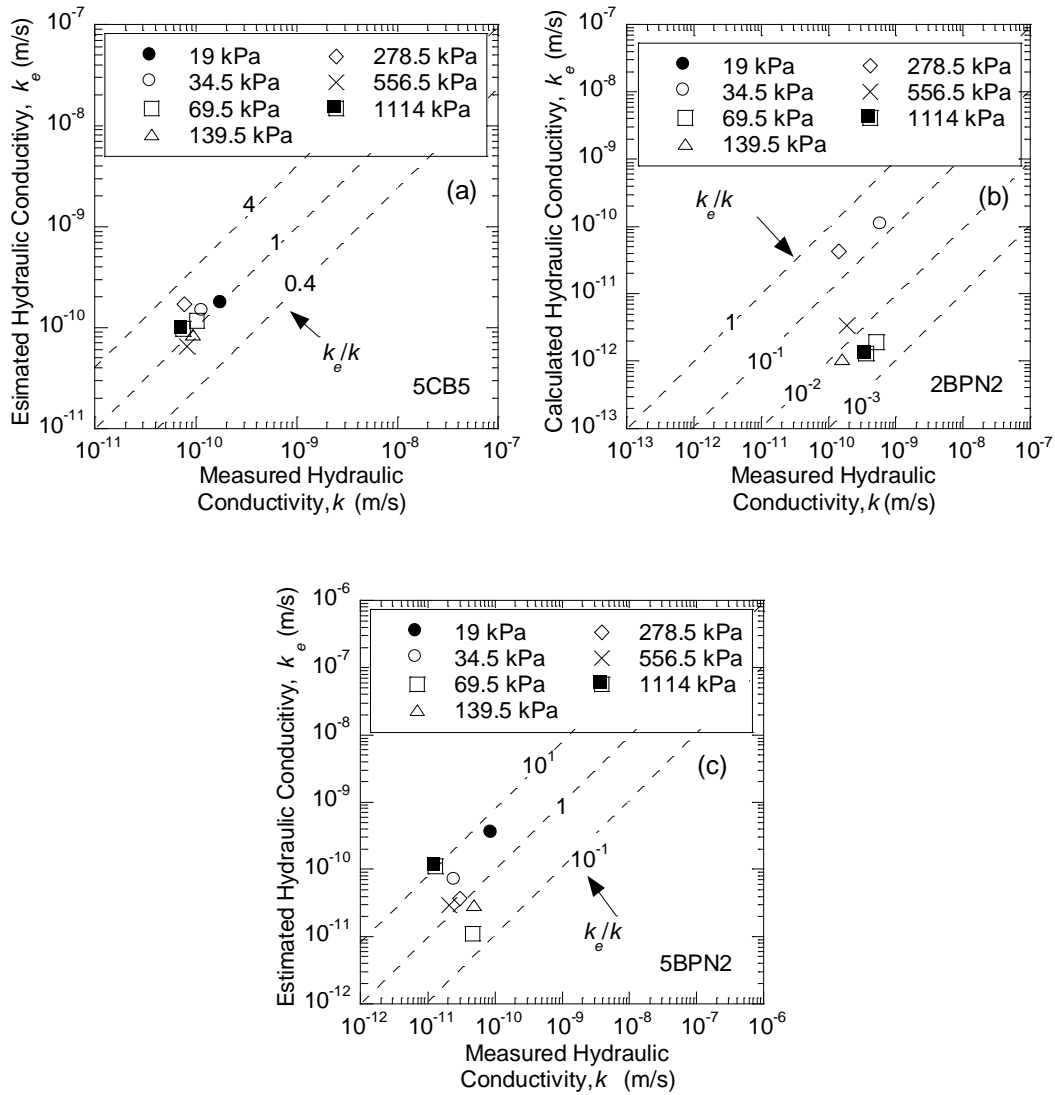


Figure 6.11. Comparison between measured and estimated hydraulic conductivity for (a) sand-bentonite backfills with 5 % conventional bentonite (CB) mixed with 5 % CB slurry (5CB5), (b) 2 % bentonite polymer nanocomposite (BPN) mixed with 2 % BPN slurry (2BPN2), (c) and 5% BPN mixed with 2 % BPN slurry (5BPN2).

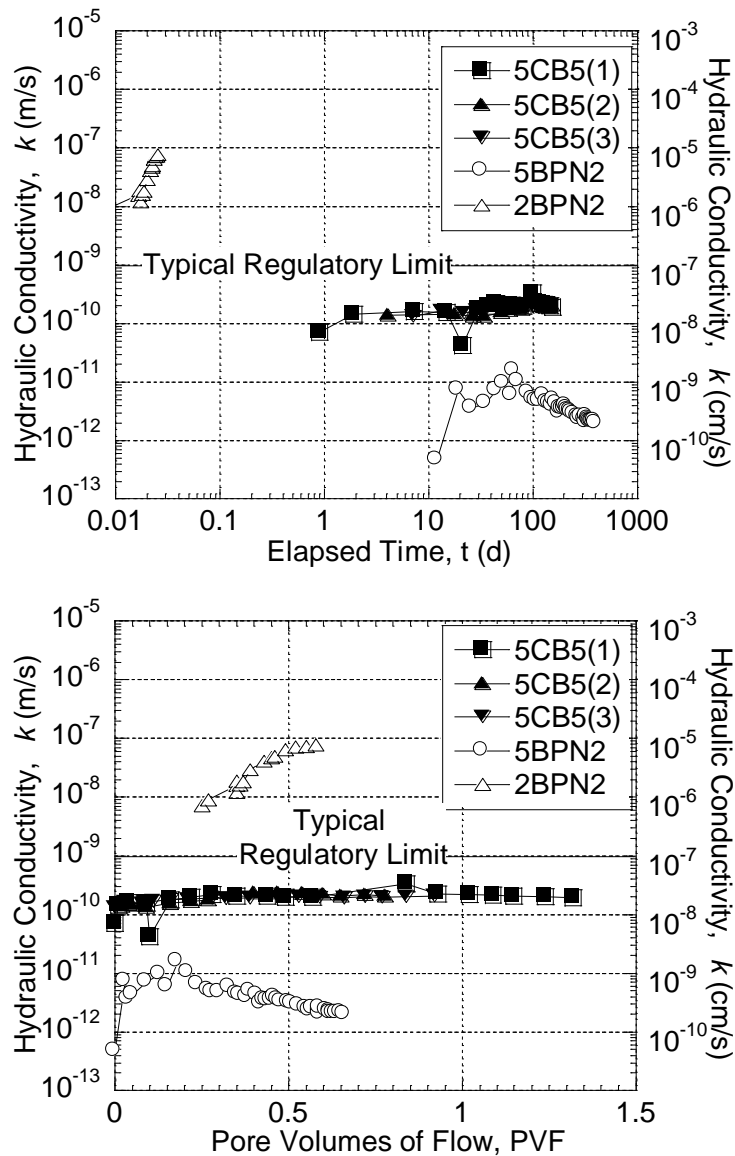


Figure 6.12. Hydraulic conductivity measured in flexible-wall cells based on permeation with water versus (a) time and (b) pore volumes of flow for replicated specimens of sand-bentonite backfills 5 % conventional bentonite (CB) mixed with 5 % CB slurry (5CB5), and individual specimens of sand-bentonite backfills with 2 % bentonite polymer nanocomposite (BPN) mixed with 2 % BPN slurry (2BPN2) and 5% BPN mixed with 2 % BPN slurry (5BPN2).

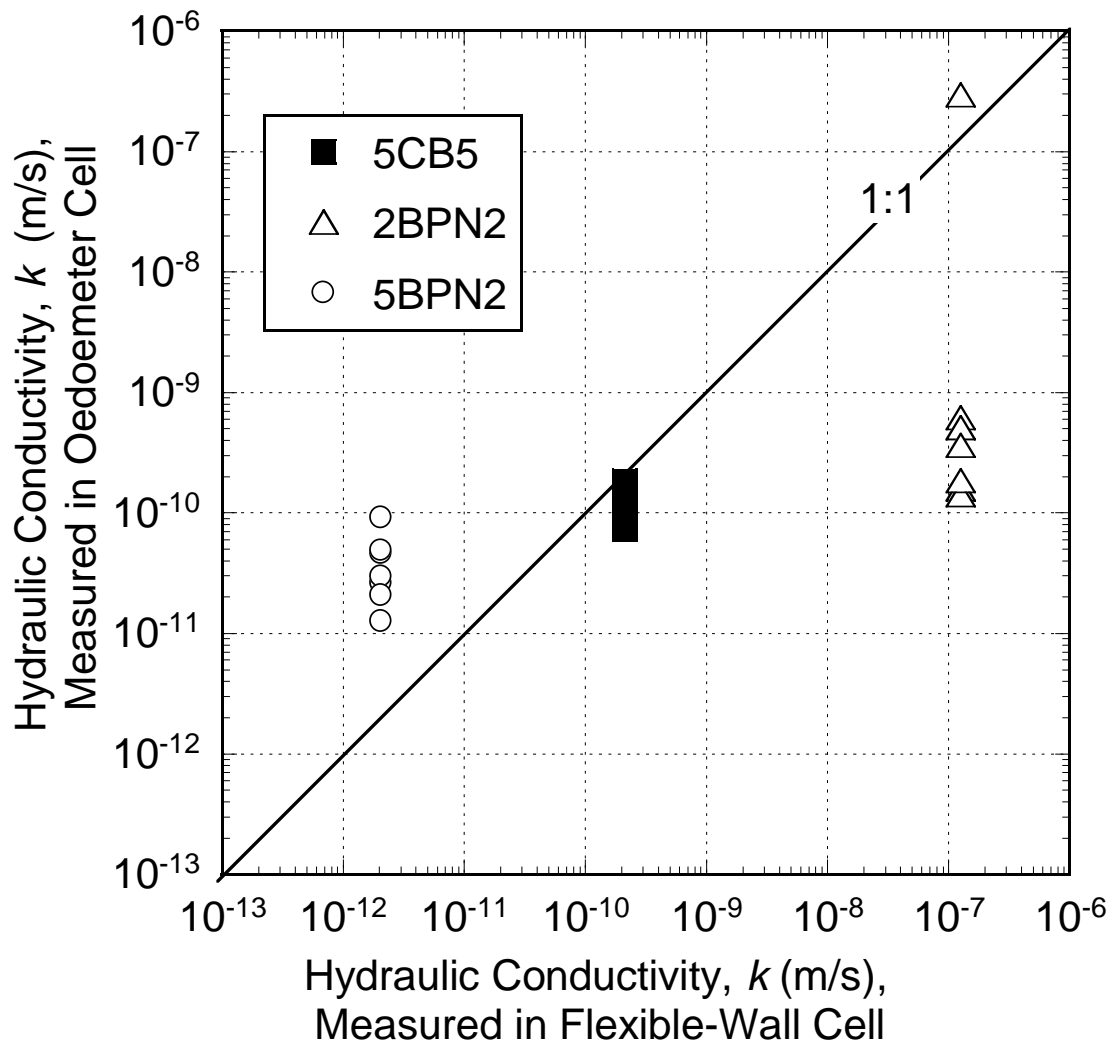


Figure 6.13. Correlation between geometric mean hydraulic conductivity measured in a flexible-wall cell at an average effective stress, σ' , of 20 kPa (2.9 psi) versus the hydraulic conductivity measured in a consolidometer cell at 23 kPa (3.3 psi) $\leq \sigma' \leq 1485$ kPa (215 psi) for sand-bentonite backfills with 5 % conventional bentonite (CB) mixed with 5 % CB slurry (5CB5), 2 % bentonite polymer nanocomposite (BPN) mixed with 2 % BPN slurry (2BPN2), and 5% BPN mixed with 2 % BPN slurry (5BPN2).

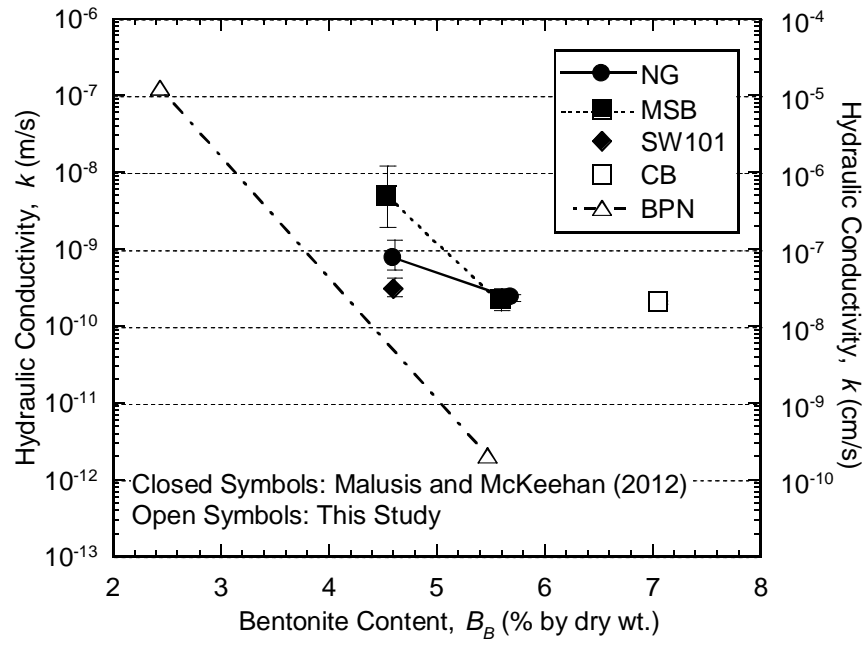


Figure 6.14. Hydraulic conductivity to tap water as a function of bentonite content for different backfills (modified after Malusis and McKeehan 2012).

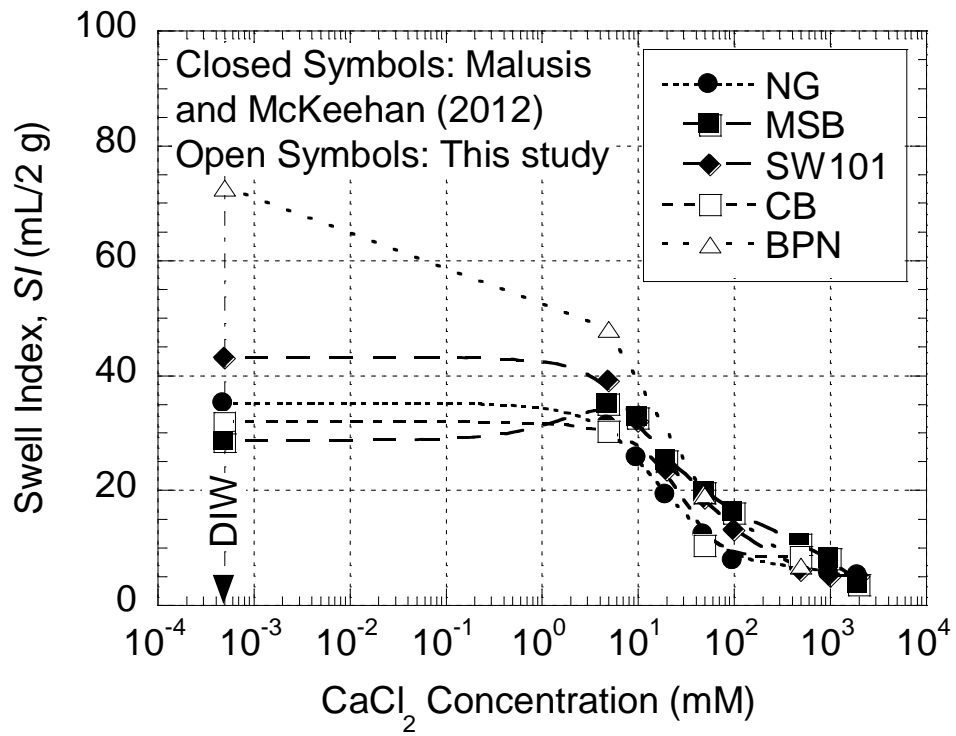


Figure 6.15. Swell index of different backfills as a function of CaCl_2 concentration (modified after Malusis and McKeehan 2012).

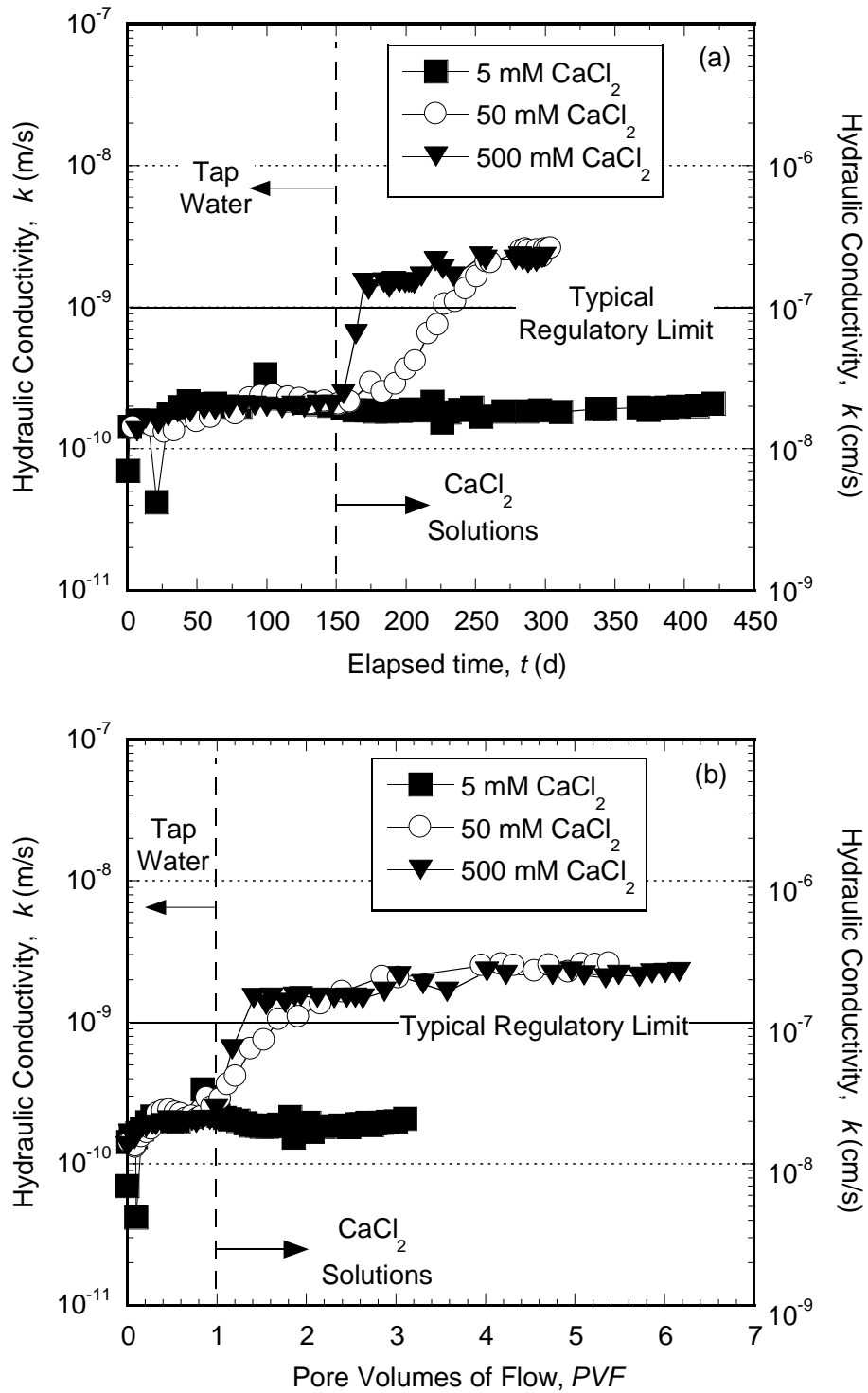


Figure 6.16. Hydraulic conductivity measured in flexible-wall cells versus (a) elapsed time and (b) pore volumes of flow for sand-bentonite backfills with 5 % conventional bentonite (CB) mixed with 5 % CB slurry (5CB5).

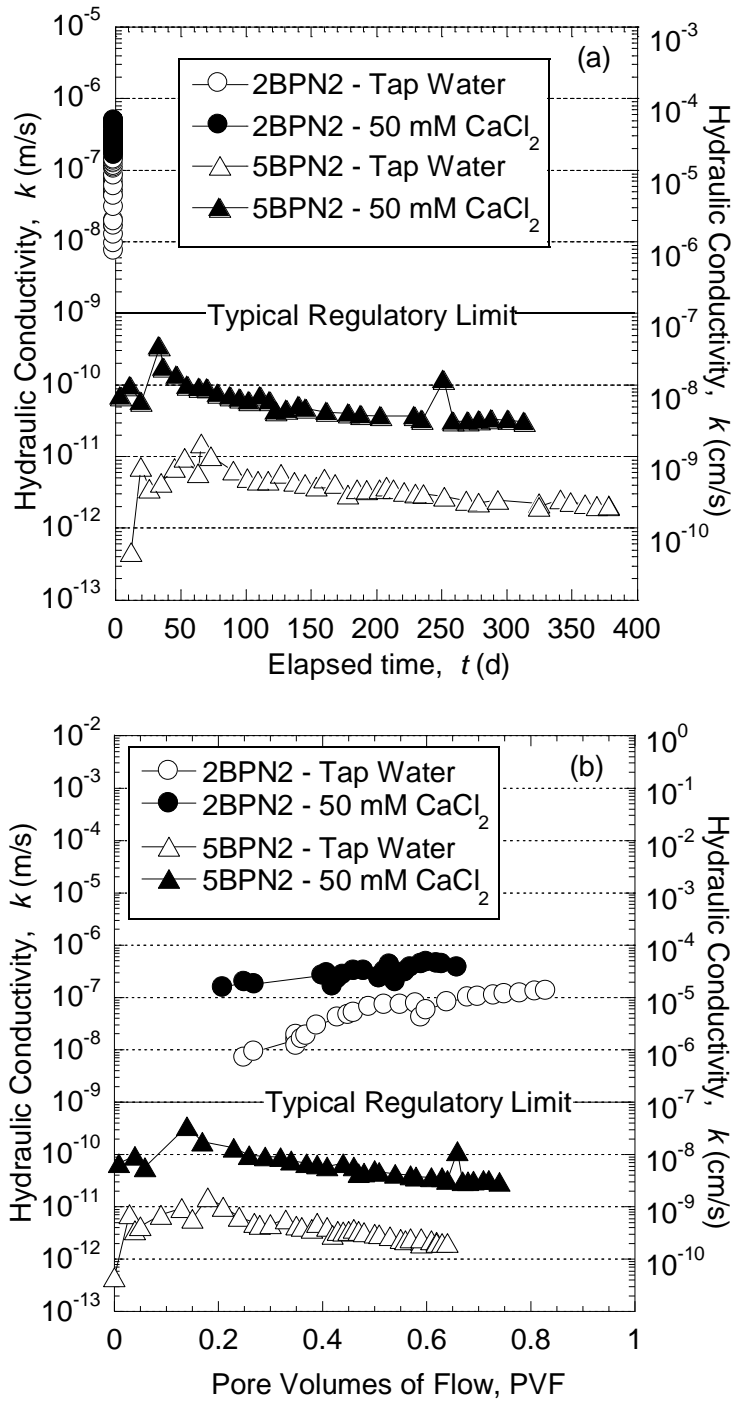


Figure 6.17. Hydraulic conductivity measured in flexible-wall cells versus (a) elapsed time and (b) pore volumes of flow for sand-backfills with 2 % bentonite polymer nanocomposite (BPN) mixed with 2 % BPN slurry (2BPN2) and 5 % BPN mixed with 2 % BPN slurry (5BPN2).

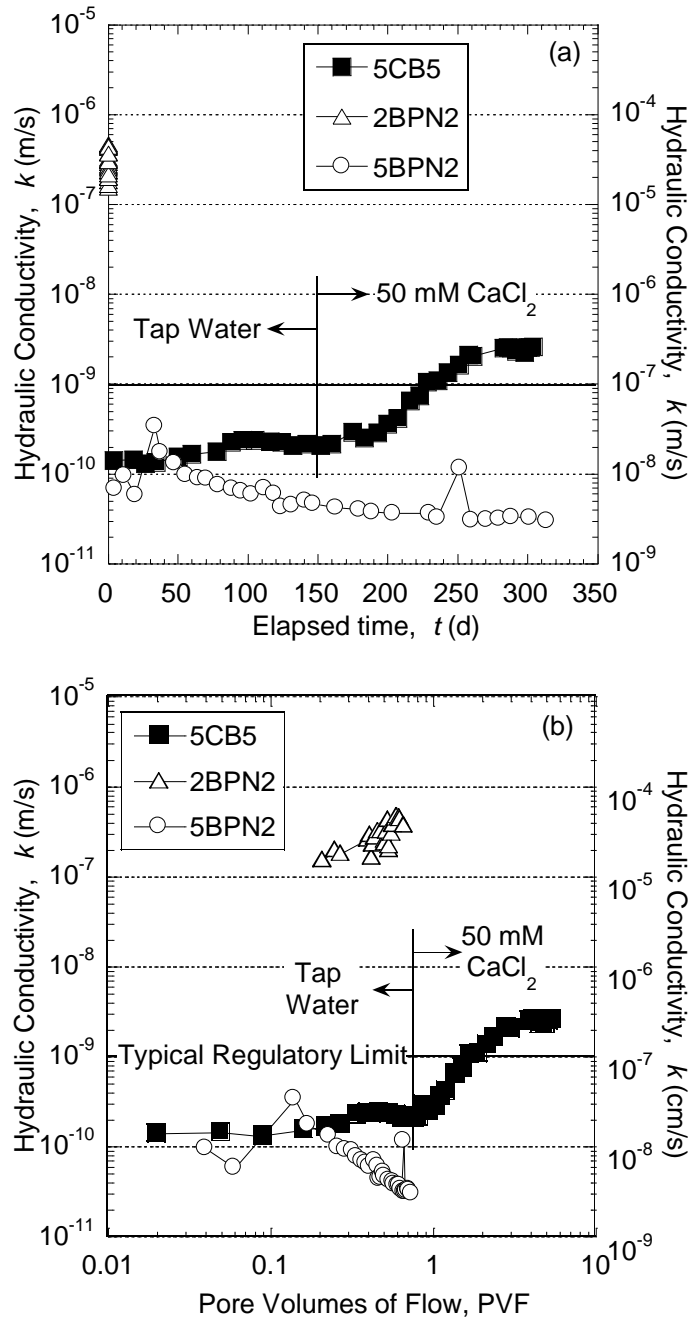


Figure 6.18. Hydraulic conductivity measured in flexible-wall cells versus (a) elapsed time and (b) pore volumes of flow measured in flexible-wall cells for sand-bentonite backfills with 5 % conventional bentonite (CB) mixed with 5 % CB slurry (5CB5), 2 % bentonite polymer nanocomposite (BPN) mixed with 2 % BPN slurry (2BPN2), and 5% BPN mixed with 2 % BPN slurry (5BPN2).

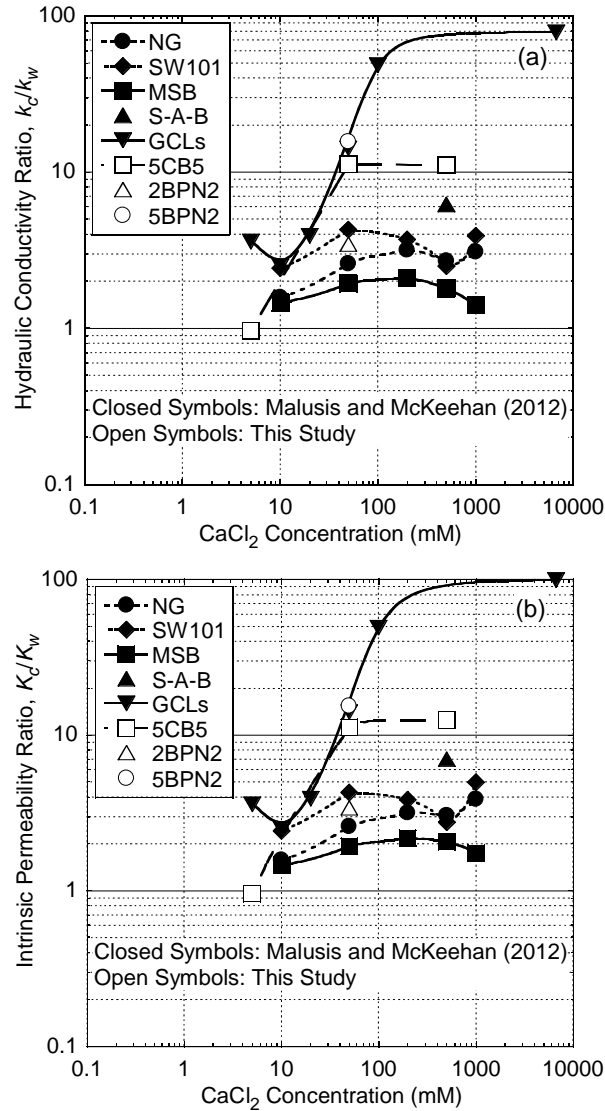


Figure. 6.19. Hydraulic conductivity ratios (k_c/k_w) and intrinsic permeability ratios (K_c/K_w) for soil-bentonite backfills containing NaturalGel (NG) bentonite, SW101 bentonite, and multi-swelling bentonite (MSB), a compacted sand-attapulgite-bentonite (S-A-B) mixture containing 10 % attapulgite clay and 10 % bentonite, granular bentonite GCLs, and sand-bentonite backfills with 5 % conventional bentonite (CB) mixed with 5 % CB slurry (5CB5), 2 % bentonite polymer nanocomposite (BPN) mixed with 2 % BPN slurry (2BPN2), and 5% BPN mixed with 2 % BPN slurry (5BPN2) (modified after Malusis and McKeehan 2012).

References

- API. (2003). "Recommended practice standard procedure for field testing water-based drilling fluids." API recommended practice 13B-1, American Petroleum Institute, Washington, D.C.
- ASTM. (2004). "Standard test methods for one-dimensional consolidation properties of soils using incremental loading." ASTM D2435, ASTM International, West Conshohocken, PA.
- ASTM. (2005). "Standard test methods for liquid limit, plastic limit, and plasticity index of soils." ASTM D4318, ASTM International, West Conshohocken, PA.
- ASTM. (2006a). "Standard test method for swell index of clay mineral component of geosynthetic clay liners." ASTM D5890 ASTM International, West Conshohocken, PA.
- ASTM. (2006b). "Standard test methods for specific gravity of soil solids by water pycnometer." ASTM D854, ASTM International, West Conshohocken, PA.
- ASTM. (2007). "Standard test method for particle-size analysis of soils." ASTM D422-63, ASTM International, West Conshohocken, PA.
- ASTM. (2009). "Standard test method for slump of hydraulic-cement concrete." ASTM C143, ASTM International, West Conshohocken, PA.
- ASTM. (2010a). "Standard practice for classification of soils for engineering purposes (Unified Soil Classification System)." ASTM D2487, ASTM International, West Conshohocken, PA.
- ASTM. (2010b). "Standard test methods for measurement of hydraulic conductivity of saturated porous materials using a flexible wall permeameter." ASTM D5084, ASTM International, West Conshohocken, PA.
- Beirck, B. R., and Chang, W. C. (1994) "Contaminant transport through soil-bentonite slurry walls: Attenuation by activated carbon." *Water Environmental Federation Specialty Conf. on Innovative Solutions for Contaminated Site Management*, Miami, 461-472.
- Buchholz, F., and Graham, A. (1998). *Modern Superabsorbent Polymer Technology*, Wiley, New York.
- D'Appolonia, D. J. (1980). "Soil-bentonite slurry trench cutoffs." *Journal of the Geotechnical Engineering* 106(4), 399-417.
- Duncan, J. M. (1993). "Limitations of conventional analysis of consolidation settlement." *Journal of Geotechnical Engineering*, 119(9), 1333-1359.

- Egloffstein, T. A. (2001). "Natural bentonites influence of the ion exchange and partial desiccation on permeability and self-healing capacity of bentonites used in GCLs." *Geotextiles and Geomembranes*, 19(7), 427-444.
- Evans, J. C. (1993). "Vertical cutoff walls." *Geotechnical Practices for Waste Disposal*, D. E. Daniel, ed., Chapman & Hall, London, 430 - 454.
- Evans, J. C., Shackelford, C. D., Yeo, S. S., and Henning, J. (2008). "Membrane behavior of soil-bentonite slurry-trench cutoff walls." *Soil & Sediment Contamination*, 17(4), 316-322.
- Hong, C. S., Shackelford, C. D., and Malusis, M. A. (2012). "Consolidation and hydraulic conductivity of zeolite amended soil-bentonite backfills." *Journal of Geotechnical and Geoenvironmental Engineering*, 138(1), 15-25.
- Jo, H. Y., Benson, C. H., Shackelford, C. D., Lee, J. M., and Edil, T. B. (2005). "Long-term hydraulic conductivity of a geosynthetic clay liner permeated with inorganic salt solutions." *Journal of Geotechnical and Geoenvironmental Engineering*, 131(4), 405-417.
- Jo, H. Y., Katsumi, T., Benson, C. H., and Edil, T. B. (2001). "Hydraulic conductivity and swelling of nonprehydrated GCLs permeated with single-species salt solutions." *Journal of Geotechnical and Geoenvironmental Engineering*, 127(7), 557-567.
- Katsumi, T., Kamon, M., Inui, T., and Araki, S. (2008) "Hydraulic barrier performance of SBM cut-off wall constructed by the trench cutting and re-mixing deep wall method." *GeoCongress 2008: Geotechnics of Waste Management and Remediation*, New Orleans, Louisiana, 628-635.
- Kolstad, D. C., Benson, C. H., and Edil, T. B. (2004). "Hydraulic conductivity and swell of nonprehydrated geosynthetic clay liners permeated with multispecies inorganic solutions." *Journal of Geotechnical and Geoenvironmental Engineering*, 130(12), 1236-1249.
- LaGrega, M. D., Buckingham, P. L., and Evans, J. C. (2001). *Hazardous Waste Management*, McGraw-Hill, Boston, MA.
- Lambe, T. W. and Whitman, R. V. (1969) *Soil mechanics*, John Wiley & Sons, Inc., New York, NY.
- Lee, J.-M., and Shackelford, C. D. (2005). "Concentration dependency of the prehydration effect for a geosynthetic clay liner." *Soils and Foundations*, 45(5), 27-41.
- Lee, J. M., Shackelford, C. D., Benson, C. H., Jo, H. Y., and Edil, T. B. (2005). "Correlating index properties and hydraulic conductivity of geosynthetic clay liners." *Journal of Geotechnical and Geoenvironmental Engineering*, 131(11), 1319-1329.

- Malusis, M. A., Barben, E. J., and Evans, J. C. (2009). "Hydraulic conductivity and compressibility of soil-bentonite backfill amended with activated carbon." *Journal of Geotechnical and Geoenvironmental Engineering*, 135(5), 664-672.
- Malusis, M. A., Evans, J. C., McLane, M. H., and Woodward, N. R. (2008). "A miniature cone for measuring the slump of soil-bentonite cutoff wall backfill." *Geotechnical Testing Journal*, 31(5), 373-380.
- Malusis, M. A., and McKeehan, M. D. (2012). "Chemical compatibility of model soil-bentonite backfills containing multiswellable bentonite." *Journal of Geotechnical and Geoenvironmental Engineering*. In press.
- Malusis, M. A., McKeehan, M. D., and LaFredo, R. A. (2010). "Multiswellable bentonite for soil-bentonite vertical barriers." Sixth International Congress on Environmental Geotechnics, McGraw-Hill, New Dehli, India, 764-769.
- Muzny, C. D., Butler, B. D., Hanley, H. J. M., Tsvetkov, F., and Peiffer, D. G. (1996). "Clay platelet dispersion in a polymer matrix." *Materials Letters*, 28(4-6), 379-384.
- Olsen, R. E., and Daniel, D. E. (1981). "Measurement of the hydraulic conductivity of fine-grained soils." *Permeability and Groundwater Contaminant Transport*, ASTM STP 746, T. F. Zimmie and C. O. Rigs, eds., ASTM, West Conshohoken, PA, 18-64.
- Olson, R. E. (1998). "Settlement of embankments on soft clays." *Journal of Geotechnical and Geoenvironmental Engineering*, 124(8), 659-669.
- Onikata, M., Kondo, M., Hayashi, N., and Yamanaka, S. (1999). "Complex formation of cation-exchanged montmorillonites with propylene carbonate: Osmotic swelling in aqueous electrolyte solutions." *Clays and Clay Minerals*, 47(5), 672-677.
- Ressi, A., and Cavalli, N. (1985). "Bentonite slurry trenches." *Engineering Geology*, 21(3-4), 333-339.
- Ryan, C. R. (1987). "Vertical barriers in soil for pollution containment." *Geotechnical Practice for Waste Disposal '87*, R. D. Woods, ed., ASCE, Reston, VA, 182-204.
- Scalia, J. (2012). "Bentonite-polymer composites for containment applications" PhD Dissertation, University of Wisconsin - Madison, Madison, WI.
- Scalia, J., Benson, C. H., Edil, T. B., Bohnhoff, G. L., and Shackelford, C. D. (2011). "Geosynthetic clay liners containing bentonite polymer nanocomposite." *Geo-Frontiers 2011*, J. Han and D. Alzamora, eds., ASCE, Reston, VA, 2001-2009.

- Shackelford, C. D. (1994). "Waste-soil interactions that alter hydraulic conductivity." *Hydraulic Conductivity and Waste Contaminant Transport in Soil*, ASTM STP 1142, D. E. Daniel and S. G. Trautwein, eds., ASTM, West Conshohocken, PA, 111-168.
- Shackelford, C. D., Benson, C. H., Katsumi, T., Edil, T. B., and Lin, L. (2000). "Evaluating the hydraulic conductivity of GCLs permeated with non-standard liquids." *Geotextiles and Geomembranes*, 18(2-4), 133-161.
- USEPA. (1984). *Slurry trench construction for pollution migration control*, EPA 540, U.S. Environmental Protection Agency, Office of Emergency and Remedial Response, Office of Research and Development, Washington DC.
- USEPA. (1992). *Slurry walls*, U.S. Environmental Protection Agency, Office of Emergency and Remedial Response, Office of Research and Development, Washington, DC.
- Xanthakos, P. P. (1979). *Slurry walls*, McGraw-Hill, New York.
- Yeo, S. S., Shackelford, C. D., and Evans, J. C. (2005). "Consolidation and hydraulic conductivity of nine model soil-bentonite backfills." *Journal of Geotechnical and Geoenvironmental Engineering*, 131(10), 1189-1198.

Chapter 7

Summary and Conclusions

7.1 SUMMARY

This document presented the results of an investigation into the feasibility of using a polymerized bentonite, referred to as a bentonite polymer nanocomposites, or BPN, in geoenvironmental containment applications. The membrane behavior and diffusive properties of BPN exposed to potassium chloride, KCl, or calcium chloride, CaCl₂, were determined and compared with those properties of conventional (unmodified) and modified bentonites reported in literature. In addition, the potential to use BPN as a substitute for conventional bentonite in soil-bentonite (SB) backfills for cutoff walls was investigated.

7.2 CONCLUSIONS

Based on the objectives and results presented in this document, the following conclusions can be drawn:

- The results of the evaluation of physical and chemical properties of the BPN, including the swell index, *SI*, and solution retention capacity, performed using calcium chloride, CaCl₂, solutions implied that the BPN would be more resistant to chemical attack than untreated or conventional bentonites when exposed to dilute solutions containing divalent cations such as CaCl₂. For example, the *SI* of BPN with 5 mM CaCl₂ was 50 mL/2g, whereas the previously reported *SI* of conventional bentonites ranged from 26.9 to 29.8 mL/2g.
- The BPN exhibited membrane behavior when exposed to potassium chloride (KCl) with concentrations ranging from 4.7 mM to 54 mM KCl, and this membrane behavior was

enhanced compared to that for a geosynthetic clay liner, GCL, containing conventional bentonite. For example, the ω value measured in this study for a BPN specimen contained within a rigid-wall cell and based on circulation of 20 mM KCl was 0.43, whereas that previously reported for a GCL specimen containing a conventional bentonite under similar testing conditions except at a lower porosity (0.74 vs. 0.92) was only 0.30.

- In agreement with previously reported results for conventional bentonite contained in a GCL, the diffusive properties of the BPN correlated well with the membrane behavior of the BPN. However, the lower matrix tortuosity for the BPN compared to that of a GCL at a similar porosity, suggested that the interconnected pores of the BPN were more tortuous than the GCL, which likely was due, in part, to the existence of the superabsorbent polymer in the pores of the BPN specimens.
- The BPN offers enhanced resistance to membrane degradation relative to that previously shown to exist for traditional (unmodified) and other polymer modified bentonites. However, the enhanced membrane behavior was only incremental with respect to CaCl_2 concentration, and was affected by the type of cell (rigid-wall vs. flexible-wall) in which the membrane behavior was evaluated.
- The use of BPN as a substitute for conventional bentonite in a soil-bentonite vertical cutoff walls is feasible. Although the BPN backfill was more sensitive to stress conditions than the CB backfill, the overall hydraulic performance backfill containing 5 % dry BPN was significantly better than that of the backfill containing 5 % dry conventional bentonite.

7.3 RECOMMENDATIONS FOR FUTURE RESEARCH

Recommendations for future research are as follows.

(1) The qualitative scenario of combined diffusion of sodium (Na^+) initially in the pores of the BPN and diffusion of either potassium (K^+) or calcium (Ca^{2+}) as a result of an imposed gradient of KCl or CaCl_2 , respectively, across the specimen needs to be modeled to confirm the observed behavior.

(2) A rigid-flex wall cell (a rigid-wall cell with a flexible membrane between the rigid side-walls and the specimen) should be considered to simultaneously measure the membrane efficiency coefficients and diffusion coefficients during multi-stage steady-state diffusion of calcium chloride (CaCl_2) through BPN. The use of the rigid-flex cell would limit the potential for short circuiting associated with the rigid-wall cell, and reduce the potential for membrane blow-out associated with a flexible-wall cell. Therefore, the concentration of CaCl_2 at which the membrane behavior of the BPN in the rigid-cell is destroyed could be more accurately determined.

(3) Specimens should be leached of soluble salts before testing using a method such as dialysis to remove the effects of excess sodium (Na^+) in the BPN on the measured effective diffusion coefficients, thereby providing a basis for comparison with the results of this study based on specimens that were largely not flushed prior to testing.

(4) The engineering properties of the “next generation” BPN (e.g., less excess polymer) should be evaluated and compared with those from this study.

(5) The potential use of BPN in other types of barriers, such as compacted sand-BPN mixtures, and for other applications, such as animal waste lagoons, mine tailings, nuclear waste repositories, should be evaluated.

Appendix A
Consolidation Test Data

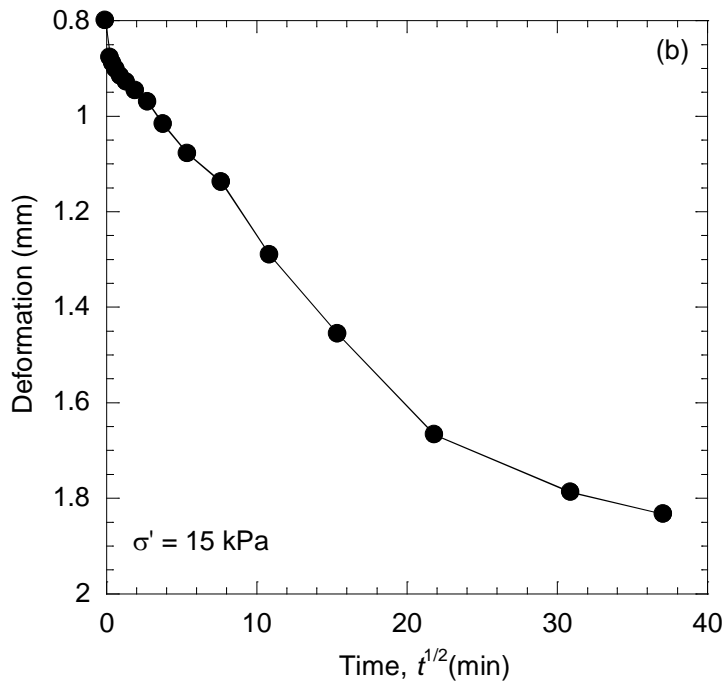
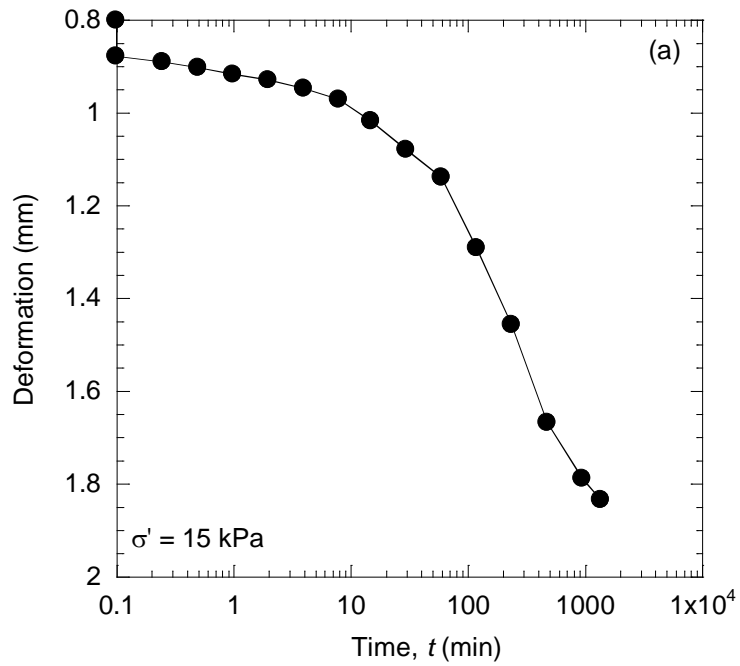


Figure A.1. Deformation versus logarithm of time (a) and deformation versus square root of time (b) during consolidation of 5CB5 backfill in an oedometer .

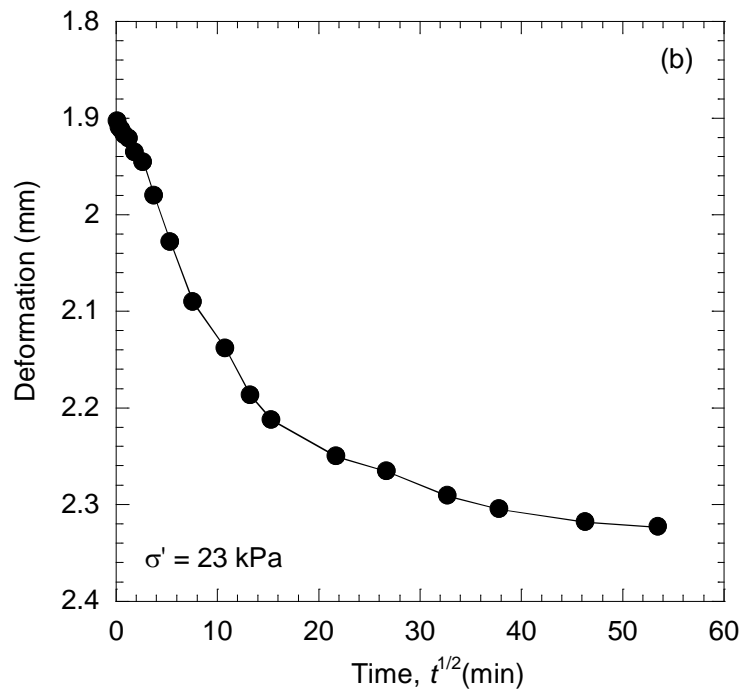
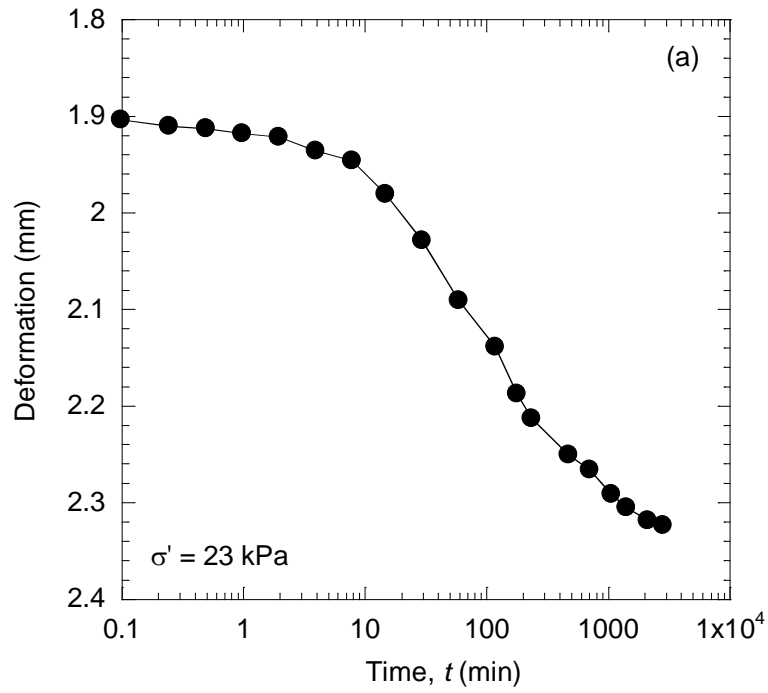


Figure A.2. Deformation versus logarithm of time (a) and deformation versus square root of time (b) during consolidation of 5CB5 backfill in an oedometer.

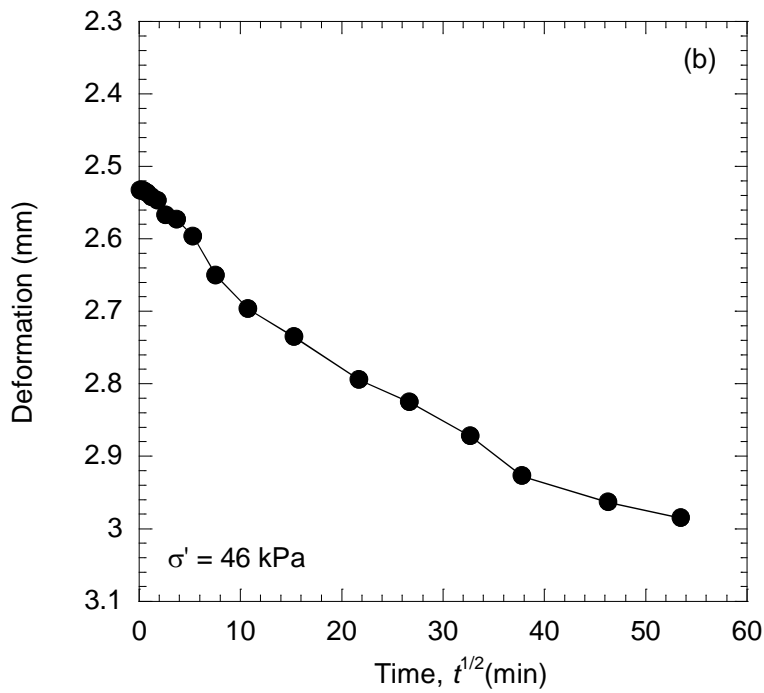
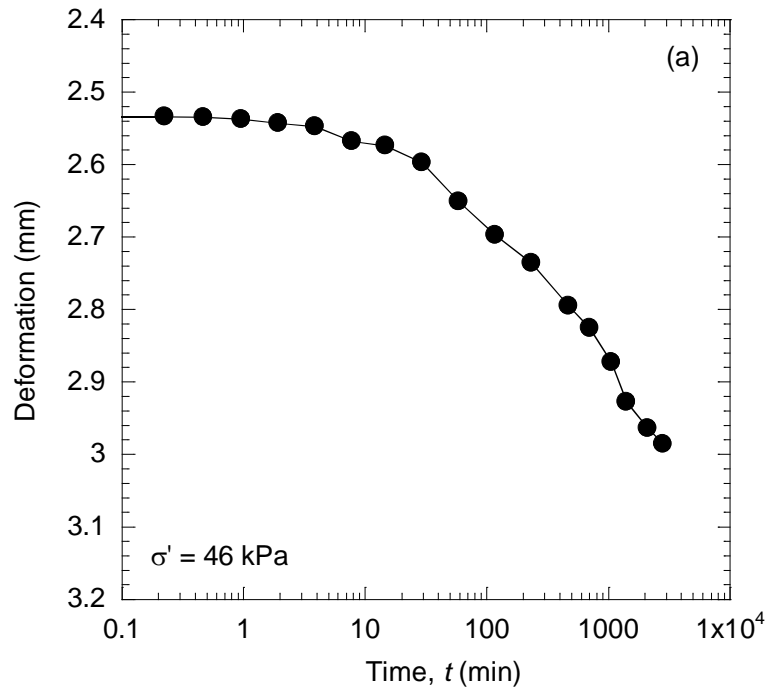


Figure A.3. Deformation versus logarithm of time (a) and deformation versus square root of time (b) during consolidation of 5CB5 backfill in an oedometer.

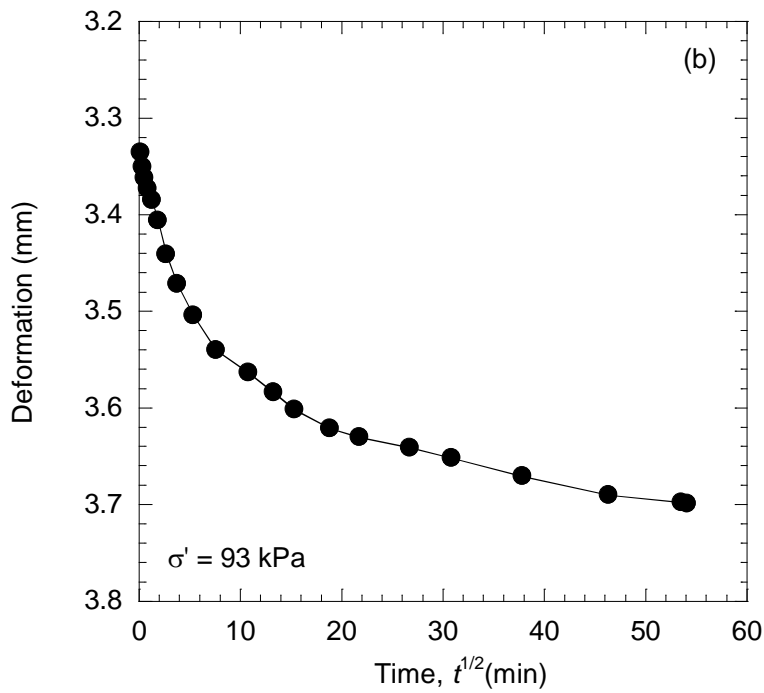
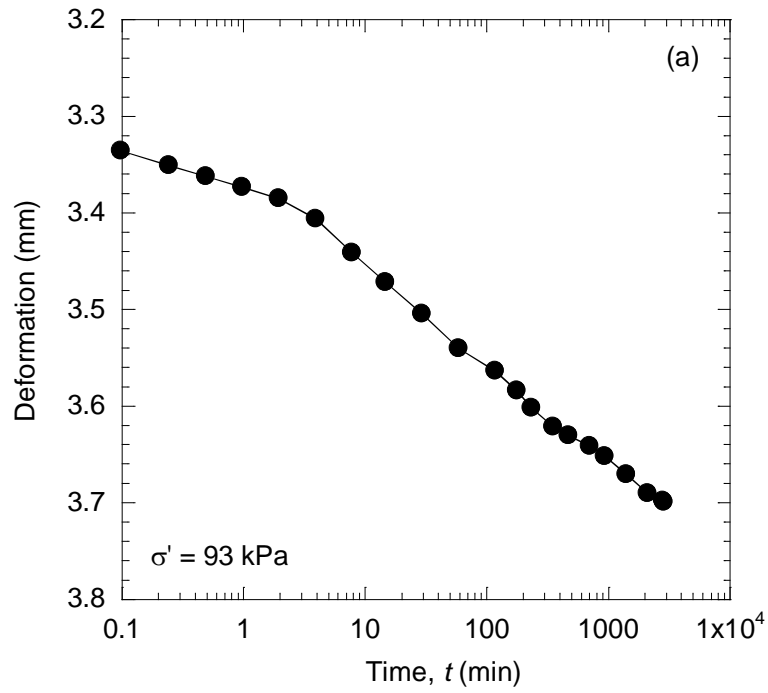


Figure A.4. Deformation versus logarithm of time (a) and deformation versus square root of time (b) during consolidation of 5CB5 backfill in an oedometer.

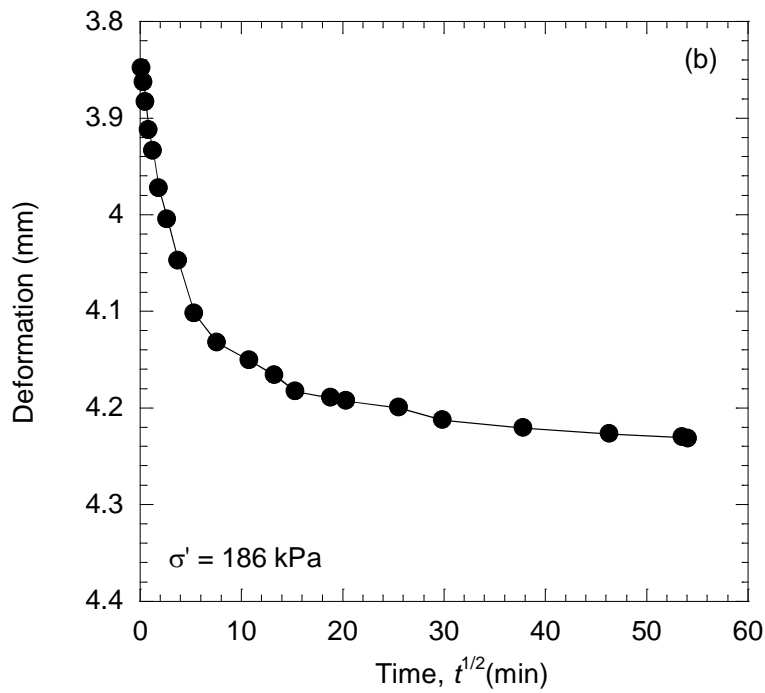
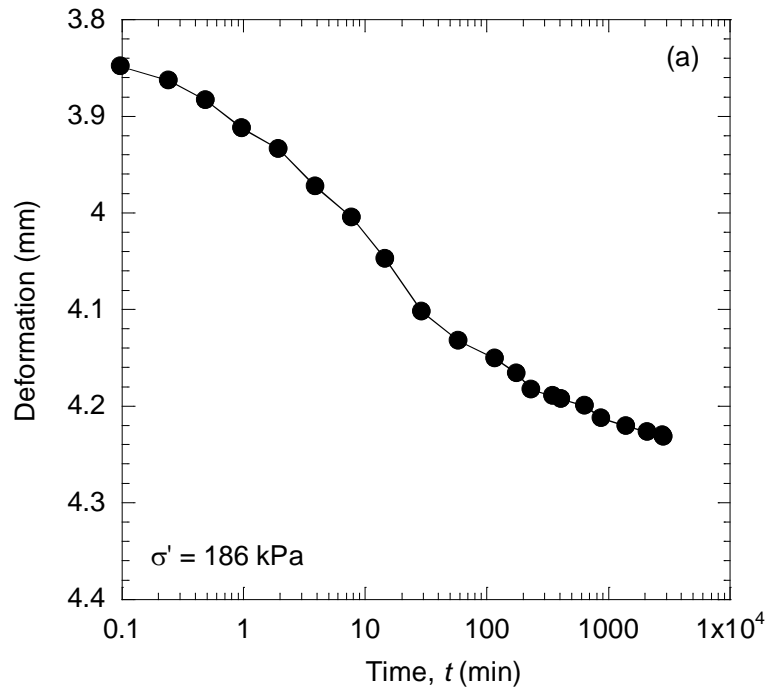


Figure A.5. Deformation versus logarithm of time (a) and deformation versus square root of time (b) during consolidation of 5CB5 backfill in an oedometer.

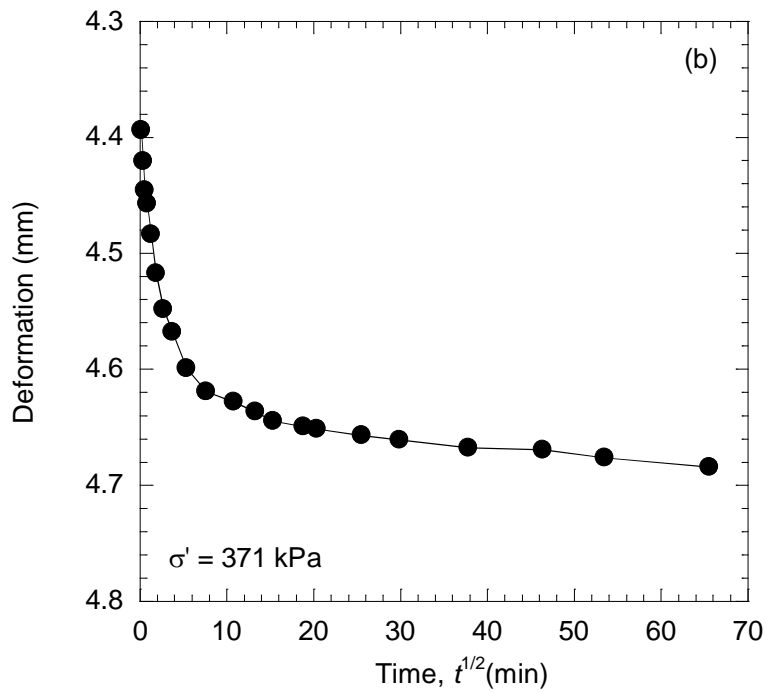
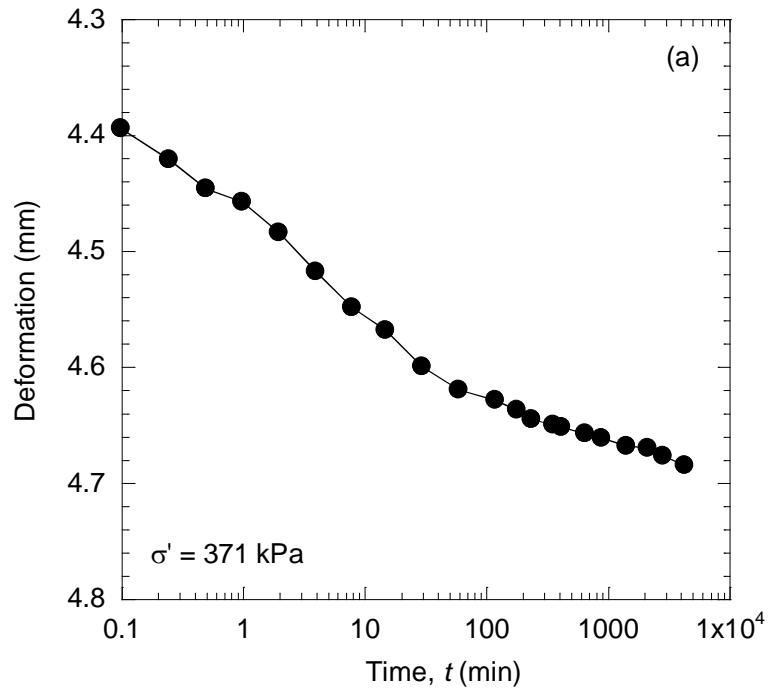


Figure A.6. Deformation versus logarithm of time (a) and deformation versus square root of time (b) during consolidation of 5CB5 backfill in an oedometer.

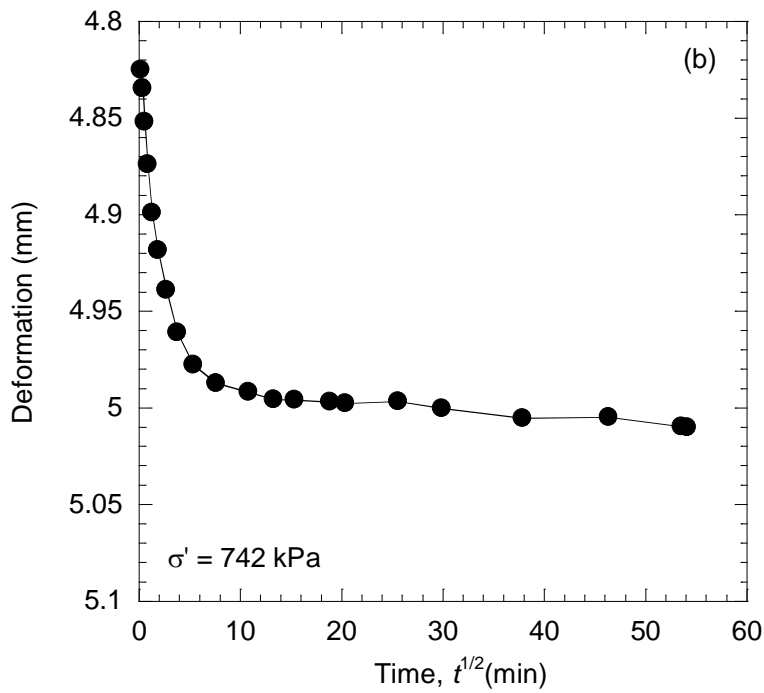
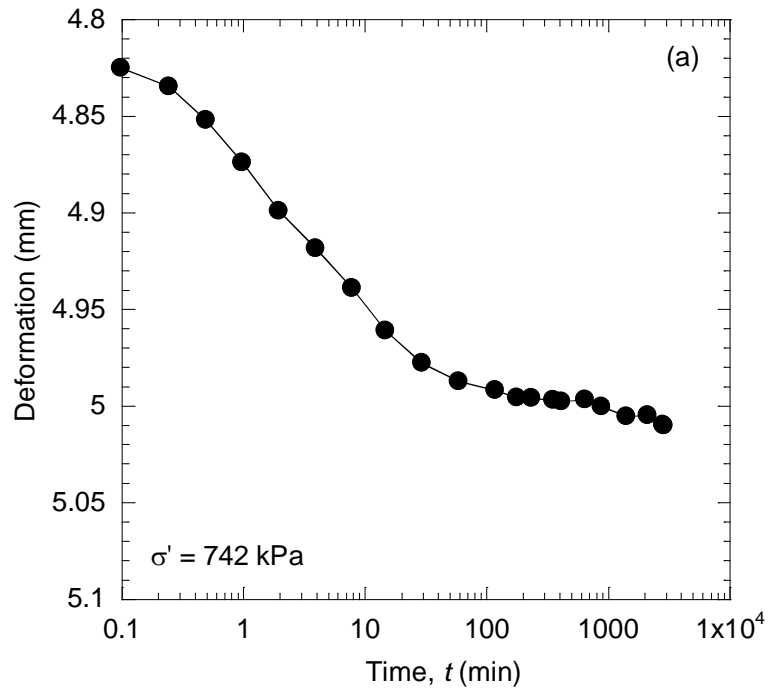


Figure A.7. Deformation versus logarithm of time (a) and deformation versus square root of time (b) during consolidation of 5CB5 backfill in an oedometer.

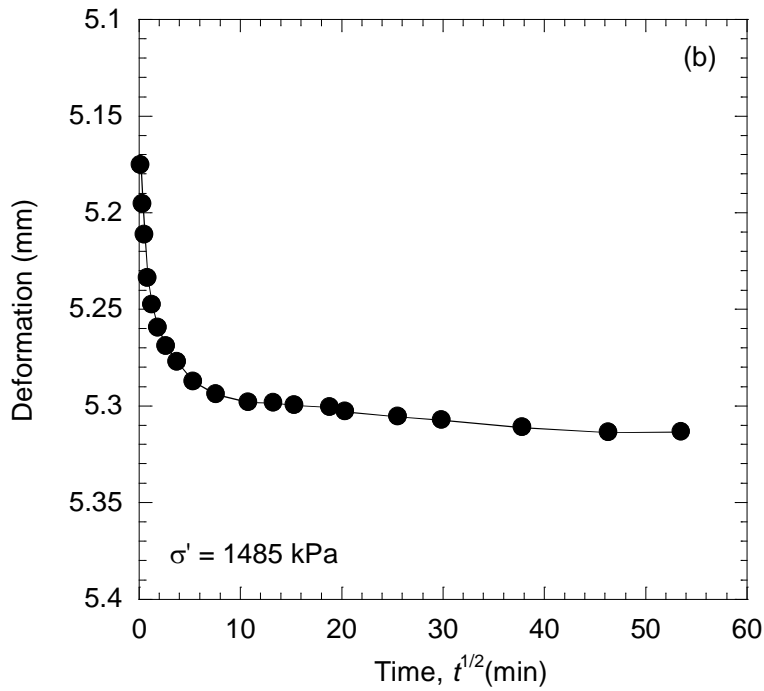
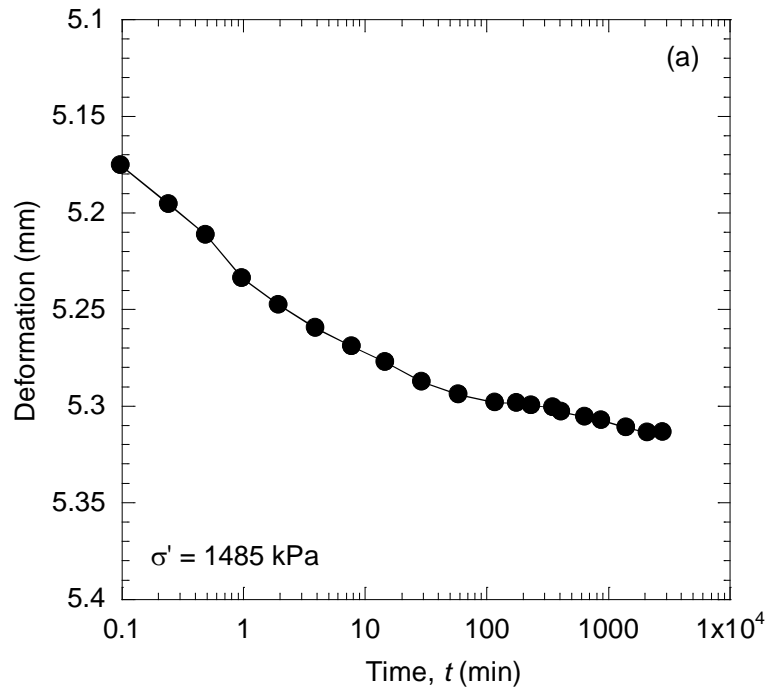


Figure A.8. Deformation versus logarithm of time (a) and deformation versus square root of time (b) during consolidation of 5CB5 backfill in an oedometer.

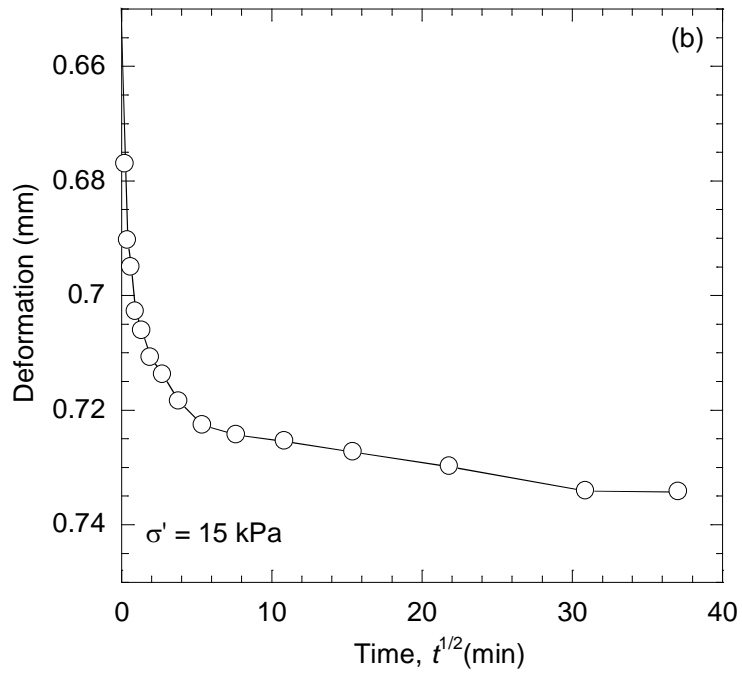
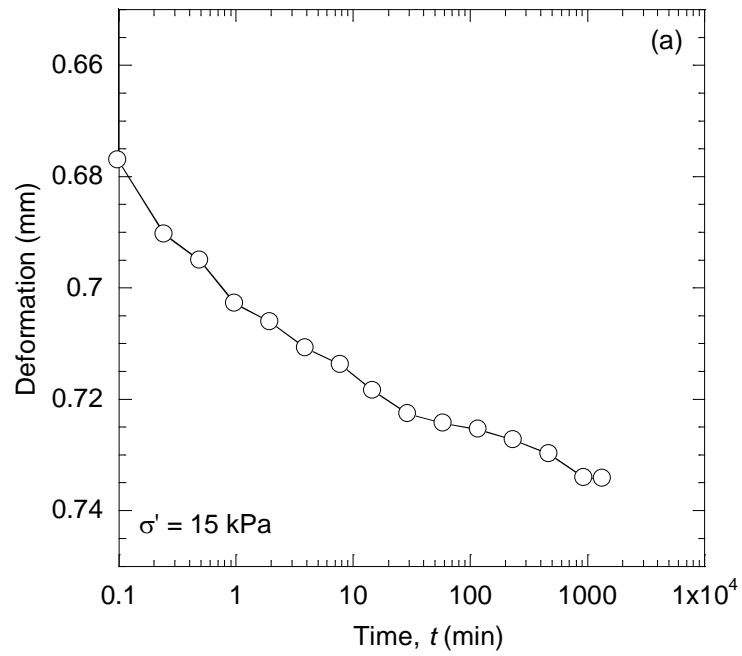


Figure A.9. Deformation versus logarithm of time (a) and deformation versus square root of time (b) during consolidation of 2BPN2 backfill in an oedometer.

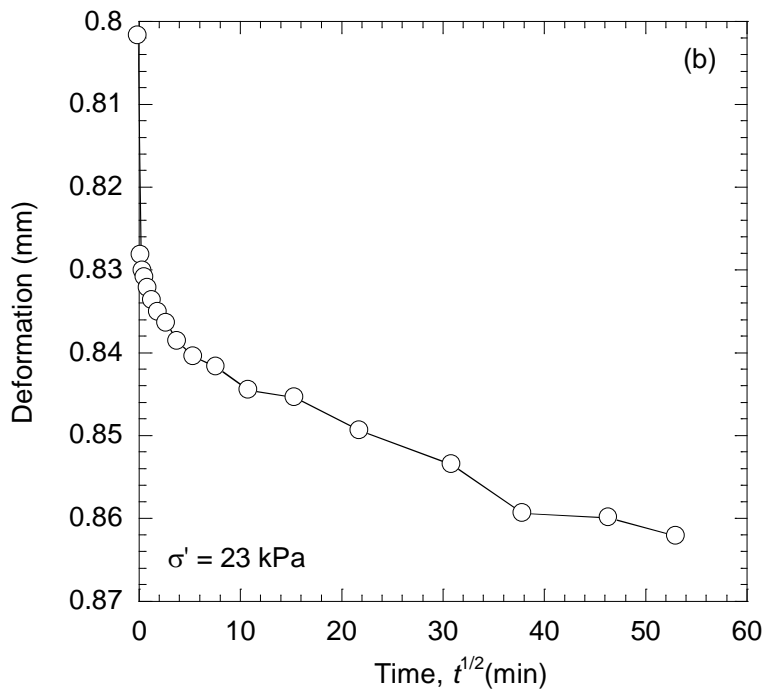
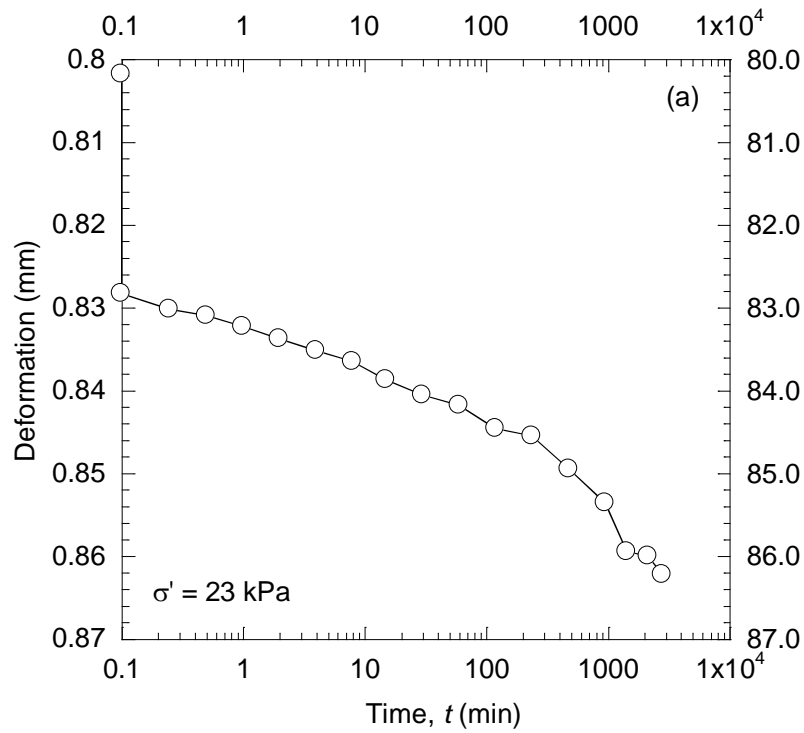


Figure A.10. Deformation versus logarithm of time (a) and deformation versus square root of time (b) during consolidation of 2BPN2 backfill in an oedometer.

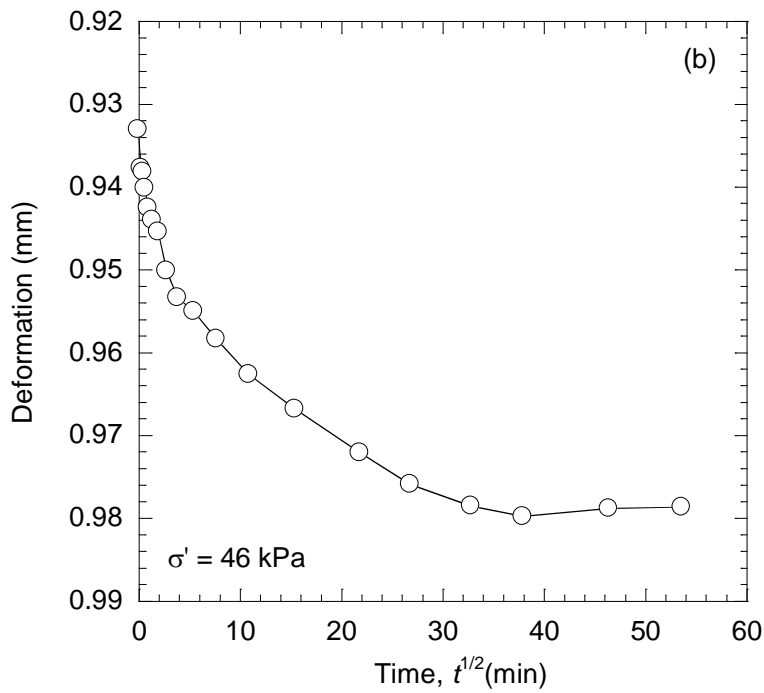
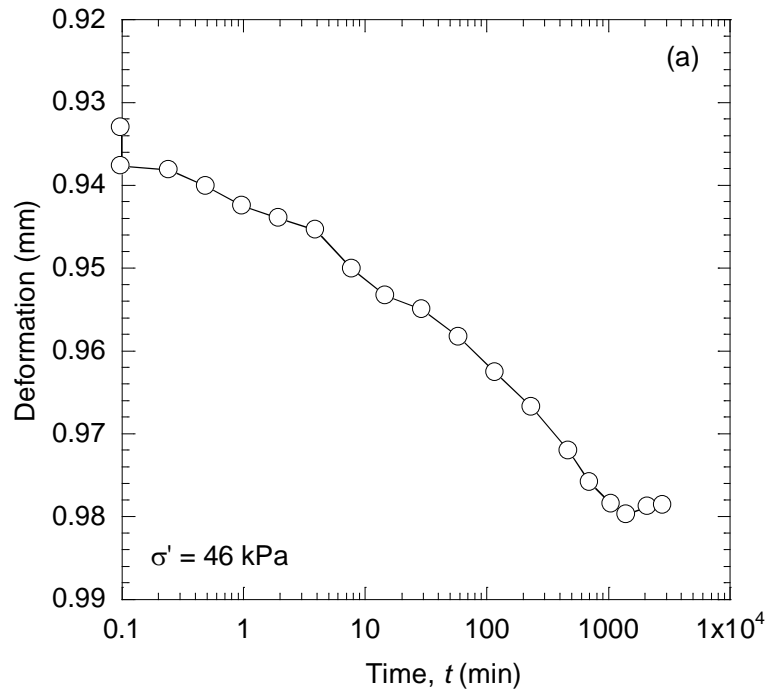


Figure A.11. Deformation versus logarithm of time (a) and deformation versus square root of time (b) during consolidation of 2BPN2 backfill in an oedometer.

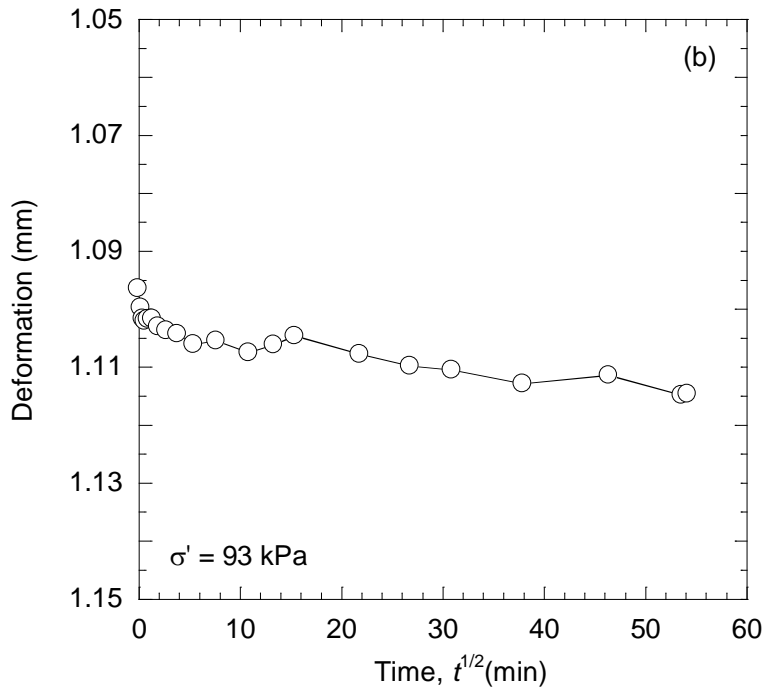
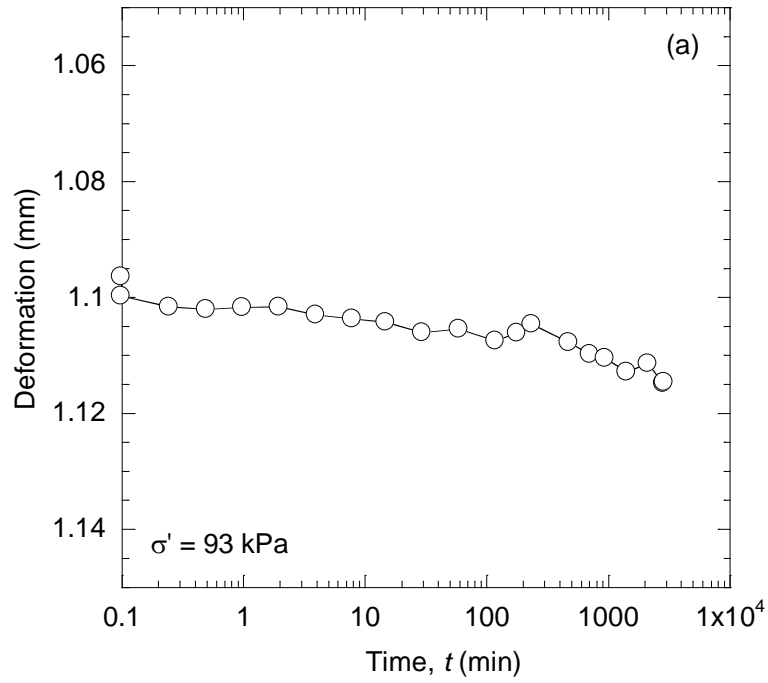


Figure A.12. Deformation versus logarithm of time (a) and deformation versus square root of time (b) during consolidation of 2BPN2 backfill in an oedometer.

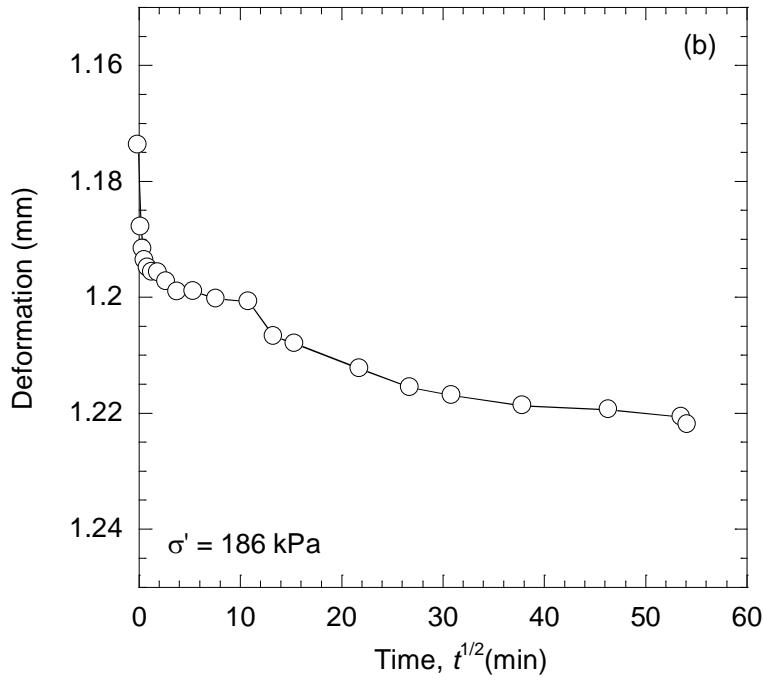
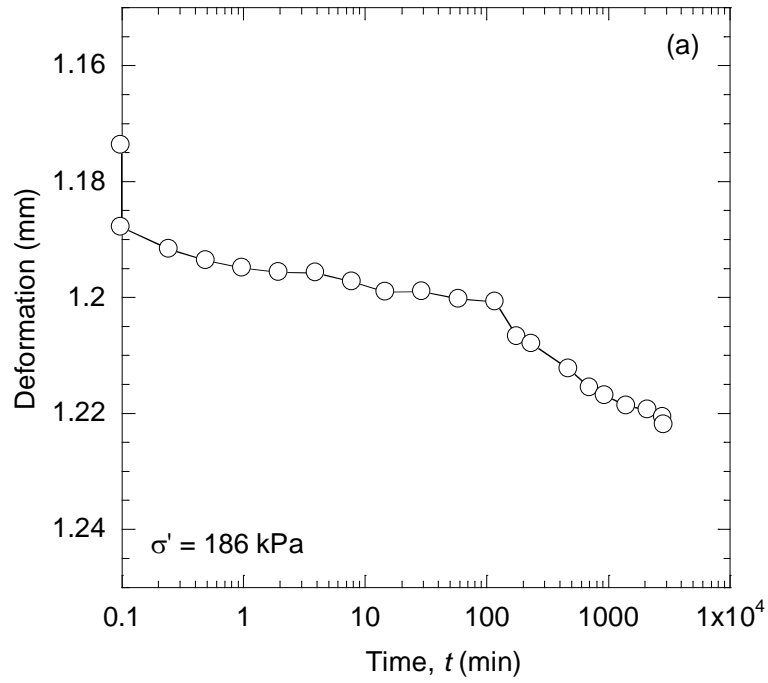


Figure A.13. Deformation versus logarithm of time (a) and deformation versus square root of time (b) during consolidation of 2BPN2 backfill in an oedometer.

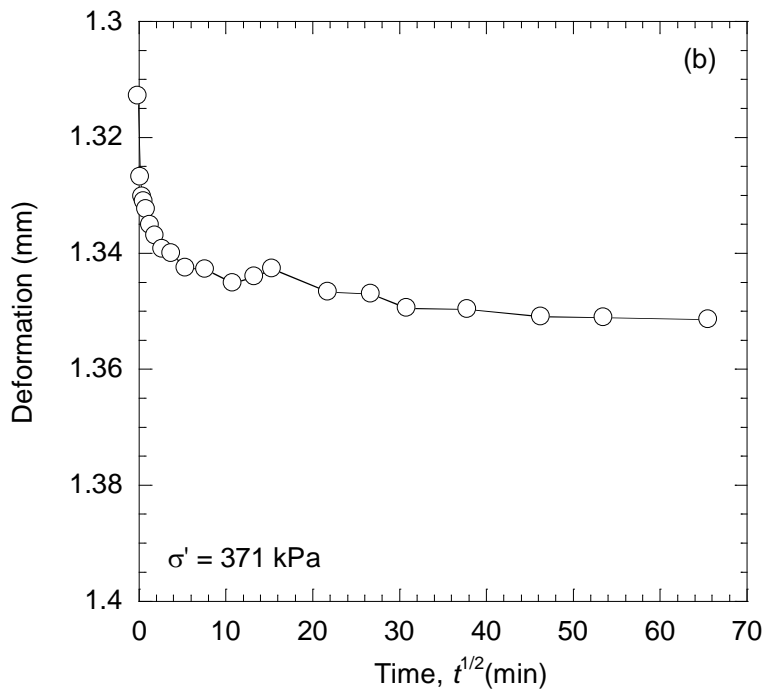
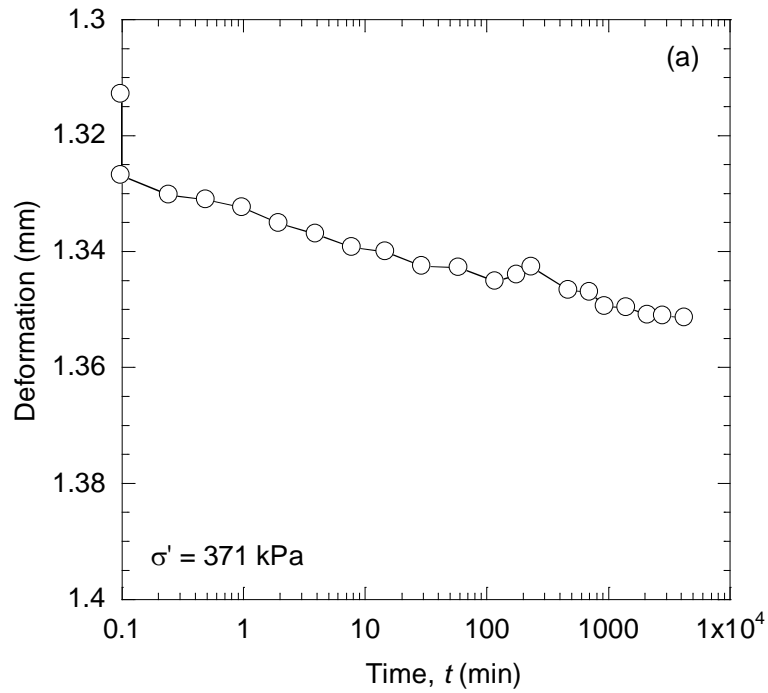


Figure A.14. Deformation versus logarithm of time (a) and deformation versus square root of time (b) during consolidation of 2BPN2 backfill in an oedometer.

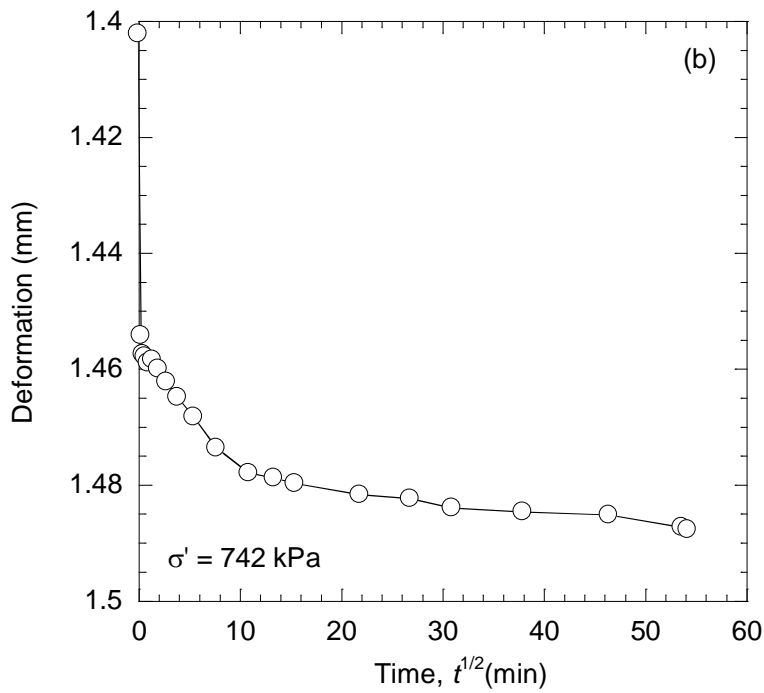
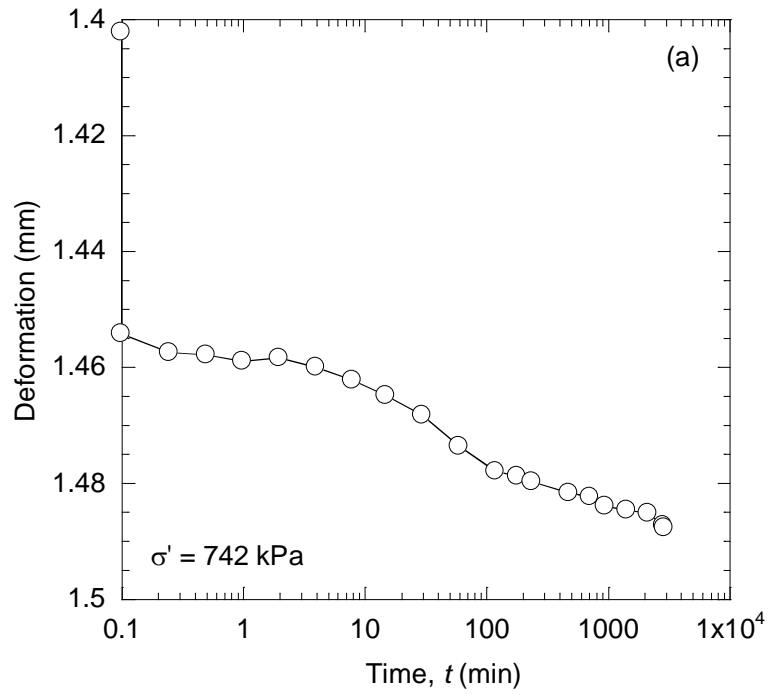


Figure A.15. Deformation versus logarithm of time (a) and deformation versus square root of time (b) during consolidation of 2BPN2 backfill in an oedometer.

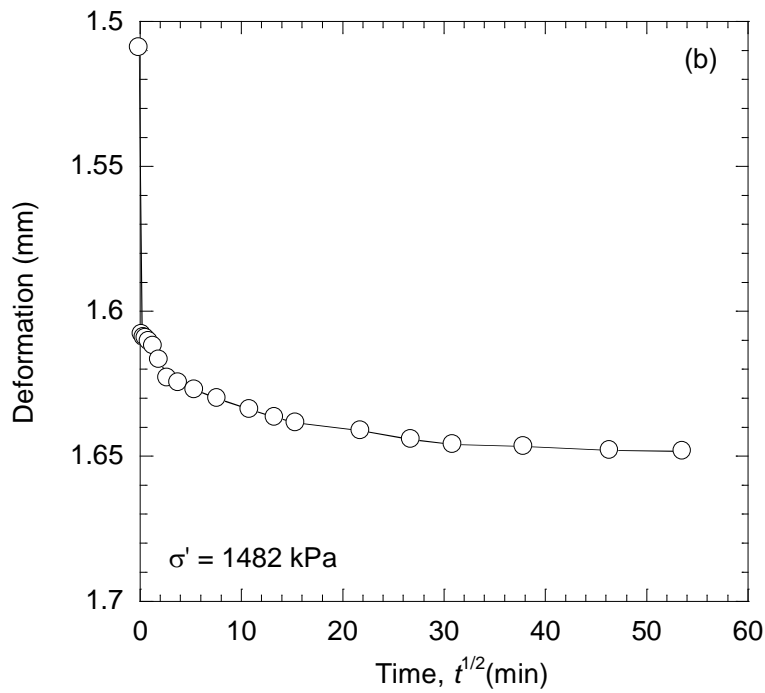
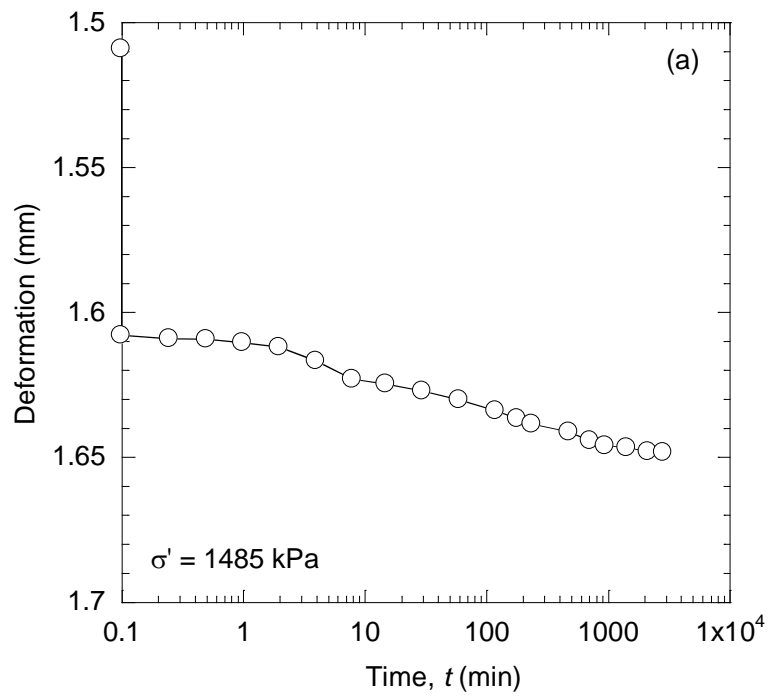


Figure A.16. Deformation versus logarithm of time (a) and deformation versus square root of time (b) during consolidation of 2BPN2 backfill in an oedometer.

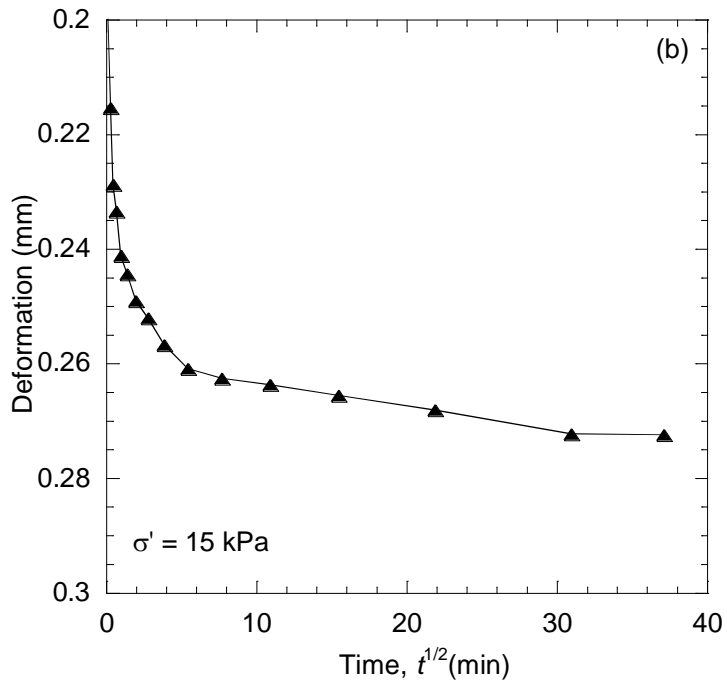
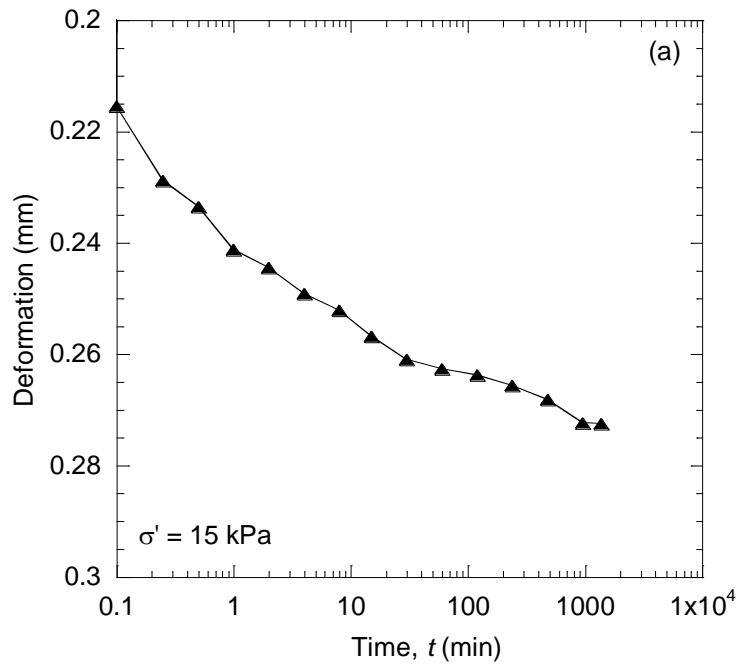


Figure A.17. Deformation versus logarithm of time (a) and deformation versus square root of time (b) during consolidation of 5BPN5 backfill in an oedometer.

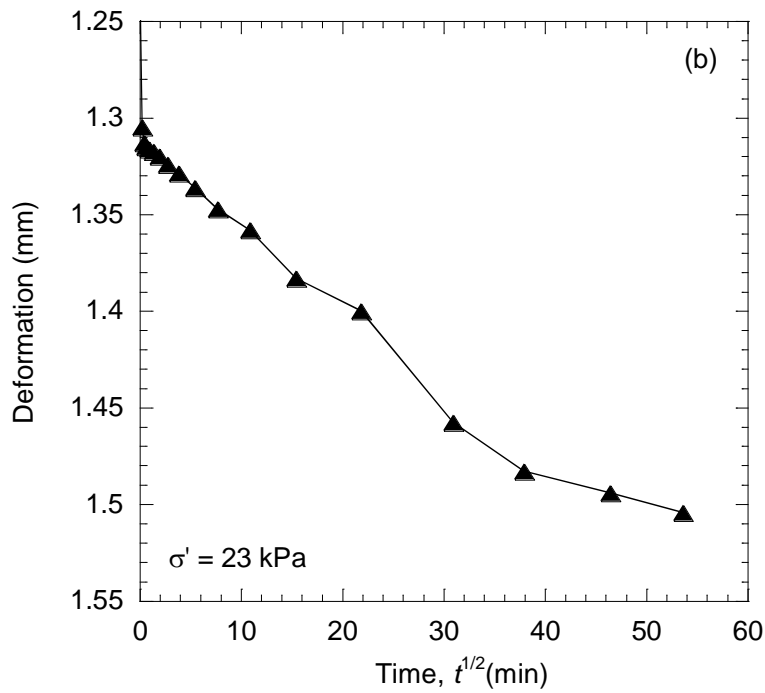
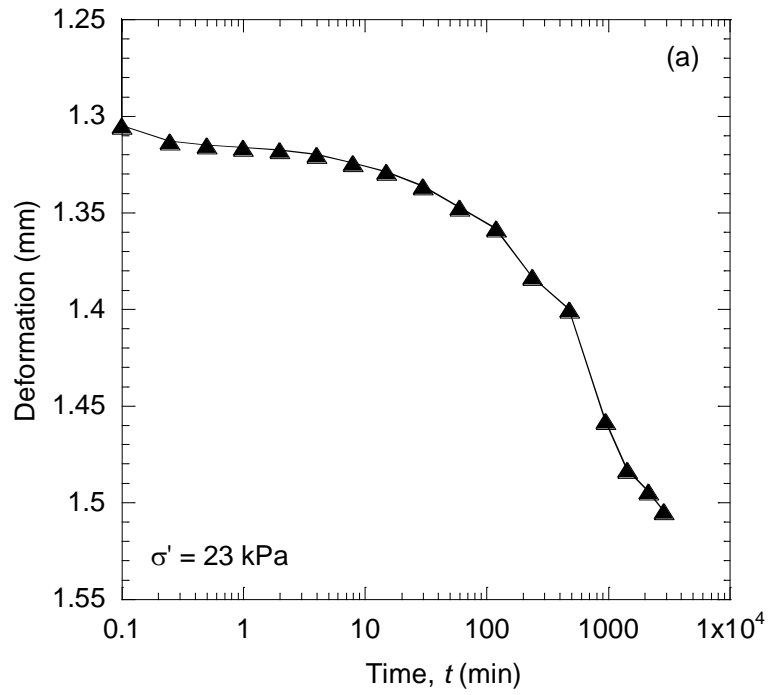


Figure A.18. Deformation versus logarithm of time (a) and deformation versus square root of time (b) during consolidation of 5BPN5 backfill in an oedometer.

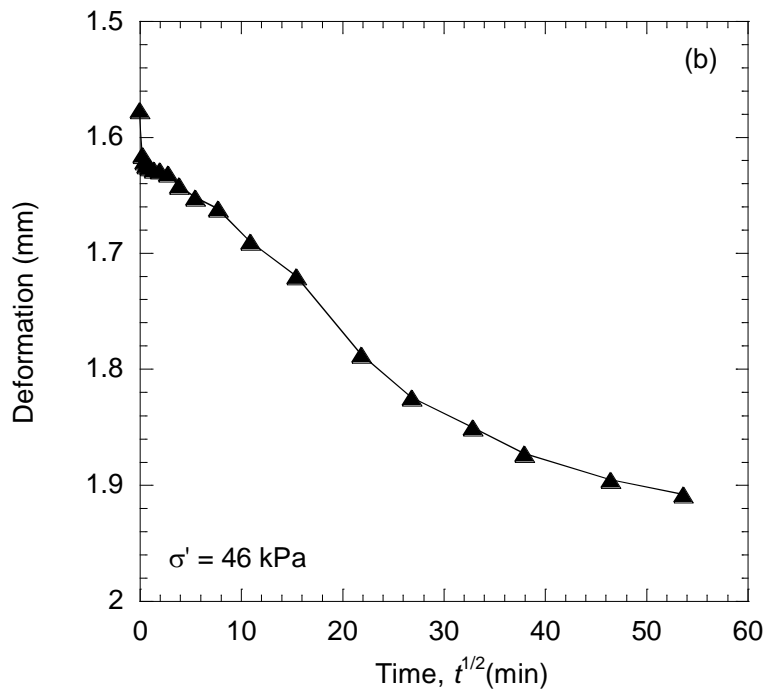
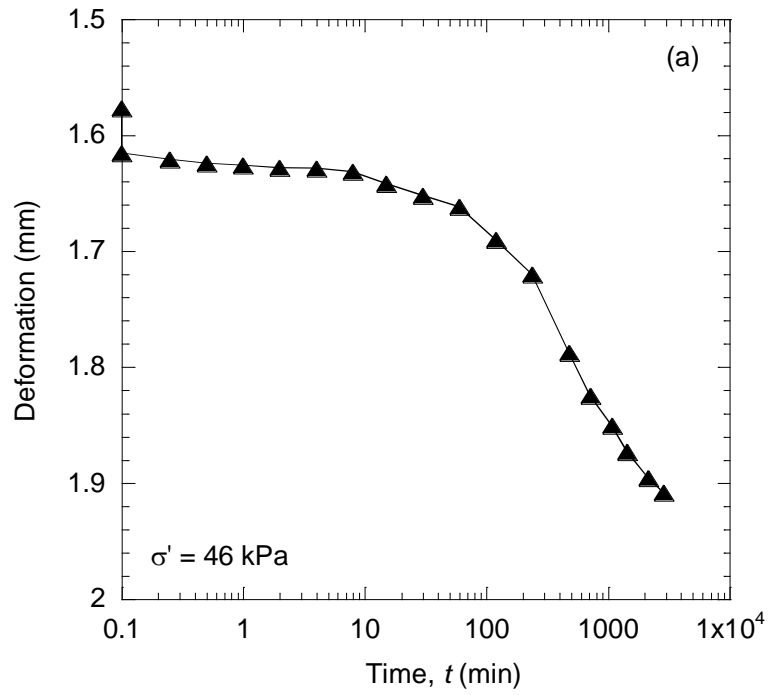


Figure A.19. Deformation versus logarithm of time (a) and deformation versus square root of time (b) during consolidation of 5BPN5 backfill in an oedometer.

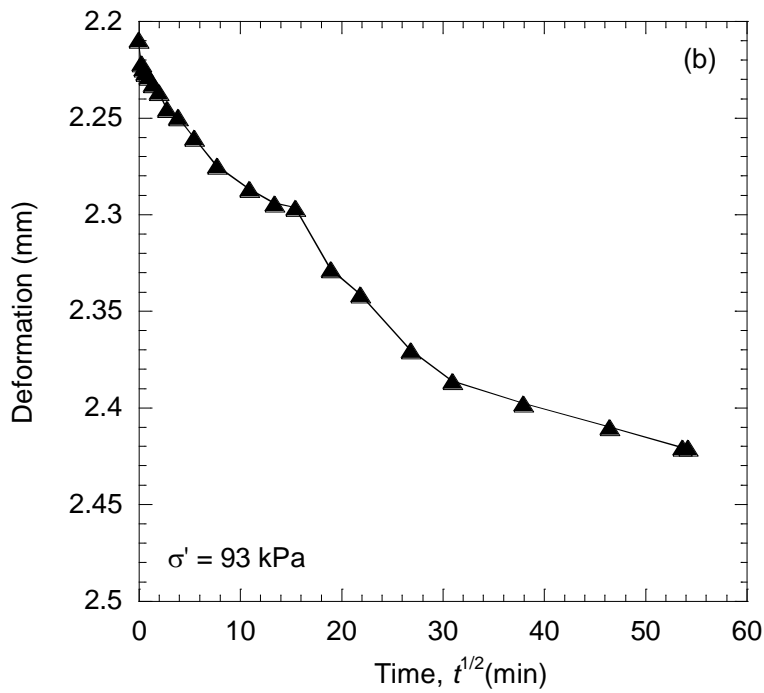
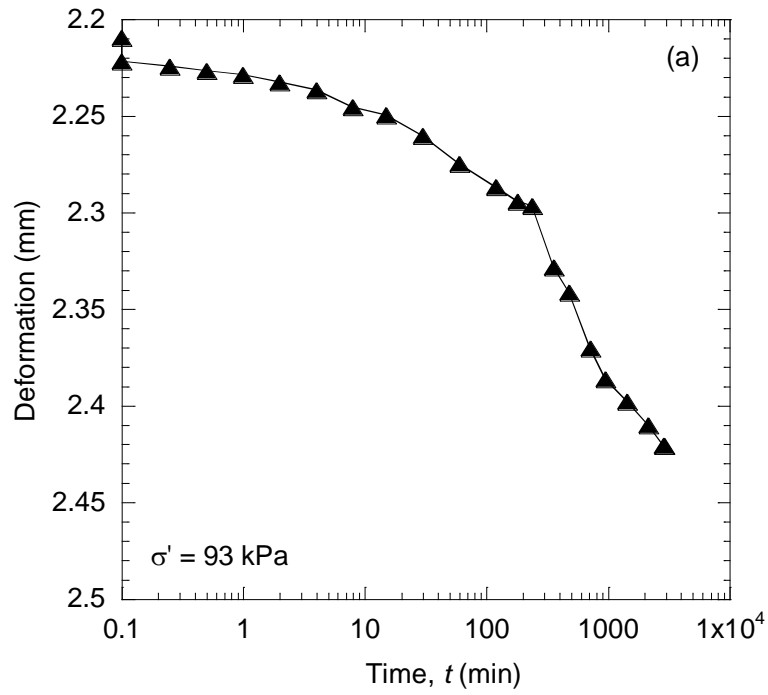


Figure A.20. Deformation versus logarithm of time (a) and deformation versus square root of time (b) during consolidation of 5BPN5 backfill in an oedometer.

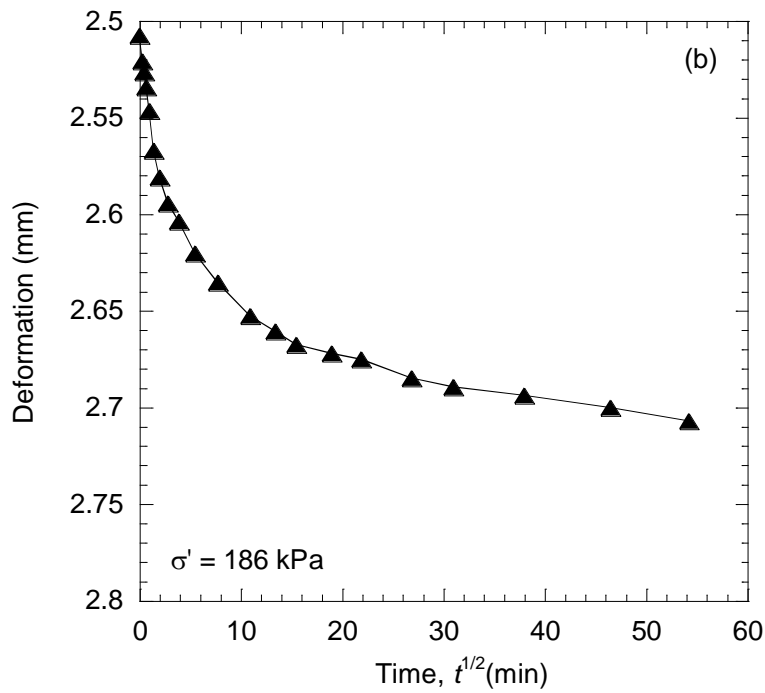
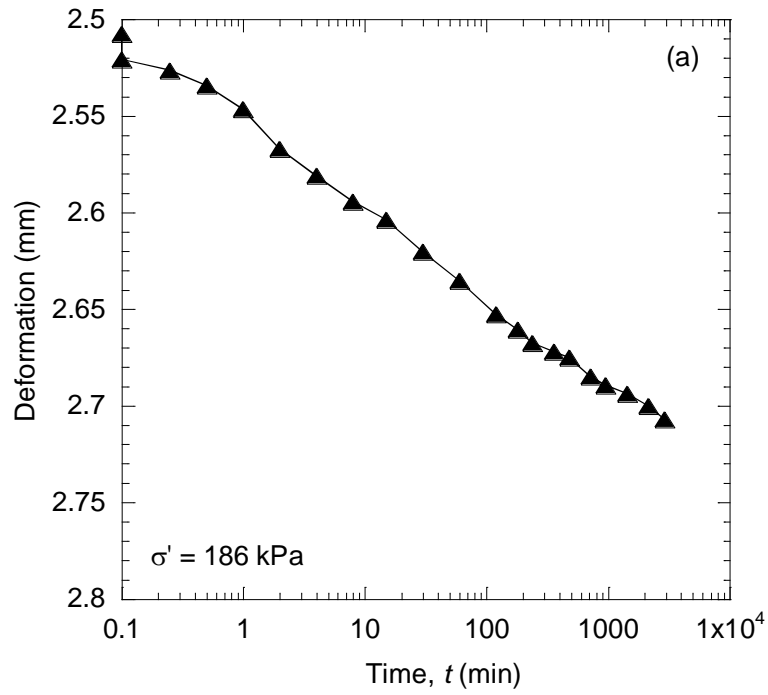


Figure A.21. Deformation versus logarithm of time (a) and deformation versus square root of time (b) during consolidation of 5BPN5 backfill in an oedometer.

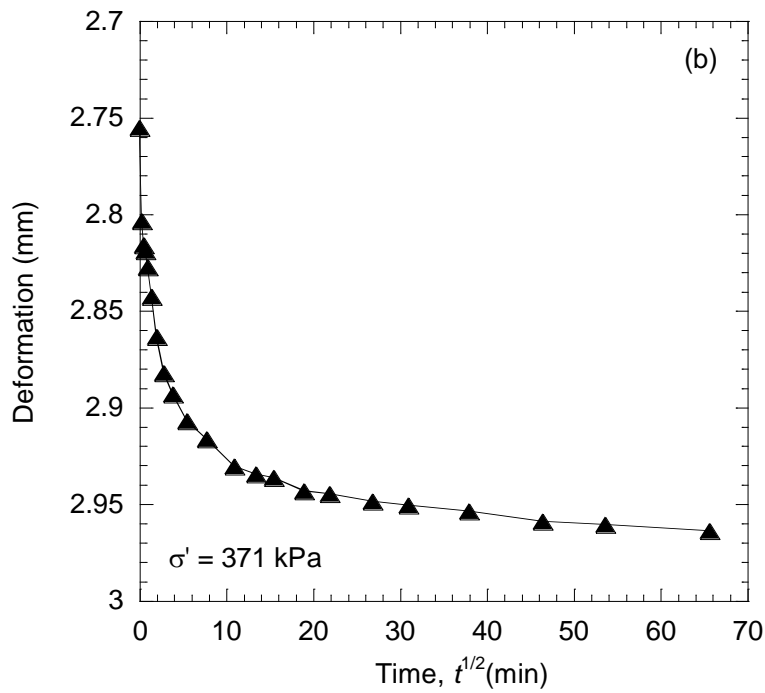
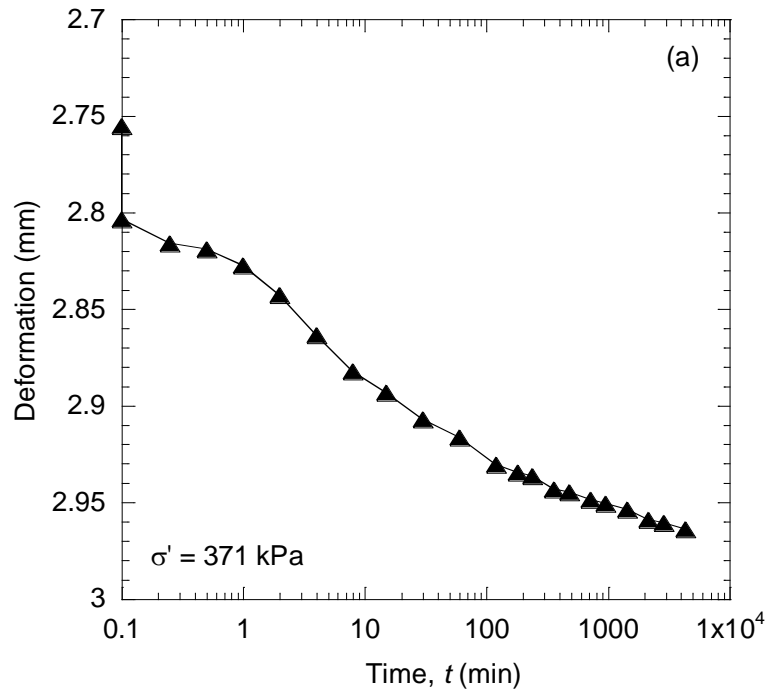


Figure A.22. Deformation versus logarithm of time (a) and deformation versus square root of time (b) during consolidation of 5BPN5 backfill in an oedometer.

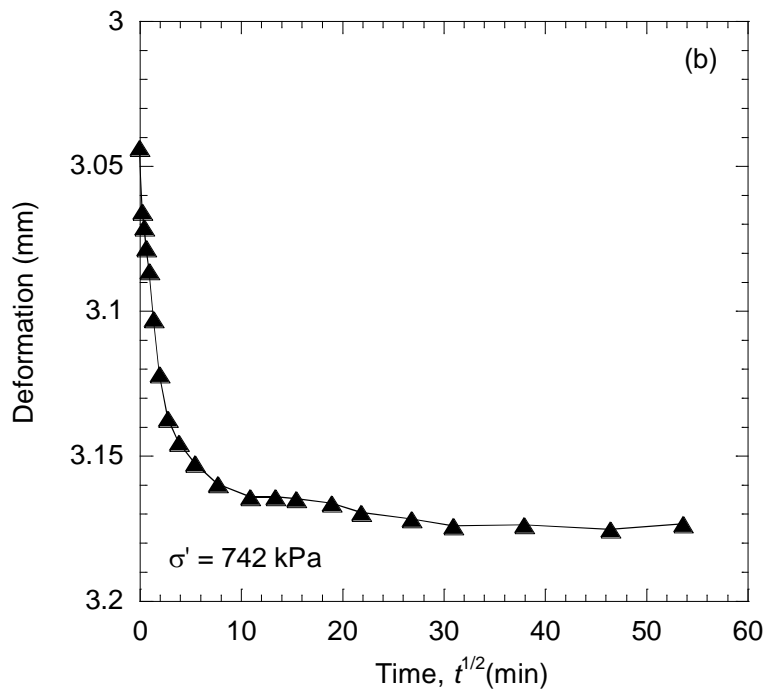
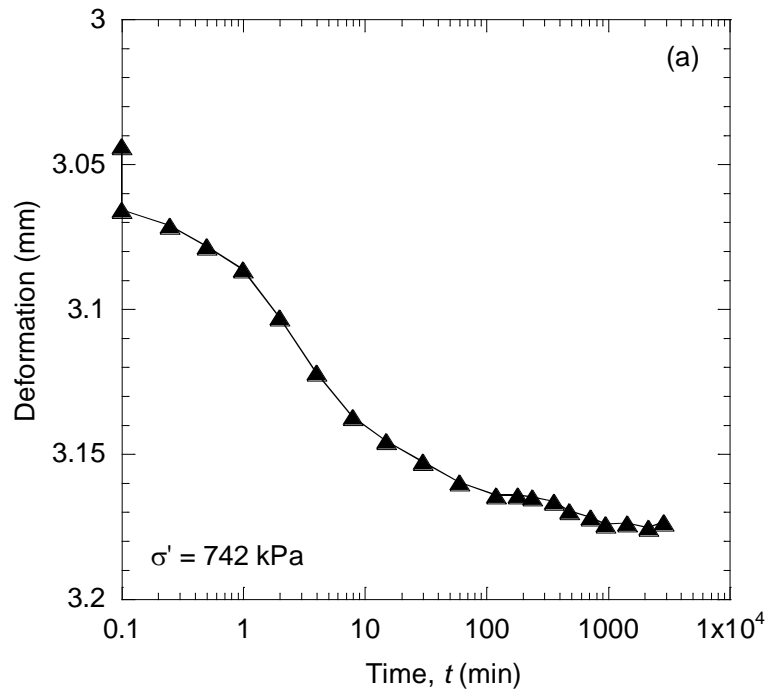


Figure A.23. Deformation versus logarithm of time (a) and deformation versus square root of time (b) during consolidation of 5BPN5 backfill in an oedometer.

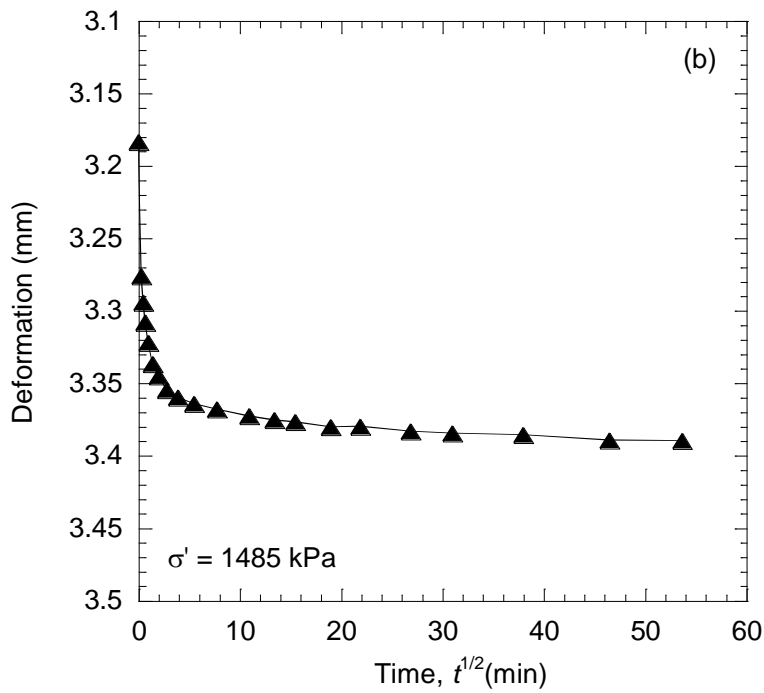
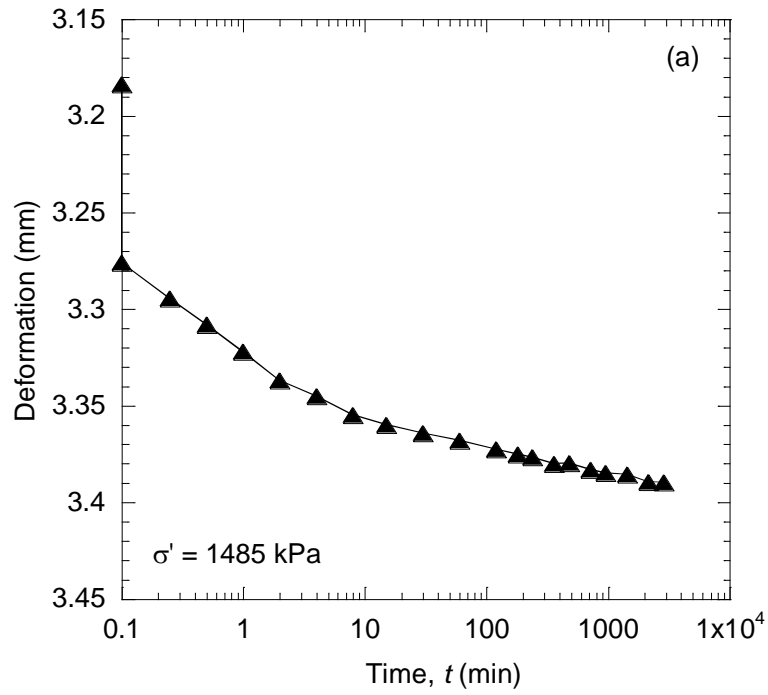


Figure A.24. Deformation versus logarithm of time (a) and deformation versus square root of time (b) during consolidation of 5BPN5 backfill in an oedometer.

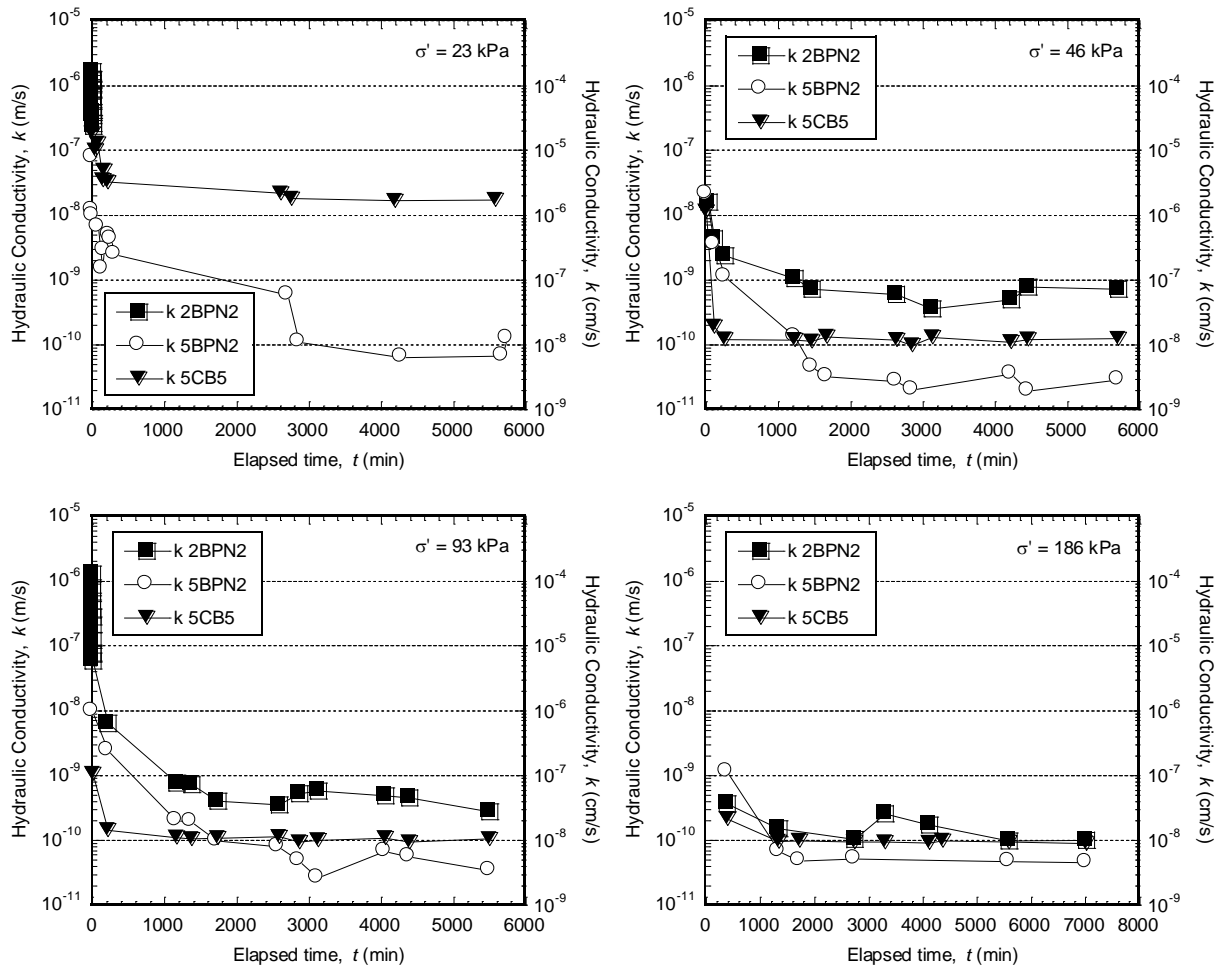


Figure A.25. Hydraulic conductivity versus elapsed time measured in a consolidometer cell for sand-bentonite backfills with 5 % conventional bentonite (CB) mixed with 5 % CB slurry (5CB5), 2 % bentonite polymer nanocomposite (BPN) mixed with 2 % BPN slurry (2BPN2), and 5% BPN mixed with 2 % BPN slurry (5BPN2).

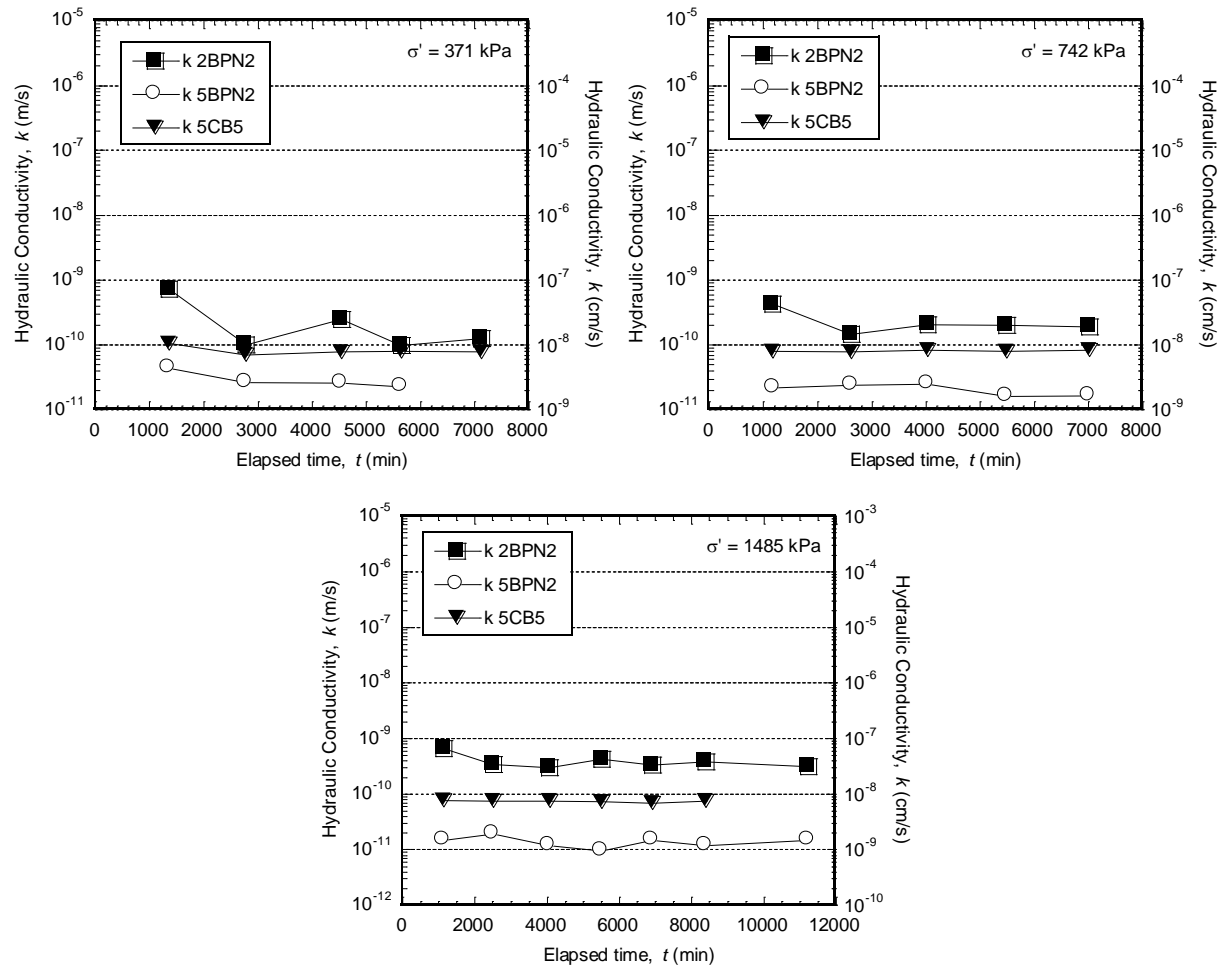


Figure A.25 (continued). Hydraulic conductivity versus elapsed time measured in a consolidometer cell for sand-bentonite backfills with 5 % conventional bentonite (CB) mixed with 5 % CB slurry (5CB5), 2 % bentonite polymer nanocomposite (BPN) mixed with 2 % BPN slurry (2BPN2), and 5% BPN mixed with 2 % BPN slurry (5BPN2).